Second Series *October 1, 1932* *Vol. 42, No. 1*

THE

PHYSICAL REVIEW

The Isotopic Weight of H^2

By KENNETH T. BAINBRIDGE
Bartol Research Foundation of the Franklin Institute

(Received August 15, 1932)

The mass of neutral H^2 was measured on a mass-spectrograph as 2.01351 ± 0.00006 referred to He and 2.01351 ± 0.00018 referred to $O^{16} = 16$. The equivalent packing fraction of H^2 is 67.5 parts in 10,000. On the assumption that the nucleus is composed of two protons and one electron the energy of binding is approximately 2×10^6 electron-volts. If the H^2 nucleus is made up of one proton and one Chadwick neutron of mass 1.0067 then the binding energy of these two particles is 9.7×10^5 electron-volts. H_3^{1+} and He^+ provided the dispersion measurements for the spectra. The presence of $H^1\,H^{2+}$ can only introduce in the mass determination a possible *maximum* error of 0.00003 mass units. Lines of mass 4.02852 on the spectra were attributed to $H_2^1\,H^2$ ions because: (1) no lines of comparable intensity appeared in this position when commercial hydrogen of low H^2 content was used; (2) under the conditions existing in the discharge tube the abundance of H_2^{2+} was negligibly small compared to the abundance of $H_2^1\,H^{2+}$; (3) the mass is less than the mass of H_4^{1+} by an amount outside of the limits of error. Two samples of enriched hydrogen were used which had been prepared by Brickwedde; both had been tested spectroscopically by Urey and Murphy, and one of them was identical with Bleakney's Sample III. From the value for the mass of H^2, the energy balance is calculated for one process of noncapture disintegration of N^{14} by neutron impact, suggested by Feather, which would result in C^{12} and H^2. It is concluded that this disintegration could not possibly occur under the conditions of his experiments.

INTRODUCTION

THE H^2 nucleus represents the simplest complex nucleus and as such may be more amenable to theoretical attack than other nuclei. Whether the nucleus is composed of two protons and one electron, or one proton and one neutron, an accurate determination of the mass of the H^2 nucleus is of interest not only in relation to the packing fractions of other nuclei but also as a clue to the possible structure of the H^2 nucleus itself. Also, the possibility exists that together with the electron, proton, neutron, and alpha-particle, H^2 may play a part in the structure of heavier nuclei.[1]

In all calculations of the energy of binding of nuclear constituents it is essential to know the masses of the component parts. Bleakney[2] has placed a lower limit on the mass of the H^2 nucleus, but spectrographs of the Dempster

[1] N. Feather, Proc. Roy. Soc. **136,** 726 (1932); J. Chadwick, ibid., 706; N. S. Grace, J. Am. Chem. Soc. **54,** 2562 (1932).

[2] W. Bleakney, Phys. Rev. **41,** 32 (1932); **39,** 536 (1932).

type such as Bleakney used are at present limited to a lower order of accuracy than mass-spectrographs which photograph mass-spectra and permit the reduction of observations from accurate mensuration of the photographic traces resulting from ionized atoms and molecules. In the future the ratio of the masses of H^1 to H^2 may possibly be obtained from band spectra with an error of only one part in 10^5. The present paper is a report of the measurement[3] of the mass of H^2 obtained with the mass-spectrograph recently described.[4]

The existence of an isotope of hydrogen of mass number two, predicted by Birge and Menzel,[5] was demonstrated by Urey, Brickwedde, and Murphy.[6] Their paper should be referred to for a bibliography of the subject and a review of previous work. Bleakney's work with his low-pressure spectrograph provided excellent confirmatory evidence of H^2, and splendid measurements were secured of the relative abundance of H^2 in various samples of hydrogen. More recently Kallman and Lasareff[7] were able to detect the presence of H^1H^2 in fractionated hydrogen.

Conditions for the Measurement of the Mass of H^2

If the mass of H^2 should be close to that of H_2^1 then the resolving power of the apparatus might not permit the separation of the doublets H^{2+}, H_2^{1+}, and H_3^{1+}, H^1H^{2+}, and the mass of H^2 could not be compared with H^1 directly. The most accurate method of measurement of the mass of H^2 by a mass-spectrograph would be by comparison of the mass of $H_2^1H^{2+}$ with He^+. Bleakney's value of a lower limit of the mass of H^2 showed clearly that $H_2^1H^{2+}$ if secured would be well separated from He^+ and the higher the mass of H^2 the greater the separation. From the suggested process of formation of triatomic hydrogen,[8] $H_2^+ + H_2 \rightarrow H_3^+ + H$, it is clear that a high concentration of ions in the discharge tube would favor the production of H_3^{1+} and $H_2^1H^{2+}$. Brasefield[9] has shown that under proper conditions of current density and pressure, an ion beam can be secured with a concentration of H_3^{1+} comparable to that of H_2^{1+}. Bleakney, and Kallman and Lasareff worked with very low pressures of hydrogen which would preclude secondary effects to a large extent and only permit measurements of ions produced by the primary process of electron impact. Relatively high current density and high gas pressure favor the formation of $H_2^1H^{2+}$.

Experimental Procedure

Fortunately the conditions essential to the production of triatomic hydrogen can be achieved in the discharge tube of the mass-spectrograph.

[3] K. Bainbridge, Phys. Rev. **41**, 115 (1932).

[4] K. Bainbridge, Phys. Rev. **40**, 130 (1932). A detailed description of this apparatus will appear in the Journal of the Franklin Institute.

[5] R. T. Birge and D. H. Menzel, Phys. Rev. **37**, 1669 (1931).

[6] H. C. Urey, F. G. Brickwedde and G. M. Murphy, Phys. Rev. **40**, 1 (1932); **39**, 164 (1932).

[7] H. Kallman and W. Lasareff, Naturwiss. **20**, 472 (1932).

[8] H. D. Smyth, Rev. Mod. Phys. **3**, 370 (1931).

[9] C. Brasefield, Phys. Rev. **31**, 52 (1928).

A cylindrical discharge tube was used, 8 cm in diameter, with a 2.5 cm diameter aluminum cathode of the shape described by Thomson.[10] The top of the cathode was 2 cm above the surface of an iron plate which served as a magnetic shield for stray fields and also as a base for the discharge tube. The pressure of the gas in the discharge tube was in the range of 0.5 to 5 microns of mercury. The current was 75 ± 25 m.a. for different exposures at potentials from 7000 to 15,000 volts, which experience had shown produced $H_2{}^1H^{2+}$ with sufficient intensity.

Two Thordardson 1 K.V.A., 25,000 volt transformers, controlled by an induction voltage regulator, provided the current for the discharge. The combination of two kenetrons with two transformers gave full wave rectification. The output was not filtered in any way, as a wide range of energies in the discharge tube is essential to the proper functioning of the mass-spectrograph.

In addition to ordinary commercial tank hydrogen, two samples of enriched hydrogen were used which had been fractionated at the triple point by Dr. Brickwedde of the U. S. Bureau of Standards. These samples were placed at the disposal of the author through the kindness of Professor Urey, Dr. Brickwedde, Dr. Murphy, and Dr. Bleakney. One sample was from the same lot Bleakney used and designated *Sample III*. The other was fractionated later by Dr. Brickwedde and had been tested by Professor Urey and Dr. Murphy, who reported a greater concentration of H^2 than in *Sample III*.

The magnetic field and the potential across the velocity selector plates of the mass-spectrograph were adjusted to bring $H_3{}^{1+}$ and He^+ within the first 8 cm of the recording plate. This region had been exposed for more than 15 spectra of C, CH_1, CH_2, CH_3, CH_4, and CH_5, and also for the series O, OH_1, OH_2, OH_3, and the mass scale had been found to be linear to within one part in 10,000.

The first 21 exposures showed that $H_2{}^1H^{2+}$, or possibly $H_4{}^{1+}$ or $H_2{}^{2+}$, was present but in such small concentration that no measurements of the mass could be made to aid in determining the nature of the ion. In agreement with Thomson's results,[11] it was found that the presence of mercury vapor in the tube greatly weakens the triatomic hydrogen line. Subsequently, before photographing each series of spectra the discharge tube was cleaned out and baked by the energy of the discharge itself until no discharge could be run at voltages even as high as 25,000. The great amount of power dissipated in the discharge tube, about 500 watts, was sufficient to raise the walls of the tube to 200°C. At the same time the cathode and iron base were thoroughly cleaned by positive ion bombardment.

Ordinarily gases are admitted through a leak into the discharge tube and then are pumped out into the atmosphere. The valuable fractionated hydrogen, however, was not pumped out, but was circulated continuously by a diffusion pump. The gas was pumped out through the cathode slit, 0.005 cm $\times$ 0.3 cm, and then was readmitted to the discharge through a hole under the side of the cathode. The gas passed through two liquid air traps, one on

[10] J. J. Thomson, *Rays of Positive Electricity*, 2nd. ed., p. 30.

[11] Reference 10, p. 200.

each side of the circulating pump. In certain cases still further concentration of the H^2 in the enriched samples was achieved in the discharge tube itself

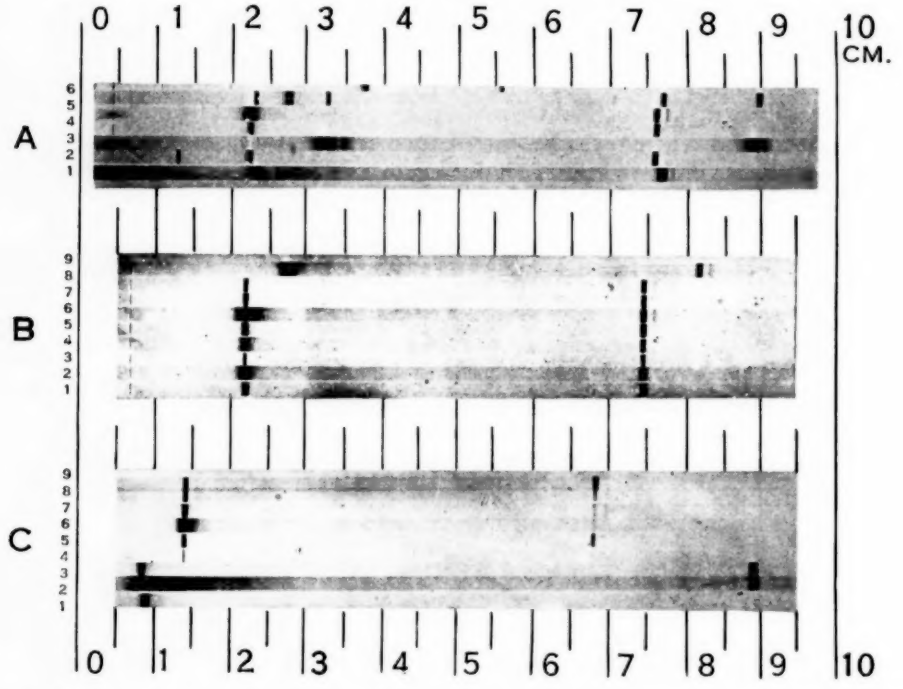

Fig. 1. Mass-spectra of hydrogen and helium ions. The descriptions of the spectra are given below in condensed form. The three samples of hydrogen used are designated: OH, for ordinary commercial tank hydrogen; BH, for Sample III Bleakney hydrogen; UH, for Urey-Brickwedde hydrogen. Spectra A June 10, Spectra B June 11, Spectra C June 14, 1932. Spectra are numbered in order as they were taken. T=exposure time in minutes. Description of ion is followed by number to nearest mm referring to attached cm scale as aid in locating specific lines. Lines which may not be or cannot be reproduced in half-tone are designated weak (w), or very weak (vw). Sharp lines on the left are fiducial lines to mark the plate position.

A1, BH, T63, H_3^1 2.3, He 7.7, $H_2^1H^2$ 7.8:
A2, BH, T .16 H_2^1 1.3; T 15, H_3^1 2.2, He 7.6, $H_2^1H^2$ 7.7 w:
A_3, UH, H_3^1 3.5 premature exposure before velocity selector potential and discharge potential were set, $T60$ H_3^1 3.2, He 8.9, $H_2^1H^2$ 9.0:
A4, UH, T 16H_3^1 2.3, He 7.6, $H_2^1H^2$ 7.7 vw taken with 60 sec.$^{-1}$ pulsating current, one transformer disconnected:
A5, UH, T 17.5, H_3^1 2.2, He 7.6, $H_2^1H^2$ 7.7:
A6, UH, three separate spectra, No. 1 $T5$, H_3^1 2.3, He 7.7, $H_2^1H^2$ 7.8 w:
No. 2 $T12.5$, He 2.8, $H_2^1H^2$ 2.9 w, HeH 7.1:
No. 3 $T4$, H_3^1 3.3, He 9, $H_2^1H^2$ not reproducible on print.

B1, OH, $T16$, H_3^1 2.2, He 7.5:
B2, OH, $T30$, H_3^1 2.2, He 7.5:
B3, OH, $T3$, H_3^1 2.2, He 7.5:
B4, BH, $T15$, H_3^1 2.2, He 7.5, $H_2^1H^2$ 7.6 vw:
B5, BH, $T30$, H_3^1 2.2, He 7.5, $H_2^1H^2$ 7.6 w:
B6, UH, $T30$, H_3^1 2.2, He 7.5, $H_2^1H^2$ 7.6:
B7, UH, $T15$, H_3^1 2.2, He 7.5, $H_2^1H^2$ 7.6:
B8, UH, $T4$, H_3^1 2.2, He 7.5, $H_2^1H^2$ 7.6:
B9, UH, $T15$, H_3^1 2.7, He 8.15, $H_2^1H^2$ 8.3:

C1, UH, $T5$, H_2^1 .9, H_3^1 9 w, Hg present:
C2, UH, $T30$, H_2^1 .8, H_3^1 8.9:
C3, UH, $T1$, H_2^1 .8, H_3^1 8.9:
Pressure in discharge changed.
C4, UH, $T1$, H_3^1 1.4, He 6.8 w:
C5, UH, $T15$, H_3^1 1.4, He 6.8, $H_2^1H^2$ 6.9 vw:
C6, UH, $T30$, H_3^1 1.4, He 6.8, $H_2^1H^2$ vvw:
Discharge voltage too low.
C7, UH, $T15$, H_3^1 1.4, He 6.8, $H_2^1H^2$ 7:
H^2 content increased by separation by diffusions.
C8, OH, $T15$, H_3^1 1.4, He 6.8, $H_2^1H^2$ 7 vw:
C9, OH, $T33$, H_3^1 1.4, He 6.8, $H_2^1H^2$ 7 vw.

by the method of differential diffusion. A dose of hydrogen was admitted and the excess gas pumped out through the slit while the discharge was running. When the gas pressure had been reduced to the right value for an exposure the process of circulation was started. Small but positive and useful increased concentrations of H^2 were obtained in this way.

Fig. 1 is a reproduction of contact prints of the spectra of hydrogen. A small amount of helium was added to the hydrogen to provide a reference mass.

Identification of $H_2{}^1H^2$ Ion

A line adjacent to and on the heavier mass side of He^+ might be due to $H_4{}^1$, $H_2{}^2$, or $H_2{}^1H^2$ ions. However, the following considerations demonstrate that the trace actually observed at that position on the plate could only be produced by $H_2{}^1H^2$ ions.

From Aston's data,[12] the mass of He is taken as 4.00216 ± 0.00013, of H^1 as 1.00778 ± 0.00005,[13] and of the electron as 0.000547 mass units, all referred to $O^{16} = 16$. The measurements of the separation of He^+ and the adjacent heavier ion gave 0.02691 ± 0.00006 mass units, as will be described later. This value added to the mass of the helium ion results in a mass of 4.02852 ± 0.00015 for the line adjacent to $He^+ \cdot H_4{}^{1+}$ is ruled out as a possibility since its mass, 4.03057 ± 0.00010 is quite outside of the limit of error of the measurements.

$H_4{}^{1+}$ is also ruled out, because no lines adjacent to helium appeared when ordinary commercial hydrogen was used in the discharge tube. Spectra 1, 2 and 3B, Fig. 1 were taken with tank hydrogen in the spectrograph discharge tube and no lines appeared near the helium traces. The discharge tube was then evacuated and fractionated enriched hydrogen was admitted which produced lines corresponding to a mass of 4.02852 units on the immediately succeeding spectra 4, 5, 6, 7, 8, 9B. The lines are weak for spectra 4 and 5B as the electrodes and walls of the tube were still contaminated with ordinary hydrogen which reduced the concentration of H^2 in the first dose of fractionated hydrogen. The objection might be raised that the possible presence of mercury in the tube for the first few spectra so inhibited the appearance of a line at 4.0285 that such a line would have been absent in any case regardless of the source of the hydrogen. In order to disprove any such contention spectra 7, 8 and 9C were taken. Spectra 8 and 9C were photographed using commercial hydrogen in the discharge tube *after* successful runs had been made in which $H_2{}^1H^{2+}$ appeared. Faint lines did appear, but as may be seen in Fig. 1, they are weaker on 8C, a 15 minute exposure, and on 9C, a 33 minute exposure, than the $H_2{}^1H^2$ lines on spectrum 7C (15 minutes exposure). All three exposures were taken under conditions as nearly identical as possible. The faint traces of $H_2{}^1H^2$ on 8 and 9C were present owing to the practical impossibility of washing out the tube and cleaning the electrodes entirely free from the gas used in earlier exposures taken immediately before 8C and 9C. As the

[12] F. W. Aston, Proc. Roy. Soc. **115**, 502 (1927).

[13] All succeeding calculations are made on the basis that Aston's limits of error are three times the probable error of his measurements.

line at 4.0285 only appeared in abundance when fractionated hydrogen was used, it was concluded that the ions responsible for that line contained H^2 and might be $H_2{}^1H^2$ or $H_2{}^2$ but could not be $H_4{}^1$ ions.

$H_2{}^{2+}$ is eliminated as a possibility when the relative abundance of $H_2{}^{2+}$ and $H_2{}^1H^{2+}$ is considered. From Bleakney's measurements the ratio $H^1H^{2+}/H_2{}^{1+}$ is approximately 0.002. The atomic ratio of H^2/H^1 is 0.001 and the ratio $H_2{}^{2+}/H_2{}^{1+}$ is 10^{-6}. The suggested mode of formation of triatomic hydrogen is

$$H_2{}^+ + H_2 \rightarrow H_3{}^+ + H.$$

The production of $H_2{}^1H_2{}^{2+}$ is given by

$$H_2{}^{1+} + H^1H^2 \rightarrow H_2{}^1H^{2+} + H^1$$
$$H^1H^{2+} + H_2{}^1 \rightarrow H_2{}^1H^{2+} + H^1$$

and for each reaction of this type, assuming that H^1 and H^2 behave similarly, the probability is that three out of every four triatomic molecules will contain H^2. If these reactions proceed in proportion to the product of the partial pressures of the constituents, the ratio $H_2{}^{2+}/H_2{}^1H^{2+}$ can be calculated. In the discharge tube the partial pressures for different molecules and ions are respectively: for $H_2{}^1$, p; for $H_2{}^{1+}$, ap; for H^1H^2, 0.002 p; and for H^1H^{2+}, 0.002 ap, where a is proportional to the amount of ionization extant. The amount of $H_2{}^1H^{2+}$ is $2\times3/4\times0.002\ ap$ and the abundance of $H_3{}^{1+}$ is ap. The ratio of $H_2{}^{2+}/H_2{}^1H^{2+}$ is equal to

$$H_2{}^{2+}/H_2{}^{1+} \times H_2{}^{1+}/H_3{}^{1+} \times H_3{}^{1+}/H_2{}^1H^{2+}$$

wherein all ratios are known except $H_2{}^{1+}/H_3{}^{1+}$ which is a function of the conditions existing in the discharge tube. The value of $H_2{}^{1+}/H_3{}^{1+}$ must be obtained experimentally. From Fig. 1, spectra 2, 3 and 4C, the ratio $H_2{}^{1+}/H_3{}^{1+}$ was estimated at from 1 to 20 under varying conditions in the discharge tube. If the measured values of this ratio are substituted, the ratio of abundance of $H_2{}^{2+}/H_2{}^1H^{2+}$ is in the range 0.67×10^{-2} to 0.33×10^{-3}. The low abundance of $H_2{}^{2+}$ precludes its appearance on the mass-spectra and the line of mass 4.02852 must be attributed to $H_2{}^1H^{2+}$.

Exactly the same relative abundance of $H_2{}^{2+}/H_2{}^1H^{2+}$ is obtained if the calculations are made without regard to the process of formation of triatomic hydrogen, on the basis of unweighted probability considerations alone.

Dispersion Measurements

The separation of $H_3{}^{1+}$ and He^+ was measured by a comparator to secure the dispersion measurements for these spectra. The presence of H^1H^{2+} can only introduce a negligible correction to the mass scale measurements. If H^1H^{2+} were present to an abundance equal to that of $H_3{}^{1+}$ then the dispersion figure would be in error by one part in 1100, equivalent to 0.00003 mass units in the value for the mass of H^2. This possible systematic error is only one half of the probable error in the measurement of the isotopic weight of H^2. As the ratio of abundance of $H^1H^{2+}/H_3{}^{1+}$ could not be greater than 0.002×20 or

1/25, the effect of H^1H^2 ions was negligible and no correction to the dispersion measurements is necessary.

Method of Measurement of He^+ $H_2^1H^{2+}$ Separation

The faintness of the $H_2^1H^{2+}$ lines in most cases prevented direct measurements by a comparator. The separations of the $H_2^1H^{2+}$ and He^+ lines on different spectra were measured by running the plates through a Goos-Koch microphotometer at a ratio of plate distance to record distance of approximately 1 to 40. For the first report[3] of this work the densitometer records of 14 spectra had been measured and reduced to plate distances by a subsequent determination of the ratio of densitometer travel to plate travel. The microphotometer does not maintain the same multiplication ratio throughout its travel so that for this report, twelve spectra were remeasured with a glass reticle, (1/20 mm divisions), directly superimposed on the spectrum plates. The reticle was compared with one ruled on the Swarthmore College Observatory comparator and also measured directly on a Gaertner comparator. Two of the spectra measured for the first report of this work could not be measured by this method. The densitometer records were coated with a frosting coating and smooth curves were drawn in by pencil. Fig. 2 is a reproduction of some of the records of spectra used in the measurement of the mass of

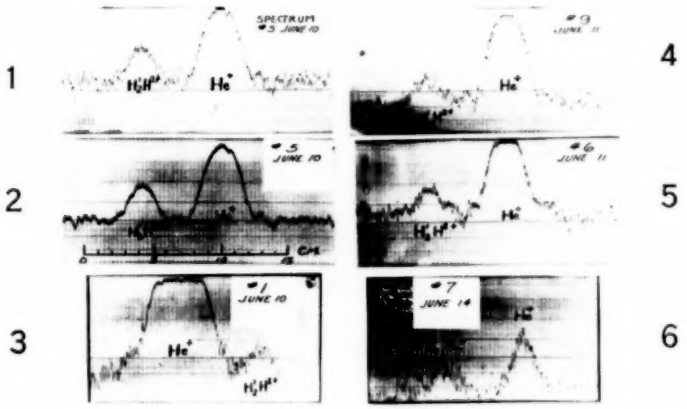

Fig. 2. Densitometer records of several $He^+ - (H_2^1H^2)^+$ doublets. Scale under record No. 2. Ratio of densitometer record distance to spectrum plate distance approximately 40 to 1. Micrometer slit 0.002 cm wide.

$H_2^1H^{2+}$. These records, taken without the superposition of the reticle, illustrate the remarkable symmetry of the ion traces.[14] Record No. 2 is of the

[14] The symmetry of the spectral lines is a direct consequence of the design of the mass-spectrograph. *Measurements of the separation of lines can be made referred to the centers of traces of unequal density,* an advantage which can hardly be overestimated in cases in which it is impractical or impossible to obtain traces of equal density. The symmetry of the traces is a result of the fact that *the ion beams are not brought to a focus at the surface of the recording plate. Any focussing action takes place in the circular path of the ions* 90° *from the ion source,* or last slit of the velocity selector in the mass-spectrograph. The velocity selector introduces an essentially

same spectrum as No. 1 but it was made with a different adjustment of the densitometer to minimize the effect of the grain of the plate.

The separation of the traces was measured by superposition of the densitometer records on accurate millimeter cross-section paper and by direct scale measurement of the centers of the peaks. The probable error of a single observation, ± 0.00024 mass units, corresponds to an error of about ± 0.5 mm in a distance of 43 to 60 mm on the densitometer records of different spectra.

Results

The results and their weight values for the mass difference between He^+ and $H_2{}^1H^{2+}$ are given in Table I.

Table I.

Fig. 1 spectrum	1A	2A	3A	4A	5A	6A
Mass difference	0.02749	0.02702	0.02688	0.02721	0.02688	0.02668
Weight	1	2	1	1	3	1
Fig. 1 spectrum	5B	6B	7B	8B	9B	7C
Mass difference	0.02627	0.02657	0.02742	0.02627	0.02714	0.02703
Weight	1	3	2	1	1	2

The averaged difference is 0.02691 ± 0.00006. The probable error is a composite value of a probable error of one part in one thousand in measuring the reticle and the probable error of the above mass difference *per se*.

The mass of neutral H^2 is $M_{He} + 0.02691 - M_{H_2{}^1} = 2.01351 \pm 0.00006$ when referred directly to Aston's value for helium. The masses of He^+ and $H_2{}^{1+}$ were compared directly by Aston with a probable error of only ± 0.000008 mass units in the determination of the mass of H^1 in terms of helium.[15]

The absolute value of H^2 is 2.01351 ± 0.00018 mass units referred to $O^{16} = 16$ and calculated on the basis that Aston's limits of error are equal to three times the probable error of his measurements. The equivalent packing fraction of H^2 is 67.5 parts in 10,000.

parallel beam of ions into the uniform magnetic field, or camera section of the spectrograph, so that the ions converge at 90°, then diverge, and at 180° from the source are again traveling in a parallel beam where the beam is normally incident on the surface of the recording plate. Spectrographs which deal with divergent nonparallel beams of ions bring the beams to a focus at the recording plate. A sharp edge (W. A. Wooster, Proc. Roy. Soc. **114,** 729 (1927)), or high density of ions at one position results, but the position of the edge of a trace shifts with changes in density and the separation of two adjacent traces of different density cannot be measured accurately (F. W. Aston, Proc. Roy. Soc. **115,** 496 (1927)). A complete discussion will appear in the Journal of the Franklin Institute.

[15] Aston (Proc. Roy. Soc. **115,** 502 (1927) gives three measured values for the difference in the packing fractions of helium and hydrogen, 73.7, 73.6 and 73.9. The correction for the mass of the electron gives a value of 72.4 for the excess of the packing fraction of hydrogen over that of helium. Ordinary error theory, of course, cannot be applied for the calculation of the probable error of only three measurements, but the theory of errors for small samples (W. A. Shewhart, Bell System Tech. J. **5,** 308 (1926)) may be applied and the error in Aston's measurements was calculated on that basis.

Discussion

Nuclear structure of H^2

The energy of binding of the H^2 nucleus corresponds to 0.00205 mass units or approximately 2×10^6 electron-volts if the nucleus is composed of two protons and one electron. It is interesting to speculate that if the H^2 nucleus is composed of one proton and one Chadwick neutron,[16] of mass 1.0067, then the binding energy would be 9.7×10^5 electron-volts. The energy of binding of the neutron itself has been given as 1 to 2×10^6 electron-volts. When more concentrated samples of H^2 are available, it may be possible to distinguish between the two suggested structures of the H^2 nucleus.

The possibility of H^2 as a nuclear structural unit

The binding energy of H^2 is small compared to the 35×10^6 electron-volts accorded helium nuclei. Grace[1] has suggested that the H^2 nucleus may be a constituent of other nuclei and suggests its inclusion in Li^6 and B^{10}. On this basis the binding energy of a Li^6 nucleus, composed of one H^2 nucleus and one helium nucleus, is 3.7×10^6 electron-volts. The binding energy of two helium nuclei and one H^2 nucleus combined as a B^{10} nucleus is 4.3×10^6 electron-volts. Such structures appear possible but the presence of H^2 in heavier nuclei, above mass 22, seems doubtful. While there is good evidence from various sources that α-particles retain their identity inside of nuclei, the small energy of binding of H^2 may not be sufficient to maintain the structure of that entity when it is subjected to the fields and perturbing forces of other particles in heavy complex nuclei.

Feather[17] has suggested the process

$$N^{14} + n^1 \rightarrow C^{12} + H^2 + n^1$$

for noncapture disintegration of nitrogen by neutron impact. When the known masses of the constituents are substituted the result is that at least 9×10^6 electron-volts energy must be supplied by the impacting neutron in order that this disintegration may proceed. The maximum energy of neutrons resulting from the disintegration of Be^9 is 5.7×10^6 electron-volts, entirely insufficient to promote the suggested noncapture disintegration of nitrogen. Feather decided on different grounds that H^2 does not result as a disintegration product of N^{14} but left the possibility open. Until positive evidence is obtained of the inclusion of H^2 in nuclei it is best not to complicate further the structure of nuclei by the addition of H^2 as a possible component, since what evidence is available militates against the addition of this unit.

The author is particularly indebted to Dr. Brickwedde who made this investigation possible by his preparation of the samples of enriched hydrogen at the U. S. Bureau of Standards, to Professor Urey and Dr. Murphy of Columbia University who placed a tested sample at the disposal of the author, to Br. Bramley and Dr. Bleakney for their interest and helpful discus-

[16] J. Chadwick, Proc. Roy. Soc. **136,** 270 (1932).
[17] N. Feather, Proc. Roy. Soc. **136,** 721, 726 (1932).

sions, and to Professor John A. Miller and the members of the Swarthmore College Observatory for their generous permission to use their measuring instruments.

Note added in proof: It has been the author's privilege to see the manuscript of a paper on the infrared spectrum of H^2Cl by J. D. Hardy, E. F. Barker, and D. M. Dennison. They have observed and measured the fundamental absorption bands due to H^2Cl^{35} and H^2Cl^{37} which lie in the neighborhood of 4.8μ. The value obtained for the mass of H^2 is 2.01367 ± 0.00010 if H^1 is 1.00778 as given by Aston. The details will be published shortly.

Professor R. T. Birge has pointed out to the writer that Aston's values for the mass of H^1 and He are probably too low. If the chemical value for the mass of H^1 is correct (R. T. Birge, Phys. Rev. Supplement 1, 1 (1929)), then the mass of H^1 is 1.00796 on the $O^{16}=16$ scale and Aston's value is too low by 1.8×10^{-4} units. The calculation of the mass of H^1 is made on the basis that the abundance of H^2 is 1 in 30,000 (W. Bleakney, Phys. Rev. **41,** 32 (1932)) and that Mecke and Childs' value for the relative abundance of the oxygen isotopes is correct (Zeits. f. Physik **68,** 362 (1931)).

If $H^1=1.00796$, then from the measurements of Hardy, Barker, and Dennison, the mass of $H^2=2.01403\pm0.00010$. The measurement of the mass of H^2 on the mass-spectrograph involves a knowledge of the mass of H^1 and of He also. Aston measured the ratio H/He and He/O. If the error 1.8×10^{-4} in H^1 is divided equally between H^1 and He then the mass of $H^1=1.00796$ and $He=4.00252$. On this basis my measurements give $H^2=2.01351\pm0.00018$ referred to O^{16}, a result identical with the value obtained before. The agreement between the band spectrum and mass-spectrograph values for the mass of H^2, calculated on this new basis, can no longer be considered satisfactory.

Ionization of Helium, Neon and Argon under Impact of their own Atoms and Positive Ions[1]

By CHARLES J. BRASEFIELD
Sloane Physics Laboratory, Yale University

(Received June 30, 1932)

The number of electrons liberated from neutral rare gas atoms under impact of their own atoms and positive ions was measured as a function of the kinetic energy of the impinging particles. When the impinging beam is composed mostly of neutral atoms, it is found that helium is ionized at about 60 equivalent volts, neon at about 50 volts and argon at about 40 volts. If the impinging beam is composed of atoms and positive ions in about equal proportions, additional ionization is found to set in in argon at around 330 volts. No ionization by positive ions was observed in either helium or neon up to 500 volts. Curves are shown which indicate the efficiency of ionization of the rare gases under impacts of their own atoms and positive ions.

INTRODUCTION

IONIZATION by positive ions has been considered one of the processes necessary for the maintenance of a gaseous discharge. Earlier attempts made to detect this effect directly were inconclusive due to the difficulty of distinguishing electrons produced by ionization of gas atoms from secondary electrons which are emitted from metal parts under impact of positive ions.[2] However, the experiments of Sutton, Beeck and Mouzon[3,4] indicate quite conclusively that the rare gases are ionized under impact of the alkali positive ions, although the process is inefficient compared with ionization under electron impact. Beeck and Mouzon[5] have found definite values of the minimum kinetic energy which an alkali ion must have in order to ionize a rare gas atom. More recently Wolf[6] has reported that argon is ionized slightly by its own positive ions in the neighborhood of 300 equivalent volts. Still more recently, Beeck[7] has reported preliminary experiments on the ionization of argon and neon by slow argon atoms.

Attempts to find a theoretical solution of the problem have been made, among others, by Franck,[8] Joos and Kulenkampff,[9] and Zwicky.[10] About all

[1] This paper was presented before the American Physical Society at the New Haven meeting, June 23, 1932. The abstract printed in the program of this meeting should be disregarded.

[2] As a matter of fact, the skeptical may still claim with some justification that, even in the most recent experiments, the electrons are not products of ionization of gas atoms but are secondary electrons from the metal parts which are inherent in any experimental apparatus.

[3] R. M. Sutton and J. C. Mouzon, Phys. Rev. **37**, 379 (1931).

[4] O. Beeck and J. C. Mouzon, Ann. d. Physik **11**, 737 (1931).

[5] O. Beeck and J. C. Mouzon, Ann. d. Physik **11**, 858 (1931).

[6] F. Wolf, Zeits. f. Physik **74**, 575 (1932).

[7] O. Beeck, Proc. Nat. Acad. Sci. **18**, 311 (1932).

[8] J. Franck, Zeits. f. Physik **25**, 312 (1924).

[9] G. Joos and H. Kulenkampff, Phys. Zeits. **25**, 257 (1924).

[10] F. Zwicky, Proc. Nat. Acad. Sci. **18**, 314 (1932).

that can be said at present is that for central impacts between uncharged particles of the same mass, approximately one-half the kinetic energy of the impinging particle is available for ionization of the particle struck. Thus helium, neon and argon should be ionized under impacts of their own neutral atoms if the atoms have kinetic energy of approximately 49, 43 and 31 equivalent volts, respectively. Ionization of the rare gases under impact of their own positive ions might be expected at somewhat higher energies, for in this case the ejected electron escapes while in the field of force of two positive ions.

Apparatus and Procedure

The apparatus used in this investigation is a modification of that used by Sutton and is shown drawn to scale in Fig. 1. The experimental tube was divided into two parts by a glass partition which separated the discharge chamber from the chamber in which ionization of the gas by the impinging

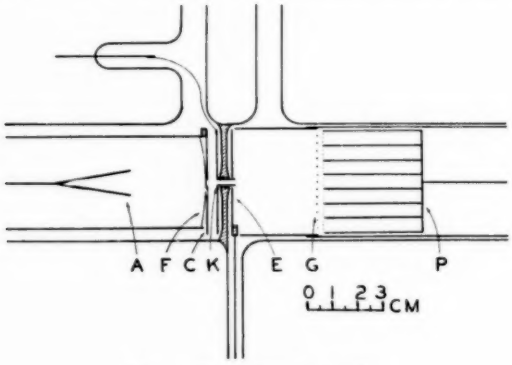

Fig. 1. Experimental tube.

particles was detected. A discharge was produced between the oxide-coated filament[11] F and the anode A. Positive ions of the gas are produced by electron impact and drift toward the filament. Since the voltage across the discharge, V_d, is concentrated at the filament, most of the positive ions that pass through the 2 mm hole in the virtual cathode C will have an energy of V_d equivalent volts. Between C and K they are further accelerated by an applied potential V_a so that most of the ions enter the canal K with an energy of V_d+V_a equivalent volts. The canal is 7 mm long and 2 mm in diameter. Emerging from the canal, the particles in the beam (now a mixture of positive ions and neutral atoms) enter the ionization chamber where they are free to collide with the atoms of the gas. The ionization chamber is 3.3 cm long. Its walls are of sheet nickel and the far end is closed by a large mesh fine wire grid G, both of which are at the same potential as the plate K. At the near end of the ionization chamber is the electrode E to which a positive potential is applied to collect any electrons resulting from the impacts. In general 15 volts were found sufficient to saturate the electron current to E. The positive ions in the beam continue through the grid G and are collected by P. The

[11] Kindly supplied by Dr. M. J. Kelly of the Bell Telephone Laboratories.

face of P is covered by a wire grid to give a more uniform field between G and P. The distance from G to P is about 2 mm and P is kept at a positive potential with respect to G in order to prevent the escape of any secondary electrons resulting from the impact of positive ions upon P. We might expect secondary electrons with velocities as high as 16 volts in helium, 13 volts in neon and 7 volts in argon.[12] However, it was found that only a few volts were sufficient to stop most of the secondary electrons emitted from P, but to be on the safe side the potential between G and P was kept at 15 volts for helium and 12 volts for neon and argon. The metal parts of the tube were made of nickel and were outgassed by an induction furnace. The rare gases were obtained spectroscopically pure and were used without further purification. The tube was completely evacuated and a fresh supply of gas admitted before each run.

Keeping V_d and I_d (the discharge current) constant, the accelerating potential V_a was varied and readings were taken of the electron current to the plate E and the positive ion current collected by P. The same galvanometer was used to measure each of these currents. It had a sensitivity of 2324 megohms.

It has been assumed that the moving particles enter the ionization chamber with a velocity of V_d+V_a equivalent volts. To check this, measurements were made of the positive ion current collected by P as the retarding potential between G and P was increased, for given values of V_d and V_a. It was found that the fastest ions reaching P did have a velocity of V_d+V_a equivalent volts.

We are quite certain that all the particles leaving the neighborhood of the filament are positive ions. Knowing the distance the ions go from the filament until they reach the ionization chamber (1.1 cm) and also knowing the mean free path of the ions for neutralization, we can compute the fraction of ions and of atoms in the impinging beam as it enters the ionization chamber. The most reliable value of the mean free path for neutralization of A^+ in argon, obtained from the work of Wolf,[6] is 1.6 cm at 0.01 mm pressure. For the mean free paths for neutralization of Ne^+ in neon and He^+ in helium we must make use of the more qualitative measurements of Kallman and Rosen[13] which yield values of 2.5 cm at 0.01 mm pressure in each case.

Results

If the discharge is operated at such a pressure that 95 percent of the particles entering the ionization chamber are neutral atoms, curves such as are shown in Fig. 2 are obtained. Here the electron current collected by the electrode E, I_e, is plotted against the energy of the impinging atoms in (V_d+V_a) equivalent volts. It will be noticed that in all cases the initial electron current is not zero but has a definite constant value. It is thought that this is due to secondary electrons ejected from the canal K by the impinging positive ions, and of course it is impossible to eliminate such secondaries.

[12] See for example Rev. Mod. Phys. **2**, 180 (1930) and references given there.
[13] H. Kallman and B. Rosen, Zeits. f. Physik **61**, 61 (1930).

When the impinging atoms have a certain minimum energy, ionization is observed to set in. This occurs in helium at about 60 volts, in neon at about 50 volts and in argon at about 40 volts. These values are in each case approximately 10 volts higher than we would expect theoretically. Further ionization also appears to take place in neon and argon at about 110 and 75 volts, respectively. Two possible explanations of these higher ionization potentials are suggested. They may represent the minimum energies which an atom must have in order to ionize successively two times. Or they may represent the minimum energy necessary to ionize one of the colliding particles and excite the other—a process which has been suggested in a recent paper by Weizel and Beeck.[14]

In order to increase the proportion of positive ions in the impinging beam, the tube was now operated at as low a pressure as possible. The minimum pressure was determined in the case of helium and neon by the lowest pressure

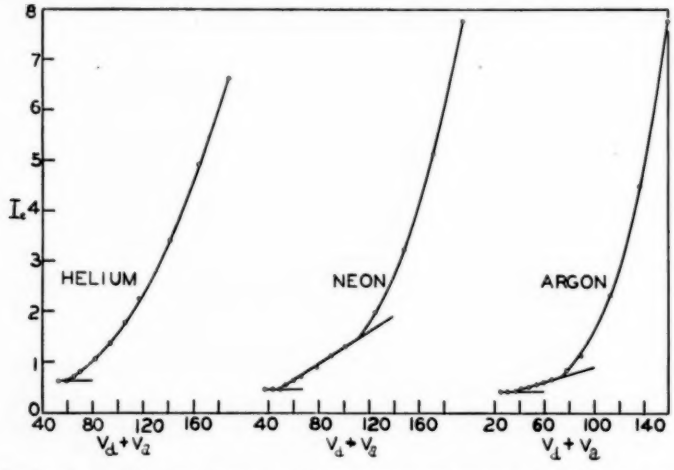

Fig. 2. Ionization of helium, neon and argon under impact of their own atoms. Helium: pressure = 0.07 mm, $V_d = 47$ v., $I_d = 20$ m.a.; neon: pressure = 0.07 mm, $V_d = 31$ v., $I_d = 20$ m.a.; argon: pressure = 0.036 mm, $V_d = 19$ v., $I_d = 40$ m.a.

at which a discharge could be maintained; in argon by the lowest pressure at which there was an appreciable electron current collected by E. The results obtained under these conditions are shown in Fig. 3, where again the electron current collected by the electrode E, I_e, is plotted against the energy of the impinging particles in $(V_d + V_a)$ equivalent volts. The impinging beam in argon on entering the ionization chamber is composed of 60 percent A^+ and 40 percent A° (neutral atoms); in neon 55 percent Ne^+ and 45 percent Ne°; and in helium 30 percent He^+ and 70 percent He°. As at the higher pressures, we again observe in neon and argon an increase in the ionization current (here at about 120 and 85 volts) due to successive impacts or to simultaneous ionization and excitation. No further abrupt increases in the ionization current are observed except in argon where further ionization seems to set in at about 330 volts. This is ascribed to ionization by argon ions and confirms

[14] W. Weizel and O. Beeck, Zeits. f. Physik **76**, 250 (1932).

Wolf's observation[6] that argon is ionized slightly by its own positive ions around 300 volts. If helium and neon are ionized by their own positive ions, the process must either be inefficient compared with the ionization of argon by its own positive ions, or it must take place at energies greater than 500 equivalent volts.

From the data used for Fig. 3 it is also possible to calculate roughly the efficiency of ionization of the rare gases under impact of their own atoms and positive ions. Knowing the number of positive ions collected by P,[15] the distance they have gone since entering the ionization chamber (3.5 cm) and also the mean free path of the ions, it is possible to calculate the number of initial positive ions entering the ionization chamber. Also, since the composition of

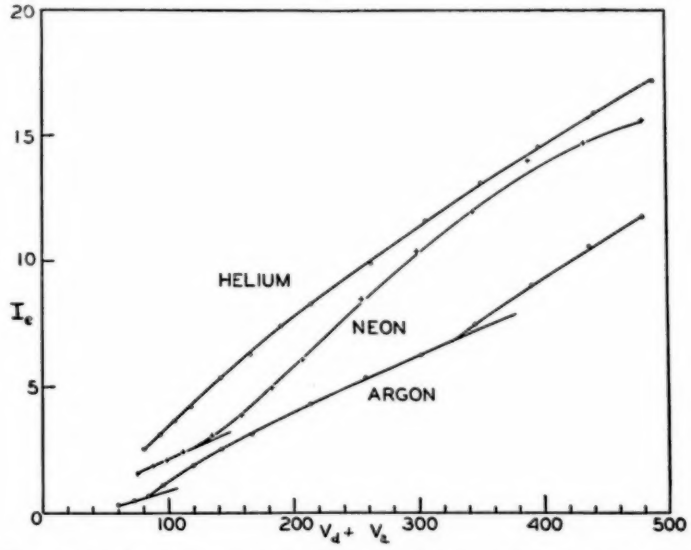

Fig. 3. Ionization of helium, neon and argon under impact of their own atoms and positive ions. Helium: pressure = 0.028 mm, V_d = 70 v., I_d = 10 m.a.; neon: pressure = 0.013 mm, V_d = 65 v., I_d = 10 m.a.; argon: pressure = 0.0072 mm, V_d = 26 v., I_d = 20 m.a.

the beam on entering the ionization chamber is known, it is possible to calculate the number of atoms entering the ionization chamber. If now the ratio of the number of electrons produced (corrected for secondary electrons) to the number of initial atoms (or positive ions as the case may be) is divided by the gas pressure in mm and also by the length of the path of the particles in the ionization chamber (3.3 cm) we get N, the number of electrons produced per initial atom (ion) per cm path at 1 mm pressure. The variation of N with the kinetic energy of the impinging particles in $(V_d + V_a)$ equivalent volts is shown for helium, neon and argon in Fig. 4. These curves should only be con-

[15] If any of the ions produced by collisions in the ionization chamber had succeeded in reaching P, we would expect to observe a marked increase in the positive ion current collected by P after ionization set in. No such increase was detected except when argon was ionized by A^+. In calculating the efficiency of ionization of argon by A^+, an attempt was made to correct for these additional positive ions by neglecting the increase in the positive ion current after ionization set in.

sidered as accurate as the measurements of the mean free path of the ions; in other words, only qualitatively correct.

If these curves are compared with similar curves of Sutton[3] and Beeck[16] for the efficiency of ionization of the rare gases under impact of the alkali positive ions, it can be seen that the rare gases are considerably more efficiently ionized

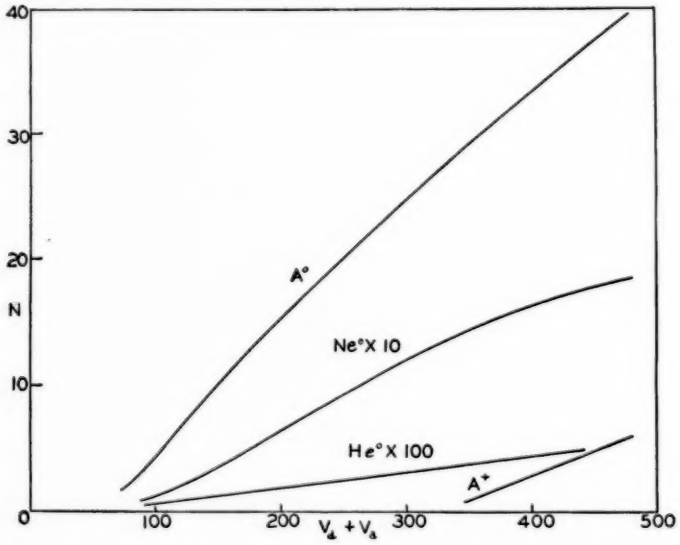

Fig. 4. Efficiency of ionization of helium, neon and argon under impacts of their own atoms (He^0, Ne^0, A^0) and positive ions (A^+). Ne^0 curve magnified 10 times; He^0 curve magnified 100 times.

by their own atoms (but less efficiently ionized by their own positive ions) than by alkali ions of approximately the same mass as the rare gas atom. As a matter of fact, in the case of argon and neon, the efficiency of ionization by their own atoms is comparable with the efficiency of ionization under electron impact.[17]

[16] O. Beeck, Ann. d. Physik **6**, 1018 (1930).
[17] K. T. Compton and C. C. Van Voorhis, Phys. Rev. **27**, 729 (1926).

The Scattering of Slow Electrons. Part II

By EUGENE FEENBERG
Harvard University

(Received June 9, 1932)

The scattering equations derived in an earlier paper are here found by a variation method, which is closely related to the Fock-Slater method of determining single electron functions for complex atoms. The equations for scattering in helium and the other inert gases are treated in detail and put into a form suitable for numerical integration. For scattering in helium excellent agreement with experiment is found in the neighborhood of the resonance potential; at 10.75 volts the agreement is poor. This discrepancy at low potentials is undoubtedly to be accounted for by atomic distortion which is neglected in the scattering equation.

IN AN earlier paper[1] the writer discussed the problem of electron scattering by an N electron atomic system from the standpoint of the $N+1$ Schroedinger equation for the scattering system and the external electron. The discussion is here extended.

We treat a simplified problem obtained by representing the atom as an outer electron shell in the potential field $V(r)$ of the core. N is then the number of electrons in the outer shell. Let $u(1, \cdots, N)$ represent the normal state unperturbed atomic wave function and $v(1, \cdots, N, x_0)$ the atomic wave function perturbed in an unspecified manner by the field of the external electron at x_0, y_0, z_0. In particular v may be the unperturbed function u, independent of x_0, y_0, z_0, or a solution of the wave equation for the atomic system in the field of a unit negative charge fixed at the point x_0, y_0, z_0. We require of v that

$$\begin{gathered}\sum_{\text{spin}} \int \cdots \int v^*(1, \cdots, N, x_0) v(1, \cdots, N, x_0) d\tau \cdots d\tau_N = 1, \\ \sum_{\text{spin}} \int \cdots \int v^*(1, \cdots N, x_0) \nabla_0 v(1, \cdots, N, x_0) d\tau_1 \cdots d\tau_N = 0, \\ \lim_{r_0 \to \infty} v(1, \cdots, N, x_0) = u(1, \cdots, N).\end{gathered} \tag{1.1}$$

We write an approximate solution $\psi\ (0, 1, \cdots, N)$ of the $N+1$ electron problem, antisymmetric in the space-spin coordinates $0, 1, \cdots, N$, in the form

$$\psi(0, 1, \cdots, N) = \sum_j \pm P_j v(1, \cdots, N, x_0) f(0) s(0) \tag{1.2}$$

in which P_j is a permutation operator, $f(0)$ the scattering function, and $s(0)$ a spin function for the external electron. With W_1 the energy of the atomic system, W the kinetic energy of the external electron, and H the energy operator for the complete system,

[1] Feenberg, Phys. Rev. **40**, 40 (1932); referred to in text as S.S.E.

$$H = -\tfrac{1}{2}\sum_0^N \nabla_i^2 - \left(\sum_0^N V(i) - \sum_0^N{}' 1/r_{ij}\right), \tag{1.3}$$

we can briefly describe the method used in S.S.E.[1] to set up scattering equations as follows: Because ψ is only an approximation to the exact solution $(H-W-W_1)\psi$ does not vanish identically. We multiply $(H-W-W_1)\psi$ by the atomic wave function $v^*(1, \cdots, N, x_0)$ and the external electron spin function $s(0)$, integrate over space coordinates $1, 2, \cdots, N$ and sum over all spin coordinates and require that the resulting averaged value of $(H-W-W_1)\psi$ vanish identically. We find in this way an integral-differential equation for the scattering function f:

$$\sum_{\text{spin}} s(0) \int \cdots \int v^*(1, \cdots, N, x_0)(H - W - W_1)\psi d\tau_1 \cdots d\tau_N = 0. \tag{1.4}$$

(1.4) is simplified by introducing the differential equation satisfied by v and the conditions (1.1).

I show that the function f determined by (1.4) gives the integral

$$K(f) = \sum_{\text{spin}} \int \cdots \int \psi^*(H - W - W_1)\psi d\tau_0 d\tau_1 \cdots d\tau_N \tag{1.5}$$

an extreme value. Some preliminary remarks are desirable before stating the variation problem. For large values of r the scattering function reduces to a plane wave plus a scattered wave: $f \sim e^{-ikz} + (1/r)e^{ikr}F(x/r, y/r, z/r)$. Thus neither $\int \cdots \int \psi^* H \psi d\tau_0 \cdots d\tau_N$ nor $\int \cdots \int \psi^*(W+W_1)\psi d\tau_0 \cdots d\tau_N$ exist. However it is possible to define a manifold of functions $R(x)$, $S(x)$ such that $K(f)$ is finite if f is a solution of an equation of the form $(\nabla^2 + 2W + R)f = S$. Eq. (1.4) provides a particular determination of the functions R and S. The condition for the conservation of charge is expressed by

$$\iint_\infty (f^* \nabla f - f \nabla f^*) \cdot dS = 0, \ (S.S.E.,[1] \text{ section } 3), \tag{1.6}$$

which in turn implies that $K(f)$ is a real number. Finally

$$\begin{aligned} \delta K(f) &\equiv \sum_{\text{spin}} \int \cdots \int [\delta\psi^*(H - W - W_1)\psi + \psi^*(H - W - W_1)\delta\psi] d\tau_0 \cdots d\tau_N \\ &= \sum_{\text{spin}} \int \cdots \int [\delta\psi^*(H - W - W_1)\psi + \delta\psi(H - W - W_1)\psi^*] d\tau_0 \cdots d\tau_N \\ &\quad + C(N) \iint_\infty (f^* \nabla \delta f - \delta f \nabla f^*) \cdot dS. \end{aligned}$$

With this introduction we are prepared to state the variation problem: Given a scattering function f satisfying (1.6) and a manifold of comparison functions $f+\delta f$ such that;

(a) $$f + \delta f \sim e^{-ikz} + (1/r)e^{-ikr}(F(x/r, y/r, z/r) + \delta F)$$

for large values of r,

(b) $K(f+\delta f)$ exists,

(c) $$\iint_{\infty}(f^*\nabla\delta f-\delta f\nabla f^*)\cdot dS=0,$$

(d) $\delta K(f)=0$ for all comparison functions satisfying (a), (b), (c); to prove

(e) f a solution of (1.4).

The proof is simple. Subtracting from $\iint_{\infty}(f^*\nabla\delta f-\delta f\nabla f^*)\cdot dS$ its conjugate complex we find $\delta\iint_{\infty}(f^*\nabla f-f\nabla f^*)\cdot dS=0$; or, neglecting terms in $\delta F\delta F^*$, the comparison functions satisfy the condition for the conservation of charge. Because of the symmetry properties of ψ we may write

$$\delta K(f)=C(N)\sum_{\text{spin}}\int\cdots\int[v^*(1,\cdots,N,x_0)\delta f^*(0)s(0)(H-W-W_1)\psi + v(1,\cdots,N,x_0)\delta f(0)s(0)(H-W-W_1)\psi^*]d\tau_0 d\tau_1\cdots d\tau_N.$$

Then, seeing that the real and imaginary parts of δf are independently variable (except at infinity where they are connected by the relation(c)), (1.4) is an immediate consequence of (d).

It seems probable that (1.4) is the best scattering equation derivable from the assumption that the wave function has the form (1.2). The variation method of deriving (1.4) does not differ essentially from the Fock-Slater method of determining single electron functions for complex atoms. One point of difference may be noted: the atomic wave function, perturbed or unperturbed, is given; only the scattering function is varied.

Scattering by the Inert Gases

Using unperturbed atomic wave functions the solution is

$$\psi(0,1,\cdots,N)=u(1,\cdots,N)f(0)s(0)+u(2,\cdots,N,0)f(1)s(1)+\cdots+u(0,1,\cdots,N-1)f(N)s(N). \quad (1.7)$$

The discussion applies to any atom with an even number of electrons in the outer shell, but in general there are several solutions and a corresponding number of scattering functions. With

$$V_1(0,1,\cdots,N)=2\left(V(0)-\sum_1^N 1/r_{0j}\right),$$

$$U(0)=\sum_{\text{spin}}\int\cdots\int u^*(1,\cdots,N)V_1(0,1,\cdots,N)u(1,\cdots,N)d\tau_1\cdots d\tau_N,$$

$$V_2(0,1,\cdots,N)=V_1(0,1,\cdots,N)-U(0),$$

$$L(0,1,\cdots,N)=\nabla_0^2+2W+V_1(0,1,\cdots,N),$$

$$L(0)=\sum_{\text{spin}}\int\cdots\int u^*(1,\cdots,N)L(0,1,\cdots,N)u(1,\cdots,N)d\tau_1\cdots d\tau_N$$

$$=\nabla_0^2+2W+U(0)$$

we have

$$-2(H-W-W_1)\psi = u(1,\cdots,N)s(0)L(0,1,\cdots,N)f(0)$$
$$+u(2,\cdots,N,0)s(1)L(1,\cdots,N,0)f(1)$$
$$\vdots$$
$$+u(0,1,\cdots,N-1)s(N)L(N,0,1,\cdots,N-1)f(N)$$

and (1.4) becomes

$$L(0)f(0) = N\sum_{\text{spin}} s(0)s(1)\int\cdots\int u^*(1,\cdots,N)u(0,2,\cdots,N) \cdot L(1,2,\cdots,N,0)f(1)d\tau_1\cdots d\tau_N. \tag{1.8}$$

Using (1.8) and the differential equation satisfied by u it is not difficult to verify the relation (1.6). If we attempt to solve (1.8) by the method of successive approximation the obvious and most suitable first approximation f_0 is the solution of the equation $Lf_0=0$ subject to the scattering problem boundary conditions: f_0 everywhere finite and $f_0\sim e^{-ikz}+(1/r)e^{-ikr}F(z/r)$ for large values of r. With f_0 in the right hand member (1.8) reduces to

$$L(0)f(0) = N\sum_{\text{spin}} s(0)s(1)\int\cdots\int u^*(1,\cdots,N)u(0,2,\cdots,N) \cdot V_2(1,2,\cdots,N,0)f_0(1)d\tau_1\cdots d\tau_N. \tag{1.9}$$

Note that the potential function in the integrand is V_2 and not V_1. The right-hand member of (1.9) is conveniently described as an exchange integral. It contributes a term to the scattering amplitude which may be interpreted as resulting from interchange of atomic and external electrons. (1.9) is certainly valid when the exchange term is so small that f does not differ appreciably from f_0 inside the region of high charge density. But it is neither a final nor very useful equation. To make further progress toward an understanding of (1.8) we must replace the exact atomic wave function by an approximate solution constructed from single electron functions:

$$u(1,\cdots,N)\rightarrow(1/N!^{1/2})\,|\,u_n(m)s_n(m)\,|,\quad n,m=1,2,\cdots,N,$$

with $u_n=u_{n+N/2}$, $n\leqq N/2$, $u_1, u_2, \cdots u_{N/2}$ normalized and mutually orthogonal,

$$s_1=s_2=\cdots=s_{N/2}=s,\quad s_{N/2+1}=\cdots=s_N=s',$$

$$\sum_{\text{spin}} s(1)s'(1)=0,\quad \sum_{\text{spin}} s(1)s(1)=\sum_{\text{spin}} s'(1)s'(1)=1.$$

With a suitable choice of single electron functions $u_1,\cdots,u_{N/2}$ the error introduced by the substitution $u(1,\cdots,N)\rightarrow(1/N!^{1/2})\,|u_n(m)s_n(m)\,|$ is quite negligible. Arguments to support this statement will appear as the discussion develops.

HELIUM

$$u(1,2) \rightarrow (1/2^{1/2})u(1)u(2)(s(1)s'(2) - s(2)s'(1)),$$

$$U(0) = 2\int\cdots\int u(1)u(2)u(1)u(2)(2/r_0 - 1/r_{01} - 1/r_{02})d\tau_1 d\tau_2$$

$$= 4(1/r_0 - (1/r_0)) \text{ with } (1/r_0) = \iiint u(1)u(1)(1/r_{01})d\tau_1,$$

$$V_2(0,1,2) = 2(2(1/r_0) - 1/r_{01} - 1/r_{02}).$$

Eliminating the spin functions from (1.8) there remains

$$L(0)f(0) = u(0)\iiint u(1)[L(1) + 2((1/r_1) - 1/r_{01})]f(1)d\tau_1. \quad (2.1)$$

We write $f=\sum_0^\infty f_k$ with f_k defined by the system of equations

$$L(0)f_0(0) = 0,$$

$$L(0)f_{k+1}(0) = u(0)\iiint u(1)[L(1) + 2((1/r_1) - 1/r_{01})]f_k(1)d\tau_1.$$

We find then (S.S.E.,[1] section 2) that $\iiint uLf_k d\tau = 0$ and therefore $\iiint uLf\, d\tau = 0$. Thus the function f defined by the process of successive approximation outlined above is also a solution of the equation

$$L(0)f(0) = 2u(0)\iiint u(1)((1/r_1) - 1/r_{01})f(1)d\tau_1. \quad (2.2)$$

Now it is easily verified that (2.2) implies the relation $\iiint uLf d\tau = 0$. It is not true that every solution of (2.1) is a solution of (2.2). We shall see that for a particular choice of the one electron function u, (2.1) has an infinite number of distinct solutions, all satisfying the scattering problem boundary conditions and all yielding the *same scattering amplitude*. However the most practical procedure for accurately solving (2.1) is the method of successive approximation and this method leads directly to the orthogonality condition $\iiint uLf\, d\tau = 0$ and Eq. (2.2). The scattering amplitude is (S.S.E.,[1] section 2)

$$F(z/r) = (-1/4\pi)\int\cdots\int u(1,2)e^{ikr_0\cos(r_0,r)}[V_1(0,1,2)u(1,2)f(0)$$

$$- V_2(2,1,0)u(1,0)f(2)]d\tau_0 d\tau_1 d\tau_2$$

$$= (-1/4\pi)\iiint e^{ikr_0\cos(r_0,r)}[U(0)f(0) \quad (2.3)$$

$$- 2u(0)\iiint u(1)((1/r_1) - 1/r_{01})f(1)d\tau_1]d\tau_0.$$

Since f is not known (2.3) is useful only for the qualitative survey afforded

when f is replaced by a simple approximation and the integrals then evaluated.

We assume now that the single electron function u is determined by a Hartree[2] equation:

$$(\nabla^2 + 2(E + 2/r - (1/r)))u = 0.$$

By Green's theorem $\iiint uLf d\tau = \iiint fLu d\tau$; (2.1) assumes the form

$$L(0)f(0) = 2u(0)\iiint u(1)(W - E - 1/r_{01})f(1)d\tau_1. \tag{2.4}$$

Then

$$\iint_\infty (f^*\nabla f - f\nabla f^*)\cdot dS = \iiint (f^*Lf - fLf^*)d\tau$$

$$= 2\int\cdots\int u(0)u(1)(W - E - 1/r_{01})(f^*(0)f(1) - f(0)f^*(1))d\tau_0 d\tau_1 = 0,$$

a verification of (1.6). This is the first step in justifying the introduction of the approximate atomic wave function.

The Hartree equation may be written

$$(\nabla_0^2 + 2(W + 2/r_0 - 2(1/r_0)))u(0) = 2(W - E - (1/r_0))u(0)$$

$$= 2u(0)\iiint u(1)(W - E - 1/r_{01})u(1)d\tau_1.$$

We see that a solution of the Hartree equation is also a solution of (2.4). If f is a solution of (2.4) satisfying the scattering problem boundary conditions so also is $f+cu$ with c an arbitrary constant. With u determined by the Hartree equation, (2.1) has an infinite number of solutions and (2.2) presumably only one, but all satisfying the scattering problem boundary conditions and yielding the *same scattering amplitude*. (2.1) and (2.2) are thus equivalent physically, but not mathematically.

The freedom in the definition of f has this consequence: we are at liberty to impose practically arbitrary orthogonality conditions on f. Each such condition combined with (2.4) leads to a differential equation differing in form from (2.4), but having at least one solution in common with it. For example (2.2) is such an equation, imposing on its solutions the orthogonality condition $\iiint uLf d\tau = 0$, having a solution in common with (2.1) for unrestricted single electron function u and a solution in common with (2.4) if u is the Hartree function. We try the condition $\iiint uf d\tau = 0$; combined with (2.4) the equation

$$L(0)f(0) = -2u(0)\iiint u(1)(1/r_{01})f(1)d\tau_1 \tag{2.5}$$

results. We verify that a necessary consequence of (2.5) and the Hartree equa-

[2] Hartree, Proc. Cam. Phil. Soc., Jan. (1928).

tion for u is the orthogonality of u and f. For from (2.5) and the Hartree equation

$$\nabla_0 \cdot (u(0)\nabla_0 f(0) - f(0)\nabla_0 u(0)) + 2(W - E)u(0)f(0)$$
$$- 2(1/r_0)u(0)f(0) = -2u(0)u(0)\iiint u(1)(1/r_{01})f(1)d\tau_1.$$

Integrated this yields

$$2(W - E)\iiint uf d\tau - 2\iiint u(1/r)f d\tau = -2\iiint u(1/r)f d\tau$$

or $\iiint uf d\tau = 0$. For numerical integration by successive approximation (2.2) is far preferable to (2.5), in part because the derivation of (2.2) does not involve the assumption that u is a solution of the Hartree equation, but primarily because of the more rapid convergence brought about by the presence of the term $(1/r_1)$ in the exchange integral and because in (2.2) the orthogonality condition $\iiint uLf d\tau = 0$ is satisfied automatically by each successive approximation: thus $\iiint uLf_k d\tau = 0$.

There follows an argument that supplies an adequate justification of the substitution $u(1, 2) \rightarrow (1/2^{\frac{1}{2}})u(1)u(2)(s(1)s'(2) - s(2)s'(1))$ provided that the single electron function u is determined by the Hartree equation. Eq. (2.1) is derived by a method that proceeds as far as possible with the accurate atomic wave function before introducing an approximation. If now we begin with the approximate atomic wave function and evaluating (1.4) find an equation almost identical with (2.1) we must conclude that the substitution brings with it no serious error. Letting $u(1, 2)$ in (1.7) represent the approximate atomic wave function we have

$$\begin{aligned}
&-2(H - W - W_1)\psi \\
&= u(1,2)[\nabla_0^2 + 2(W + W_1 - 2E + 2/r_0 - 1/r_{01} - 1/r_{02} - 1/r_{12} \\
&\qquad + (1/r_1) + (1/r_2))]f(0)s(0) \\
&+ u(0,1)[\nabla_2^2 + 2(W + W_1 - 2E + 2/r_2 - 1/r_{01} - 1/r_{02} - 1/r_{12} \\
&\qquad + (1/r_0) + (1/r_1))]f(2)s(2) \\
&+ u(2,0)[\nabla_1^2 + 2(W + W_1 - 2E + 2/r_1 - 1/r_{01} - 1/r_{02} - 1/r_{12} \\
&\qquad + (1/r_2) + (1/r_0))]f(1)s(1)
\end{aligned}$$

Combined with (2.4) this yields

$$(L(0) + 2(W_1 - W_1'))f(0) \qquad (2.6)$$
$$= u(0)\iiint u(1)(L(1) + 2(W_1 - W_1') + 2(1/r_1 - 1/r_{01}))f(1)d\tau_1$$

in which W_1' is the value of the helium normal state energy given by the Hartree function: $W_1' = 2E - \int \cdots \int u(1)u(1)\ (1/r_{12})u(2)u(2)d\tau_1\ d\tau_2$ and $W_1' - W_1 = 0.8$ volts.[3] (2.1) with kinetic energy W is identical with (2.6) with

[3] Gaunt, Proc. Cam. Phil. Soc. **24**, 328 (1928).

kinetic energy $W+W_1'-W_1$. We may conclude that the use of the Hartree atomic wave function to simplify (1.8) is certainly permitted for kinetic energies greater than 2 or 3 volts. It must be emphasized that (2.6) is not an alternative scattering equation; it is a check on the validity of a simplifying assumption.

For the numerical integration of (2.1), f_k is written as a sum of Legendre polynomials in the scattering angle with coefficients depending only on the distance from the scattering center:

$$f(x, y, z) = \sum_0^\infty f_k(x, y, z) = \sum_0^\infty \sum_0^\infty f_{kn}(r) P_n(\cos\theta). \tag{2.7}$$

Then

$$(L(0) - n(n+1)/r_0^2) f_{0n}(0) = 0, \tag{2.8}$$

$$L(0) f_{k+1,0}(0) = 8\pi u(0) \int_0^\infty u(1)((1/r_1) - \gamma_0(0, 1)) f_{k0}(1) r_1^2 dr_1,$$

$$(L(0) - n(n+1)/r_0^2) f_{k+1,n}(0) = -8\pi/(2n+1) u(0) \int_0^\infty u(1)\gamma_n(0, 1) f_{kn}(1) r_1^2 dr_1, \quad n > 0,$$

$$\gamma_n(0, 1) = r_0^n/r_1^{n+1}, \quad r_0 \leqq r_1,$$
$$= r_1^n/r_0^{n+1}, \quad r_0 > r_1.$$

The convergence is quite rapid in both k and n.

Neon, Argon, Krypton, Xenon; $N=8$

As might be expected most of the results found for scattering in helium have their parallel here. The Fock[4] equations for determining single electron functions are related to the N electron scattering problem as the Hartree equation to the helium scattering problem. But in the helium problem the Fock equation reduces to Hartree's. Thus the parallel is very close. With spin functions eliminated from the several defining equations

$$U(0) = 2\left(V(0) - \sum_1^N (1/r_0)_n\right),$$

$$V_2(0, 1, \cdots, N) = 2\sum_1^N ((1/r_0)_n - 1/r_{0n}),$$

and

$$L(0) f(0) = \sum_1^{N/2} u_n(0) \iiint u^*(1)(L(1) - 2/r_{01}) f(1) d\tau_1 + 2\sum_1^{N/2} u_n(0) \sum_1^{N/2} \iiint u_m^*(1)(1/r_1)_{nm} f(1) d\tau_1 \tag{3.1}$$

[4] Fock, Zeits. f. Physik **61**, 126 (1930).

in which

$$(1/r_0)_n = \iiint u_n^*(1)(1/r_{01})u_n(1)d\tau_1,$$

$$(1/r_0)_{nm} = \iiint u_n^*(1)(1/r_{01})u_m(1)d\tau_1.$$

The simpler equation

$$\begin{aligned} L(0)f(0) = &- 2\sum_1^{N/2} u_n(0) \iiint u_n^*(1)(1/r_{01})f(1)d\tau_1 \\ &+ 2\sum_1^{N/2} u_n(0) \sum_1^{N/2} \iiint u_m^*(1)(1/r_1)_{nm}f(1)d\tau_1 \end{aligned} \tag{3.2}$$

imposes on its solutions the orthogonality condition $\iiint u_n^* L f d\tau = 0$ and therefore has at least one solution in common with (3.1). This common solution is in fact found when (3.1) is solved by the method of successive approximation.

We assume for u_n the representation

$$u_1 = (1/4\pi)^{1/2}R_1(r),\ u_2 = (3/4\pi)^{1/2}R_2(r)\cos\theta,$$

$$u_3 = u_4^* = (3/8\pi)^{1/2}R_2(r)e^{i\varphi}\sin\theta.$$

R_1 and R_2 are functions which give the energy integral for the atomic problem a minimum value. In terms of R_1 and R_2

$$\sum_1^N (1/r_0)_n = 2\int_0^\infty (R_1(r_1) + 3R_2(r_1))\gamma_0(0, 1)r_1^2 dr_1,$$

$$u_2(0)\iiint u_2^*(1) + u_3(0)\iiint u_3^*(1) + u_4(0)\iiint u_4^*(1)$$

$$= (3/4\pi)R_2(0)\iiint R_2(1)\cos(r_0, r_1),$$

$$\sum_1^{N/2} u_n(0)\iiint u_n^*(1)(1/r_{01})f(1)d\tau_1 =$$

$$(1/4\pi)R_1(0)\iiint R_1(1)(1/r_{01})f(1)d\tau_1$$

$$+ (3/4\pi)R_2(0)\iiint R_2(1)(1/r_{01})f(1)\cos(r_0, r_1)d\tau_1,$$

$$u_1(0)\sum_1^{N/2} \iiint u_m^*(1)(1/r_1)_{1m}f(1)d\tau_1$$

$$(1/4\pi)R_1(0)\iiint R_1(1)(1/r_1)_1 f(1)d\tau_1 + (1/3)(3/4\pi)^2 R_1(0)\iiint R_2(1)f(1)$$

$$\cdot \iiint R_2(2)(1/r_{12})R_1(2)\cos(r_1, r_2)d\tau_2 d\tau_1,$$

$$\sum_2^{N/2} u_n(0) \sum_1^{N/2} \iiint u_n^*(1)(1/r_1)_{nm} f(1) d\tau_1$$

$$(3/4\pi)^2 R_2(0) \iiint R_2(2) + (1/r_{12}) f(1) \cos(r_0, r_2)(R_2(1)R_2(1)\cos(r_1, r_2)$$

$$+ (1/3)R_1(1)R_1(1))d\tau_1 d\tau_2.$$

The angle functions combine into terms invariant under rotation of the axis of the atomic representation. It is convenient to take the axis in the direction of the incident electron beam. We expand f in a series of Legendre polynomials, $f = \sum f_n(r)P_n(\cos\theta)$, and find for the coefficients $f_n(r)$ the set of equations

$$\begin{aligned} L(0)f_0(0) &= 2R_1(0)\int_0^\infty R_1(1)((1/r_1)_1 - \gamma_0(0, 1))f_0(1)r_1^2 dr_1 \\ &\quad + 2\Big[R_1(0)\int_0^\infty R_2(1)\Big(\int_0^\infty R_2(2)\gamma_1(1, 2)R_1(2)r_2^2 dr_1\Big)f_0(1)r_1^2 dr_1 \\ &\quad - R_2(0)\int^\infty R_2(1)\gamma_1(0, 1)f(1)r_1^2 dr_1\Big] \end{aligned} \tag{3.3}$$

$$\begin{aligned} &(L(0) - 2/r_0^2)f_1(0) \\ &= 2R_2(0)\int_0^\infty R_2(1)\Big(\int_0^\infty R_2(2)\gamma_0(1, 2)R_2(2)r_2^2 dr_1 - \gamma_0(0, 1)\Big)f_1(1)r_1^2 dr_1 \\ &\quad + (4/5)R_2(0)\int_0^\infty R_2(1)\Big(\int_0^\infty R_2(2)\gamma_2(1, 2)R_2(2)r_2^2 dr_1 - \gamma_2(0, 1)\Big)f_1(1)r_1^2 dr_1 \\ &\quad + (2/3)\Big[R_2(0)\int_0^\infty R_1(1)\Big(\int_0^\infty R_2(2)\gamma_1(1, 2)R_1(2)r_2^2 dr_1\Big)f_1(1)r_1^2 dr_1 \\ &\quad - R_1(0)\int_0^\infty R_1(1)\gamma_1(0, 1)f_1(1)r_1^2 dr_1\Big] \end{aligned}$$

$$\begin{aligned} &(L(0) - n(n+1)/r_0^2)f_n(0) \\ &\quad = -1/(2n+1)\Big[R_1(0)\int_0^\infty R_1(1)\gamma_n(0, 1)i_n(1)r_1^2 dr_1 \\ &\quad + 3R_2(0)\int_0^\infty R_2(1)(\gamma_{n-1}(0, 1)(n/(2n+1)) \\ &\quad + \gamma_{n+1}(0, 1)(n+1)/(2n+3))f_n(1)r_1^2 dr_1\Big], \quad n \geqq 2. \end{aligned}$$

The writer must correct an error in the note added in proof to S.S.E.[1] There appears the statement "The scattering intensity does not tend toward

spherical symmetry with decreasing electron velocity." The statement is false. Each equation of the set (3.3) involves only one coefficient $f_n(r)$. $f_n(r)$ is roughly proportional to the coefficient of $P_n(\cos\theta)$ in the expansion of e^{ikz} in a series of Legendre polynomials. Thus $f_n(r)$ vanishes uniformly in r as $k\to 0$ and the scattered wave approaches spherical symmetry for sufficiently low velocities. If a generalization is permitted from results obtained for helium, the effect of exchange is to lower the limiting velocity below which scattering is sensibly spherically symmetric. There is apparently an effective cancellation of terms of opposite sign in the exchange integrals for f_0 and f_1. Again if we generalize from results obtained for helium, this apparent cancellation is real. There arises the possibility that for quite low velocities the scattering amplitude proportional to $P_2(\cos\theta)$ is much larger than the scattering amplitude proportional to $P_1(\cos\theta)$. If this occurs in the neighborhood of the Ramsauer minimum cross section, the distribution in angle will depart strongly from spherical symmetry, but will retain more or less symmetry about the plane of right angle scattering. We have here a possible explanation of the distribution in angle in the inert gases found by Ramsauer and Kollath.[5] The argument suffices to make the integration of (3.3) a problem of considerable interest. There is however one feature of the experimental distribution in angle at low velocities which is not reproduced by the exchange equations. The sharp rise in the krypton and xenon intensity curves below 30° may be explained by the reaction of the distorted atom on the incident wave. The effect of atomic distortion or polarization is to excite the partial scattering functions of high order; the partial scattering amplitudes then decrease slowly with increasing n and yield a large sum for small angles, but interfere effectively everywhere else

In the remainder of the discussion the single electron functions u_n are solutions of the Fock equations

$$\left(\nabla^2 + 2(E_n + V(r) - \sum_{m\neq n}^{N}(1/r)_m)\right)u_n = -2\sum_{m\neq n}^{N/2}(1/r)_{mn}u_m + \sum_{m\neq n}^{N/2}\lambda_{mn}u_m,$$

$$\lambda_{pn} = \iiint u_p^*\left(\nabla^2 + 2(E_n + V(r) - \sum_{m\neq n}^{N}(1/r)_m)\right)u_n d\tau + 2\sum_{m\neq n}^{N/2}\iiint u_p^*(1/r)_{mn}u_m d\tau.$$

The condition $\lambda_{mn}=\lambda_{nm}^*$ implies the mutual orthogonality of the u's. Using the Fock equations to simplify the exchange integral, (3.1) transforms into

$$L(0)f(0) = 2\sum_{1}^{N/2}u_n(0)\iiint u_n^*(1)(W - E_n - 1/r_{01})f(1)d\tau_1 - \sum_{1}^{N/2}u_n(0)\sum_{m\neq n}^{N/2}\lambda_{nm}\iiint u_m^*(1)f(1)d\tau_1. \tag{3.4}$$

[5] Ramsauer and Kollath, Ann. d. Physik, Feb. (1932), March (1932).

Then

$$\iint_{\infty}(f^*\nabla f - f\nabla f^*)\cdot dS$$
$$= \sum_{n=1}^{N/2}\sum_{m\neq n}^{N/2}\int\cdots\int\Big(u_n(1)u_m^*(0)f^*(1)f(0)\lambda_{mn}^* - u_n^*(1)u_m(0)f(1)f^*(0)\lambda_{mn}\Big)d\tau_0 d\tau_1 = 0;$$

the relation (1.6) is satisfied. We verify by substituting u_p for f that solutions of the Fock equations are also solutions of (3.4). If f is a solution of (3.4) satisfying the scattering problem boundary conditions so also is $f+\sum_1^{N/2}c_n u_n$. We fix f by the orthogonality conditions $\iiint u_n^* f d\tau = 0$; (3.4) becomes

$$L(0)f(0) = -2\sum_1^{N/2}u_n(0)\iiint u_n^*(1)(1/r_{01})f(1)d\tau_1. \tag{3.5}$$

The orthogonality of u_n and f is a necessary consequence of (3.5) and the Fock equations. (3.5) is apparently much simpler than (3.2), but for numerical integration by the method of successive approximation (3.2) is preferable for reasons already discussed in connection with Eqs. (2.2) and (2.5).

If the atomic wave function $u(1, \cdots, N)$ in (1.7) is replaced by $|u_n(m)\ s_n(m)|, \psi(0, 1, \cdots, N)$ can be written as a determinant with $N+1$ rows and columns. But the determinant form of ψ discloses immediately that it is unchanged when fs is replaced by $fs+\sum_1^N c_n u_n s_n$. A scattering equation derived by a process which begins with the approximate atomic wave function constructed from single electron functions will have these functions as solutions. If now the single electron functions are solutions of the Fock equations, this scattering equation cannot differ essentially from (3.4) which also has as solutions the single electron functions. We conclude that the use of an approximate atomic wave function to simplify (1.8) is justified, particularly so when the approximate atomic wave function is constructed from solutions of the Fock equations.

TABLE I. *W=21.5 volts.*

k	0	1	2
F_{k0}	0.243–i0.711	−0.138–i0.104	−0.064–i0.001
F_{k1}	0.192–i0.016	0.301–i0.049	0.042–i0.046

	FF^*	$\iint FF^* d\Omega$	$(2\pi i/k)\,(F(1)-F^*(1))$†
Without exchange	$0.563+0.117\cos\theta+0.039\cos^2\theta$	7.24	7.24
With exchange	$0.668+0.225\cos\theta+0.299\cos^2\theta$	9.65	9.25

† S.S.E.,[1] section 3. The relation $\iint FF^* d\Omega = (2\pi i/k)\,(F(\cos\theta)-F(\cos\theta))_{\cos\theta=1}$ is equivalent to (1.6). The calculation was carried through with the single electron function $u=(\alpha^3/\pi)^{1/2}e^{-\alpha r}$, $\alpha=27/16$. The ratio 9.65–9.25/9.25 is a measure of the error introduced into the total cross section by the use of a single electron function different from the Hartree function.

TABLE II. *W = 10.75 volts (with the Hartree function).*

k	0	1	2
F_{k0}	0.138–*i*1.105	−0.124–*i*0.025	−0.028+*i*0.010
F_{k1}	0.141–*i*0.006	0.288–*i*0.026	0.034–*i*0.030

	FF^*	$\int\int FF^* d\Omega$	$(2\pi i/k)(F(1)-F^*(1))$
Without exchange	$1.239+0.052\cos\theta+0.020\cos^2\theta$	15.66	15.66
With exchange	$1.255+0.125\cos\theta+0.214\cos^2\theta$	16.68	16.65

INTEGRATION OF 2.8. HELIUM

The partial waves f_{kn} yield partial scattering amplitudes $F_{kn}P_n(\cos\theta)$ which combine into the total scattering amplitude $F(\cos\theta)=\sum_0^\infty\sum_0^\infty F_{kn}P_n(\cos\theta)$.

Results of the numerical integration of (2.8) are found in Tables I and II.

For $n=2$ the partial scattering amplitudes are estimated from (2.3) with f replaced by e^{-ikz}:

$$\begin{aligned} F'(\cos\theta) &= F_a(\cos\theta) + F_b(\cos\theta) \\ F_a(\cos\theta) &= (1/4\pi)\int\int\int e^{ik(r_1\cos(r,r_1)-z_1)}U(r_1)d\tau_1 \end{aligned} \tag{4.1}$$

the Born first order scattering amplitude, and

$$F_b(\cos\theta) = (1/2\pi)\int\cdots\int e^{ik(r_1\cos(r,r_1)-z_2)}u(1)(1/r_{12}-(1/r_2))u(2)d\tau_1 d\tau_2,$$

$$U(r) = (4/r)e^{-2\alpha r}(1+\alpha r),\ u(r) = (\alpha^{3/2}/\pi^{1/2})e^{-\alpha r},\ \alpha = 27/16.$$

Letting $q=k/a$

$$\alpha^2 F_a(\cos\theta) = [1/(1+q^2\sin^2\theta/2) + 1/(1+q^2\sin^2\theta/2)^2].$$

We write

$$F_a(\cos\theta) = \sum_0^\infty F_{an}P_n(\cos\theta)\quad F_b(\cos\theta) = \sum_0^\infty F_{bn}P_n(\cos\theta)$$

and remembering that $\sin\theta d\theta = 2d(\sin^2\theta/2)$ find

$$\begin{aligned} \alpha^2 F_{a0} &= ((1/q^2)\log(1+q^2) + 1/(1+q^2)) \\ \alpha^2 F_{a1} &= 3[(1/q^2)\log(1+q^2) - 1/(1+q^2)]. \end{aligned}$$

The coefficients F_{bn} are taken from a recent paper by Massey and Mohr:[6]

$$\begin{aligned} \alpha^2 F_{b0} &= -2/(1+q^2)^2[(3-q^2)/(1+q^2) - 8(15+q^2)/(9+q^2)^2] \\ \alpha^2 F_{b1} &= -4/(1+q^2)^2[1/q^2(1-(1/q^2)\log(1+q^2)) \\ &\quad -(21/2+(6/q^2)\log(1+q^2) - (16/q)\tan^{-1}q) \\ &\quad -q^2(3/2-(3/q^2)\log(1+q^2))] \end{aligned}$$

[6] Massey and Mohr, Proc. Roy. Soc. **A132**, 605 (1931).

$$\alpha^2 F_{b2} = -4/(1+q^2)^3[(6/q^4)((1/q^2)\log(1+q^2) - 1/(1+q^2) - 0.5q^2/(1+q^2)) + (15/q^2)((1/q^2)\log(1+q^2) - 1/(1+q^2)) + ((48/q)\tan^{-1}q - 54.5/(1+q^2)) + q^2((15/q^2)\log(1+q^2) - 45/(1+q^2) - 2.5q^2/(1+q^2))].$$

F_{b0} differs from the corresponding term computed by Massey and Mohr because we are using a different and more accurate form of the exchange integral. At 21.5 volts, $q^2=0.555$, $F_{b2}=0.040$,

$$\left.\begin{aligned} F_{a0} &= 0.505 \\ F_{00} &= 0.243 - i0.711 \end{aligned}\right\} \qquad \left.\begin{aligned} F_{a1} &= 0.160 \\ F_{01} &= 0.192 - i0.016 \end{aligned}\right\}$$

$$\left.\begin{aligned} F_{b0} &= -0.061 \\ F_{10}+F_{20} &= 0.202 - i0.105 \end{aligned}\right\} \qquad \left.\begin{aligned} F_{b1} &= 0.244 \\ F_{11}+F_{21} &= 0.343 - i0.095 \end{aligned}\right\}.$$

From the comparison we conclude that for $n \geqq 2$ the partial amplitudes given by (4.1) agree well with the amplitudes found by numerical integration of (2.8). The complete scattering amplitude is then

$$F(\cos\theta) = \sum_0^2 (F_{k0} + F_{k1}\cos\theta) + (F_a(\cos\theta) - F_{a0} - F_{a1}\cos\theta + F_{b2}P_2(\cos\theta)). \tag{4.2}$$

TABLE III. *W=21.5 volts.*

θ	$F_a(\cos\theta)$	$F_a(\cos\theta)-F_{a0}-F_{a1}\cos\theta$	$F_{b2}P_2(\cos\theta)$	$\sum_0^2(F_{k0}+F_{k1}\cos\theta)$	FF^*
0	0.702	0.037	0.040	0.576–*i*0.927	1.29
20	0.682	0.027	0.033	0.544–*i*0.920	1.21
40	0.637	0.009	0.015	0.451–*i*0.901	1.04
60	0.578	−0.007	−0.005	0.309–*i*0.872	0.85
80	0.516	−0.017	−0.018	0.134–*i*0.835	0.71
100	0.465	−0.012	−0.018	−0.052–*i*0.797	0.64
120	0.422	−0.003	−0.005	−0.227–*i*0.761	0.63
140	0.392	0.010	0.015	−0.369–*i*0.731	0.65
160	0.374	0.019	0.033	−0.462–*i*0.712	0.68
180	0.370	0.025	0.040	−0.494–*i*0.705	0.68

Measurements in helium are not available at 21.5 volts. Ramsauer and Kollath[5] give a series of intensity measurements over the energy range 1.8 to 19.2 volts.* The points labeled experimental in the 21.5 volt diagram are obtained from the 15.8 and 19.2 volt experimental points by a linear extrapolation. To change from the R. and K. units to atomic units the experimental intensity is multiplied by the factor $1/(0.532)^2=3.533$. The 15.8 volt curves for scattering with and without exchange are rough approximations found by averaging the calculated 10.75 and 21.5 volt amplitudes.

Except in the region below 30° the agreement at 21.5 volts is excellent. At 15.8 volts a discrepancy appears which becomes important at 10.75 volts. This discrepancy as well as the large difference below 30° is undoubtedly to

* The R. and K. intensities are absolute; those given by Bullard and Massey in an earlier paper (Proc. Roy. Soc. **A133,** 637 (1931)) are relative. To compare the two sets of measurements the B. and M. intensities are multiplied by a factor chosen for each velocity to make the fit as close as possible. Excellent agreement is found (see R. and K.).

be accounted for by atomic distortion which is neglected in deriving the exchange scattering equation. Considering the extreme difficulty of a calculation including atomic distortion it is disappointing to find the discrepancy at 10.75 volts so great.

The writer has had the privilege of many stimulating discussions with Dr. H. Bethe. He is indebted to Dr. R. Peierls for suggesting the derivation of scattering equations by a variation method and to Professor G. Wentzel and Professor E. C. Kemble for helpful criticism.

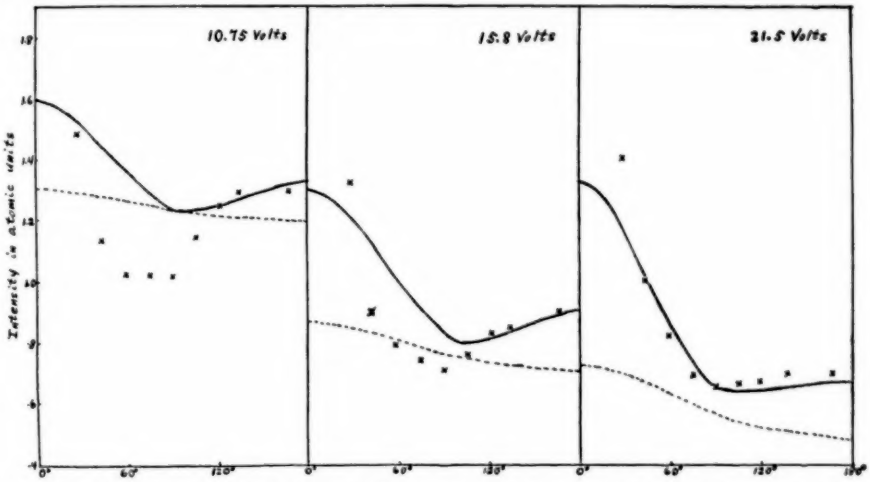

Fig. 1. Elastic scattering in helium. Crosses, experimental points from Ramsauer and Kollath.[5] Full line, calculated intensity with exchange. Dotted line, calculated intensity without exchange.

Note added in proof: Massey and Mohr[7] derive exchange scattering equations resembling only remotely the equations found by the writer. The discrepancy arises in M. and M.'s treatment from the introduction of unnecessarily crude approximations into an accurate equation. M. and M. write an exact solution of the two-electron problem (scattering in atomic hydrogen) in the form

$$\begin{aligned}\psi(1,2) &= \sum_n u_n(1)f_n(2) + \int_E u_E(1)f_E(2)dE \\ &= \sum_n u_n(2)g_n(1) + \int_E u_E(2)g_E(1)dE\end{aligned} \qquad \text{(I)}$$

in which $(\nabla^2+2(E_n+1/r))u_n=0$, $(\nabla^2+2(E+1/r))u_E=0$ and asymptotically $f_1\sim e^{-ikz}+1/re^{-ikr}F(z/r)$, $g_1\sim 1/re^{-ikr}G(z/r)$. The solutions with correct symmetry and physical meaning are $\psi\pm(1,2)=\psi(1,2)\pm\psi(2,1)$. The equations given by M. and M. for the determination of f_1 and g_1 are

$$\begin{aligned}(\nabla_2^2 + 2W)f_1(2) &= -2\iiint u_1(1)\,(1/r_2-1/r_{12})\psi(1,2)d\tau_1, \qquad \text{(II)}\\ (\nabla_2^2+2W)g_1(2) &= -2\iiint u_1(1)\,(1/r_2-1/r_{12})\psi(2,1)d\tau_1.\end{aligned}$$

Orthogonality properties implicit in (I) are involved in the derivation of (II). In particular use is made of the relations

[7] Massey and Mohr, Proc. Roy. Soc. **A85**, 289 (1932).

$$\iiint u_1(1)\,(\psi(1,2) - u_1(1)f_1(2))d\tau_1 = 0, \qquad \text{(III)}$$
$$\iiint u_1(2)\,(\psi(1,2) - u_1(2)g_1(1))d\tau_2 = 0.$$

It is thus clearly a dubious procedure to introduce into Eq. (II) an approximation for $\psi(1, 2)$ which is inconsistent with Eq. (III). The equations obtained by M. and M. following this procedure are at best of doubtful validity. For details the reader is referred to their paper. The reduction of (II) to the form given by the writer (S.S.E., section 2) is not difficult, but because the analysis is somewhat lengthy cannot be reproduced here.

Analytic Atomic Wave Functions

By J. C. SLATER
Massachusetts Institute of Technology

(Received July 26, 1932)

A method is suggested for setting up analytic atomic wave functions which form good approximations to Hartree's functions. These functions are of the form $\Sigma cr^n e^{-ar}$, where the exponent a as well as c and n vary from one term to another. The constants are determined for 1, 2, and 3-quantum electrons by fitting Hartree's values numerically for five selected atoms, and interpolation methods are presented for dealing with the intermediate atoms. A method is suggested for setting up exactly orthogonal functions, with no loss of accuracy. It is shown that the analytic wave functions are the solutions of central field problems in which the field is slightly different for different quantum numbers, on account of the inaccuracy in the function, but a table shows that the discrepancy between this and the correct field is small over the region where the wave function is large. Suggestions are made for future work, on the one hand in extending the tables, on the other in using the wave functions in investigating atomic energies, exchange integrals, etc.

FOR any detailed calculations dealing with atomic or molecular structure, good approximations to the atomic wave functions are essential. The most satisfactory method, in general, for building up such functions seems to be by the use of one-electron functions which are solutions of the problem of an electron moving in a central field, setting up sums of products of such functions, antisymmetric in the electrons. But no completely satisfactory set of one-electron functions has been developed. It is the purpose of this paper to suggest a considerable improvement in such functions.

The best one-electron functions which we have are those of Hartree.[1] It is to be regretted that these functions are not in more accessible form; but they have been computed, by Hartree or his collaborators, for the atoms He, Li^+, Be^{++}, Be, B^{+++}, O^{+++}, O^{++}, O^+, O, F^-, Ne, Na^+, Al^{+++}, Al^+, Si^{+4}, Cl^-, A, K^+, Ca^{++}, Cu^+, Rb^+, Cs^+. It has been shown by the writer and by Fock[2] that these are the best one-electron functions which can be set up, if we neglect exchange terms, and it is to be presumed that the corrections made by introducing exchange would be small. We should state at the outset that the functions suggested in this paper are no improvement on Hartree's in the matter of accuracy; they are in fact somewhat inferior, but are much more convenient. For there are two important points in which Hartree's functions are far from satisfactory. First, and most important, they exist only as tables of values, and as such cannot be used for any analytical calculations. Second, the functions for different quantum numbers with the same atom are not exactly orthogonal to each other, and this introduces great complications when

[1] D. R. Hartree, Proc. Camb. Phil. Soc. **24**, 89, 111 (1928) and later papers by Hartree and others. For Si^{+4}, J. McDougall, Proc. Roy. Soc., to appear shortly. I am much indebted to Dr. Hartree for the list of atoms whose structure has been investigated, and for tables of values of wave functions.

[2] J. C. Slater, Phys. Rev. **35**, 210 (1930); V. Fock, Zeits. f. Physik **61**, 126 (1930).

calculations using antisymmetric combinations are made. Our present functions are analytical approximations to Hartree's functions, modified to make them orthogonal.

Among analytic wave functions, two types may be mentioned as extreme examples. First, Pauling[3] has used hydrogen-like functions of the form $e^{-Zr/n}$ times polynomial in r, the coefficients of the polynomial being given as for a hydrogen problem with nuclear charge Z. He has set up a set of screening constants, giving Z for each electron of each atom. By comparison of one of Pauling's functions with the corresponding one of Hartree's (see Fig. 1), we see that the nodes in Pauling's functions lie at too large values of r. The reason is that the nodes get closer together for large Z. Now the nodes lie in any

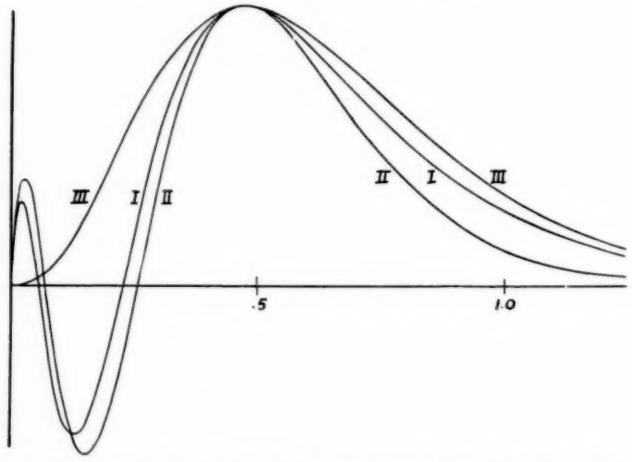

Fig. 1. Wave functions for Rb^+ $3s$. I. Present wave function. On this scale, Hartree's curve departs from this by negligible amounts. II. Hydrogen-like curve. III. Single term r^3e^{-ar}. Constants for II and III are chosen so as to make all curves coincide at the maximum, rather than to agree with the screening constants of Pauling and the writer, respectively.

case at smaller values of r than the principal, outer maximum of the function, and in an actual atom this region near the nucleus has a larger effective Z than the range around the maximum, compressing the nodes; while Pauling uses a constant Z all over the wave function. On account of this behavior of the nodes, Pauling's functions are rather badly in error.

The other extreme in the way of wave functions was suggested by the writer.[4] These functions were of the form $r^{n-1}e^{Zr/n}$, without any nodes at all. It is plain that the correct wave functions, having nodes larger than in the writer's functions, but smaller than in Pauling's, lie between these two sets. In all these sets of functions, the maxima are so adjusted that they approximately agree in position.

Analytical Expression for Wave Functions

As a method of improving these functions, one may proceed according to the following line of thought. A $3s$ function for instance, has a wave function

[3] L. Pauling, Proc. Roy. Soc. **A114,** 181 (1927).

[4] J. C. Slater, Phys. Rev. **36,** 57 (1931).

in hydrogen (multiplied by r) of the form $e^{-Zr/3}(r^3-ar^2+br)$, where a and b are definitely determined. The three terms of this correspond roughly to the outer, middle, and inner maxima of the function: $e^{-Zr/3}\ r^3$ has its maximum at $9/Z$; the next term has its maximum at $6/Z$, and the inner one at $3/Z$. But now really the middle maximum lies in a range of larger Z then the outer one, and the inner maximum has still higher Z. Let us then use different Z's for each maximum, taking a function of the form $r^3e^{-Z_1r/3}-a'r^2e^{-Z_2r/3}+b're^{-Z_3r/3}$, where a', b' are no longer the same as a and b. The maxima will then lie at $9/Z_1$, $6/Z_2$, $3/Z_3$, and if Z_2, Z_3 are much larger than Z_1, the inner maxima, and hence the nodes, will lie much further in than with the hydrogen-like function of Pauling. It is now actually found that functions of this form, as for example $c_1re^{-a_1r}-c_2r^2e^{-a_2r}+c_3r^3e^{-a_3r}$, can form good representations of Hartree's functions, by proper choice of constants.

One further refinement of these functions proves to be necessary, if we are to get really satisfactory agreement with Hartree's functions. This can be seen most clearly from the $3d$ function, for which our method would give

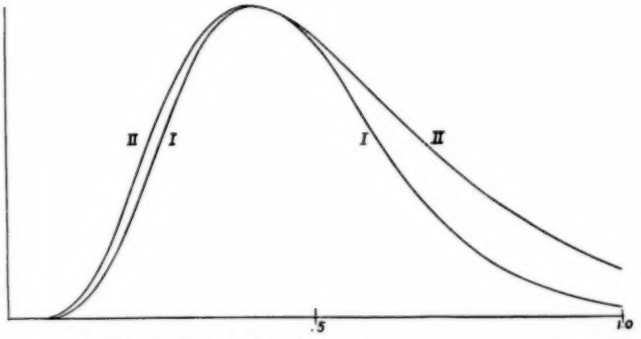

Fig. 2. Wave functions for Rb^+ $3d$. I. Hydrogen-like curve. II. Present wave function, agreeing with Hartree's curve.

r^3e^{-ar}. This has but one parameter, a, and if it is chosen to make the maximum agree with that of Hartree's curve, the general form of the curve is evidently wrong, as we may see from Fig. 2. Hartree's function falls off much more slowly for large r. The reason is clear; in the outer part of the orbit, the effective Z is smaller, resulting in a more gradual change of the function. This can be remedied by using two exponentials connected with the same power of r, as $r^3(c_1e^{-a_1r}+c_2e^{-a_2r})$, the smaller exponent giving the outer part of the function, the larger one the inner part. It is found that this gives a good representation, except for Cu^+, where the $3d$ electrons lie at the outside of the atom. There the effect is so pronounced that three exponentials are necessary, and it was found that even as far along as Rb three exponentials improve the agreement, though they are not so necessary. Now the $3d$ is an extreme case, but for the other orbits as well it was found helpful to use two exponentials for the outer maximum, though not for the inner ones. The only wave functions represented sufficiently well without this were the $1s$ and $2s$. Thus for $3s$ we should use a function $c_1re^{-a_1r}-c_2r^2e^{-a_2r}+r^3(c_3e^{-a_3r}+c_4e^{-a_4r})$. Such a function

is capable of representing Hartree's solutions with very good accuracy. We give in Table I three examples of agreement between such analytical functions and Hartree's tables of values.

TABLE I. *Comparison of analytic functions with Hartree's for 2s, 3s, and 3d electrons of Rb^+.*

r	2s		3s		3d	
	Hartree	*Anal.*	*Hartree*	*Anal.*	*Hartree*	*Anal.*
0.01	0.679	0.695	0.678	0.637	0.001	0.001
0.02	0.882	0.896	0.874	0.846	0.006	0.005
0.03	0.796	0.795	0.772	0.736	0.019	0.014
0.04	0.546	0.538	0.504	0.480	0.040	0.031
0.06	−0.138	−0.156	−0.211	−0.209	0.108	0.088
0.08	−0.795	−0.825	−0.867	−0.854	0.207	0.176
0.10	−1.290	−1.300	−1.308	−1.292	0.329	0.289
0.12	−1.601	−1.602	−1.492	−1.495	0.466	0.420
0.14	−1.752	−1.747	−1.476	−1.478	0.623	0.562
0.16	−1.777	−1.773	−1.276	−1.282	0.752	0.709
0.18	−1.715	−1.709	−0.954	−0.965	0.889	0.853
0.20	−1.597	−1.597	−0.557	−0.574	1.017	0.989
0.25		−1.213	0.540	0.519	1.284	1.278
0.30	−0.827	−0.842	1.508	1.496	1.462	1.468
0.35	−0.535	−0.546	2.198	2.199	1.556	1.575
0.40	−0.333	−0.340	2.600	2.611	1.583	1.601
0.45	−0.202	−0.205	2.763	2.786		1.570
0.5	−0.120	−0.121	2.750	2.778	1.505	1.498
0.6	−0.041	−0.039	2.416	2.441	1.335	1.316
0.7	−0.013	−0.012	1.927	1.950	1.138	1.107
0.8	−0.004	−0.004	1.449	1.472	0.944	0.915
0.9	−0.001	−0.001	1.052	1.070	0.767	0.748
1.0			0.742	0.762	0.614	0.606
1.2			0.350	0.364	0.382	0.386
1.4			0.160	0.165	0.230	0.235
1.6			0.072	0.071	0.137	0.139
1.8			0.032	0.030	0.080	0.079
2.0			0.014	0.012	0.047	0.045

METHOD OF DETERMINING CONSTANTS

After choosing a form of analytical wave function, at least two methods are available for determining the constants. One would be to construct a wave function for the whole atom from such functions, and determine the constants by the variation method, minimizing the whole energy. This would be a very interesting method, essentially that which Zener[5] has used on the light atoms, except that Zener did not use our wave functions with the adjustable exponents. The second method, however, is simpler and more available, and that is to choose the functions to fit Hartree's curves as well as possible. This was the method adopted. Dr. Hartree very kindly supplied the complete tables of wave functions of the five atoms Si^{+4}, K^+, Cu^+, Rb^+, Cs^+, and these were fitted by numerical methods. The two schemes should, of course, arrive at substantially the same results. In the present paper, the coefficients and exponents are given for the 1, 2, and 3 quantum electrons of these atoms. They are tabulated in Table II, and plotted in Fig. 3.

[5] C. Zener, Phys. Rev. **36**, 51 (1930); Guillemin and Zener, Zeits. f. Physik **61**, 199 (1930).

TABLE II. *Exponents in analytic wave functions for five atoms.*

Explanation: The wave function for a 1*s* electron (multiplied by r) is re^{-ar}, where a is tabulated. For a 2*s*, it is $re^{-ar}-cr^2e^{-br}$ where a and b are tabulated (for example, for Si^{+4}, $a=12.25$, $b=4.53$). For a 3*s*, it is $re^{-ar}-cr^2e^{-br}+r^3(de^{-fr}+ge^{-hr})$, where for example in K^+, $a=15.35$, $b=5.89$, $f=3.27$, $h=2.30$. The coefficients are determined for orthogonal functions as follows: c in the 2*s* is determined to make 2*s* orthogonal to 1*s*; in 3*s*, d and g are related by the condition that $de^{-fr}=ge^{-hr}$ for $r=3/2.67$ (where 2.67 is in the column "3*s* intersection," and c, and d, are determined to make the 3*s* orthogonal to 1*s* and 2*s*.

For a 2*p*, the function is $r^2(ae^{-br}+ce^{-dr})$, where the exponents are given by the entries "2*p* inner" and "2*p* outer," and the relation between coefficients is such that the terms are equal when $r=2/$"2*p* intersection." For 3*p*, we have $r^2e^{-ar}-r^3(be^{-cr}+de^{-fr})$. For 3*d*, in Cu^+ and Rb^+, the functions are $r^3(ae^{-br}+ce^{-dr}+fe^{-gr})$, where the exponents are tabulated, and also the values "3d inner intersection" and "3*d* outer intersection" from which the corresponding r's are the values where the first two, or last two, exponentials are equal.

The curves are sufficiently straight so that linear interpolations between adjacent atoms should be fairly good. But extrapolations are dangerous, since the curves break at the completion of shells of electrons.

The constants as given do not suffice to describe the functions agreeing with Hartree's curves, but only the slightly different orthogonal functions.

Power of r	Orbit	Si^{+4}	K^+	Cu^+	Rb^+	Cs^+
r	1*s*	13.70	18.70	28.70	36.70	54.70
	2*s*	12.25	16.00		30.00	44.02
	3*s*		15.35	21.62	25.30	31.70
r^2	2*s*	4.53	6.67		14.80	23.03
	3*s*		5.89	10.35	13.40	19.92
	2*p* inner	6.00	8.98	14.69	18.80	27.95
	2*p* intersection	4.56	7.12	12.11	16.10	24.41
	2*p* outer	3.59	5.77	10.10	13.67	21.85
	3*p*		7.05	12.32	15.78	23.00
r^3	3*s* inner		3.27	6.62	9.17	15.76
	3*s* intersection		2.67	4.68	6.40	11.27
	3*s* outer		2.30	4.19	6.02	11.10
	3*p* inner		2.99	5.84	8.21	14.25
	3*p* intersection		1.72	3.55	5.43	10.66
	3*p* outer		1.72	3.57	5.54	10.60
	3*d* inner			6.29	9.20	15.46
	3*d* inner intersection			3.78	5.55	10.62
	3*d* middle			2.65	4.74	10.10
	3*d* outer intersection			1.15	1.12	
	3*d* outer			1.28	2.60	

The actual methods used for fitting Hartree's functions may be of interest. Suppose we wish to fit a 3*s* function, and that by interpolation or otherwise we can get first, rough estimates of the terms. Then first we subtract the estimated values of the terms in r and r^2 from Hartree's function, leaving approximately the term which should be represented by r^3 times the sum of two exponentials. We divide the difference by r^3, take the logarithm to base two exponentials. We divide the difference by r^3, take the logarithm to base 10, for convenience. The result would give a straight line if one exponential were enough. As it is, however, the line is likely to be bent sharply at small r's, on account of inaccurate estimates of the terms in r and r^2; this can be disregarded. But more important, the line as a whole is curved, and must be represented, not by one term $a-br$, but by two, in the form $\log_{10}(10^{a-br}+10^{c-dr})$. The graph of this function has two asymptotes, the straight lines $a-br$ and $c-dr$; at the point where these lines cross, the graph lies a distance $\log_{10}2$ above the intersection. We can make a further useful set of observa-

tions: where one line is, for example, 0.1 above the other, the graph lies a distance $\log_{10}(1+10^{-0.1})=0.2539$ above the upper straight line, and 0.3539 above the lower. Using a table constructed according to this model, making use of the positions of the asymptotes, and making a few trials, we may readily get the constants a, b, c, d. Then we compute the term $r^3(10^{a-br}+10^{c-dr})$, subtract it and the approximate first term from Hartree's curve, and get the term which should be represented by $r^2\,10^{e-fr}$. Dividing by r^2 and plotting the logarithm, we find a straight line, from which e and f are determined. Finally we subtract the difference of the correct second and third terms from

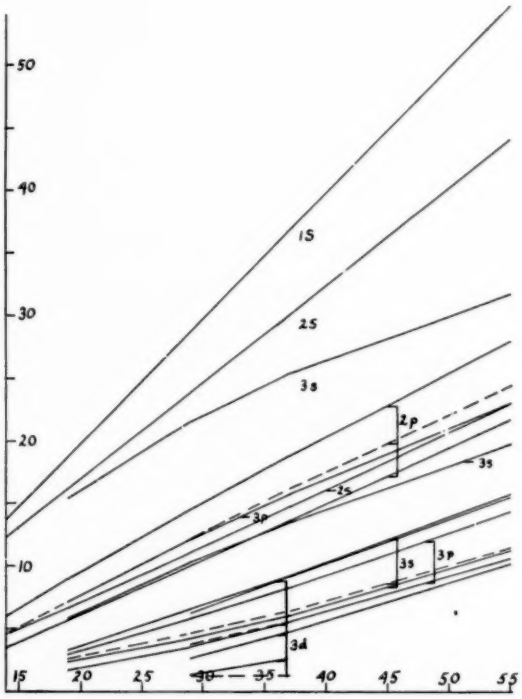

Fig. 3. Diagram of exponents and coefficients as function of atomic number. Drawn from the data of Table II, with linear interpolation. See Table II for explanation. The curves for intersections are drawn with dotted lines.

Hartree's function, divide by r and take the logarithm, and read off from this straight line the coefficient and exponent of the term in r. If the original estimates were far wrong, the process can be repeated, yielding good results fairly rapidly. The final straight lines turn out in all cases to be remarkably straight. The same method can be used on all the functions. It was found in many cases that the constants were by no means uniquely determined. It was possible to choose sets of constants varying over quite a wide range, giving equally good agreement with the curve. In these cases, constants were chosen to give smooth curves of exponents against atomic number, as described in the next section.

Interpolation Methods; Orthogonality of Wave Functions

The wave functions for five isolated atoms would be of small value; the real use of the present method is that it provides a means of interpolation, by which wave functions of intermediate atoms can be found. The interpolation can be thrown into a form suggesting Moseley curves of x-ray term values. The reason is that the exponent Z/n, is of the same form as the square root of an x-ray term, which is plotted in those diagrams. In Fig. 3 we show the exponents as functions of atomic number, giving approximately straight lines, but breaking for the outer electrons when shells are completed, as in x-ray diagrams. Not only the exponents, but some of the coefficients as well, can be put in this form. Thus in an expression $r^n(ce^{-ar}+de^{-br})$, which we have in the outer parts of the wave functions, we may compute the value r_0 for which the two exponentials are equal: $c\,e^{-ar_0}=de^{-br_0}$. This point generally proves to be between the maxima of the two exponentials. Now these maxima come for $r=n/a$, and n/b, respectively. Thus we can define a quantity, analogous to a and b, equal to n/r_0, which will lie generally between a and b, and will fall on the interpolation diagram just as the exponents themselves do. These quantities are plotted in Fig. 3. We discuss the other coefficients in the next paragraph.

The functions of Hartree, which we approximate, are not exactly orthogonal, as we mentioned above. Thus if we use our analytical expressions for Hartree's functions, we find that $(1s, 2s)$ (meaning by this the integral of the product of the functions) for Rb^+ is 0.0072, $(1s, 3s)$ is -0.0078, $(2s, 3s)$ is -0.0015, showing that the departure from orthogonality is of the order of a percent. Now when one constructs antisymmetric wave functions in the form of determinants, one has a certain freedom in choosing the one-electron functions entering into it. The reason is that the determinant has the same value, apart from a constant factor, if the elements of each row (or column) are replaced by arbitrary linear combinations of the corresponding elements of the other rows. For example, the determinant

$$\begin{vmatrix} 1s(1) & 1s(2) & 1s(3) \\ 2s(1) & 2s(2) & 2s(3) \\ 3s(1) & 3s(2) & 3s(3) \end{vmatrix}$$

has the same value as

$$\begin{vmatrix} 1s(1) & 1s(2) & 1s(3) \\ 2s(1)+a1s(1) & 2s(2)+a1s(2) & 2s(3)+a1s(3) \\ 3s(1)+b2s(1)+c1s(1) & 3s(2)+b2s(2)+c1s(2) & 3s(3)+b2s(3)+c1s(3) \end{vmatrix}$$

except for a constant factor which drops out on normalizing. As a result, we shall have the same wave function for an atom if, instead of using Hartree's one-electron wave functions, we use a set constructed after the following model: For $1s$: Hartree's $1s$; for $2s$: Hartree's $2s$+constant times his $1s$; for $3s$: Hartree's $3s$+constant times $2s$+constant times $1s$, and so on. And here

the constants can be so chosen as to make the resulting functions orthogonal. Thus a set of orthogonal functions can be set up, similar to Hartree's, and giving just the same atomic wave function as Hartree's.

From our analytic functions, we can proceed in a very similar way to set up orthogonal functions. For the correct $2s$, we should subtract some of our $1s$ from the $2s$ as determined from Hartree's function. But the $1s$ is so nearly the same as the inner term of the $2s$, that we can subtract some of that instead. In other words, we merely change the coefficient of the term in r, to make the function orthogonal to $1s$. Similarly, in the $3s$ function, we can change the coefficients of the terms in r, r^2 to get orthogonality with both $1s$ and $2s$. It is easily seen that conditions of this sort give just enough equations to determine all the coefficients of our final orthogonal functions. We thus have the following rule: we use orthogonal wave functions of the form $c_1re^{-a_1r}-c_2r^2e^{-a_2r}+\cdots$, where the coefficients are so chosen that the functions are all orthogonal (and of course normalized). The exponents are taken from our interpolation graph. In this process, the sum of exponentials occurring in the outer maximum is treated as a single term. Of course, this rule applies to the part of the wave function which is a function of r; it is to be multiplied by the proper spherical harmonic of the angle.

As an example, let us choose the s states of Rb. For $1s$ the exponent from the graph is 36.70. Thus the function is $cre^{-36.70r}$, and if we normalize to unity, we have $c^2\int r^2e^{-73.40r}dr=1=c^2\,2!/(73.40)^3$, $c=444.7$. Next, for the $2s$ we have $c_1re^{-30.00r}-c_2r^2e^{-14.80r}$. For orthogonality, the integral of the product of this with $re^{-36.70r}$ must be zero:

$$c_1\int r^2e^{-66.70r}dr-c_2\int r^3e^{-51.50r}dr=0,\ c_2'/c_1=(51.5)^4/3(66.7)^3=7.903.$$

Finally for normalization we have

$$c_1^2\int r^2e^{-60.0r}dr-2c_1c_2\int r^3e^{-44.8r}dr+c_2^2\int r^4e^{-29.6r}dr$$
$$=1,\ c_1^2\{2/(60.0)^3-2c_1c_26/(44.8)^4+c_2^224/(29.6)^5\}=1.$$

Solving these simultaneously gives $c_1=139.1$, $c_2=1099$. Lastly, for the $3s$ we have $c_1re^{-25.30r}-c_2r^2e^{-13.40r}+r^3(c_3e^{-8.97r}+c_4e^{-6.02r})$. The value giving the intersection of the last two is 6.40, so that $c_3e^{-8.97\times3/6.40}=c_4e^{-6.02\times3/6.40}$, giving $c_4=0.2512\,c_3$. Then applying the conditions of orthogonality with $1s$ and $2s$, and normalizing, we find $c_1=49.65$, $c_2=534.8$, $c_3=572.5$, $c_4=143.8$, determining the function completely.

Differential Equation Satisfied by the Wave Function

It is interesting to consider what differential equation is satisfied by our analytical wave functions. Let us write the function $u=\Sigma u_n=\Sigma c_nr^ne^{-a_nr}$, times function of angle, where we may have more than one term for a given exponent n. This can be written as the solution of an equation $Hu=Eu$, where $H=-\nabla^2-2Z(r)/r$, provided $Z(r)$ is properly chosen; for to get it we need

only set $Z(r) = -(r/2)\ (\nabla^2 u/u + E)$. Computing the derivatives, we have $\nabla^2 u = \Sigma([n(n-1) - l(l+1)]/r^2 - 2a_n n/r + a_n^2)u_n$, where l is the azimuthal quantum number, from which $Z(r)$ can be at once computed, if we assume a value of E. Since our functions are essentially the same as Hartree's, and since his are solutions of central field problems for which he has found the energy values, we take those values for E. We give in Table III for illustration

TABLE III. *Effective nuclear charge for 3-quantum electrons of Rb, compared with Hartree's value.***

r	Z Hartree	Z $3s$	Z $3p$	Z $3d$
0.01	35.14	34.94		
0.02	33.56	32.97	31.49	
0.03	32.16	32.86		
0.04	30.89	32.75*	29.99	
0.06	28.65	23.47	28.38	
0.08	26.69	25.59	26.84	
0.10	24.92	24.56	25.34	22.40
0.15	21.41	21.57	22.09	
0.2	18.73	19.62*	— —*	18.59
0.3	14.64	14.44	14.56	15.04
0.4	11.66	11.70	11.60	11.95
0.5	9.55	9.63	9.54	9.53
0.6	8.06	8.12	8.10	7.78
0.7	7.05	7.22	7.05	6.64
0.8	6.29	6.30	6.26	5.97
0.9	5.66	5.80	5.68	5.68
1.0	5.12	5.38	5.16	5.32
1.2	4.25	4.71	4.35	4.77
1.4	3.60	4.07	3.61	4.00
1.6	3.12	3.27	2.84	3.15
1.8	2.77	2.23	1.93	2.34
2.0	2.52	1.34	0.96	1.71
2.5	2.19	−1.96	−2.00	1.60
3.0	2.07	−5.41	−5.26	4.09

** An electron moving in the field of potential $-2Z/r$, where Z has the tabulated value, would have just the analytic wave functions we have found. Asterisks mark the nodes, at which particularly large errors of Z are found.

the resulting values of $Z(r)$ for the 3-quantum orbits of Rb, computed for each wave function. We see that they are all different, as they naturally would be since we have not a real solution of a single central field problem. On the other hand, the curves agree with each other over wide ranges of variables, in fact over the whole range where the individual wave functions are large. Not only that, but they agree well with what we should expect from Hartree's calculations. We give also in Table III the values calculated from Hartree's field, representing the $Z(r)$ which, divided by r, gives the potential in which a 3-quantum electron moves (strictly different for $3s$, $3p$, $3d$, but nearly enough the same so that we can use a sort of average).

On a graph of $Z(r)$ it is easily shown that a hydrogen-like curve, as used by Pauling, is represented by a straight line, and a single exponential term, as used by the writer, by a parabola-like curve opening downward. Obviously both of these are far less accurate than the functions of the present paper. The principal inaccuracies in our present values come at the nodes of the functions (where, since u appears in the denominator, a very small error in

the position of the node can result in a behavior of the Z curve resembling anomalous dispersion), and at large r's , where the curves approach straight lines which generally are not horizontal, as they should be. Both these inaccuracies come in regions where the wave function is small, showing that at all points where it is large it satisfies rather accurately the differential equation which it should.

Suggestions Regarding Further Work

It seems that the present wave functions are accurate enough to form good approximations, and at the same time are as simple as they could possibly be—they are scarcely more complicated than hydrogen wave functions. They should be useful, in the first place, in further calculations of atomic structure by Hartree's method. For by interpolation, a decidedly accurate approximation to the wave function can be obtained, to use as a starting point for the method of self-consistent fields. Of course, the curves of constants given in the present paper are far from satisfactory. No doubt they are not even the best approximations for the five atoms which have been computed. They cover only a few of the atoms for which calculations have been made, and not all the wave functions even of those. It is hoped that further work may improve and extend these curves, as the Moseley x-ray term diagrams have been continuously improved. In particular, attention is called to the fact that almost all the atoms which have been calculated by Hartree's method, except for a few light atoms, consist entirely of closed shells. If a few atoms were worked out containing uncompleted shells, as for instance in the iron group, it would be possible to extend the curves to the outer, optical electrons, adding greatly to their usefulness. Fairly reliable extrapolations can be easily made, though they are not indicated in this paper. The wave functions of the present paper should be useful, then, both in stimulating and in guiding further calculations by the method of self-consistent fields, and it is to be hoped that those who make such calculations will at the same time find analytical approximations to their results, so as to improve the curves.

The wave functions themselves are good enough so that a number of calculations become possible which could not be done before. These deal principally with applications of the perturbation theory to atomic structure; for here we have a really good set of orthogonal functions, which can be used as a starting point for perturbation calculations. It will be possible to compute the total energy of atoms, by integration of the energy operator over the orbits, as Zener has done for the light atoms. Further, the exchange integrals coming into the theory of atomic spectra can be calculated from these wave functions, if they are extended to the optical levels. Other interesting applications would be to the effect on the wave function of the perturbations produced by relativity in heavy atoms, and by exchange. The wave functions would be useful in the theory of hyperfine structure. Still another use, of course, is in forming atomic approximations to use with Heitler and London's method of treating molecular structure. Most of these applications demand

rather definitely the order of accuracy, as well as the analytical convenience, attained in the present wave functions, and which have been impossible before. In addition, there are other calculations which can be made better with these functions, but were possible before, as diamagnetism, polarizability, atomic diameters, etc., previously studied with less accurate analytic functions, and atomic scattering, etc., studied with Hartree's or the Thomas-Fermi functions. In conclusion, the writer wishes again to acknowledge his gratitude to Dr. Hartree for his kindness in providing the tables of wave functions, and for many useful suggestions.

The Nuclear Spin and Magnetic Moment of Li^7

By L. P. GRANATH
Department of Physics, New York University, University Heights

(Received July 25, 1932)

Measurements have been made on the hyperfine structure of the $^3P_0-^3S_1$ group of the λ5485 line of $(Li^7)^+$ with a Fabry-Perot etalon crossed with a 21 ft. Paschen-mount concave grating. The method of using the etalon with an astigmatic grating is discussed. The results of the measurements on the Fabry-Perot patterns of the $^3P_0-^3S_1$ group indicates a nuclear spin of 3/2 for Li^7 and a nuclear magnetic moment of 3.29 times the theoretical magnetic moment of the proton.

INTRODUCTION

THE hyperfine structure of the $1s2p\ ^3P\rightarrow 1s2s\ ^3S$ (λ5485) line of Li^+ has been investigated with the object of determining the spin and the magnetic moment of the Li^7 nucleus. Schüler[1] was the first to observe the hyperfine structure of this line and in his original paper ascribed a spin of $\frac{1}{2}$ to the Li^7 nucleus, discarding as a ghost the third component of the group $^3P_0-^3S_1$. The author[2] found this group to be composed of three components thus removing the possibility of a spin of $\frac{1}{2}$ but the measurements were not of sufficient accuracy to decide between a value of 1, 3/2 and 2.

There are three ways of determining the nuclear spin from the hyperfine structure of the λ5485 line.

(a) Agreement of the observed pattern with a theoretical calculated pattern for all of the hyperfine structure components.
(b) Measurements of relative intensities of specially chosen hyperfine structure components such as 3, 2, 1 ($^3P_0-^3S_1$).
(c) Measurement of interval ratio of specially suitable components, in particular 3, 2 and 1.

The method (a) could be considered the best in theory provided the accuracy of the measurements were high enough. The difficulty of resolving closely spaced groups of lines such as Schüler's 4, 5, 6 group is however considerable and the theoretically expected difference between the appearance of the pattern as a whole for different spins is not very pronounced. This method has been used by Güttinger and Pauli[3] and Goudsmit and Inglis.[4] A precise determination of the nuclear magnetic moment is difficult by this method for reasons just mentioned.

Method (b) could be used provided intensity measurements could be made well enough. It is unnecessary to point out the pitfalls present in such measurements; even if the measurements could be made with sufficient cer-

[1] Schüler, Zeits. f. Physik **42**, 487 (1927); Schüler and Brück, Zeits. f. Physik **58**, 735 (1929).
[2] Granath, Phys. Rev. **36**, 1018 (1930).
[3] Güttinger and Pauli, Zeits. f. Physik **67**, 743 (1931).
[4] Goudsmit and Inglis, Phys. Rev. **37**, 328 (1931).

tainty only a few of the hyperfine structure components could be used without ambiguity on account of the large influence of the intermediate stages of coupling[3] between the nuclear spin, the electron spin and the electronic total angular momentum.

For components 3, 2 and 1 the question of intermediate coupling does not arise and it may be possible to determine the spin from the relative intensities of these components.

Method (c) has the advantage of greater possible accuracy, it is unaffected by the intermediate coupling, it gives at the same time the spin and the effective nuclear magnetic moment.

The measurements given by Schüler on the position of components 1, 2 and 3 are not of sufficient accuracy to give quite definite information about the spin. In the present work the accuracy of the measurements of the relative position of 1 and 2 with respect to 3 has been increased in comparison with that of Schüler. It is believed that it is sufficiently high to establish the value of the spin as 3/2, to show that the interval rule is obeyed, and to give the effective magnetic moment to at least 0.5 percent.

Working on the 3, 2, 1 ($^3P_0 - {}^3S_1$) group the author[2] obtained an interval ratio of $\Delta\lambda_{32}/\Delta\lambda_{21} = 1.61(5) \pm 0.02(3)$ as against a value of 1.62 determined from Schüler's[1] data.*

The theoretical value of this interval ratio is, according to Goudsmit and Bacher,[5]

$$(i+1)/i = 2,\ 5/3,\ 3/2 \text{ for } i = 1,\ 3/2,\ 2.$$

The value $1.61(5) \pm 0.02(3)$ indicated that the interval rule did not apply. This value was obtained from measurements on plates taken in the second order of a 21 ft. concave grating** and while the probable error was small on 100 measurements taken on 2 plates it was felt that not much weight could be attached to the ratio since the proximity of the components may have influenced each other. The problem then was to obtain photographs of the group with increased resolution and dispersion.

Photographs were obtained in the third order of the grating and measurements on these gave an unmistakeable interval ratio of $\Delta\lambda_{32}/\Delta\lambda_{21}$ between 1.33 and 1.41 indicating a spin greater than 3/2. Next an exposure was obtained in the fourth order of the grating. This gave an interval ratio of about 1.66 which agreed somewhat with the second order but definitely not with the value obtained from the third order plate taken during the same run. The intensity of the grating was low in this order and it was necessary to expose for 50 hours over a period of two weeks so only one exposure was taken. Moreover grating ghosts were present which tended to make the lines slightly blurred (due perhaps to nonperiodic irregularities in the ruling). Conse-

* The alleged inaccuracy in Schüler's conversion of the wave-length of component 3 was due to an oversight on my part of the position of the number 4 in Schüler's table.

[5] Goudsmit and Bacher, Phys. Rev. **34**, 1501 (1929).

** The Anderson grating used at present in this mounting is the property of Townsend Harris Hall, College of the City of New York.

quently it was felt that the grating should be discarded in favor of the Lummer plate or Fabry-Perot interferometer.

A glass Lummer plate was then crossed with the second order of the grating by placing the Lummer plate behind the grating plate holder. (The mounting of this is identical with that for the Fabry-Perot which is described later.)

The results obtained with the Lummer plate are given in Table I, and a photograph of one of the patterns appears in Fig. 1.

TABLE I. *Intervals and interval ratio as obtained with the Lummer plate.*

Plate	$\Delta\lambda_{32}$	$\Delta\lambda_{21}$	
July 9 No. 2	0.2014	0.1189	
July 9 No. 2	0.1965	0.1189	
July 19 No. 2	0.2007		0.4991 cm Lummer
July 20	0.1954	0.1220	
July 20	0.1945	0.1231	
July 26	0.1950	0.1233	
July 27	0.1943	0.1199	
March 24	0.1972	0.1172	0.4853 cm Lummer
Average	0.1971	0.1204	$\Delta\lambda_{32}/\Delta\lambda_{21}=1.637$

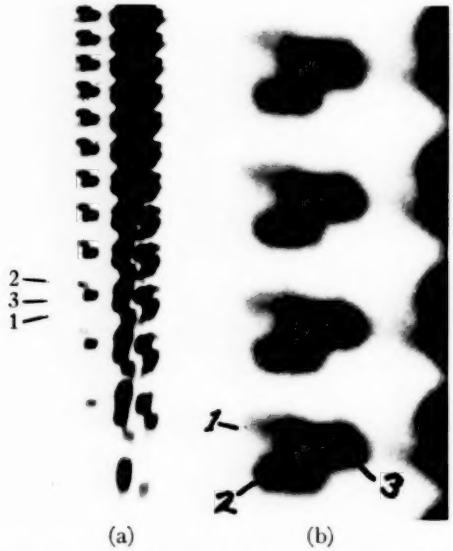

(a) (b)

Fig. 1. Lummer plate crossed with second order of grating. (a) Complete pattern of λ5485. (b) $^3P_0-{}^3S_1$ group of λ5485.

These patterns were taken with a 17 cm camera on Cramer Isopresto plates with the exception of the plate of March 24 which was taken on an Eastman 3G plate which is of finer grain than the Cramer but considerably slower.

The agreement between the several values is fair but due to the overlapping of orders component 3 falls between components 1 and 2. This may have caused a consistent error in measuring the intervals. In addition to the over-

lapping of orders the dispersion was small and the grain of the plate not as fine as could be desired. The values obtained were not considered sufficiently accurate to decide the validity of the interval rule, consequently a method was sought which would give a greater dispersion with no overlapping of orders.

This was accomplished by using a Fabry-Perot interferometer with spacers of such thickness that there would be no overlapping of orders. The results thus obtained are believed to be the most reliable.

An attempt was also made to determine the intervals by so choosing the Fabry-Perot spacers as to obtain coincidence of 2 with 3 and the results thus obtained indicated that the ratio was 1.66 ± 5 percent.

Apparatus and Method

A Paschen-Schüler lamp excited by a 1500 volt d.c. motor generator was used as a source. Commercial helium, purified by chabazite kept at liquid air temperature was continually circulated through the tube. The 21 ft. concave grating (Paschen mounting) was used as a monochromator to single out the

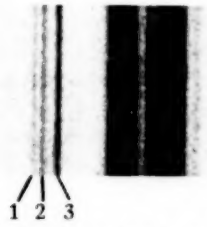

Fig. 2. Pattern of λ5485 taken in 4th order of grating.

λ5485 line of Li^+, a slit being placed at the plate holder so that the $^3P_0 - ^3S_1$ group could be separated from the rest of the line, a photograph of which taken in the fourth order is shown in Fig. 2. A condensing lens of 28 cm focus (the collimating tube of a Hilger constant deviation spectrograph) rendered the light parallel which then went through a Fabry-Perot interferometer of 4 cm aperture. A camera of 35 cm focal length was used to photograph the pattern.

This method of using the Lummer plate or the Fabry-Perot interferometer with an astigmatic grating mount has several good features; it is fast, the exposure time necessary with the Fabry-Perot being not much more than that required for a straight grating exposure; the resolution and dispersion of the grating is sufficient to enable one to identify the order of the lines in the interference pattern immediately. The lines in the Fabry-Perot pattern taken with the grating also appeared much sharper than when the same Fabry-Perot plates were used with a Hilger E_2 spectrograph in the customary manner. The interference instrument is inside the grating room and therefore at constant temperature. It has the disadvantage however in that only one line may be photographed at a time.

The bull's-eye of the Fabry-Perot pattern was centered on the line by placing a mercury arc in front of the grating and then moving the interferometer until the pattern was centered. It is then centered for the line for which the pattern is desired. A diagram of the apparatus is given in Fig. 3.

The Fabry-Perot plates were coated with silver sublimed on them in a vacuum. The method is essentially that described by Ritschl,[6] except that the films were not treated with acid. The spacers used were 1.78, 2.22 and 2.90 mm thick. Cramer Iso presto plates, the fastest that could be obtained for the green region of the spectrum, were used. These are excellent plates where speed in the green is required, but they must be used while fresh. The plates

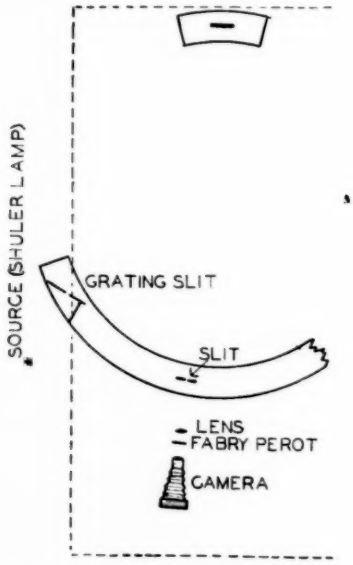

Fig. 3. Method of crossing Fabry-Perot etalon with astigmatic grating.

were developed for about twenty minutes in a fine grain boric acid developer. Exposure times were of the order of three to six hours.

Results

Several patterns of the $^3P_0-{}^3S_1$ group are shown in Fig. 4. These were taken with a wide slit on the grating, with the rest of the pattern screened off by the slit at the grating plate holder. The spacers 1.78, 2.22, 2.90 mm yield a pattern with no overlapping of components of this group, the distance between orders being 0.519, 0.685, and 0.845A, respectively.

Microphotometer traces of the patterns were measured and from these measurements the wave-length intervals were calculated by the usual formula for the Fabry-Perot interferometer. The intervals were also calculated from measurements taken directly on the plates with a comparator. The results are given in Table II.

[6] Ritschl, Zeits. f. Physik **69**, 578 (1931).

In calculating the final value of $\Delta\lambda_{32}$ and $\Delta\lambda_{21}$ the intervals $\Delta\lambda_{32}$ for the spacer 1.78 have been discarded. It was found that perfect resolution was not obtained for components 2 and 3 due to the presence of the edge of component 5 of the $^3P_2-{}^3S_1$ group. This is a comparatively very intense component and it seems that some of the light from it was scattered by the slit and so appeared on one side of the pattern. This can be seen in Figs. 4c and 5c. It should be noted that practically all of the $\Delta\lambda_{32}$ intervals due to the 1.78 spacer

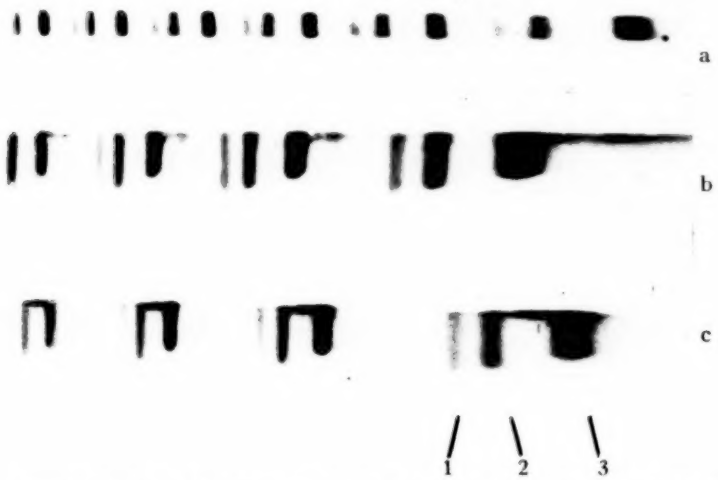

Fig. 4. Fabry-Perot pattern of the $^3P_0-{}^3S_1$ group. (a) 2.90 mm spacer plate April 28, No. 2. (b) 2.20 mm spacer plate May 16. (c) 1.78 mm spacer plate May 18.

TABLE II. *Intervals and interval ratio as obtained with the Fabry-Perot interferometer.*

Plate	Spacer (mm)	Intervals calculated from microphotometer traces: A Calculated intervals $\Delta\lambda_{32}$	A $\Delta\lambda_{21}$	B Corrected intervals $\Delta\lambda_{32}$	B $\Delta\lambda_{21}$	C Chosen intervals $\Delta\lambda_{32}$	C $\Delta\lambda_{21}$	Intervals calculated from comparator measurements $\Delta\lambda_{32}$	$\Delta\lambda_{21}$
April 28 No. 1	2.90	0.2005	0.1183	0.2005	0.1200	0.2005		0.1976	0.1113
April 28 No. 2	2.90	0.1995	0.1175	0.1995	0.1190	0.1995		0.2017	0.1146
May 5	2.90	0.1983	0.1135	0.1983	0.1150	0.1983		0.2003	0.1123
May 6	2.90	0.1971		0.1971		0.1971			
May 16	2.20	0.2000	0.1179	0.2000	0.1179	0.2000	0.1179	0.2006	0.1154
May 16	2.20	0.2001	0.1183	0.2001	0.1183	0.2001	0.1183		
May 17	2.20	0.2003	0.1213	0.2003	0.1213	0.2003	0.1213	0.1997	0.1177
May 18	1.78	0.1967	0.1213	0.2000	0.1213		0.1213	0.2023	0.1202
May 19	1.78	0.1964	0.1179	0.2000	0.1179		0.1179	0.1970	0.1212
May 20	1.78	0.1948	0.1223	0.1990	0.1223		0.1223	0.1998	0.1202
June 7	1.78	0.1985		0.1985					
June 9	1.78	0.1961	0.1209	0.2000	0.1209		0.1209		
Ave.		0.1982	0.1189	0.1994	0.1194	0.1994	0.1199	0.1999	0.1166
$\Delta\lambda_{32}/\Delta\lambda_{21}$		1.666		1.670		1.663		1.714	

are smaller than the others except the trace of June 7 which has the best resolution of any of these for the 2-3 distance. A 2 percent change in the position of component 2 seems reasonable, based on calculations which will be described later.

The interval $\Delta\lambda_{21}$ is discarded for the 2.90 spacer since it was found that with this spacer the isotope component ${}^3P_0-{}^3S_1$ for Li^6 came midway between components 2 and 1. This would tend to decrease the distance between 1 and 2 and it is seen that they are somewhat smaller than those for the other spacers. Here again, judging from the resolution of 1 and 2, a 2 percent correction would seem reasonable. A microphotometer trace of one of the groups for this spacer is given in Fig. 5a (see also Fig. 4a).

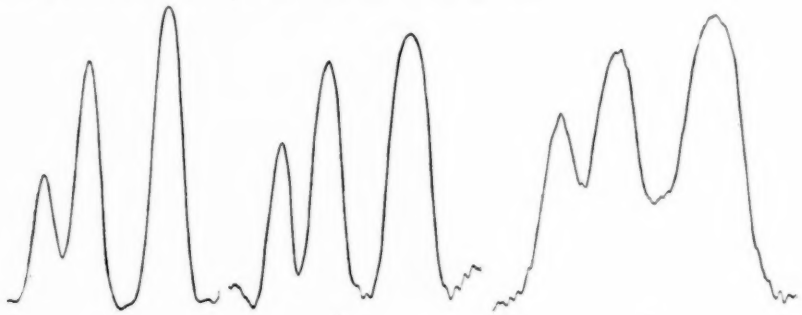

Fig. 5. Microphotometer traces of Fabry-Perot pattern. (a) 2.90 mm spacer plate April 28, No. 2. (b) 2.20 mm spacer plate May 16. (c) 1.78 mm spacer plate May 18.

The plates taken with the 2.90 and 2.20 spacers have the best resolution for the $\Delta\lambda_{32}$ interval. The second trace of the May 16 plate appears on the whole to be the best for both intervals. A reproduction of this trace appears in Fig. 5b (see also Fig. 4b).

The $\Delta\lambda_{21}$ interval for the 1.78 mm plates is assumed to be correct. Component 2 was undoubtedly shifted towards component 3 by about 2 percent and this would increase the $\Delta\lambda_{21}$ interval; consequently a correction to it was deemed unnecessary.

The correction to the intervals was estimated as follows: Immediately after obtaining a pattern the Fabry-Perot interferometer was removed and a mercury arc with a green filter was placed in front of the grating and different positions of the plate exposed to it for different times. Then by using the microphotometer a curve giving the relation between density and exposure was obtained for the plate containing the pattern. An intensity curve was plotted for component 3 and a Gauss error curve was then fitted to it thus giving the constant (a) in the equation $I=Ae^{-ax^2}$.

It was then supposed that the intensity due to components 1 and 2 was given by $I=A_1e^{-ax^2}+A_2e^{-a(x-x_0)^2}$ where A_2/A_1 should be approximately 2 (assuming the spin is 3/2). Knowing (a) it may then be calculated that the maximum of component 1 should be displaced by approximately 2 percent. A like correction was also deemed necessary on a few of the $\Delta\lambda_{23}$ distances as previously mentioned.

On account of absorption of lines in the cathode, 3 is likely to be somewhat wider than 2 and 1. Thus, by supposing the width of 1 and 2 to be the same as 3, one is likely to overestimate the correction. The mean value of the intervals $\Delta\lambda_{32}$ for the spacer 2.90 and 2.20 is 0.1994 and $\Delta\lambda_{21}$ for spacers 2.20 and 1.78 mm is 0.1200. (These are believed to be the most reliable values, those obtained by measuring the plates directly with the comparator being left out due to a possibility of a personal error in measurement. It will nevertheless be noted that the agreement between the comparator and microphotometer measurements is quite good.)

This yields an interval ratio $\Delta\lambda_{32}/\Delta\lambda_{21}=1.662$ which indicates a spin of 3/2 and a fair agreement with the interval rule.

From the formulas of Goudsmit and Bacher[5] with the correction factor $(1+\epsilon)=1.06$ of Breit and Doermann[7] applied to these formulas one can calculate the magnetic moment of the Li^7 nucleus.

$$^3S_1 = (1+\epsilon)0.228[g(i)/2](i, -1, -i-1).$$

Solving for $g(i)$

$$g(i) = \frac{2 \times 0.1994 \times 10^{-8}}{5485^2 \times 10^{-16} \times 0.228 \times 1.06 \pm 5/2} = 2.19$$

and

$$1840\mu = ig(i)\mu_0 = 3.29\mu_0.$$

This indicates that the magnetic moment of the Li^7 nucleus is about $3+\frac{1}{3}$ times the theoretical magnetic moment of the proton.

In conclusion the writer wishes to express his appreciation to Professor G. Breit for his generous interest and advice throughout the progress of the investigation, and to Dr. R. Garman and Mr. G. Shriver of the Department of Chemistry for their kindness in microphotometering the plates. Thanks are also due to Mr. H. Beck for construction of parts of the apparatus used. The lithium used in this investigation was obtained through the courtesy of the Maywood Chemical Works of Maywood, New Jersey.

[7] Breit and Doermann, Phys. Rev. **36,** 1732 (1930).

The Thermionic and Photoelectric Work Functions of Molybdenum

By LEE A. DUBRIDGE* AND W. W. ROEHR
Washington University, St. Louis

(Received August 20, 1932)

The photoelectric and thermionic emission from pure molybdenum was studied during a prolonged process of outgassing by heat treatment at temperatures up to 2100°K. In a sealed-off tube an equilibrium condition was reached which was not changed by further treatment extending up to 1600 hours. Photoelectric curves taken at room temperature and at 940°K and analyzed by Fowler's method yielded a true work function for the outgassed Mo of 4.15 ± 0.02 volts. Thermionic data for the same specimen also yielded a work function of 4.15 volts, and a value of the constant A close to the theoretical value of 60 amp./cm² deg.².

THE present investigation was undertaken as a part of a program of examining the photoelectric and thermionic properties of metals after a prolonged heat treatment in the highest attainable vacuum. Its aim was twofold: (1) to clear up if possible the discrepancies between the various published values for the surface work function of molybdenum, and (2) to obtain a further experimental test of Fowler's theory of photoelectric emission.

The thermionic work function of Mo has been determined under good vacuum conditions by Dushman and his co-workers[1] and by Zwikker.[2] The values obtained by these observers, 4.44 and 4.38 volts, respectively, are in good agreement with each other and undoubtedly represent the best values heretofore obtained for the outgassed metal. However, Dushman reported that great difficuity was encountered in eliminating the last traces of oxide from the molybdenum specimens so that completely consistent values of the thermionic emission were never obtained. The results of the present investigation indicate that it is possible to eliminate residual gas effects only by a very prolonged treatment and that the work function for the more thoroughly cleaned metal is slightly lower (4.15 volts) than the values obtained by the above observers.

Martin[3] studied the photoelectric properties of Mo during outgassing treatment and found that after about 150 hours of heating at temperatures up to 1700°K the work function reached an apparently stable value of about 3.2 volts, while the value of the thermionic work function for the same specimen was 3.48 volts. While these two values are in fair agreement, the large discrepancy between these values and those obtained by Dushman and Zwikker led Dushman[4] to suggest that the heat treatment had not been car-

* The work described in this paper was made possible by assistance to the first named author from a grant made by the Rockefeller Foundation to Washington University for research in science.

[1] Dushman, Rowe, Ewald and Kidner, Phys. Rev. **25,** 338 (1925).

[2] C. Zwikker, Proc. Amst. Acad. Sci. **29,** 792 (1926).

[3] M. J. Martin, Phys. Rev. **33,** 991 (1929).

[4] S. Dushman, Rev. Mod. Phys. **2,** 395 (1930).

ried out in this case at high enough temperatures to eliminate all impurities. In any case it appeared worth while to examine again the photoelectric and thermionic emission from Mo after a very prolonged treatment at the highest possible temperatures, to see whether a more gas-free condition could be reached than had hitherto been obtained.

Apparatus and Procedure

With the few exceptions mentioned below the experimental technique was the same as that used by the authors in a recently reported study of palladium[5] and need not be described again. The specimens, in the form of ribbons, were cut from a piece of very pure Mo foil about 0.01 mm thick. Temperatures were obtained from optical pyrometer readings, using the temperature scale determined by Worthing, and also from the resistance of the filament using Worthing's data.[6]

After a thorough baking of the tube, the outgassing of the filament was begun at a temperature in the neighborhood of 1750°K, since it was found that prolonged heating at higher temperatures during the early stages caused a failure of the filament before complete outgassing was attained. As the outgassing progressed the specimen was heated for long periods at 1900°K and for shorter periods up to 2100°K, at which temperature it soon burned out. It was found that if the tube was left sealed to the pumps it never reached a condition where consistent values of the photoelectric and thermionic emission could be obtained, even though the treatment was continued for 1000 hours. By sealing the tube from the pumps and allowing the residual gas to clean up by the getter action,[7] it was found that a stable and apparently gas-free condition could be reached which was not changed by further heating. One specimen withstood continuous heating for about six weeks after being sealed from the pumps, during most of which time there was no change in the work function. Most of the data given below were obtained from this specimen, though other specimens which burned out more quickly showed a similar behavior.

The single-prism monochromator used in previous investigations was replaced by a Van Cittert double quartz-prism monochromator to obtain more nearly pure monochromatic light. The relative intensities of the spectral lines of the mercury arc source were measured with a Burt vacuum thermopile connected to a Zernicke galvanometer. A sodium-in-quartz photoelectric cell connected to an FP-54 tube amplifier[8] was used for checking the intensities from time to time, and for determining the intensities of lines too weak to be measured with the thermopile. As before, the photoelectric currents were measured with a sensitive Cambridge Compton electrometer. The thermionic currents at the lower temperatures were measured with a Type R galvanom-

[5] L. A. DuBridge and W. W. Roehr, Phys. Rev. **39,** 99 (1932).

[6] A. G. Worthing, Phys. Rev. **28,** 190 (1926).

[7] Aluminum was found to be a more satisfactory getter than magnesium since it did not distil throughout the tube during the baking process.

[8] See L. A. DuBridge, Phys. Rev. **37,** 392 (1931).

eter and at the high temperatures with a potentiometer and standard 1-ohm resistance.

Results

1. Photoelectric emission

During the early stages of the outgassing process both the photoelectric and thermionic readings showed great irregularities and large and irregular changes with temperature, typical of a metal which has not been freed of gas. The threshold shifted at first toward the red reaching a value in the neighborhood of 3500A (3.5 volts). As the heating progressed the limit shifted again to the violet, to a minimum value near 2800A (4.4 volts), and after still longer treatment, with the tube sealed from the pumps, the threshold finally reached a stable value of 2980A (4.15 volts) as determined by the Fowler curves. This value could not be changed by further treatment at the highest temperatures.

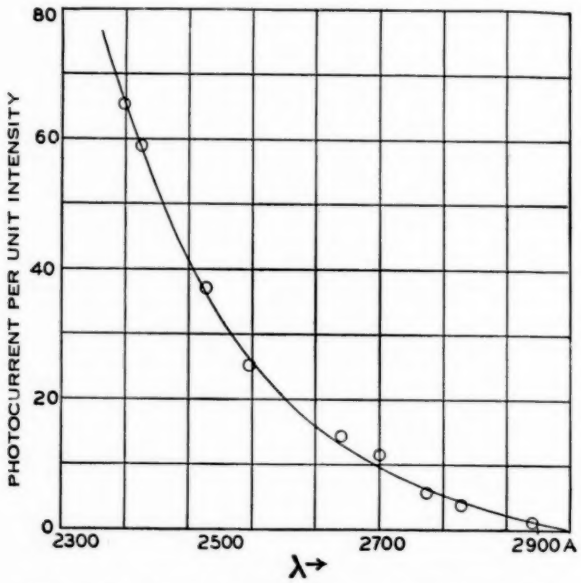

Fig. 1. Photoelectric threshold curve for outgassed Mo.

The ordinary threshold curve, taken at room temperature, for a specimen which had been outgassed for 1600 hours at temperatures up to 2100°K is shown in Fig. 1. This curve had remained practically unchanged by the last 800 hours of treatment, the tube having been sealed from the pumps after the first 400 hours. The pressure in the tube after sealing off, as read by an ionization gauge, was below 10^{-7} mm and showed a gradual decrease with time. During the last 800 hours of treatment both the photoelectric and thermionic measurements were entirely consistent and reproducible from day to day, indicating that the specimen was in a very gas-free state.

The Fowler curve for this specimen is shown in Fig. 2. The readings plotted were taken at room temperature (303°K) and at 940°K, the latter being

the temperature at which the thermionic currents just became appreciable. From the amount by which the observed points had to be shifted horizontally to fit the theoretical curve the following values of the threshold and work function were deduced:[9]

$$\text{for } T = 303°,\ \lambda_0 = 2992\text{A},\ \phi = 4.14 \text{ volts};$$
$$\text{for } T = 940°,\ \lambda_0 = 2983\text{A},\ \phi = 4.16 \text{ volts}.$$

These values are in excellent agreement, and their average, 4.15 volts, may therefore be taken as the best value of the photoelectric work function for clean molybdenum. There is a possible error of the order of 0.5 percent involved in fitting the Fowler curves.

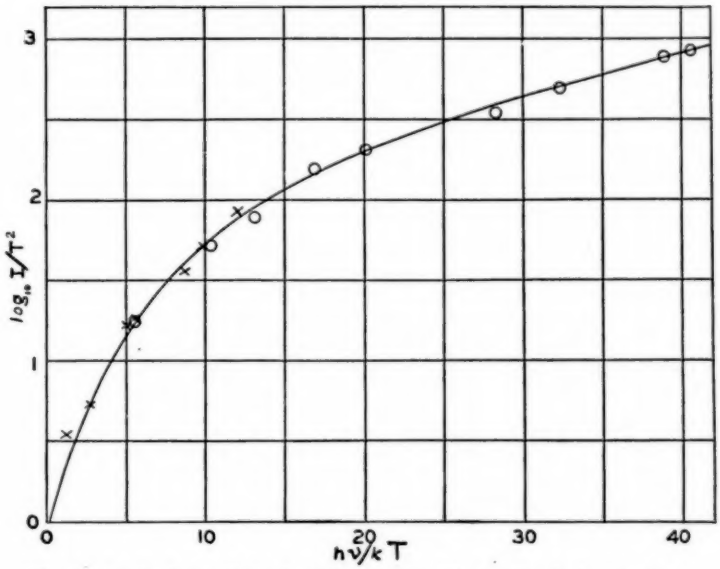

Fig. 2. Analysis of photoelectric data for Mo by Fowler's method. Circles, $T=303°$K; crosses, $T=940°$K.

The agreement between the observed points and the theoretical curve shown in Fig. 2 is within the limits of error involved in measuring the currents and the relative intensities of the spectral lines. These data for Mo thus constitute a further experimental verification of Fowler's theory.

2. Thermionic emission

During the early stages of outgassing the thermionic data did not at all fit the Richardson equation. When the observations were plotted in the usual form of log I/T^2 against $1/T$, a curve, usually concave toward the origin, instead of a straight line resulted. Hence no definite work function could be deduced. In general, however, the thermionic data ran parallel to the photoelectric data during the outgassing process. After equilibrium was reached

[9] See R. H. Fowler, Phys. Rev. **38**, 45 (1931); L. A. DuBridge, Phys. Rev. **39**, 108 (1 also reference 5. A discussion of Fowler's theory will also be found in Hughes and DuBr2 *Photoelectric Phenomena* pp. 241–248 (McGraw-Hill, 1932).

the thermionic emission showed a very consistent and reproducible behavior, again showing evidence that the specimen was quite gas-free. In Fig. 3 is shown a thermionic curve, taken after 1600 hours of treatment on the same specimen for which the photoelectric data of Figs. 1 and 2 were obtained. The value of the work function computed from the slope of this curve is 4.15 volts ($b=48{,}100$). Three other curves taken for this specimen at intervals over a period of about six weeks yielded the following values: 4.15, 4.17 and 4.14 volts. The average value is thus close to 4.15 volts and is in excellent agreement with the photoelectric value.

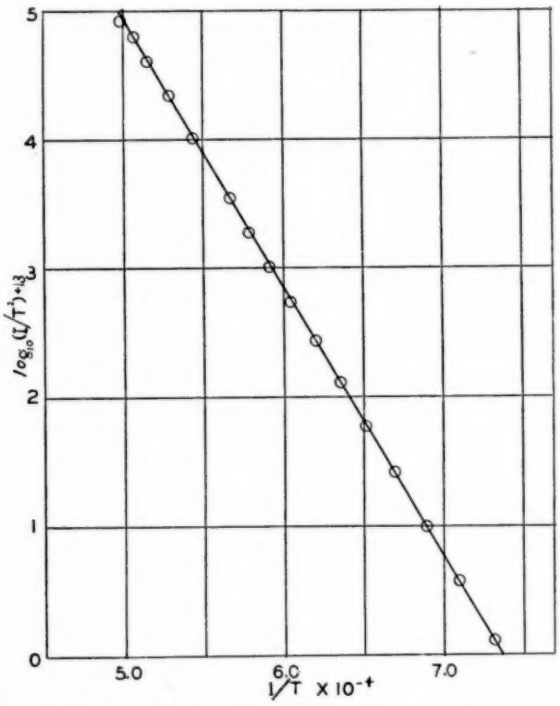

Fig. 3. Thermionic data for outgassed Mo. $\phi=4.15$ volts.

The average value of the thermionic constant A calculated from the data plotted in Fig. 3 is approximately 55 amp./cm^2 deg.^{2}, in good agreement with the theoretical value of 60.

Discussion

The results of these experiments seem to confirm the suggestion that the low value of the work function for Mo reported by Martin is to be attributed to the fact that in his experiments the heat treatment was not carried out for a sufficiently long time or at sufficiently high temperatures to eliminate all impurities. Values of the same order as those reported by Martin were observed in the present investigation only during the early stages of heating. More prolonged heating at high temperatures always caused an increase in the work function. Our failure to check exactly the values of 4.38 and 4.44

volts reported by Zwikker and Dushman was somewhat more puzzling. Apparently the value 4.4 volts is characteristic of a specimen which has been given a reasonably thorough outgassing treatment, but a very prolonged treatment results in the slightly lower value of 4.15 volts. Many of our specimens did show work functions of the order of 4.4 volts during the treatment, but those which withstood the longer heating gave the lower value, which we believe to be characteristic of a very gas-free state. It is possible, of course, that the prolonged heating also causes a microscopic recrystallization of the surface which results in a slight reduction in the work function.

Absorption Spectra of the Samarium Ion in Solids. I. Absorption by Large Single Crystals of $SmCl_3 \cdot 6H_2O$

By FRANK H. SPEDDING[1] AND RICHARD S. BEAR
Chemical Laboratory, University of California

(Received July 22, 1932)

The visible and ultraviolet absorption of large single monoclinic crystals of $SmCl_3 \cdot 6H_2O$ has been studied at seven temperatures between 15° and 298°K. Measurements of the absorption lines and bands are given as they appear at four of these temperatures. The influence of temperature on the positions of lines and multiplets and on the width and intensity of lines is discussed. All phenomena are explained on the basis of three direct effects of temperature change on the crystal: Lattice contraction and expansion, temperature vibration of the lattice with consequent fluctuations in crystal fields, and Boltzmann distribution of the ions between excited lower levels about 160, 210 and 300 cm^{-1} above the basic level.

IN THE past few years the spectra of gaseous atoms and the simpler gaseous compounds have been fairly well interpreted, and many relations between the energy levels of the substances under investigation and their physical and chemical properties have been established. Since a large part of chemistry is concerned with solids and solutions, it would be very desirable if these relations could be extended to apply to them. Unfortunately, very little is known of the energy levels of solids. This paper is the first of a series covering observations on the absorption of the samarium ion in various solid compounds and aiming at the determination of the characteristics of energy levels in solids. These papers will thus deal with one phase of a systematic study of the energy levels of ions in solids and solutions that is being carried out in this laboratory. The rare earths, as has been demonstrated elsewhere,[2] offer the simplest field for such investigation.

Freed[3] in his investigations of the magnetic susceptibility of $Sm_2(SO_4)_3 \cdot 8H_2O$ at various temperatures has predicted that the basic level of the samarium ion must have one or more levels lying near it. At higher temperatures a certain percentage of the ions, determined by the Boltzmann factor, would be distributed among these higher levels. Freed and Spedding[4] have verified this prediction by means of photographs of the absorption of $SmCl_3 \cdot 6H_2O$ at various temperatures. They have reported that the multiplets observed can be divided into two classes: one group with intensities greatest at 20°K and another that is completely absent at 20°, making its appearance at 78° and increasing in intensity with the temperature. They attributed the former group to electronic transitions arising from the basic level and considered that the latter group arises from the excited levels.

[1] National Research Fellow in Chemistry.

[2] Freed and Spedding, Nature **123,** 525 (1929); Phys. Rev. **34,** 945 (1929); Spedding and Nutting, J. Am. Chem. Soc., in press (1932).

[3] Freed, J. Am. Chem. Soc. **52,** 2702 (1930).

[4] Freed and Spedding, Nature, reference 2.

Because of the multiplicity of the lower levels of the Sm^{+++} ion it has been chosen for these investigations. The effects of temperature variation and of different crystal environments upon the lower levels are of course reflected in the spectra observed, and under such varying conditions the samarium ion should prove a powerful tool in the attempt to determine the nature of the energy levels of solids. To date we have photographed at several temperatures and under various conditions the absorption spectra of $SmCl_3 \cdot 6H_2O$, $SmBr_3 \cdot 6H_2O$, $Sm(BrO_3)_3 \cdot 9H_2O$, $Sm_2(SO_4)_3 \cdot 8H_2O$, $Sm(C_2H_5SO_4)_3 \cdot 9H_2O$, and $Sm(ClO_4)_3 \cdot xH_2O$. In this first paper we are considering only the absorption of single crystals of $SmCl_3 \cdot 6H_2O$, but in a second, which we are submitting at the same time, the conglomerate or so-called "reflection" spectrum of the chloride is described in detail. In the latter paper we give a partial energy level diagram for the samarium ion as it exists in the $SmCl_3 \cdot 6H_2O$.

The original plates made by Freed and Spedding were not suitable for this study in that they were taken with low dispersion which left most of the multiplets unresolved. We have for this reason taken new photographs at higher dispersion. This new work has been done also with conditions under better control and at several new temperatures.

Experimental Part

The photographs upon which this report is based were obtained from two large crystals and several smaller ones of $SmCl_3 \cdot 6H_2O$ which had been prepared from samarium material of exceptional purity purified by the late Professor C. James of New Hampshire College. Several such crystals have been examined by Dr. A. Pabst[5] of this university, who has reported that their external symmetry is monoclinic. The large ones were obtained as transparent yellow tablets about 1.5 cm square and 4 mm thick. These were used to secure the visible spectra, for which a 3 m Wood grating with dispersion of about 5.5A per mm in the first order was employed. A single photograph at liquid nitrogen temperature was taken with a 7 m grating but was too faint to be used for any but confirmation purposes. The larger grating proved unsatisfactory because of the long exposures required and the limited supply of liquid hydrogen available at any one time. At all other temperatures the smaller grating was found to be just as satisfactory, since the temperature blurring was larger than the resolving power of the instrument. The quartz extension of the Dewar used for the several ultraviolet photographs required smaller crystals about 5 mm wide and 1 mm thick. The ultraviolet spectra were obtained with a Hilger E 185 instrument with prisms so mounted as to give at one time about 3A per mm, at another 2, in the λ3100 region.

Most attention has been paid to the visible part of the spectrum, since most of the absorption occurs in that region and the effects of greatest interest are observed there. To facilitate work in the visible region over the temperature range employed, a special (Pyrex) Dewar was constructed and

[5] A. Pabst, Journal of Science **22,** 426 (1931).

fitted out as shown in Fig. 1. The chief features are the triangular windows left in two sides; the crystal house with filter (for elimination of frozen solids from obstruction of the light path); the crystal holder of piston shape introduced through a metal tube, which enables exchange of crystals during a run without introduction of air (especially important with liquid hydrogen); and the liquefier used to produce the liquids ethylene, methane and nitrogen, at whose boiling points pictures were taken. The liquefier, which can be removed for runs at liquid hydrogen temperature, is essentially an air-tight can fitting within the top of the Dewar with independent openings to the outside. The liquefying agent, liquid air, was introduced into the can and the desired gas

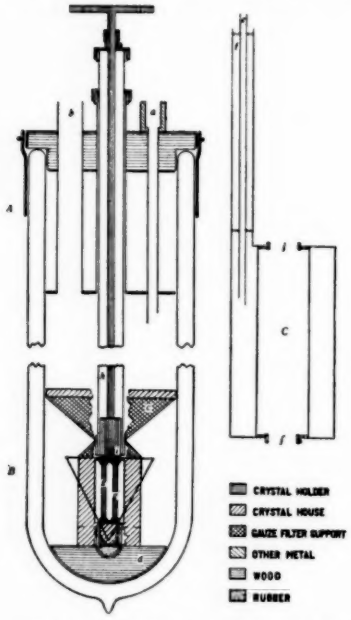

Fig. 1. Longitudinal cross section of Dewar for photography of visible absorption of solids at low temperatures, with *A*, top having inlet for liquid hydrogen, *a*, and outlet for gaseous hydrogen, *b*; *B*, crystal house with filter, *c*, and balsa "shock absorber," *d*; and *C*, liquefier for use with nitrogen, methane and ethylene having inlet for liquid air, *e*, and outlet for gaseous air, *f*. The triangular windows left in both sides of the silvered Dewar disclose the parts shown. The crystal is mounted between the two posts, *g* and *g'*, of the crystal holder, which can be introduced or withdrawn through the tube *h*. This tube is itself disconnectable from the crystal house at *i*, which permits insertion of the liquefier as follows. The liquefier when in position has the air outlet and inlet extending through and out of the hydrogen outlet of the top with the liquefier supports, *j* and *j'*, encircling the tube *h*. The inlet *a* is then used for entrance and exit of the gas to be liquefied. All of the above sets of concentric tubes and cylinders are made to fit snugly but not too tightly together, and the various metal parts, wherever possible, are constructed of German silver or Monel metal to avoid excessive conduction or corrosion. The dimensions of the Dewar are about 3 ft. by 4½ in. It was found possible to secure a charge of hydrogen lasting 15 hours.

condensed on the outside, from which it was allowed to drop to the bottom of the Dewar. To liquefy nitrogen the liquid air of the liquefier was evaporated under reduced pressure. Liquid hydrogen was transferred from the laboratory liquefier directly into the Dewar. In addition to room temperature and

those of liquid ethylene, methane, nitrogen and hydrogen, the temperatures of nitrogen and hydrogen boiling under reduced pressure, about 60° and 15°K, respectively, have been utilized.

The photographs were taken with "Speedway" and hypersensitive panchromatic plates with exposures of from two to four hours, depending on the temperature (see below). It was found that slightly overexposed plates gave the most reproducible results with respect to band edges and structure within wide intense bands. The plates were measured with a comparator us-

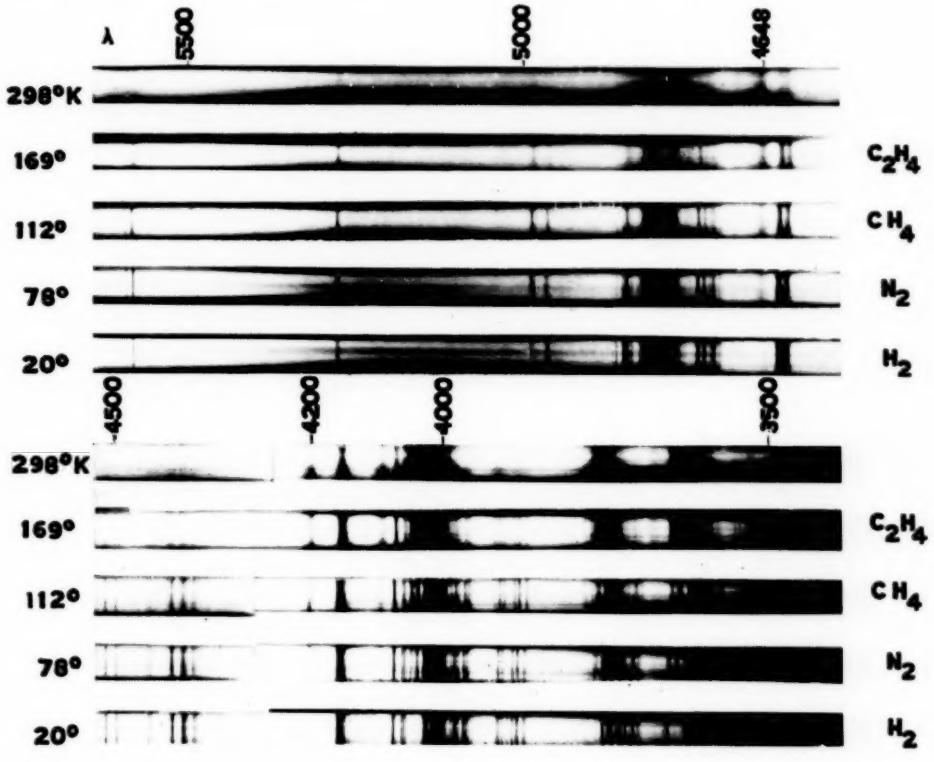

Fig. 2. Single-crystal absorption of $SmCl_3 \cdot 6H_2O$. The substances at whose boiling point the spectra were photographed are indicated on the right, the corresponding temperatures on the left. At λ4648 and λ4200 are the prominate high-temperature lines for which photometer curves are given in Fig. 3.

ing a low-power eye piece. The whole gave a magnification of five times, which somewhat limited the accuracy, but was necessary since many of the lines are faint and diffuse.

Results

In Fig. 2 are shown reproductions of the $SmCl_3 \cdot 6H_2O$ visible absorption spectrum at five of the seven temperatures investigated. (The photographs taken at "reduced-pressure" temperatures were practically identical with those for which the nitrogen and hydrogen boiled at atmospheric pressure.) An effort was made to keep the exposures as nearly comparable in intensity

as possible. The pictures at room, liquid ethylene and liquid methane temperatures were taken under absolutely identical conditions as to crystal, position, exposure, etc., except for substitution of the proper liquid baths, but an increased transparency at lower temperatures made it necessary to shorten the exposure times when liquids nitrogen and hydrogen were used.

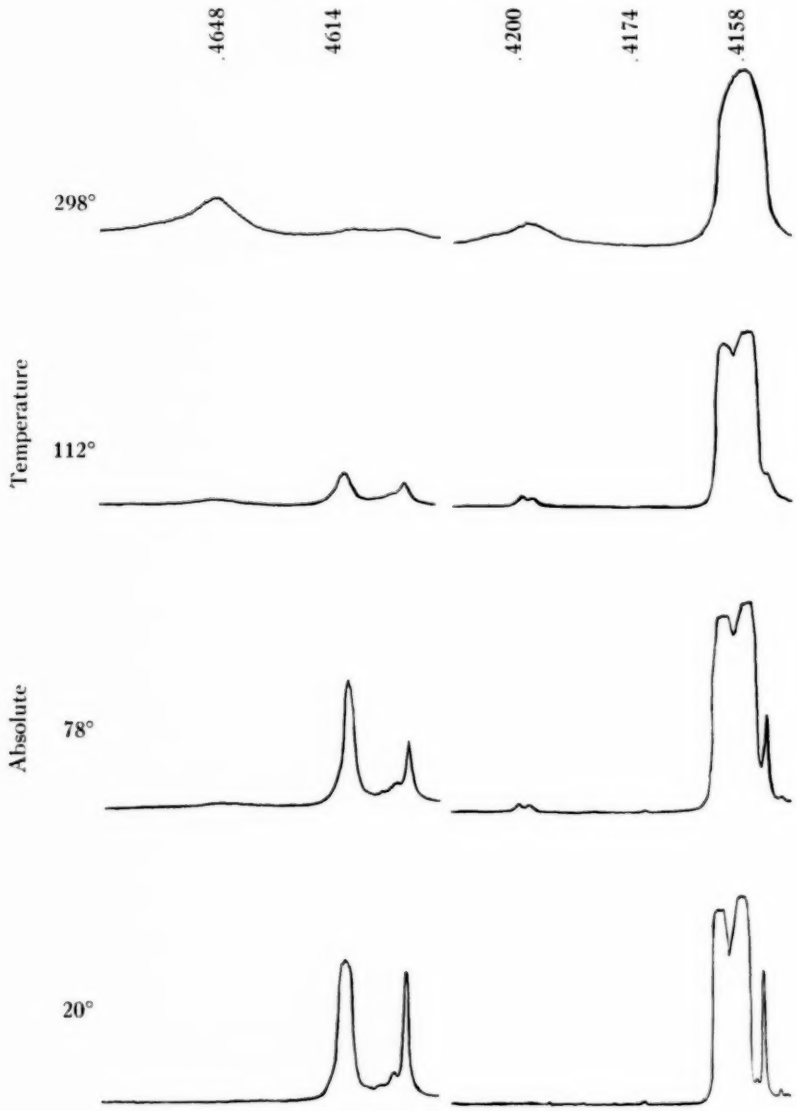

Fig. 3. Photometer curves.

Photometer curves of the two most outstanding multiplets of the visible region showing the decrease and increase of intensities are given in Fig. 3 for four temperatures. The ethylene curve is omitted because ethylene plates were found not to be comparable entirely in intensity under the high magnifi-

cation and sensitivity employed in photometering the plates. This is caused possibly by a slight absorption of the ethylene itself in these regions.

Table I gives measurements of the absorption lines and bands at four temperatures. Room and hydrogen temperatures are of interest as the extremes, nitrogen temperature because it is the lowest at which the "high-temperature" lines appear appreciably (offering their greatest sharpness), while ethylene measurements represent a temperature at which the high-temperature lines have greater intensity and still the increased definition of a low temperature. In fact the Boltzmann factor begins to cause rapid fading just below liquid ethylene temperature. Exact study of the methane-temperature absorption is of little interest because of the similarity to that occuring at nitrogen temperature.

TABLE I. *Single-crystal absorption lines and bands of* $SmCl_3 \cdot 6H_2O$.

H (Type) = high-temperature line; L (Type) = low-temperature line; HL (Type) = probably both types overlap; R.T., E.T., N.T., H.T. = columns of measurements for room, ethylene, nitrogen and hydrogen temperatures, respectively; Int. = columns of intensity, complete for hydrogen temperature but only occasionally filled for nitrogen temperature. Intensity is estimated roughly on a scale of 10, with very faint or doubtful lines given as 0; s, vs = degrees of increasing sharpness; d, vd = degrees of increasing diffuseness; b = broad line or band, most frequently found with bands; "2," "3" = possibly double or triple, respectively. Primed values represent band edges; c, centers.

Type	R.T. ν (cm^{-1})	E.T. ν (cm^{-1})	N.T. ν (cm^{-1})	Int.	H.T. λ(A)	H.T. ν (cm^{-1})	Int.
L			17095		5848.1	17095	1d
L			17156.3		5827.20	17156.2	3s
L			17230		5802.2	17230	1d
L					5720.9	17475	1b
L		17877	17875.8		5592.65	17875.7	5s
L	17905′	17908	17908.0		5582.55	17908.0	7s
L	17912′		18103		5522.4	18103	1d
L			18124		5516.00	18124.1	1s
L	18930′	18929	18927.0		5282.05	18926.7	7s
L	18939′	18938	18937.4		5279.15	18937.2	7s
L			19032		5253.10	19031.2	2s
L					5221.4	19147	0
L	20016′	20026	20024.5		4992.55	20024.2	6s
L	20050′	20044	20042.5		4988.20	20041.8	4s
L		20112′	20115.5		4969.90	20115.5	7s
L		20124′	20123.6		4967.7	20124	2d "3"
L		20170′			4964.1	20139	1d "3"
L			20192		4951.1	20192	0
L		20200′	20204		4949.1c	20200c	1d
L					4947.5c	20207c	1d
H	20239′	20248′					
	20274′	20265′					
L		20408	20404.5		4899.65	20404.0	2s
L			20520.2		4871.90	20520.1	3s
L		20547	20544.8		4866.05	20544.8	4s
L					4862.3	20560.7	0 "2"
L		20577′			4858.8	20574	0
L			20585.7		4856.40	20585.7	8s
L		20592′	20595		4854.3	20595	1d
L	20605′	20601′			4852.3′	20603′	8d
					4851.5′	20607′	
		20618′	20611		4849.5′	20615′	
L			20631′		4845.4	20633	2d
L					4843.5	20641	2d
L	20642′	20645′	20648′		4842.2	20646	2d
L					4839	20660	1d

TABLE I. (*Continued*)

Type	R.T.	E.T.	N.T.	Int.	H.T.		Int.
L					4837.	20670	1d
L					4832.	20690	1d
	20698′	20703′	20706′		4828.1′	20706′	
L					4827.2	20710	5d
L		20724′	20722′		4824.7	20721	9d
L					4822.3	20731	8d
	20739′	20738′	20736′		4820.7′	20738′	
L					4817.8	20751	1d
L					4816.0	20758	1d
			20770′		4813.4′	20769′	
L		20773′			4812.8	20772	9d
L					4811.3	20779	9d
	20784′	20788′	20782′		4810.5′	20782′	
			20811′		4804.3′	20810′	
L					4803.1	20814	8d
	20819′	20819	20822′		4799.7′	20829′	
			20836′				
L		20842′	20840		4796.9	20841	7d
L			20861		4793.8	20855	5d
L		20866′	20864′		4791.9	20863	5d
L	20895′	20892′	20893′		4787.4	20882	3d
					4784.9′	20893′	
L			20902		4782.7	20903	10d
					4781.3′	20909′	
L	20919′	20922′	20927		4778.4′	20922′	
			20935′		4775.3′	20935′	6d
L					4772.1	20949	1d
L					4766.0	20976	1d
	20992′	20985′	20980′		4763.4	20988	1d
H	21024′	21024′	21025′		4757.	21015	0
		21069′	21069′		4745.2′	21068′	
L			21074		4744.1	21073	8d
		21085′	21078′		4743.0′	21078′	
L	21104′	21109′	21108′		4735.9c	21110c	3d
L		21129′	21118′		4734.3c	21117c	3d
	21154′	21145′	21147′		4726.9′	21150′	
L					4726.1	21153	2d
			21161′		4725.1′	21158′	
		21168′	21175′		4721.5′	21174′	
L			21178		4720.3	21179	4d
	21189′	21183′	21182′		4718.8′	21186′	
		21205′	21209′		4713.9′	21208′	
L					4712.7	21213	2d
		21225′	21224′		4711.6′	21218′	
		21302′	21301′		4693.0′	21302′	2d
L	21329′	21340′	21314′		4691.5′	21309′	
H	21351′						
		21397′					
H	21423′	21426′					
H	21489′	21480′	21486′				
	21526′	21510′	21504′				
L		21517	21515.1		4646.65	21515.0	1s
			21536′		4642.1′	21536′	0
L			21548′		4640.2′	21545′	
			21607′		4626.2′	21610′	
L	21629′	21620′	21620′				8b
	21646′	21639′	21639′		4620.1′	21639′	
L			21649′		4617.8	21649	3d
L			21661.8		4615.15	21661.8	4d
L		21674′	21675.4		4612.25	21675.4	5d
	21684′	21685′					
L		21691	21690		4609.1	21690	8b
	21701′	21696′					
H	22066′	22073					
	22084′						

TABLE I. (*Continued*)

Type	R.T.	E.T.	N.T.	Int.	H.T.		Int.
L	22157′ 22169′	22153	22151.8		4513.25	22150.8	6s
L	22225′ 22237′	22227	22221.6 22228.8		4498.90 4497.45	22221.5 22228.6	2s 5s
L			22423.6		4458.50	22422.8	2s
L	22445′	22468	22466.9		4449.70	22467.1	6s
L	22494′	22488	22487.9		4445.55	22488.2	6s
L	22511′	22519′	22527.8		4437.75	22527.6	3s
L	22556′	22536′	22543.1		4434.8	22543	2d
L	22643′	22641′ 22658′	22645′ 22656′		4416.4′ 4414.5′ 4412.1′	22637′ 22646′ 22659′	8b
L	22675′				4409.4	22672	0
L					4405.1	22695	0
L L	22733′ 22762′	22729′ 22748′ 22758′ 22772′	22726′ 22739.6 22742′ 22763.6		4399.2′ 4396.35 4391.70 4391.1′	22725′ 22739.8 22763.8 22767′	6d 4d
L					4385.6	22796	1d
L L	22813′	22809′ 22824′ 22842′	22816.4 22838.1		4381.60 4377.50	22816.4 22837.6	4d 3d
L	22874′	22866′ 22885′	22876		4370.4	22875	1d
L	22922′ 22942′	22918′ 22926 22933′	22921.9		4361.45	22921.7	2d
L	22966′ 22984′		22965		4353.7	22963	1d
L			22995		4347.6	22995	3d
L		23017′	23023.8		4342.20	23023.4	2d
L		23033′	23058		4335.8	23057	2d
L	Very faintly present	23057 23086	23083		4331.1	23082	0
L		23118′ 23131′	23123		4323.5	23123	2d
H	23597′ 23653′						
H		23719					
H	23737′ 23753′	23738	23731.8	2s			
H			23778	1d			
H	23783′ 23802′	23786′ 23792 23806	23789.2 23804.9	4s 4s			
H	23824′	23811′	23840	0			
H		23857	23854	0			
H	23879′ 23902′	23879′ 23883 23901′	23881.5	1s			
H			23895.0	1s			
L			23912.3		4181.05	23910.8	1s
H			23928	1d			
L					4174.70	23947.0	2s
L		23951′	23949.8		4174.30	23949.5	3s
H		23973′	23973	1d			
H			23996	1d			
L					4165.30	24001.0	1d "2"
L					4162.85	24015.2	1d
L	24030′	24034′ 24039	24036		4159.4′	24035′	10b
L	24060′	24067	24051 24066		4156.1′ 4154.8′	24054′ 24062′	
L		24081			4152.7′	24074′	10b
L	24087′	24086′	24081		4152.7′ 4151.0′	24074′ 24084′	10b

TABLE I. (*Continued*)

Type	R.T.	E.T.	N.T.	Int.	H.T.		Int.
L					4149.65	24091.6	2s
L		24105	24102		4148.0	24101	6dw
L			24122.0		4144.45	24122.0	4s
L					4142.85	24131.1	2s
L		24136′	24140.6		4141.25	24140.4	4sw"2"
L		24152′	24152.1		4139.25	24152.2	2d"2"
L					4137.20	24164.2	1d
L		24174′	24173		4135.5	24174	2d
L		24190′	24189.8		4132.75	24190.3	2d
L		24209′			4129.4′	24210′	2d
			24213		4128.6′	24215′	
	24223′	24228′			4126.9	24225′	
L			24229		4125.9	24230	2d
					4123.8′	24243′	
					4122.4′	24251′	
			24255		4121.6	24256	2dw
L					4120.9′	24260′	
		24266′	24266		4120.2′	24264′	
L		24273	24273		4119.1′	24270′	2d
					4118.2′	24276′	
L		24282′			4118.1′	24277	2d
	24298′				4117.4′	24280′	
H			24310.1	2d			
L					4111.9	24316	2d
H	24325′	24331	24324.2	1s			
LH	24350′		24352.1	3d	4105.4	24351	2d
L					4104.3′	24358′	2d
					4103.1′	24365′	
H			24367.1	3d			
	24377′	24372′					
		24375					
HL		24384	24381.7	3d	4100.2	24383	2d
H		24388′	24395.5	1d			
HL	24408′	24411	24408.6	3d	4096.3′	24405′	1d
					4094.1′	24418′	
HL	24434′	24428	24424.7	3d	4091.5′	24434′	1d
H		24444	24440.7	3d	4090.1′	24442′	
H			24457.8	1d	4087.8′	24456′	1d
HL			24472.0	1d	4086.1′	24467′	
			24489′				
H		24503	24499	1dw			
			24508′				
			24514.0	1d			
L	24541′	24536′	24537.3		4074.30	24537.3	8sw
L	24558′	24552′	24544.5		4073.20	24543.8	8sw
L		24570	24568.6		4069.15	24568.1	4s
L		24589	24586.2		4066.20	24586.0	4s
L	24613′	24619	24617.1		4061.10	24616.9	10sw
L		24637	24634.6		4058.15	24634.8	10sw
L	24644′	24654	24652.8		4055.15	24653.0	10sw
L					4054.85	24654.9	1s
	24675′	24681′	24674′				
H		24690′	24687	3d			
H			24699	4d	4048.1′	24696′	
H	24709′		24717	1d"2"			
H			24732	1d"2"	4043.1	24727	0
					4042.1′	24733′	
H	24740′	24745′	24747	4d	4040.4	24742	0
H			24759	5d	4037.9	24758	0
?					4036.1	24769	0
?	24768′	24775′	24772′		4034.6	24778	0
L					4031.50	24798	1d

TABLE I. (*Continued*)

Type	R.T.	E.T.	N.T.	Int.	H.T.		Int.
L	24805	24805′			4029.75	24808	1d
			24823′		4027.8′	24821′	
L	24830′		24827		4027.2	24825	7d
L			24846		4023.8	24845	7d
			24850′		4022.9′	24850′	
?			24864.9				
L			24876.7		4018.70	24876.7	5d
			24890′		4016.9′	24888′	
L			24896		4016.2	24892	10b
L			24950		4007.2	24948	
			24953′		4006.5′	24953′	
					4005.6′	24958′	
L			24965		4004.8	24963	5d
					4003.9′	24969′	
L	24975′	24978′	24984		4001.40	24984.1	3s
L			24996		3999.35	24996.9	2d
L			25006′		3997.65	25007.8	4s
			25007.6				
L			25018.3		3995.90	25018.5	4s
L	25020′	25026′	25024		3994.70	25026.1	3d
L			25033′		3993.7	25033	3d
L			25047.9		3991.30	25047.6	3d
		25068′	25067′		3988.5′	25065′	
L					3987.45	25071.7	3d
L		25074			3986.40	25078.1	3d
		25079′	25080′		3985.9′	25081′	
L	25090′				3984.90	25087.8	2s
L		25101′	25097		3983.35	25097.5	3d
L			25107		3981.70	25107.7	4d
			25114′		3980.8′	25114′	
L					3980.0	25119	5d
	25120′	25123′	25123′		3979.1′	25125′	
		25140′					
L		25145	25145.3		3975.70	25145.7	5d
		25153′					
L					3973.8	25158	2d
	25195′	25191′	25188′		3969.1′	25187′	
L		25199			3968.5	25191	7d
		25207′	25201′		3966.6′	25203′	
		25219′	25221′		3963.8′	25221′	
					3963.0′	25226′	4d
L	25235′	25229′	25233′		3962.1	25232	4d
L			25250		3959.1	25251	3d
L			25275′		3955.4′	25275′	
L					3954.4	25281	2d
			25284′		3953.2′	25289′	
L			25326.8		3947.30	25326.6	2s
L	25335	25331	25335		3945.5	25338	1d
L		25361′	25360.6		3942.20	25359.4	2s
L	25368′	25368	25370		3940.2	25372	1d
	25380′	25374′					
L			25422′		3932.50	25422.1	2s
			25430′				
L			25439′		3929.5	25441	1d
			25445′				
H	25475′	25479′	25486	3d	3921.5′	25493′	0
H	25500′	25505′	25501	3d	3918.9′	25510′	
L	25520′	25525′	25527.2		3916.35	25526.7	5sw
L	25548′	25543′	25537.5		3914.80	25537.0	4s
L					3912.3	25553	1d
	25575′	25567′	25570′		3909.6′	25571′	
L					3909.1	25574	3d
		25588′	25580′				
	25600′		25593′		3906.2′	25593′	

TABLE I. (*Continued*)

Type	R.T.	E.T.	N.T.	Int.	H.T.		Int.
		25622′			3901.7′	25623′	
L	25630′		25626.2		3901.20	25625.9	4d
	25647′	25643′	25637		3899.1′	25640′	
L					3897.90	25647.4	1s
L			25658		3896.25	25658.5	2s
L	25670′	25669′	25671.2		3894.35	25671.0	5s
		25673					
L		25686	25684.6		3892.30	25684.5	4s
	25692′	25691′					
		25715′					
L	25720′	25723	25719.5		3887.00	25719.4	5d
L		25733	25730.3		3885.45	25729.9	5d
	25750′	25738′					
	25790′	25788′					
L		25791	25786.8		3877.00	25786.0	4s
L		25805	25799.8		3874.90	25799.8	4s
L		25810′	25807		3874.00	25805.8	3d
L	25825′		25822.1		3871.65	25821.4	2d
L					3868.0	25846	0
L					3865.0	25866	0
H	26310′						
	26342′						
H	26395′	26406′	26394	0			
H	26430′	26425′	26409	1d			
L			26423.3	2d	3783.60	26422.5	2s
H			26437	0			
H			26453	1d			
HL	26457′	26468	26467.8	2d	3779.2′	26453′	1wd"2"
					3776.3′	26474′	
H	26490′	26488	26482.9	2d			
H		26513	26510.5	3d			
H		26526	26524.8	3d			
HL		26544	26541.5	3d	3767.7′	26534′	1dw
H	26553′	26558	26556.3	3d	3765.0′	26553′	
H			26570	1d			
	26600′	26609′	26608′		3756.85′	26610.3′	
L			26611		3756.35′	26614.2′	8s
L					3756.35′	26614.2′	8s
L		26624′	26618		3755.75′	26618.3′	
	26630′	26629	26620′				
L			26627.1		3754.60	26626.5	9s
	26657′	26657′	26659′		3749.5′	26663′	
L		26664			3749.1	26666	10d
		26670′	26670′				
L		26682c	26680		3747.4	26678	10d
			26682′		3747.0′	26681′	
L	26688′		26690.7		3745.65	26690.2	5s
L		26704	26700.9		3744.20	26700.4	6s
L			26714.3		3742.25	26714.4	5s
L	26725′	26722"2"	26727.6		3740.55	26726.4	2d
L		26747	26744.0		3738.20	26743.2	3s
L		26768	26764.4		3735.25	26764.3	5s
L	26775′		26775.2c		3733.75	26775.2	5s
L		26782	26780.9c		3733.00	26780.5	5s
L	26795′				3730.50	26798.3	1s
L	26820′	26815	26816.3		3728.05	26816.2	2d
L			26838		3725.10	26837.5	1d
L	26856′		26856.4		3722.40	26856.7	2d
L		26874	26869.4		3720.80	26868.5	4s
L	26877′		26884		3718.6	26884	0
L					3717.4	26893	0
L		26907	26906		3715.65	26905.6	4s

TABLE I. (*Continued*)

Type	R.T.	E.T.	N.T.	Int.	H.T.		Int.
L			26931′				
L			26933.4		3711.80	26933.6	4dw
L		26935′	26937.7		3711.25	26937.4	2d
		26939	26940′				
		26944′					
	26950′						
L		26957	26954.3		3708.90	26954.5	4s
L			26967.9		3707.10	26967.8	2s
L	26980′				3705.55	26979.1	1s
		26993′					
L		27001	26999.1		3702.80	26998.9	3d
	27012′	27010′					
L			27013.7		3700.6	27014.8	2d
L					3698	27035	0
L					3695	27055	0
			27076′				
L			27092′		3691	27085	0
	27120′	27124′	27129′		3684	27135	0
H	27160′	27141′			3679	27175	0
	27210′		27203′		3673	27220	0
H	27262′	27256′	27261′				
	27295′	27280′	27276′	1b	3665	27275	0
?			27303	0	3662	27300	0
L	27340′	27334′	27333.2		3657.55	27332.9	3s
L	27362′	27348′	27344.8		3656.00	27344.4	7s
L		27378	27374.1		3652.00	27374.4	3s
H			27392	1s			
HL	27410′	27411	27412.8	4s	3646.80	27413.4	2s
HL		27432c	27431.1	4s	3644.1	27434	1d
H	27443′	27450′	27445.9	4s			
H		27466′	27466.0	1d			
H		27487′	27480	1d			
		27511′	27519′		3632.6′	27521′	
		27548			3629.1′	27542′	
L	27557′	27556	27553				9d
					3627.5′	27559′	
L		27571	27569c		3626.8′	27565′	9d
	27585′	27576′			3625.4′	27575′	
L		27594	27591.4		3623.30	27591	9d
	27610′	27608′	27606′		3622.0′	27601′	
L					3621.4	27606	
L		27614	27615		3620.3	27614	6d
L		27634	27629		3618.2	27630	9d
	27638′	27647′	27640′		3617.6′	27635′	9d
L		27663′	27668′		3616.3	27645	3d
					3613.5′	27666′	
L	27685′	27681′			3612.8	27671	6d
L		27688			3610.7	27688	8d
L		27708			3608.2	27707	8d
	27715′	27714′					
L					3605.9	27724	6d
			27726′		3605.6′	27727′	
L		27748′	27743		3603.50	27742.9	6d
L	27765′		27761′		3600.80	27763.8	3d
L			27764		3599.60	27773.1	2d
L		27771′	27783		3598.25	27783.2	3d
		27787′	27785′				
L	27795′		27795		3596.65	27795.8	2s
L			27806		3594.8	27810	1d
		27822′	27821′				
L			27826		3592.90	27824.7	2d
L		27840′	27832′		3592.0	27832	2d
L			27861		3588.2	27861	2d
L			27881		3585.6	27881	2d
L	27895′	27890′	27896′		3583.0c	27902c	3d
L	27910′	27912′	27910′		3582.1c	27909c	2d

TABLE I. (*Continued*)

Type	R.T.	E.T.	N.T.	Int.	H.T.		Int.
L			27933		3578.95	27933.3	2d
L			27961		3575.2	27963	1d "2"
L					3571.6	27967	1d
H		28003					
L					3466.0	28034	0
H	28045′	28043			3563.7	28053	0
	28068′				3561.3	28072	0
H	28100′	28097′	28094′				
	28123′	28118′	28121′				
L	28162′	28164	28161.3		3550.00	28160.8	3s
	28183′						
L			28198		3545.3	28199	1d
L			28236′		3541.0	28233	1d
L			28246′		3539.8	28242	1d
L	28250′	28258′	28256.9		3538.05	28256.2	4s
L		28264	28264.5		3537.05	28264.2	4s
L	28278′	28270′			3533.9	28290	0
L					3532.2	28303	0
	28320′	28319′					
L		28324	28322.2		3529.75	28322.5	5s
L	28340′	28328′	28334.5		3528.45	28333.2	1s
L			28662.4		3487.93	28662.1	2vs
L		28669	28667.8		3487.34	28667.0	3vs
L					3485.9	28679	0s
L		28694	28691.3		3484.49	28690.4	3vs
L					3482.8	28704	0
L			28719.8		3481.05	28718.8	3vs
L		28732	28733.2		3479.34	28732.9	2vs
L			28745		3478.25	28742.0	1s
L			28760		3475.50	28764.7	1vs
L		28768′	28772.2		3474.58	38772.3	2vs
	28780′	28797′					
H		28827′	28833.9	0			
H	28852′		28845	0			
L			28856.4		3464.55	28855.5	4s
L			28877		3462.3	28874	0
	28882′	28885′					
L			28894.3		3460.00	28893.7	5s
		28906′					
L		28928′	28926.9		3456.10	28926.2	4d
L	28933′		28939c		3454.6	28939	5d
L			28949c		3453.6	28947	5d
	28962′	28957′					
L		28990	28990		3448.50	28989.8	6d
L					3446.7	29005	1d
	29027′	29020′	29023′		3444.6′	29023′	
L			29027.7		3444.05	29027.3	6d
L			29040.8		3442.50	29040.4	6d
	29053′	29052′	29048′		3441.7′	29047′	
L		29081	29078		3438.2	29076.7	6d
L			29102.1		3435	29104	0
L			29125.4		3432.45	29125.4	1d
L			29138		3430.9	29139	2d
L		29152	29151		3429.3	29152	3d
L	29166′				3428.1	29162	2d
L	29189′	29184	29186		3425.4	29186	2d
L			29206		3422.9	29207	1d
L	29221′		29220.7		3421.30	29220.3	1d
L		29239′	29237		3419.3	29237	1d
	29248′		29256′		3417.2′	29255′	
L					3416.9	29258	3d
L	29264′				3415.9	29266	3d
	29285′	29272′	29270′		3915.6′	29269′	
L					3412.0	29300	1d

TABLE I. (*Continued*)

Type	R.T.	E.T.	N.T.	Int.	H.T.		Int.
L	29324′ 29349′	29316′ 29342′	29316′ 29356′		3410.4′ 29314′ 3407.5′ 29339′ 3406.4′ 29348′		1b
L					3402.4	29383	1d
L			29641.1		3372.85	29640.0	4s
L	29654′ 29674′	29655	29656.3		3371.10	29655.5	3s
H	29817′ 29858′						
H	29883′ 29906′						
LH	29961′		29969.8		3335.90	29968.1	4s
L	30000′ 30037′	30038′ 30047	30043′ 30048′		3327.50	30044.2	7d
L		30058′	30055 30056′		3326.50	30052.9	5d
L	30101′	30082	30076′ 30081′		3324.00	30075.8	7d
L			30137′		3317.15	30137.9	3s
L			30153′		3316.25	30145.8	3s
L			30198′		3310.30	30200.1	4s
L		30203	30205′				
L	31138′ 31157′		31141.7		3210.40	31139.8	6s
H	31197′ 31201′						
H	31233′ 31252′						
H	31283′ 31301′	Not photo-graphed					
L	31346′ 31365′		31345′ 31352′		3189.5′ 31344′ 3189.0′ 31349′		10d
L			31377.3		3186.20	31376.1	8s
L	31389′ 31405′		31385′ 31386′ 31392′		3185.4′ 31384′ 3185.2′ 31386′ 3185.0′ 31388′		10d
L	31418′		31416′ 31417.3		3182.3′ 31415′ 3182.10 31416.5		9s
L	31438′		31420.5 31423′		3181.90 31418.5 3181.8′ 31420′		9s
L			31444′		3179.30	31444.5	9d
L	31449′		31445.5		3178.70	31450.3	9d "2"
L	31462′		31453.0 31455′				
L	31492′		31479′ 31487′		3175.7′ 31480′ 3175.3′ 31484′		9d "2"
L			31549.6		3168.90	31547.5	5d
L			31564.4		3167.55	31561.0	4d
L			31576.7c 31581.2c		3165.85	31578.2	3d
L	31592′ 31646′		31588′ 31599′ 31635′		3164.8′ 31588′ 3133.7′ 31599′ 3160.9′ 31627′		10b
H	32532′ 32553′						
H	32573′		32581.1				
H	32592′		32592.3				
L	32696′		32698.0		3057.60	32696.1	10s
L	32713′		32739.6		3053.70	32737.5	5s
L	32755′ 32774′		32752′ 32767′		3052.4′ 32752′ 3051.2′ 32764′		10b
H	33503′ 33512′				Not photographed		

TABLE I. (*Continued*)

Type	R.T.	E.T.	N.T.	Int.	H.T.	Int.
	{33524′					
H	{33541′		33538.8			
L	{33695′		33700.8			
L	{34392′		34386.7			
	{34407′					
L	{34421′		34425.7			
	{34436′					
L	{34472′					
L	{34486′		34486			
L	{34510′		34513			
H	{35689′					
	{35719′					
L	{35782′		35790.3			
	{35805′					
L	{35846′		35853.1			
	{35868′					

From measurements of seven nitrogen and three hydrogen plates in a region where the lines are fairly sharp it has been found that because of the nature of the lines and the low magnification used in measuring them it is difficult to expect results to be accurate within less than 0.05A. Band edges and more diffuse or faint lines cannot be given even to this accuracy. As a result of measurements of the best parts of two plates at each temperature, with confirmation by sharp lines of others, we have the figures as quoted in the table. Wave numbers are given, with wave-lengths for hydrogen temperature only. Figures are quoted to units or tenths of units (cm^{-1}) according to the accuracy thought possible. Intensities are estimated for hydrogen temperature only, except for an occasional nitrogen-temperature line which does not appear at hydrogen temperature, i.e., a high-temperature line. These intensities are very roughly determined on a scale of ten and represent the appearance of the lines on our plates. They are meant only for rough comparison and consequently are not to be used from one region of the spectrum to another. It will be noticed that only the most intense lines have appeared in the ultraviolet region. This is probably due to the fact that much thinner crystals were used in that part of the investigation.

DISCUSSION OF RESULTS

Effect of temperature on the positions of lines and multiplets

In general the centers of the multiplets shift to the red with decreasing temperature. At the same time the separations of the lines within the multiplet become greater, so that, although most of the lines are shifted to the red, occasionally one on the high-frequency side is shifted to shorter wave-lengths. The shift in either direction is small, rarely over 5 cm^{-1}, certainly not over 10 cm^{-1}, and takes place mostly above liquid nitrogen temperature. These results are in good accord with those already reported for gadolinium compounds.[6] Such shifts are probably caused by effects discussed in the

[6] Freed and Spedding, Phys. Rev., reference 2.

previous report, briefly, the contraction of the crystal which brings the neighboring ions closer to the samarium ions and thus increases the field acting on them. This would result in a greater spreading of the levels, just as an increased external electric field would. The closer approach also would be expected to affect the higher excited levels more than the deeper basic level, so that the multiplets would be shifted to the red. This effect is again demonstrated by the fact that the red shift of the multiplets is greater for the high-energy levels which cause the ultraviolet lines, than it is for the levels that are responsible for the lower-energy multipets to the red.

Width of lines

At liquid hydrogen temperature the lines can be divided into three classes: (1) broad sharp lines which are undoubtedly narrow multiplets with intense outer components; (2) fine sharp lines, relatively few in number, which are probably truly single; and (3) narrow diffuse bands which are also unresolved multiplets but whose edges are either faint or whose levels are not constant over the time of photographic exposure. (A similar effect of temperature is discussed for wider multiplets.) In the table these are designated respectively, by s, vs and d. In addition wide bands are indicated otherwise.

As the temperature is increased all these lines become broader and more diffuse at the edges. The higher the temperature the more pronounced the effect, with the result that at room temperature most of the multiplets have merged into broad diffuse bands. These facts are also in good accord with the theory that the multiplets are caused by the electric fields of the neighboring ions. At low temperatures the oscillating movement of the neighboring ions would be absent and the magnitudes of the fields fairly constant during the length of the photographic exposure. As the ions begin to move at higher temperatures the fields vary correspondingly, and at one instant the levels might be split but slightly, while at the next, a momentarily increased field would cause wider separations. The photograph registers the integrated effect over a large time interval, which appears as a blurring of lines.

Effect of temperature on the intensity of lines

The lines can be alternatively divided into three groups on the basis of their intensity changes with temperature.

(1) A large group, present on every plate, increase in intensity as the temperature is lowered. This group can be divided into two subgroups: in one the lines are located in the violet and ultraviolet and show very little intensity change, while in the other, which is situated between 6000 and 4320 A, a marked intensity change with temperature is observed.

(2) Many fainter lines appear on the violet sides of the multiplets. These are weak at hydrogen temperature and rapidly fade out as the temperature is raised.

(3) A group of lines located on the red side of each multiplet are absent at 20°K but appear at all higher temperatures, usually increasing in intensity with the temperature. A few, however, pass through a maximum and then decrease in intensity as the temperature is raised, for reasons which shall appear later.

The first group, which we call a low-temperature group, consists of lines which originate from transitions between the basic level and excited higher ones.[7] The lines of the second group are probably similar in origin to the first group but are fainter because of low transition probabilities.

The lines of the third group, which we term high-temperature lines, originate from transitions between several low-lying levels situated in groups separated from the basic level by about 160, 210 and 300 cm^{-1}, etc., and the same high excited levels that cause the low-temperature lines.

The intensities of both of these groups of lines will depend in part on the population in the lower levels, and this in turn will be governed by the Boltzmann factor. At hydrogen temperature the number of ions of energy corresponding to the excited lower levels will be extremely small, and consequently the lines originating from these should be absent. At liquid nitrogen temperature and higher these high-temperature lines are permitted by the Boltzmann factor and should increase in intensity. As the population in the excited lower levels increases, that of the basic level, and consequently the intensities of the lines arising therefrom, should decrease.

A factor which tends to mask the intensity changes of the low temperature lines is their great intensity. Certain strong lines and bands may be completely absorbed before the light has penetrated the whole path through the crystal. Consequently, a change in intensity would not be noticed.

The intensities of the lines depend also on the transition probabilities, which are not entirely independent of temperature in solids. In the case of the group of multiplets between 6000 and 4320A this may be responsible for the great decrease in intensity, which is enough to make some of these multiplets almost disappear at room temperature.

Probably another factor aiding this abnormal decrease in intensity is the fluctuation of the crystal field at high temperatures previously mentioned. Under such conditions the coupling between the lattice and the orbits of the electrons or between the orbital and spin momenta of the electrons may be broken, especially in the final higher levels, and many of these levels may thus become potentially unstable, just as many similar levels do in the case of diatomic molecules. An electron jumping to one of these unstable levels would not be sharply quantized and would give rise to a continuous absorption. This

[7] This basic level may be nondegenerate up to about 20 cm^{-1}, since it would be necessary for us to go to liquid helium temperature to detect the change in population between levels of this separation. It is possible to look for levels of this sort in the position of the lines themselves. However, since the separations of the sub-levels composing the "basic level" appear to be fairly small multiples of our error in measurement and because such separations frequently cause the lines to be wide or diffuse and are often unresolved, such levels would be very uncertain. Nevertheless, as we shall show in the paper on the conglomerate spectra, a degeneracy covering about five inverse centimeters is highly probable.

is observed to cause a continuous "general" absorption, which has already been mentioned to occur at high temperatures and which makes necessary at room temperature almost twice the exposure required at hydrogen temperature to secure the same blackening of the plate.

On the basis of the explanations given above for the intensity changes of the absorption lines it would appear possible to construct an energy level diagram for Sm IV. However, in the conglomerate spectra many additional lines appear or faint ones are intensified, with the result that more complete and convincing evidence is presented therein for the existence of the various lower levels we have postulated. Consequently a more complete and exact account of the various separations observed between the corresponding high- and low-temperature lines follows in the second paper of this series.

Absorption Spectra of the Samarium Ion in Solids. II.* Conglomerate Absorption of $SmCl_3 \cdot 6H_2O$ and a Partial Energy Level Diagram of the Sm^{+++} Ion as It Exists in Crystalline $SmCl_3 \cdot 6H_2O$

By FRANK H. SPEDDING[1] AND RICHARD S. BEAR
Chemical Laboratory, University of California

(Received July 22, 1932)

Additional lines of the $SmCl_3 \cdot 6H_2O$ absorption spectrum obtained from conglomerates of crystal fragments are reported for four temperatures between 20° and 300°K. These new lines, along with ones previously reported for single-crystal absorption, are used to establish the existence of excited lower levels situated at 145, 160, 204, 217, and roughly 300 cm^{-1} above the basic level. It is probable that there are other levels more than 400 cm^{-1} above the basic one. Two components of the 300 level, at 295 and 315 cm^{-1}, are thought to be present, and there are indications that the other levels, particularly the basic one, may be complex.

IT HAS been shown previously[2] that for rare earth salts the absorption or "reflection" spectra of conglomerates of small crystals are almost identical with the spectra obtained from single crystals. The chief difference is an enhancement of the fainter lines, many of which are consequently observed for the first time in the conglomerate absorption. This is brought about by the fact that the effective path length of the ray of light of frequency corresponding to that of the absorption is very much greater in the conglomerate case. The increased refractive index of the crystal fragments for such a wave-length causes the beam, once it has entered the solid, to be totally reflected, on the average, a great number of times before it strikes the surface at such an angle that it can emerge. As might be expected, the lines seem to be shifted slightly to the red. This shift is small, however, and is about of the order of our error in measurement. Comparison of Fig. 1 and the corresponding reproduction of the single-crystal spectrum in the first paper of this series[3] shows that the conglomerate also causes quite an increase in intensity of *all* lines not already completely absorbed, which is in agreement with the above explanation.

Because of its enhancement of faint lines and disclosure of new ones, the conglomerate absorption is a very valuable addition to that of the single crystal and contributes much to the determination of the energy levels of the ion in the solid. Unfortunately the conglomerate spectra are not sufficient in themselves because of the excessive enhancement and consequent blurring of large regions of the spectrum.

* Contribution from the Chemical Laboratory of the University of California.
[1] National Research Fellow in Chemistry at the University of California.
[2] Spedding and Bear, Phys. Rev. **39**, 948 (1932).
[3] Spedding and Bear, Phys. Rev. **41**, 58 (1932).

Experimental Part

The conglomerates employed were prepared from small single crystals and fragments by crushing these to a size of smallness sufficient to allow close packing in glass cells without reduction to a powder. The cells varied in thickness from 4 mm to 1 cm and were substituted for the single crystals in the apparatus described in the preceding paper. In general, the thicker layers composed of finer crystals brought out the greatest number of new lines, but this could not be continued indefinitely. Beyond certain limits the exposures required in photographing the spectra became of unreasonable and impossible length. A compromise between thickness of conglomerate and time of

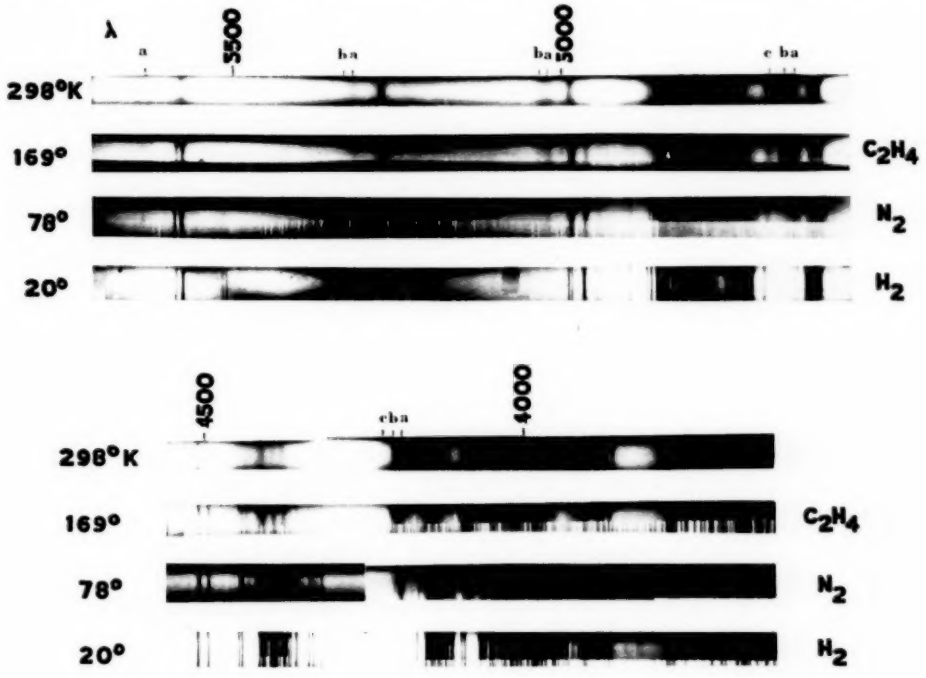

Fig. 1. Conglomerate absorption of $SmCl_3 \cdot 6H_2O$. The substances at whose boiling points the spectra were photographed are indicated on the right, the corresponding temperatures on the left. The small letters indicate various high-temperature lines of importance as explained in the text.

exposure had to be made. This varied with the region of the spectrum and the temperature, making it necessary to photograph conglomerates of several thicknesses and to use the parts of the plates which turned out to be most satisfactory.

In Table I we have given the positions of the new lines as they were observed to appear in the conglomerate absorption spectra at four temperatures. The large number of lines given in the preceding paper is not repeated here, as the wave-lengths in both types of spectrum are practically the same. Only for some of the sharp lines could differences be detected, in which cases

TABLE I. *New absorption lines of $SmCl_3 \cdot 6H_2O$ disclosed by conglomerates.*

H (Type) = high-temperature line; L (Type) = low-temperature line; HL (Type) = probably both types are present; R.T., E.T., N.T., H.T. = Columns of measurements for room, ethylene, nitrogen and hydrogen temperatures, respectively; f, vf, vvf = degrees of decreasing intensity; s, vs = degrees of increasing sharpness; d, vd = degrees of increasing diffuseness; b = broad, frequently used for bands; # = line or band appearing more distinctly in conglomerate than in single-crystal spectrum, hence repeated; incl. = the conglomerate band includes lines and bands formerly given and still approximately correct. Primed values indicate band edges; c, centers.

This table is chiefly a supplement to the single-crystal one. Lines or bands appearing only at one temperature may have been given in the former table for other temperatures. Lines with no intensity designation are quite distinct and have approximately the intensity 1 or 2 on the scale of the former table.

Type		R.T. ν(cm^{-1})	E.T. ν(cm^{-1})	N.T. ν(cm^{-1})	Character	H.T. λ(A)	H.T. ν(cm^{-1})	Character
H		16783′ 16803′						
L				17128.8	s	5837.0	17127	s
L			17154′ 17162′					
L				17251.8	s	5795′ 5734′	17250′ 17432′	Many doubtful lines
			17469′					
L			17480′	17475	d	5720.9	17475	d
H				17659	vvf			
H				17672	vvf			
H				17692	vvf			
H				17703	vvf			
H		17709′	17712′ 17723′	17716.3	s			
H		17727′	17732′	17730.6	s			
H			17744′	17748.6	s			
H			17768′	17763.1	s			
H				17848	d			
L		17872′ 17887′						
L		17902′						
L	#	17920′				5579.5	17918	f
L				17938	f	5572.4	17941	f
L				17954	f	5567.4	17957	f
L				17975	f	5561.4	17976	f
L				17991	f	5557.2	17990	f
L						5551.5	18008	vf
L						5546.2	18025	vf
L						5539.5	18047	vf
L						5536.7	18056	vf
L						5533.6	18066	vf
L						5530.2	18078	vf
L						5527.3	18087	vf
L						5520.1	18111	vf
L						5511.4	18139	vf
L				18197	fd	5495.5	18192	fd
L						5487.7	18218	vf
H		18720′ 18737′	18705′ 18733′					
H		18766′	18765′	18768.0	f			
H				18780.4	f			
H		18784′	18791′	18792.2	f			
L				18971	fd	5269.5	18972	fd
L			18998	18994.9	fs	5263.35	18994.1	fvs
L						5262.05	18998.8	fvs
L		19005		19016.3	fvs	5257.45	19015.4	fvs
L		19026	19023	19021.0	fvs	5255.90	19021.0	fvs
L			19031′ 19041′					

TABLE I. (*Continued*)

Type	R.T.	E.T.	N.T.	Character	H.T.		Character
L			19070	fd	5242.9	19068	f
L			19084	f	5238.5	19084	f
L			19097	fd	5235.0	19097	f
L					5232.0	19108	f
L			19146	vfd	5229.1	19118	f
L					5226.3	19129	f
H			19811	vfd			
H		19825′ 19834′	19825	f			
	19837′ 19868′						
H			19865.5	f			
H		19881′ 19887′	19882.7	s			
H	19898′ 19915′	19897′ 19805′	19897.0	s			
			19925′ 19945′	vf			
H		19953′ 19978′	19956′ 19981′	vfb			
HL			20070′ 20078′	vvfb	4982.6c	20064c	vvf
HL			20088′ 20097′	vvfb	4975.9c 4972.1	20091c 20107	vvf
L			20136	d			
L					4960.0c	20156c	vvf
L					4954.8c	20177c	
		#20194′ 20207′					
			20218	f	4949.5′	20213′	vfb
			20230	f	4940.5′	20235′	
			20246	d			
H		#20242′ 20253′ 20267′					
			20259	d			
H			20280	vf			
H			20299	vf			
H			20328	vf			
H	20359′		20361	f			
H			20386	f			
H	20432′		20421	fd			
H		20517′ 20527′					
L							
L			21356′ 21393′	fb	4676.2′ 4673.2′	21379′ 21393′	fb
			21474′		4654.1	21480	vfs
		#		db	4651.4	21493	vfs
			21514′		4648.30	21507.2	s
			21553′				
					4613.2′	21671′	
L					# 4610.0′	21686′	db
					4606.1′	21704′	
					4598.7′	21739′	
L			21773′ 21789′	vfb	4592.1′ 4588.5′	21771′ 21787′	vfb
L			21826′ 21839′	vfb	4580.5′ 4577.8′	21825′ 21839′	vfb
	to next band 21843′						
L			21887	vf	4567.3′	21889′	vfb
L			21898	vf	4565.3′	21898′	
L			21950′ 21968′	vf	4552.9′ 4550.4′	21958′ 21970′	vfb
H	21991′		21994	d			
H	22016′		22006	d			
H			22069	d			
H			22082	d			
H			22172	vf			
H			22190′ 22203′	vfb			

TABLE I. (*Continued*)

Type	R.T.	E.T.	N.T.	Character	H.T.		Character
L			22248′	vf	4493.5	22248	vf
L			22263′		4491.0	22260	vf
L					4488.4	22273	vf
L			22303	vfd	4482.4	22303	vf
H	22309′		22327	vf			
H	22337′		22341	vf			
H	22374′		22384	vf			
H	22402′		22399	vfd			
			22567′	fd			
L			22577′		4429.0	22572	d
L		22599′	22592′		4424.5	22595	d
L					4420.7	22615	d
		incl.	22626′		4418.6′	22625′	
L		#			#4416.4′	22637′	b
			22669′		4411.5′	22662′	
		22681′	to next band				
L					4400.85	22716.5	s
L		22960′					
		22979′					
L	23126′				4327.6	23101	d
L	23144′				4318.9	23148	d
H			23272	vf			
H			23282.9	s			
H	23352′						
	23387′						
H	23507′						
	23535′						
H	# 23589′						
	23612′						
H	# 23629′	23621′					
	23651′	23647′					
H			23717	fd			
H			23750	fd			
H			23761	fd			
H			23823	fd			
H			#23840	f			
H			#23852	f			
L		23907′					
		23921′					
	23943′	23948′					
L		23953					
	23966′	23957′					
		24019′					
L		incl.					
	to next bd.	24108′					
	24160′						
L					4133.15	24187.8	s
L					4132.55	24191.3	s
L					4127.45	24221.2	s
L					4122.45	24250.7	s
L					4121.55	24256.0	s
L					4120.6	24262	d
L					4118.60	24273.2	s
L					4117.85	24277.6	s
L					4116.80	24283.8	s
L					4116.15	24287.7	s
L					4112.9	24307	d
L					4109.40	24327.7	s
L					4108.30	24334.0	s
		24349′					
H		incl.					
					4100.7′	24379′	
L					4099.5′	24386′	fb
					4098.4′	24393′	
		24482′					

TABLE I. (*Continued*)

Type	R.T.	E.T.	N.T.	Character	H.T.		Character
L					4071.40	24554.7	s
L					4070.90	24557.7	s
L					4070.30	24561.3	s
L					4067.60	24577.7	s
		24609′			4061.8′	24613′	
L					# 4061.35	24615.4	intense
L					4060.65	24619.7	intense
					4060.3′	24622′	
L					4054.00	24660.1	s
L					4052.35	24670.2	s
L		incl. 25163′			4050.55	24680.9	s
L		25419′ 25448′					
L			25646.2	f			
L					3854.9	25934	fd
		25960′			3850.2′	25966′	fb
		25994′	25992	bd	3845.2′	25999′	
L			26041	fd	3839.5	26038	fd
L			26070	vfd	3835.2	26067	fd
L		26104′	26097′		3830.3	26100	d
L				fd	3828.50	26112.4	s
		26131′	26120′				
H		26205′ 26226′					
H		26263′ 26274′					
H		26309′ 26324′					
H		26391′ 26424′					

the average shift was about 0.3 wave number to the red. This is about the error of measurement for sharp lines, and of course is even less important for diffuse or broad lines and bands.

In the violet, where the multiplets of greatest intensity are located, the conglomerates cause even greater absorption. The result is a blurring of the multiplets into wide bands which make it impossible to examine very accurately the absorption occurring beyond about 3700A. (No ultraviolet investigation of the conglomerate absorption was undertaken, mainly because of the long exposures required.)

DISCUSSION OF RESULTS

Most of the new lines which are reported here belong unmistakably to one or the other of two classes. Some owe their low absorption coefficients to the small population in the lower levels producing them and are usually found on the red sides of the more intense multiplets. They thus resemble (and are) "high-temperature" lines (see the first paper of this series[3]), being similar to them in all ways. Lines of a second class have low absorption coefficients because of small transition probabilities for the electronic changes producing them. These occur on the violet sides of the multiplets and are identical with one type of "low-temperature" line discussed previously. The first class of the new conglomerate lines is valuable in determining the positions of the

lower levels lying near the basic one, while the others are useful in showing how the final excited levels are split in the crystal field and in locating levels which do not easily form electronic transitions with the basic level because of selection rules, etc.

The absorption lines at temperatures near the absolute zero can be considered as an energy-level diagram of the excited levels, since at these temperatures all lines must arise from a single basic level. As the temperature is raised the population in slightly higher levels increases as the Boltzmann factor dictates. As a consequence new lines appear which are separated from the more intense lines by amounts equal to the separation of the excited lower levels from the basic one.

At 15°K, the lowest temperature photographed by us, lines arising from levels more than 50 cm^{-1} from the basic level would likely be distinguishable

TABLE II. *Doublets of 160 cm^{-1} separation (78°K).*

Low-temperature line	High-temperature line	$\Delta\nu$ (cm^{-1})
17875.8	17716.3	159.5
17908.0	17748.6	159.4
18927.0	18768.0	159.0
20024.5	19865.5	159.0
20042.5	19882.7	159.8
20404.5	20246	158.5
20544.8	20386	158.8
20520.2	20361	159.2
22151.8	21994	157.8
22228.8	22069	159.8
22487.9	22327	160.9
22543.1	22384	159.1
23949.8	23789.2	160.6
24001	23840	161
24015	23854	161
25646.2	25486	160.2
26611	26453	158
26627.1	26467.8	159.3
26700.9	26541.5	159.4
27570	27412.8	157.2
27591.4	27431.1	160.3

TABLE III. *Doublets of 145 cm^{-1} separation (78°K).*

Low-temperature line	High-temperature line	$\Delta\nu$ (cm^{-1})
17875.8	17730.6	145.2
17908.0	17763.1	144.9
18937.4	18792.2	145.2
20042.5	19897.0	145.5
20404.5	20259	145.5
22151.8	22006	145.8
22228.8	22082	146.8
22487.9	22341	146.9
22543.1	22399	144.1
23949.8	23804.9	144.9
25646.2	25501	145.2
26627.1	26482.9	144.2
26700.9	26556.3	144.6
26714.3	26570	144.3
27591.4	27445.9	145.5

in the photographs taken, and we should be able to detect lines resulting from levels 20 cm^{-1} or more distant from the lowest one. The first new lines to make their appearance, however, do so between 20° and 60°K and appear to originate from levels differing in energy from the basic level by about 145 and 160 cm^{-1}. In Tables II and III are given the frequencies of lines forming doublets of these separations; each doublet is composed of a high-temperature line and a low-temperature line. Only lines well separated from others are used for these tables, although in almost every multiplet evidence of these separations

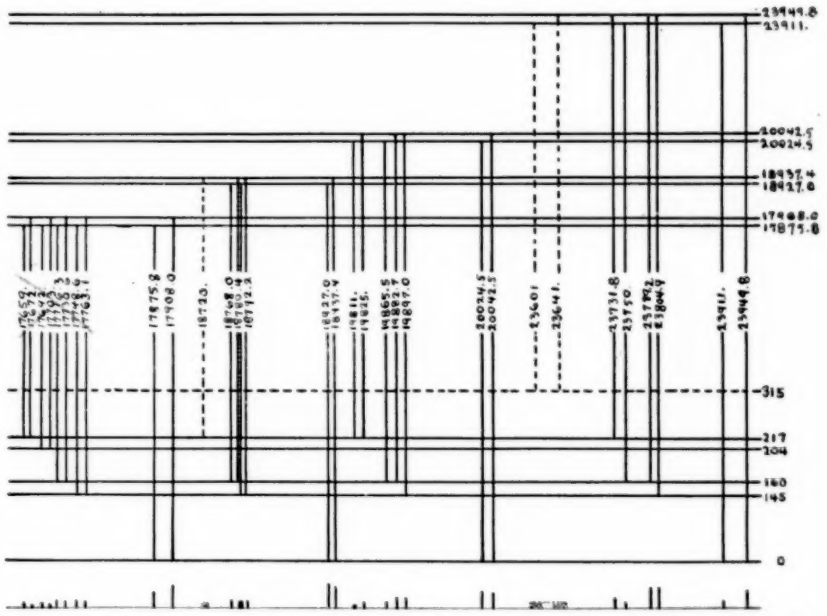

Fig. 2. Diagram of some of the multiplets of the $SmCl_3 \cdot 6H_2O$ absorption spectrum. Below the energy levels appears a representation of the lines as they appear on photographs, plotted however, within the multiplets, according to wave numbers. Relative intensities are indicated roughly by the heights of the lines used, though faint absorption is somewhat exaggerated. The solid lines in the levels or transitions indicate low-temperature values. The dotted lines show dependence on high-temperature measurements.

can be found. No other values for such differences are found to occur with nearly the same frequent repetition, and at liquid nitrogen temperature these two levels are sufficient to account for nearly all of the important, more intense high-temperature lines found in both the single-crystal and the conglomerate spectra. (See lines *a*, Fig. 1.)

At higher temperatures another group of lines which indicate two more levels at 204 and 217 cm^{-1} make their appearance (lines *b*). At liquid ethylene and room temperatures a third group resulting from one or more levels about 300 cm^{-1} (295 to 315 cm^{-1}) can be discerned (lines *c*). Finally, one or two bands found only at room temperature seem to require separations of more than 400 cm^{-1}, since they occur quite far from the nearest low-temperature lines.

In Fig. 2 is given a diagram of several multiplets that occur well apart from other lines and offer most clear and convincing proof of the existence of most of the levels described above. Except for the levels and transitions indicated by dotted lines, the values given are those at liquid nitrogen temperature. As a general rule the intensities of the lines arising from the 160 and 217 levels are a little greater than those of lines from the 145 and 204 levels, respectively. The lines from the 145 and 160 levels are, of course, much stronger than those from higher levels.

Each of the levels listed above not only has been established by from four to thirty measurements of lines whose temperature behavior supports the explanation given for them, but they also are consistent with many other lines that occur in complex regions of the spectra and cannot be determined with the same accuracy. The levels may very well be complex with a spread of from 2 to 30 cm^{-1}, but the accurate determination of this complexity is difficult for two reasons. In the first place the lines broaden as the temperature is increased with the result that at room temperature they are more than 10 cm^{-1} in width. Since the levels in many of the excited multiplets are separated by about this amount, it is impossible to tell whether the broad bands which make their first appearance at high temperatures are caused by transitions from one or more lower levels. The same is true for smaller separations in the lines appearing at lower temperatures. As a result we could not distinguish lines which might indicate 2 cm^{-1} separations in the 160 and 145 cm^{-1} levels or a 30 cm^{-1} separation in those at 300 cm^{-1}.

A second confusing factor is the fluctuating fields caused by the vibrations of the crystal, most important at higher temperatures. These probably cause partial uncoupling of the orbits or spins of the electrons with the field and produce instability in some of the upper levels. The multiplets then tend either to contract to a new center or else fade out entirely. While this latter effect is very pronounced in the case of $PrCl_3 \cdot 6H_2O$, which has been studied by one of us,[4] for the samarium salt the fading is not very great until room temperature is reached.

It is rather interesting that the separations given in Tables II and III are spread over a range of 159 ± 2 and 145 ± 2. This range is thought to be somewhat larger than the usual error would allow, though the combined errors of two lines might be that great. It is particularly noteworthy that the residuals, when plotted, instead of giving the ordinary Gaussian curve, seem to fall roughly into three groups. If this is true it would indicate that perhaps the

[4] Spedding, unpublished work. Discussion of this will probably appear in Physical Review. Many lines which are strong at 80°K are faint at 195° and absent at 300°. $PrCl_3 \cdot 6H_2O$ also appears to have electronic isomers spread over some distance (105 cm^{-1}, etc.). In this case, however, these low levels are apparently affected at high temperatures in a manner similar to that indicated for the excited upper levels of the Sm^{+++} ion. As a consequence an increase in temperature results at first in an accompanying increase in the intensity of the lines arising from these levels, whose populations are governed by the Boltzmann factor. Finally, as the temperature becomes still higher, these lines fade because of the disappearance of the levels from which they originate. Similar phenomena have been observed by J. Becquerel (J. Becquerel, Gedenboek H. Kammerlingh Onnes, Leiden, 1922) in the case of Nd^{+++}.

basic level is split into three components, a very attractive result. The basic level of Sm IV as predicted by Hund[5] is a $^6H_{5/2}$, and it would be expected to split into three doubly degenerate levels in a moderate electric field.[6] However, without additional evidence it can only be mentioned as highly probable.

Conclusions

As a result of the above evidence it is safe to conclude that in $SmCl_3 \cdot 6H_2O$ the samarium ion has levels situated at 145, 160, 204, 217 and 300 cm^{-1} above the basic one. It is highly probable that these levels are complex, especially that the 300 level is double, with components at 295 and 315, and that other levels exist at 400 and greater wave-number separations from the lowest level. These levels are in good agreement with the predictions of one of us from magnetic data.[7]

[5] Hund, Zeits. f. Physik **33,** 855 (1925).

[6] Kramers, Proc. Amst. Acad. **32,** 1176 (1929). Bethe, Ann. d. Physik **3,** 133 (1929).

[7] Spedding, J. Am. Chem. Soc. **54,** 2593 (1932). While these levels are for $SmCl_3 \cdot 6H_2O$ and the predictions are for $Sm_2(SO_4)_3 \cdot 8H_2O$, preliminary photographs and measurements show that the levels of the two salts are similar.

The Luminescence of Solid Nitrogen

By JOSEPH KAPLAN
University of California at Los Angeles

(Received August 18, 1932)

An explanation is proposed for nearly all of the radiations that have been observed by McLennan and his collaborators in the luminescence of solid nitrogen. The bands are associated with known bands of the second-, fourth- and first-positive groups of nitrogen; with hitherto unobserved second-positive bands; with a possible new system and with new modifications of the first-positive bands. These new modifications of the first-positive bands are related to the spectra of the aurora, night-sky and planetary absorption spectra. As a result of this correlation, it is now possible to see why Vegard identified the aurora spectrum as the spectrum of solid nitrogen and then proposed his theory of the upper atmosphere.

I. INTRODUCTION

THE purpose of the present paper is to discuss the identification of the spectrum of the brilliant luminescence which is observed when solid nitrogen is bombarded by cathode rays or canal rays.

The studies of the luminescence of solid nitrogen have been carried on mainly by Vegard[1] in the Cryogenic Laboratory in Leiden and by McLennan[2] and his collaborators in Toronto. It may be remembered that the work was originally an outgrowth of a hypothesis in which Vegard[3] proposed that the green aurora line originated in the luminescence of solid nitrogen suspended in a state of fine division in the upper atmosphere. Further investigation by McLennan and Shrum[2] showed that the yellow-green band, which Vegard associated with the green aurora line, was broad and diffuse and consisted of three main components, none of which overlapped the green line. The work which has since followed[4,5] has proved conclusively that the green line is a sharp narrow arc line of oxygen and its identification is now a matter of well-known record. Thus, Vegard's theory of the nature of the aurora and the upper atmosphere has not been confirmed.

It is interesting to mention at this point two other bands that Vegard and others have observed in the luminescence spectrum. These two bands, known as N_2 and N_4 and having wave-lengths of 5230A and 5945A, respectively, were associated by Vegard with two bands in the spectrum of the Aurora Borealis and hence were used as proof of the existence of solid nitrogen in the upper atmosphere. It will be shown in the present paper that it is now

[1] Commun. Phys. Lab. Univ. Leiden, No. 175; Ann. d. Physik **79**, 377 (1926).

[2] McLennan and Shrum, Proc. Roy. Soc. [A] **106**, 138 (1924). McLennan, Ireton and Thomson, Proc. Roy. Soc. [A] **116**, 1 (1927). McLennan, Ireton and Samson, Proc. Roy. Soc. **120**, 303 (1928).

[3] Phil. Mag. **46**, 193 (1923).

[4] Proc. Roy. Soc. [A] **108**, 501 (1925): ibid., **114**, 766 (1927).

[5] Babcock, Astrophysikal J. **57**, 209 (1923).

possible to understand the agreement between some of the bands in the spectrum of solid nitrogen and those in the auroral spectrum, but it will also be shown that, while this agreement has a real significance, it is not a proof of the presence of solid nitrogen in the upper atmosphere. The explanation which is to be presented here is an outcome of the author's recent work on the auroral spectrum and on predissociation in nitrogen.[6]

II. The Luminescence Spectrum

The data which are to be discussed here are taken from a paper by McLennan, Ireton and Samson,[7] and since the only purpose of this paper is to analyze the data, the reader will be referred to that and other papers for the experimental details. A part of the luminescence spectrum was arranged by the above writers into two series of bands in the violet and ultraviolet and these series are given in Table I, which has been taken directly from McLennan, Samson and Ireton's paper. Series *B* consists of narrow bands and Series *C* of broad bands, both series degrading to the red. In Table II are given the wave-lengths of all of the bands which have been observed in the luminescence.

Table I.

B_1	B_2	B_3	B_4	B_5	B_6	B_7	B_8
2347	2479	2623	2781	2961	3158	3388	3644
C_1	C_2	C_3	C_4	C_5	C_6	C_7	
3105	3285	3502	3732	3980	4255	4585	

Table II. *Wave-length in angstroms of all bands observed in luminescence.*

2347	2781	3055	3285	3732	4585	5552	6187	
2479	2903	3105	3388	3980	4775	5616 N_1	6400	N_3
2623	2961	3158	3502	4255	5230 N_2	5659	6725	
2765	3009	3234	3644	4493		5945 N_4	8535	

In an earlier paper,[2] McLennan, Ireton and Thomson called attention to the fact that the violet and ultraviolet bands might be related to the second-positive bands of nitrogen, but the agreement was apparently not very convincing because the idea was not carried further. Vegard,[8] on the other hand, had recognized the similarity between the luminescence spectrum and the auroral spectrum and he suggested that the same positive and negative bands were present in both spectra. A comparison of the auroral spectrum[9] and Table II shows, however, that while some of the second-positive bands are common to the aurora and to the solid luminescence, most of the bands in Table II are not present in the auroral spectrum. Furthermore, none of the negative bands of nitrogen, which are by far the strongest bands in the auroral spectrum, are observed in the spectrum of the solid luminescence.

[6] Kaplan, Phys. Rev. **38**, 582 (1931).
[7] McLennan, Ireton and Samson, Proc. Roy Soc. **120**, 303 (1928).
[8] Vegard, Nature **114**, 357 (1924).
[9] Vegard, Phil. Mag. **46**, 193, 577 (1923).

As far as the writer knows, no further attempts have been made to correlate the spectra of solid nitrogen and gaseous nitrogen.[10]

In the following discussion it will be shown that not only are bands related to the second-positive group of nitrogen present in Table II, but that bands related to the fourth-positive, first-positive and to a hitherto undiscovered group of bands, are also present. The bands of the fourth-positive group are not very well known, appearing under very unusual excitation conditions only, hence the relationship between them and the bands in Table II are not at all obvious. Even more interesting will be the identification of two of the bands in Table II as second-positive bands which have never been observed in gaseous nitrogen, but whose wave-lengths can be predicted from the constants of the energy levels which are involved in the emission of the known bands of the system.

III. Bands Related to the Second-Positive Group

An examination of Tables II and III will show that many of the bands in the luminescence of solid nitrogen agree with bands of the second-positive group. Thus, for example, 2961 in the luminescence spectrum corresponds very well with 2962 in the second-positive group. Similarly, 3105 corresponds

Table III. *Nitrogen second-positive bands.*

v' \ v''	0	1	2	3	4	5	6	7	8	9	10	11
0	3371	3577	3805	4059	4344	4666						
1	3159	3339	3536	3755	3998	4269	4574	4917				
2	2977	3136	3309	3500	3710	3942	4201	4490	4814			
3	2820	2962	3116	3285	3469	3671	3894	4131	4416	4723		
4		2814	2953	3104	3267	3446	3642	3857	4094	4356	4648	4975

to 3104, 3158 with 3159, 3285 with 3285, 3502 with 3500, 3644 with 3642 and 4493 with 4490. The above-mentioned bands are the ones which are rather easily correlated with the second-positive bands. It is surprising that this remarkable agreement did not impress previous writers more than it has.

In a recent paper in this journal, the writer[11] discussed the sudden curtailment of the second-positive bands at $v'=4$. No one has ever observed bands which originate on $v'=5$, in spite of the fact that the total energy of the electronic level on which these bands originate is 15 volts and the energy in the $v'=4$ level is only 13.9 volts. The writer noticed, however, that 13.9 volts corresponds almost exactly to the energy necessary to dissociate a nitrogen molecule into two ^2D metastable atoms and hence the idea was proposed that the absence of bands, which originate higher than $v'=4$, was due to an interaction between the higher vibrational states and the Heitler and London level which corresponds to the repulsive interaction of two ^2D atoms. Thus if

[10] In some recent papers Vegard has correlated gaseous and solid nitrogen spectra. The same criticism however that is presented here can be applied to Vegard's work. This will be done in detail in a later paper. Zeits. f. Physik **75**, 30 (1932).

[11] Kaplan, Phys. Rev. **37**, 1406 (1931).

any of the vibrational levels higher than $v'=4$ are excited, the molecule dissociates either by a radiationless transition to the repulsive energy level or perhaps by a transition in which radiation is emitted. At any rate, the corresponding second-positive bands are not emitted. The second-positive bands are but one of many similar cases of predissociation which were discussed by the writer in the above-mentioned paper, so that the explanation which was proposed had much evidence in its favor.

If it is assumed, therefore, that the absence of bands originating higher than $v'=4$ is accounted for by predissociation, it should be possible to calculate the wave-lengths of missing band-heads and under some circumstances to obtain these bands. That it is reasonable to expect conditions under which one might observe bands which are in general missing due to predissociation has been shown recently by the writer[12] in some work on the first-positive bands of nitrogen. With the well-known constants of the C and B levels, the predicted wave-lengths of the second-positive bands C_6-B_0 and C_7-B_2 are found to be 2479A and 2621A, respectively. A glance at Table II will show that there are two bands in the luminescence spectrum at 2479A and 2623A.

The agreement is quite remarkable and should remove any doubts that some relationship exists between the spectra of solid and gaseous nitrogen. It is worth while noting once more that in the luminescence spectrum we obtain for the first time second-positive bands which originate on levels higher than $v'=4$, thus substantiating the writer's notions regarding the absence of such bands in electrical discharges through gaseous nitrogen. Their presence in the luminescence spectrum indicates that one might find a consideration of Heitler and London levels profitable in the discussion of the spectrum of solid nitrogen. It will be seen in what follows that Heitler and London levels do play an important role in this problem.

A third band which agrees quite well with a predicted second-positive band is the band at 2765A. The predicted C_9-B_4 band falls at 2761A, the difference in frequencies being about 40 cm. The agreement is once again quite satisfactory.

The $\omega^e:v$ graph for the C level of N_2 is one which possesses such an enormous negative curvature that the resulting energy equation for the vibrational levels contains third and fourth degree terms with very large coefficients.[13]

$$E = 2018.67v' - 26.047v'^2 + 0.9873v'^3 - 0.546v'^4.$$

This equation was used to calculate the energies of the C_6, C_7 and C_9 levels. The remarkable coincidence between the predicted bands and those observed in the luminescence is such, that the function given above for E, as calculated from known levels, must also give good values for the unobserved vibrational levels. This is very interesting when considered along with Birge's[14] last discussion regarding the determination of heats of dissociation from band spectra. In that paper he discussed the failure of the linear extra-

[12] Kaplan, Phys. Rev. **38**, 373 (1931).
[13] Birge and Sponer, Phys. Rev. **28**, 259 (1926).
[14] Birge, Trans. Farad. Soc. **25**, 718 (1929).

polation method in determining heats of dissociation. It was shown that in general it is necessary to use two functions to represent the entire $\omega^v:v$ curve; one to represent the portion having negative curvature (or positive), the second function having positive (or negative) or zero curvature. Professor Birge had previously attempted to obtain a single analytical expression to represent the function $\omega^v=^6(v)$ in the cases of I_2 and O_2, where the entire $\omega^v:v$ graphs are known and he found that in no case could he get a satisfactory fit. The function for E which is used here must therefore represent at least the vibrational levels $v'=0$ to $v'=9$ and no more, because the energy in $v'=9$ is 14.6 volts, which is the maximum of the function. Since the predicted total energy is 15.0 volts, the vibrational levels in the range from 14.6 to 15.0 volts must be calculated from a second function. It will be an interesting problem not only to attempt to obtain the bands 2479, 2623 and 2765 in electrical discharges in gases, but also to obtain bands which arise in the 14.6–15.0 volt range.

IV. Bands Related to the Fourth-Positive Group

The fourth-positive bands of nitrogen arise in transitions between the D and the B levels. This group of bands was discovered in condensed discharges and it is almost never observed in uncondensed discharges, except under very unusual excitation conditions.[15,16] In general these bands are much weaker than the second-positive bands and this is easily understood when one remembers that not only is the D level the highest known level in the molecule but that once more a repulsive level prevents the emission of bands which originate higher than $v'=0$.[11]

In Table IV are given the wave-lengths of the known fourth-positive bands, each band consisting of five heads. A comparison with Table II shows

Table IV. *Wave-lengths in the fourth-positive bands.*

v'' / v'	0	1	3	3	4	5	6
0	2260.8	2351.4	2448.0	2550.7	2660.5	2777.9	2903.9
	59.6	50.3	47.0	49.7	59.3	76.5	02.0
	58.4	49.0	45.6	48.4	57.9	75.1	00.3
	57.1	47.5	44.0	46.6	55.8	72.8	2898.1
	56	46.4	42.8	45.3	54.5	71.4	96.6

that the bands 2347, 2781 and 2903 agree quite well with the bands 2347.5 or 2346.4; 2777.9 and 2903.9 or 2902. The band 2765, which was identified as C_9-B_4 in the previous section, may be the fourth-positive band 2771.4. It is of some interest to note that only part of the fourth-positive group is present in Table II. This absence of part of the group was a characteristic of the second-positive bands as well. It will be shown later that this modification of the gaseous spectrum is not at all an unreasonable one when going from a gas to a solid.

[15] Strutt, Proc. Roy. Soc. [A] **85**, 377 (1917).
[16] Kaplan, Phys. Rev. **33**, 189 (1929).

V. Bands Related to the First-Positive Group

The relationship between the luminescence spectrum and the first-positive bands of nitrogen is even more striking and interesting than the relationships discussed in the previous sections. We will consider first the luminescence band N_2, which has eight components lying between 5204A and 5240A. The wave-lengths given by McLennan and his collaborators for these components are as follows:

(1)	(2)	(3)	(4)
5204.4	5210.4	5214.3	5220.1
(5)	(6)	(7)	(8)
5224.4	5228.8	5235.0	5240.0

This band was identified by Vegard with an aurora band, whose wave-lengths have been given by various observers as 5269, 5205, 5200, 5233, 5210, 5239, 5207, 5200, 5228, 5235, 5166, 5230. This identification was advanced by Vegard[8] as proof that solid nitrogen existed in the upper atmosphere. It was criticized on the grounds that the 5230 band in the aurora is probably the fourth member of the first-negative band system of N_2, the first three members of which are very strong in the aurora. This criticism was well based and undoubtedly the negative band 5227 does appear in the aurora, but the large variation in wave-lengths which have been reported in this region indicates that other bands also appear in the aurora. It will be shown that, not only is it possible to identify the N_2 band of the luminescence spectrum with some nitrogen bands, but that the same type of modification of the gaseous bands can account for both the N_2 band and the nitrogen bands in the aurora.

The first-positive bands of nitrogen are best known on account of their presence in the afterglow of active nitrogen. On a small dispersion spectrogram most of the individual bands of this system appear to consist of three strong and one weak head, while some of the bands consist of but one strong head. The recent rotational analysis of these bands by Naudé[17] has shown that the three strong heads are in reality three groups of three strong branches which are P_1, Q_1, R_1; P_2, Q_2, R_2 and P_3, Q_3, R_3 branches belonging to the transitions ${}^3\Pi_{\text{low}}\,{}^3\Sigma$, ${}^3\Pi_{\text{medium}}\,{}^3\Sigma$ and ${}^3\Pi_{\text{high}}\,{}^3\Sigma$. In this paper we will continue to refer to these groups as heads.

A calculation of the positions of the first heads corresponding to the transitions $B_{17}-A_{12}$ and $B_{16}-A_{11}$, where A and B refer to the ${}^3\Sigma$ and ${}^3\Pi$ levels, respectively, shows that they have wave-lengths 5207 and 5240. These two wave-lengths approximately include the eight components of the N_2 luminescence band. The average separation of the components of the N_2 band is about 20 cm^{-1}, whereas the average separation of the first-positive band heads of any one band is about 22 cm^{-1}, thus giving us an additional reason for believing that the N_2 band is related to the first-positive bands 5207 and 5240. One objection to the attempt to compare the N_2 band with first-positive bands is that the luminescent band degrades to the red, whereas the first-positive bands degrade to the violet. This was also true, however,

[17] Naudé, Phys. Rev. **38**, 372 (1931).

for the second- and fourth-positive groups, yet the correlation in these cases was quite good.

The band N_1 in the solid luminescence spectrum consists of three diffuse components, the wave-lengths of which are 5556A, 5619A, and 5654A. There are no auroral radiations whose wave-lengths agree with these values, although Vegard attempted to correlate this band with the green auroral line. There are, however, three first-positive nitrogen bands, $B_{16}-A_{12}$, $B_{15}-A_{11}$, and $B_{14}-A_{10}$, which include the three components of the N_1 band. These bands are usually single-headed, with only the long wave-length head appearing, these heads having wave-lengths of about 5565A, 5617A, and 5665A, of which the 5617 head agrees very well with the second component of the N_1 band. It is to be noticed also that the B_{16} and B_{17} levels were involved in the identification of the N_2 band, while the B_{16}, B_{15}, and B_{14} levels are considered in connection with the N_1 band.

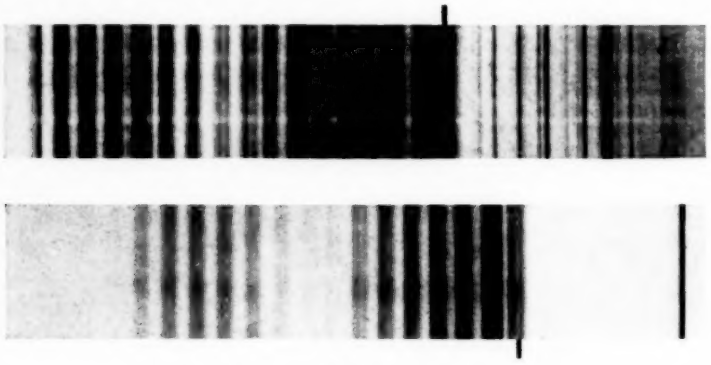

Fig. 1.

The band, the wave-length of which is given as 5552 in Table II and 5556 in McLennan, Ireton and Thomson's paper, probably corresponds to the second head of the $B_{16}-A_{12}$ band. This is in agreement with the results of a long series of experiments in nitrogen, and in nitrogen-oxygen mixtures, in which the writer has produced highly selective excitation of single heads of the first-positive group, and, what is even more interesting, single heads which correspond to radiations observed in the auroral spectrum and in the spectrum of the night-sky. Thus, it is possible for the first time to definitely identify certain auroral and night-sky radiations as nitrogen bands and also to show such marked variations in the appearance of this group of bands that the correlation of this group with the luminescence spectrum appears quite reasonable.

The band $B_{12}-A_8$, shown in Fig. 1, will illustrate the emission of single-heads in the writer's aurora experiments. It will be noted that the third head is very strong on one plate and almost missing on the other plate which was obtained from an ordinary discharge. This adds to other convincing demonstrations of the very striking variations that can be produced in the band spectrum of nitrogen.

The luminescence band N_4 at 5945A can be compared with an auroral band at 5945 and also with a first-positive band. Bands have been reported in the auroral spectrum[18] at 5929A and 5945A, and various writers have suggested that these bands were first-positive bands. Since no evidence has existed until now, regarding the significance of single-headed excitation of these bands, no one was willing to be very definite regarding the identification of the so-called nitrogen bands in the aurora and perhaps in other astrophysical spectra, and such identifications have even been regarded as incorrect.[19] The 5945A band in the luminescence is accompanied by two weak components at 5939A and 5932A, and these three wave-lengths correspond to within 1A to the second, third, and fourth heads of the 5959 band B_8-A_4. It is really very nice once again to have the second head, the strongest head in the group, as was the case for the $B_{16}-A_{12}$, $B_{15}-A_{11}$ and the $B_{14}-A_{10}$ bands in the auroral experiments, and for the $B_{16}-A_{12}$ and the $B_{14}-A_{10}$ bands in the luminescence spectrum.

The luminescence band at 6187A can be identified either as the B_4-A_0 band at 6187 or the $B_{12}-A_9$ band at 6185. Since the $B_{12}-A_8$ band was used previously to show the enhancement of the weakest of the four heads, it is tempting to identify the 6187 bands as $B_{12}-A_9$. However the luminescence band 8535 corresponds very closely to the B_3-A_2 band 8541, and the luminescence band 6725 might quite readily be a part of the B_5-A_2 band at 6704. (Strong single heads are often excited on the long wave-length side of the first head.) Thus, for no other reason than to fill the gap, the 6187 band should be identified as B_4-A_0. This procedure is especially tempting when one notes that Slipher[20] has obtained radiation in the light of the night-sky at 6870A, and this is without a doubt the band B_3-A_0 at 6875. He has also reported a band at 7270A which is very close to the B_6-A_4 band at 7273. It may be mentioned that Slipher has recently reported bands in the absorption spectra of the major planets at 6190, 7265 and 6467. Now 6468 is the first head of the B_8-A_5 band and the B_8-A_4 band is 5959, three heads and fourth of which make up the 5945 band in the solid luminescence, and the second heads of which appear in the aurora. To summarize briefly, the 6187 (or 6190) band appears in the first-positive group, the solid luminescence and in planetary absorption spectra. The 7265 (7270, 7273) band appears in the light of the night-sky, planetary absorption and first-positive group. The 6465 band appears in the same three spectra as the 6187 band. The meaning of these remarkable relationships between four such totally different phenomena will be discussed in other papers.

We come now to the band N_3, which extends from 6360 to 6500, and has a maximum of intensity at 6400A. This range includes not only the 6465 band, which was discussed above, but also the 6394 band and part of the $B_{10}-A_7$ band at 6323. Now the 6323 band has been observed both in the aurora and in the light of the night-sky, so that the notion of correlating the

[18] McLennan, Proc. Roy. Soc. **120**, 334 (1928).
[19] Sommer, Zeits. f. Physik **57**, 582 (1929).
[20] Slipher, Ast. Soc. Pac. **41**, 262 (1929).

6323 and the 6465 bands with the N_3 band is not at all unreasonable. McLennan, Ruedy and Anderson[21] have shown that in the active nitrogen which is produced in a mixture of argon and nitrogen, containing only one-half percent nitrogen, the glow consists of the three bands 6394, 6469 and 6545 only. The normal afterglow in pure nitrogen does not include any of these bands except with very feeble intensity, so that the effect of argon must be a very violent one. Other writers have usually explained this effect by saying that the effect of the argon is to simply increase the population of the levels upon which the three bands originate. That this explanation is an insufficient one is seen readily when one considers that the 6394 band is B_9-A_6, and that B_9-A_5 and other usually strong members of the progression which arise on B_9 are absent. This is an effect that cannot be explained merely as the result of a change in population in the B_9 level, and, as the writer has shown, it must be due to an enhanced interaction between the B_9 level and a new level in the molecule, for example, a Heitler and London level. The overlapping of N_3 and these three "ultimate" nitrogen bands, as well as the fact that the 5945 band, N_4, has been correlated with the B_8-A_4 band 5959, can be presented therefore as evidence for the above identification.

Two of the luminescence bands N_2 and N_4 have appreciable periods of decay, whereas the band N_1 vanished the instant the source of excitation was cut off. The analogy here with the afterglow of active nitrogen is quite striking, especially so, since the same group of bands is present in both. Here, as well as in the nitrogen afterglow, two bands which originate on the same level can appear in the exciting discharge but not in the afterglow. Thus, for example, in the argon-nitrogen afterglow, the band B_8-A_5 was present, but B_8-A_4 was absent. In the solid luminescence, on the other hand, B_8-A_4 was present in the phosphorescence, whereas B_8-A_5 was absent. In both experiments, however, each one of these bands appeared in the exciting discharge. Further study will be needed in order to completely understand this rather interesting phenomenon.

VI. New Nitrogen Bands

In addition to the bands which have been discussed, there are others for which no ready correlation with known nitrogen systems has been found. There are, however, other possibilities in nitrogen which may help to explain these bands. They may correspond to an intercombination system, in which case any attempts to explain them would be premature in view of the uncertainty regarding the absolute values of the energy levels of the triplet systems in nitrogen. In calling attention to the existence of these bands in the luminescence of solid nitrogen we wish at the same time to point out the fact that their existence indicates that there must be some undiscovered nitrogen bands in the visible and in the near ultraviolet. The relatively recent discovery by Hopfield of a system of bands in the ultraviolet gives us some hope that much more remains to be discovered in the spectrum of the nitrogen molecule.

[21] Proc. Roy. Soc. **120**, 334 (1928).

VII. Discussion

A very interesting consequence of the method used in this paper to explain some of the second-positive bands, is a fairly good identification for two unknown radiations in the auroral spectrum. These two lines or bands have wave-lengths of 3208A and 3432A and are the only two unexplained radiations in the aurora which fall in that region of the spectrum. A simple calculation predicts that the C_8-B_7 band in the second-positive group should have a frequency of 31,153 cm^{-1}, and that the C_5-B_6 transition should correspond to 29160 cm^{-1}. The two bands given above correspond to 31166 cm^{-1} and 29,138 cm^{-1}, respectively, thus giving some evidence in favor of the suggestion that the two aurora radiations are second-positive bands.

McLennan, Ireton and Samson[2] have discussed briefly the possibility that a small amount of hydrogen could be responsible for the luminescence spectrum attributed to solid nitrogen. Their supposition is based on the fact that a small quantity of a metal in solid solution in a diluting medium, is often responsible for the phosphorescent spectrum. A similar fact is true for gases; for example, in mixtures of argon and nitrogen or helium and nitrogen, in which only small amounts of nitrogen are present, the afterglow is a very strong and highly modified afterglow of nitrogen. Therefore, the doubt cast by McLennan and his collaborators, on the origin of the luminescence in solid nitrogen, is worth mentioning. It is, however, not a very serious one, in view of the striking correlation between the luminescence spectrum and the spectrum of gaseous nitrogen.

At this point it is worth while calling attention to another work of McLennan, Samson and Ireton[22] in which they describe the results of irradiating solid argon with cathode rays. They found a great similarity between the spectrum of solid argon and that of solid nitrogen, which led them to the conclusion that hydrogen was responsible in both cases for the luminescence. It is more probable that the solid argon contained enough nitrogen so that it was a reproduction in the solid state, of the argon-nitrogen gas mixtures, which yield such beautiful and highly modified afterglows. In the case of the gaseous mixture the modifications which are introduced are so radical that it is not surprising to find that in the spectrum of solid argon, the nitrogen bands are slightly different from those in solid nitrogen. The experiments in solid argon should be repeated and it would also be of considerable interest to obtain the solid luminescence of known mixtures of argon and nitrogen.

It will be of some interest to recall briefly the Raman scattering experiments of McLennan and McLeod,[23] in which they obtained modified scattering from liquid oxygen, nitrogen and hydrogen, corresponding to vibrational and to rotational changes in those molecules. The magnitudes of the displacements agreed well with those that would be obtained from gases and the displaced lines were sharp. Since the intermolecular forces produce very small changes in the molecular energy levels, it is not surprising that there is such a clear relationship between the spectra of solid and gaseous nitrogen.

[22] McLennan, Samson and Ireton, Roy. Soc. Canada Trans. **23**, 25 (1929).

[23] McLennan and McLeod, Nature **123**, 160 (1929).

The purpose of this paper has been to account in some way for the radiations emitted by solid nitrogen and this has been done. In closing, we wish to recall the many striking phenomena with which the first-positive bands of nitrogen have been connected, in this paper. These are, the spectrum of active nitrogen, the auroral spectrum, the light of the night-sky, planetary absorption spectra, and, finally, the spectrum of solid nitrogen. A general reason for the extreme modifications which this group of bands can undergo lies in the large number of Heitler and London (and possibly other) levels which lie in the energy range in which these bands arise. More will be said about this point in other communications.

Products of Dissociation in Nitrogen

By JOSEPH KAPLAN
University of California at Los Angeles

(Received August 17, 1932)

Use is made of four regions of predissociation in the triplet band systems of nitrogen in order to determine the products of dissociation from the known triplet states. Mulliken's proposal that the products of dissociation in the $^3\Sigma\mu^+$ level are two ^4S atoms does not agree with the evidence which is presented here. This evidence proves that the products are a ^4S and a ^2D atom. The bearing of these results on the heat of dissociation of nitrogen is briefly discussed.

IT IS the purpose of this note to present experimental evidence showing that the $^3\Sigma$ level of nitrogen (lower level of the well-known first-positive bands) dissociates into a ^4S atom and a ^2D atom. These products of dissociation are not in agreement with the ones recently proposed by Mulliken,[1] according to whom the products of dissociation are two ^4S atoms. We will also discuss the products of dissociation from the other triplet states of nitrogen.

Naudé's[2] recent analysis of the first-positive bands shows that the lower state of these bands must be a $^3\Sigma\mu^+$ state, and Mulliken has identified it as one of the states which can be obtained from two ^4S atoms. The vibrational levels of the $^3\Sigma\mu^+$ state have been followed to 2.1 volts above $v=0$, so that the heat of dissociation into two unexcited atoms must be equal to or greater than 2.1 volts plus the energy of $v=0$ of $^3\Sigma\mu^+$ to which we will sometimes refer as A_0. Recent experimental evidence has indicated that the heat of dissociation into normal atoms must be lower than the value of 9.1 volts, which has been proposed by Birge[3] and others,[4,5,6] probably as low as 8.2 volts. The $^3\Sigma\mu^+$ level must therefore be no higher than $9.1-2.1=7.0$ volts, and it may even be as low as $8.2-2.1=6.1$ volts, provided Mulliken's suggestion as to the products of dissociation is correct. The 6.1 volt value seems to be extremely low when compared with Sponer's 8.2 volt value for that energy.

We will now present the argument which will show that the products of dissociation of the $^3\Sigma\mu^+$ state are a ^2D and a ^4S atom. Elsewhere,[7] we have called attention to the phenomenon of missing heads in the first-positive bands in nitrogen, and this was ascribed to predissociation of the molecule. The effect is beautifully shown in bands which originate on $v=13$, 14, 15 of the

[1] Mulliken, Rev. Mod. Phys. **4,** 53 (1932).
[2] S. M. Naudé, Proc. Roy. Soc. **136,** 114 (1932).
[3] Birge, T. Faraday Soc. **25,** 713 (1929).
[4] Kaplan, Proc. Nat. Acad. **15,** 226 (1929).
[5] Tate and Lozier, Phys. Rev. **39,** 224 (1932).
[6] Sutton, Nature **130,** 132 (1932).
[7] Kaplan, Phys. Rev. **37,** 1406 (1931).

$^3\Pi g$ upper state of the first-positive bands. The one head, which does appear with any appreciable intensity, is very weak compared with the intensity of the corresponding head of the normal neighboring bands. Now the energy of $v=13$ is about 3.6 volts higher than the energy of $v=0$ of $^3\Sigma\mu^+$ and since strong predissociation occurs at this energy, it is certainly equal to or greater than the energy required to dissociate the molecule into two atoms. It is of course impossible to give the exact value of D in terms of the energy of $^3\Sigma\mu^+$ and this 3.6 volt value, because we cannot say definitely what the setting in of predissociation at $v=13$ means. The energy of $v=13$ may correspond very closely to the energy required to dissociate N_2 into two particles and again it may be somewhat larger.

There is another region of predissociation, however, similar to the one at $v=13$, and this region of single-headed bands begins at $v=20$. The difference between $v=20$ and $v=13$ is about 1.1 volts, and the difference between the $^2P(3.56)$ and $^2D(2.37)$ metastable states of atomic nitrogen is about 1.2 volts. The agreement between the two values suggests that the first region of predissociation involves a ^2D atom, and that the second region involves a ^2P atom. The only reasonable interpretation of the above results is that the first region corresponds to dissociation into a ^4S and a ^2D atom, and that the second region corresponds to dissociation into a ^4S and a ^2P atom. Hence, if A_0 is the energy of $v=0$ of $^3\Sigma\mu^+$, then $D \leqq A_0+3.6-2.37=A_0+1.2$ volts.

The predissociation at $v=13$ can also be compared with the predissociation at $v=4$ in the initial $^3\Pi$ state of the second-positive bands. The bands which arise in $v=4$ are the last ones of a sequence; there are no bands originating on $v=5$ or higher. This sudden curtailment of the band system is ascribed to predissociation. The energy of $v=4$ is 5.76 volts higher than the energy A_0, so that if $D \leqq A_0+1.2$, the energy $A_0+5.76$ volts must correspond to dissociation into two ^2D atoms, since that would require an energy of $D+2$ (2.37) or $A_0+5.94$ volts. The agreement between the calculation and the experiment is quite good since in order to compare with the previously discussed predissociation we should use the energy of $v=5$ rather than that of $v=4$. The energy of $v=5$ is about $A_0+5.95$ volts, so the agreement in this case is almost perfect.

The energy of the $v=5$ level of the initial state of the second-positive bands is about $A_0+5.95$ volts, and the energy in $v=13$ is $A_0+3.6$ volts. The difference between these two is 2.35 volts, and the energy of ^2D is 2.37 volts. This remarkable agreement certainly indicates that our arguments are consistent and probably correct.

The initial state of the fourth-positive group of nitrogen is the so-called D level, and only the $v=0$ level has ever been observed. The energy of the $v=1$ level is about $A_0+6.9$ volts, and the energy required for the production of a ^2D and a ^2P atom is equal to or less than $A_0+1.2+2.37+3.56$, i.e., $A_0+7.1$ volts. It seems reasonable once more to assign the non-appearance of higher vibrational levels to predissociation. It should be noted that we have made no use of an actual value for the energy of A_0, since this energy is known only by electron impact measurements. A strong point in the present argument lies in the fact that we have made no use of this value.

We concluded from the first example of predissociation, namely, the one at $v=13$ in $^3\Pi g$, that the heat of dissociation D was equal to or less than $A_0+1.2$ volts. Since the $A^3\Sigma\mu^+$ level has been followed to at least 2.1 volts of vibrational energy, it must be concluded that the products of dissociation are not two ^4S atoms as Mulliken suggested, but that at least one excited atom is involved.

If we assume that D lies between 9.1 and 8.2 volts, then A_0 will lie between 7.9 and 7.0 volts, if the products of dissociation in $v=13$ are ^4S and ^2D. If we assume with Mulliken that the products of dissociation in $^3\Sigma\mu^+$ are two ^4S atoms, then D cannot be equal to $A_0+1.2$ volts, since the vibrational levels have been followed to $A_0+2.1$ volts. We must conclude then that the predissociation at $v=13$ corresponds to dissociation into two ^4S atoms, and D will be equal to or less than $A_0+3.6$. This would yield values for A_0 lying between 5.5 and 4.6 volts, and it is obvious that not even excitation potential measurements would account for the enormous difference between these values and the 8.2 volt value of Sponer. We must conclude that the products of dissociation from the $^3\Sigma\mu^+$ level are ^4S and an excited atom, probably ^2D. The triplet level due to two ^4S atoms is therefore not known, and it will be an interesting problem to try to obtain evidence for its existence.

The predissociation phenomena which have been discussed in this note, enable us to suggest the identity of the products of dissociation from the several triplet states of N_2. We have proved that the $^3\Sigma\mu^+$ level dissociates into an excited atom and a normal atom, and if we say that, in general, a linear extrapolation of the vibrational levels yields a value of the total energy which is too high, then there is no choice for the excited atom but the ^2D metastable state. The linear extrapolation yields a value of 11.9 volts, and predissociation sets in at 11.8 volts, and this makes $D \leqq 9.4$ volts. For the B level the linear extrapolation yields 14.62 volts, and if we use the 9.4 volt value for D the energy required to produce two ^2D atoms is 14.2 volts, hence the identity of the products of dissociation as two ^2D atoms is quite reasonable. For the C level, the products cannot be two ^2D atoms because predissociation sets in at that energy in a manner which shows that higher vibrational levels exist. The linear extrapolation yields a value of 14.62 volts for the total energy, and 15.3 volts are required to produce one ^2D and one ^2P atom. This is therefore an exceptional case in which the linear extrapolation must be too low.

TABLE I.

Predissociating level	Energy based on $A_0=8.2$	Products of dissociation	Heat of dissociation
B_{13}	11.78	$^4S+^2D$	9.4 or less
B_{20}	12.87	$^4S+^2P$	9.3 " "
C_5	14.14	$^2D+^2D$	9.4 " "
D_1	About 15.05	$^2D+^2P$	9.1 " "

The results of this paper are summarized in Tables I and II. The derived values of D are obviously too high in most cases because predissociation sets in at an energy in general higher than that required to dissociate the molecule.

TABLE II.[8]

Birge	9.04 ± 0.2 volts
Kaplan	9.0 "
Tate and Lozier	8.4 ± 0.5 volts
(corrected by Sutton)	9.0 volts

This is in good agreement with Table II of recent values of D, taken from a letter by Sutton.[8] The evidence indicates that D is probably slightly less than 9.0 volts because the data of Table I are based on Sponer's 8.2 volt value for A_0, and all of these values will have to be lowered by the same amount as the 8.2 volt value is lowered. Even though no definite conclusion can be drawn regarding the value of the heat of dissociation of nitrogen it is clear from this paper that the upper limit is about 9.3 volts, and probably even lower, because the 8.2 value of Sponer is too high.

[8] Sutton, Nature **130**, 132 (1932).

Momentum Relations in Crossed Fields

By LEIGH PAGE
Sloane Physics Laboratory, Yale University

(Received July 9, 1932)

It is shown that the mechanical linear or angular momentum gained by ions moving in crossed electric and magnetic fields is at the expense of the electromagnetic linear or angular momentum already present. Hence Ross Gunn's theory of the acquisition of angular momentum by a star as the result of ion motions in its external electric and magnetic fields cannot be upheld.

Three cases are analyzed in detail: (a) Newtonian motion in uniform crossed fields, (b) Newtonian motion in the field of a uniformly magnetized charged sphere, (c) relativity motion in uniform crossed fields.

DURING the last three years Ross Gunn[1] has developed a promising theory of the formation of double stars and of planetary systems based on electromagnetic forces rather than on conventional gravitational attractions. While many of the features of his theory are undoubtedly significant, it will be shown that the mechanism which he invokes to account for the angular momentum of a star would not give rise to the effect which he anticipates. Gunn supposes that a star has combined electric and magnetic fields similar to those of the earth. Ions formed in its atmosphere acquire momentum in the direction of the vector $\boldsymbol{E}\times\boldsymbol{H}$, as shown in an earlier paper of the writer.[2] This momentum, which is in the same sense for ions of opposite signs, is transferred to the star as a consequence of collisions and gives rise to a continuing increase in the angular momentum of that body until finally fission occurs.

In a lecture some thirty years ago J. J. Thomson pointed out that outside a uniformly magnetized charged sphere there exists a Poynting flux everywhere in the direction of the parallels of latitude. This implies the presence of energy and momentum circulating around the axis of the sphere without ever departing from it. While this phenomenon leads to no predictions embarassing to electromagnetic theory, no particular significance appears to have been attached to it. In the course of this paper it will be shown that this flux of momentum plays a very vital role in connection with the motion of ions in the atmosphere of a star.

While certain fundamental theorems of electrodynamics prove that the laws of conservation of both linear and angular momentum hold for an isolated electromagnetic system provided account is taken of both electromagnetic and mechanical momentum, and therefore that Gunn's argument

[1] Ross Gunn, Phys. Rev. **32**, 133 (1928); **33**, 614, 832 (1929); **34**, 335, 1621 (1929); **35**, 107, 635 (1930); **36**, 1251 (1930); **37**, 283, 983, 1129, 1573 (1931); **38**, 1052 (1931); **39**, 130, 311 (1932).

[2] Page, Phys. Rev. **33**, 553 (1929).

cannot be upheld, we shall investigate here the details of the process by which these laws are satisfied in some simple cases, including the case of a uniformly magnetized charged sphere in whose atmosphere ions are present.

A. Uniform Crossed Fields

Consider a uniform electric field E in the direction of the y axis of a set of right-handed rectangular axes x, y, z combined with a uniform magnetic field H in the direction of the z axis. Then, as shown in an earlier paper,[2] ions of both signs progress in the x direction with a drift velocity cE/H which is independent of the charge or mass of the ion. The ion paths are cycloids, being prolate, common or curtate in accord with the magnitude and direction of the initial velocity. The cycloidal paths for the negative ions are obtained from those for the positive ions by rotating the latter through the angle π about the x axis. The integrated equations of motion are[3]

$$x - x_0 = \frac{mc}{e}\left\{\frac{v_{0y}}{H}\left(1 - \cos\frac{eH}{mc}t\right) + \left(\frac{v_{0x}}{H} - \frac{cE}{H^2}\right)\sin\frac{eH}{mc}t\right\} + \frac{cE}{H}t,$$

$$y - y_0 = \frac{mc}{e}\left\{-\left(\frac{v_{0x}}{H} - \frac{cE}{H^2}\right)\left(1 - \cos\frac{eH}{mc}t\right) + \frac{v_{0y}}{H}\sin\frac{eH}{mc}t\right\},$$

$$z - z_0 = v_{0z}t,$$

where x_0, y_0, z_0 are the coordinates of the starting point and v_{0x}, v_{0y}, v_{0z} the components of the initial velocity.

Differentiating the first of these we find for the x component of the momentum

$$p_x = m\left\{v_{0y}\sin\frac{eH}{mc}t + \left(v_{0x} - \frac{cE}{H}\right)\cos\frac{eH}{mc}t + \frac{cE}{H}\right\},$$

and comparing with the second

$$y - y_0 = (c/eH)(p_x - p_{0x}), \tag{1}$$

where $p_{ox} = mv_{ox}$ is the x component of the initial momentum.

This equation states that the displacement of the ion in the direction of the electric field is proportional to the gain of momentum in the direction at right angles to the two fields, that is, in the direction of the Poynting flux. Increase in momentum involves a displacement of positive ions in the same direction as the electric field, and of negative ions in the opposite direction.

Now suppose that at a certain instant n ion pairs per unit volume are formed. Under the action of the fields they separate, acquiring at the same time momentum in the direction at right angles to the two fields. Whether they make collisions with neutral particles and thereby transfer part of their momentum to the latter or not, the total mechanical momentum generated is proportional to the separation of the ions. If Δy denotes the mean separation of the positive from the negative ions, an effective electric moment

[3] Page and Adams, *Principles of Electricity*, p. 289. In the present paper we are using Heaviside-Lorentz units.

$ne\Delta y$ is set up in the region under consideration. This gives rise to an electric field of the same magnitude in the direction opposite to that originally existing. Consequently the electromagnetic momentum g per unit volume increases in the amount $\Delta g = -(1/c)ne\Delta yH$.

However, if Δp is the increase in mechanical momentum per unit volume, it follows from (1) that

$$\Delta p = neH\Delta y/c$$

and consequently

$$\Delta p + \Delta g = 0. \tag{2}$$

So the increase in mechanical momentum of the ions is at the expense of the electromagnetic momentum already present. Production of ions acts as a mechanism for converting the latter into the former. When all the electromagnetic momentum has been transformed, the electric field is reduced to zero, and no more transverse momentum is acquired by the ions. Since electromagnetic momentum is consumed in the same region of space as that in which mechanical momentum is generated, Eq. (2) applies to angular momentum about any arbitrary axis as well as to the case of linear momentum for which it was derived. However, we shall discuss in the next section the specific angular momentum relations existing in the case of a uniformly magnetized sphere which has an electric charge.

B. Uniformly Magnetized Charged Sphere

Take origin at the center of the sphere with polar axis in the direction of magnetization. The spherical coordinates consisting of the radius vector r, polar angle θ and azimuth ϕ are chosen so as to constitute a right-handed set in the order named. If Q is the charge on the sphere and M its magnetic moment, the nonvanishing field components are

$$E_r = \frac{Q}{4\pi r^2}, \quad H_r = \frac{2M}{4\pi r^3}\cos\theta, \quad H_\theta = \frac{M}{4\pi r^3}\sin\theta,$$

and the equation of motion of an ion with charge e and mass m is

$$m\mathbf{f} = e\{\mathbf{E} + (1/c)\mathbf{v} \times \mathbf{H}\},$$

which is equivalent to the three component equations

$$\ddot{r} - r\dot{\theta}^2 - r\sin^2\theta\dot{\phi}^2 = \frac{e}{4\pi m}\left\{\frac{Q}{r^2} - \frac{M}{cr^2}\sin^2\theta\dot{\phi}\right\},$$

$$2\dot{r}\dot{\theta} + r\ddot{\theta} - r\sin\theta\cos\theta\dot{\phi}^2 = \frac{e}{4\pi m}\left\{\frac{2M}{cr^2}\sin\theta\cos\theta\dot{\phi}\right\},$$

$$2\sin\theta\dot{r}\dot{\phi} + 2r\cos\theta\dot{\theta}\dot{\phi} + r\sin\theta\ddot{\phi} = \frac{e}{4\pi m}\left\{\frac{M}{cr^3}\sin\theta\dot{r} - \frac{2M}{cr^2}\cos\theta\dot{\theta}\right\}.$$

The third equation is the significant one for our purposes. It can be written

$$\frac{d}{dt}(r^2 \sin^2\theta\dot{\phi}) = -\frac{eM}{4\pi mc}\frac{d}{dt}\left(\frac{\sin^2\theta}{r}\right),$$

or, if we put $p \equiv mr^2 \sin^2\theta\dot{\phi}$ for the angular momentum of the ion about the axis of the sphere,

$$dp = -(eM/4\pi c)d(\sin^2\theta/r). \tag{3}$$

Next we must calculate the change in electromagnetic angular momentum due to motion of the ion. To do this we shall first compute the electromagnetic angular momentum of an isolated system (Fig. 1) consisting of a point pole m and a point charge e. It is evident from symmetry that the resultant angular momentum is entirely about the line connecting m to e. As

$$F = e/4\pi\rho^2, \quad H = m/4\pi r^2,$$

the component of angular momentum parallel to this line is

$$g = -(me/16\pi^2 cr\rho^2)\sin\theta\sin\alpha$$

per unit volume. Therefore the total angular momentum can be written

$$G = -\frac{mea}{8\pi c}\int_0^\infty\int_0^{2\pi}\frac{r\sin^3\theta}{\rho^3}\,d\theta dr$$

if we eliminate α by the relation $\rho\sin\alpha = a\sin\theta$. First we shall integrate with respect to θ, keeping r constant. In doing this it will be convenient to change

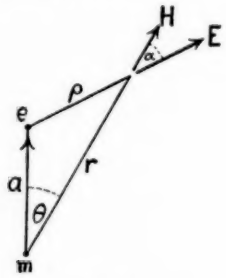

Fig. 1.

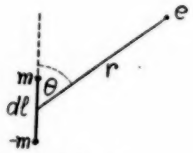

Fig. 2.

the variable of integration to ρ by means of the relation $\rho^2 = r^2 - 2ar\cos\theta + a^2$. We have then

$$ar\int\frac{\sin^3\theta}{\rho^3}\,d\theta = \int\left\{1-\left(\frac{r^2+a^2-\rho^2}{2ar}\right)^2\right\}\frac{d\rho}{\rho^2}$$

$$= \left\{\frac{(r^2-a^2)^2}{4a^2r^2}\frac{1}{\rho} + \frac{r^2+a^2}{2a^2r^2}\rho - \frac{1}{12a^2r^2}\rho^3\right\}.$$

When $r<a$ the limits of ρ are $a-r$ and $a+r$, whereas when $r>a$ the limits are $r-a$ and $r+a$. For the first region

$$G_1 = -\frac{me}{6\pi a^2 c}\int_0^a r\,dr = -\frac{me}{12\pi c},$$

and for the second

$$G_2 = -\frac{mea}{6\pi c}\int_a^\infty \frac{dr}{r^2} = -\frac{me}{6\pi c}.$$

Adding, the total electromagnetic angular momentum is found to be

$$G = G_1 + G_2 = -me/4\pi c. \tag{4}$$

At first sight it seems strange that the angular momentum should be independent of the distance a between the charge and the pole. A little consideration, however, shows that this is to be expected. For if the charge is projected directly toward the pole the magnetic field exerts no force on it and its mechanical angular momentum along the line joining the two remains constant. So the electromagnetic angular momentum should be independent of a.

The magnetic field in which we are interested is that of a dipole. If the line joining the center of the dipole to the charge e (Fig. 2) has a length r and makes an angle θ with the axis of the dipole, the component of the electromagnetic angular momentum of the system along the axis of the dipole is

$$G = -\frac{me}{4\pi c}d(\cos\theta) = \frac{me}{4\pi c}\sin\theta d\theta.$$

Now if dl is the length of the dipole, $d\theta = dl \sin\theta/r$, and

$$G = (eM/4\pi c)(\sin^2\theta/r), \tag{5}$$

where M is the magnetic moment mdl of the dipole. Comparing (5) with (3) we have

$$dp + dG = 0. \tag{6}$$

This equation shows that any gain in mechanical angular momentum by an ion is accompanied by an equal loss in electromagnetic angular momentum. Suppose that the uniformly magnetized sphere is initially uncharged electrically and that ions of one sign (electrons, for instance) are projected toward it from a great distance, the impinging ions having on the average no initial angular momentum about the axis of the sphere. When these ions strike the sphere they impart to it mechanical angular momentum in one sense while giving rise to an equal amount of electromagnetic angular momentum in the opposite sense. If, after the sphere has been charged by the impacting ions, ion pairs are formed in its atmosphere, the action of these ion pairs is to transform the electromagnetic angular momentum into mechanical angular momentum until finally the mechanical angular momentum imparted by the ions impinging from outside is just annulled. Therefore the electromagnetic process postulated by Gunn cannot lead to a continuing increase in mechanical angular momentum of the sphere.

If we replace the point pole by a finite sphere of magnetic charge in deducing (4) we are led to a different result, obtaining in addition to the term appearing on the right-hand side of that equation a second term containing

in the denominator the square of the distance a between the center of the sphere and the point charge. This additional term remains when we superpose two slightly displaced spheres of opposite sign so as to construct a uniformly magnetized sphere. Its presence is due to the fact that we erroneously employ H inside the magnetized sphere in calculating the electromagnetic momentum when we should in fact make use of B. The added term disappears when this error is corrected, and (5) is found to hold rigorously for a uniformly magnetized sphere as well as for a magnetic dipole. The analysis, which is somewhat laborious, will not be reproduced here.

C. Relativity Dynamics

The preceding analysis is inapplicable to the case where the ions have velocities comparable with the velocity of light. In such an event the variation of mass with velocity must be taken into account. We shall develop the theory for the case of uniform crossed fields on the relativity dynamics.

As before we shall take E in the direction of the y axis and H in that of the z axis of a right-handed set of rectangular axes fixed in the observers' inertial system S. In addition we shall have occasion to refer to a set of parallel axes x', y', z' located in an inertial system S' moving in the x direction relative to S with the constant velocity $u=cE/H$. As shown in a previous paper[2] the electric field vanishes in S' and the ions describe helices around the lines of magnetic force with angular velocity

$$\omega' = - eH'/m_t c,$$

where m_t is the transverse mass. If v_0' is the initial velocity of an ion relative to S', the components of velocity at any time t' are

$$\begin{aligned} v_x' &= v_{0x}' \cos \omega' t' - v_{0y}' \sin \omega' t', \\ v_y' &= v_{0x}' \sin \omega' t' + v_{0y}' \cos \omega' t', \\ v_z' &= v_{0z}'. \end{aligned}$$

Now the displacement of an ion along the electric field is

$$\begin{aligned} y - y_0 = y' - y_0' &= (1/\omega')\{v_{0x}'(1 - \cos \omega' t') + v_{0y}' \sin \omega' t'\} \\ &= - (1/\omega')(v_x' - v_{0x}'). \end{aligned}$$

Making use of the relativity transformations for the components of velocity,

$$y - y_0 = - \frac{1}{\omega'}\left\{\frac{v_x - u}{1 - \beta\dfrac{v_x}{c}} - \frac{v_{0x} - u}{1 - \beta\dfrac{v_{0x}}{c}}\right\},$$

where $\beta \equiv u/c$ is the ratio of the relative velocity of the two inertial systems to the velocity of light. Now

$$v_x'^2 + v_y'^2 + v_z'^2 = v_{0x}'^2 + v_{0y}'^2 + v_{0z}'^2 \equiv v'^2$$

since the speed relative to S' does not change with the time. Transforming to system S we find

$$\frac{(1 - v^2/c^2)^{1/2}}{1 - \beta v_x/c} = \left(\frac{1 - v'^2/c^2}{1 - \beta^2}\right)^{1/2} \equiv \text{constant}.$$

Also

$$-\frac{1}{\omega'} = \frac{m_t c}{eH'} = \frac{m_0 c}{eH} \frac{1}{[(1 - \beta^2)(1 - v'^2/c^2)]^{1/2}},$$

where m_0 is the rest mass of the ion.

Therefore

$$y - y_0 = \frac{m_0 c}{eH} \frac{1}{1 - \beta^2}\left\{\frac{v_x - u}{(1 - v^2/c^2)^{1/2}} - \frac{v_{0x} - u}{(1 - v_0^2/c^2)^{1/2}}\right\}$$

$$= \frac{c}{eH} \frac{1}{1 - \beta^2}\left\{p_x - p_{0x} - \frac{u}{c^2}(T - T_0)\right\}$$

where p_x is the momentum and T the kinetic energy of the ion. Now

$$(u/c^2)(T - T_0) = (\beta/c)eE(y - y_0) = (eH/c)\beta^2(y - y_0).$$

Solving for $y - y_0$, we find identically the same relation

$$y - y_0 = (c/eH)(p_x - p_{0x}) \tag{7}$$

between the displacement along the electric lines of force and the gain in momentum at right angles to the two fields as was obtained on the Newtonian dynamics. Therefore electromagnetic momentum is converted into mechanical momentum by ions produced in the atmosphere of a star or planet in precisely the same manner as in the cases previously discussed.

The Effect of Strain on Magnetostriction and Magnetization in Nickel

By C. W. HEAPS
Rice Institute, Houston, Texas

(Received June 20, 1932)

With a heterodyne beat method, magnetostrictive hysteresis loops have been obtained for a nickel wire under three different tensions. Magnetic hysteresis loops for the same wire and same tensions were also secured. The magnetostrictive contraction, dL/L, for the tensions 6.82 and 3.70 kg/mm² is given quite accurately by the one equation, $dL/L = -1.93\times10^{-10}\ I^2$, where I = intensity of magnetization. For a tension 0.72 kg/mm² the equation $dL/L = -1.30\times10^{-10}\ I^2$ holds somewhat less accurately. The effect of compression and of stretch on the residual magnetization of a nickel wire in a demagnetizing field is determined experimentally. From this experiment, and from the magnetostriction curves, it is shown that at certain field strengths the magnetism of a nickel wire, bent elastically into a circular arc, becomes unstable. Thus the large discontinuities in the magnetization curve observed by Forrer may be explained. It is suggested that the small Barkhausen jumps of magnetization may be due to similar magnetic instability produced in small regions by local strains.

THE phenomenon of hysteresis in magnetostriction has been observed by a number of investigators,[1] but a detailed study of the effect of strain on magnetostrictive hysteresis does not appear to have been made. The importance of strain, both in theories of magnetism and in experiments on particular phases of the subject, has recently been emphasized; for example, the very great influence which strains in the material may have on the Barkhausen effect or on the magnetic hysteresis loop.

The present paper reports experiments in which the magnetostrictive hysteresis loops and the magnetic hysteresis loops have been determined for a nickel wire under different tensions. Nickel was chosen for the experiments because the magnetostriction curves of a nickel crystal are not greatly affected by the orientation of the crystalline axis;[2] hence in a polycrystalline wire the effect of crystal size or crystal orientation should be of little importance in modifying magnetostriction. Furthermore, it is in nickel that very striking discontinuities of magnetization have been produced by strains in the material.[3] The explanation of these discontinuities was one of the objects of the experiment.

THE EXPERIMENTAL METHOD

For observing magnetostriction the heterodyne beat method of measuring small capacity changes or small displacements was used. Two oscillating elec-

[1] H. Nagaoka, Phil. Mag. [5] **37,** 131 (1894); L. W. McKeehan, J. Franklin Inst. **202,** 737 (1926); A. Schulze, Ann. d. Physik [5] **11,** 937 (1931); G. Dietsch, Zeits. f. techn. Physik **12,** 380 (1931).

[2] Y. Masiyama, Sci. Rep. Tohoku Imp. Univ. [1] **17,** 945 (1928).

[3] R. Forrer, J. de Physique [6] **7,** 109 (1926); **10,** 247 (1929).

trical circuits have their beat note (of audiofrequency) picked up by a detector, amplified, and impressed upon an oscillograph. One plate of a condenser in one of the oscillating circuits is supported by the nickel wire under test. This wire is surrounded by a solenoid. If the field in the solenoid is varied the length of the nickel wire changes, thus changing the capacity of the oscillating circuit. The frequency of the heterodyne beat note is therefore altered by an amount which can be determined from the oscillograph record. From a knowledge of the calibration constant of the apparatus the change of length of the wire may thus be calculated. Details of the electric circuits have been described elsewhere.[4]

Fig. 1 shows the arrangement of the condenser, the capacity of which is changed by the magnetostriction of the nickel. This condenser is connected in parallel with an adjustable precision condenser which was set to have the same large capacity throughout the experiment. The upper plate *B* has a

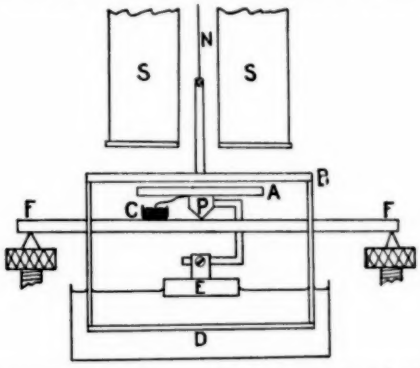

Fig. 1. Arrangement of condenser in the magnetostriction apparatus.

diameter 5 cm and is connected to earth through the nickel wire *N*. Three light, vertical rods, of which two are shown, are fixed to the edge of the upper plate and support a flat ring *D* of aluminum, immersed in oil to serve as a damping fluid. Plate *A*, of diameter 2 cm, is insulated by Bakelite from the point support *P* and counterbalance *E*. A wire from this plate dips into the mercury cup *C* by means of which connection is made to the oscillating circuit.

The micarta cross-bar *FF*, is supported on three leveling screws, of which two are shown. These screws are used to vary the capacity of the condenser. The plate *A* is carefully leveled by adjusting the counterweight *E*, which also serves as a damping plate. Weights may be placed on top of *B* to produce tension in the wire *N*. To level *B* accurately a small, easily movable weight was carefully adjusted on the top of the plate.

The solenoid, *SS*, of which only the lower part is shown, is 30.3 cm long and has 7195 turns. It is supported on a stand separate from that which supports the wire *N*. The nickel wire is 15 cm long and 0.018 cm in diameter. It is carefully centered in the solenoid so as to be in a uniform field. The current through the solenoid may be given a series of values by opening or closing a

[4] A. B. Bryan, Phys. Rev. [2] **34,** 615 (1929); C. W. Heaps and A. B. Bryan, Phys. Rev. [2] **36,** 326 (1930).

series of switches which short circuit sections of a rheostat. These switches consisted of a series of metal contacts spaced equally along a vertical micarta bar which could be pushed down into a jar of mercury. With this device it was possible to put the nickel wire through the entire hysteresis loop in only a few seconds, the successive changes of length being indicated by frequency changes on a section of oscillograph film about 10 feet long. A condenser in series with a heavily damped vibration galvanometer was connected across the switching device, so that every time the solenoid current changed, the galvanometer received an impulse which was recorded on the oscillograph film.

The oscillograph consisted of a telephone receiver to the diaphragm of which a light mirror was connected. Records were obtained on positive motion picture film and developed by the contrast developer recommended by Town.[5] The time scale was obtained by interrupting a beam of light by the cogs in the wheel of an electric clock running on 60-cycle current. Fig. 2

Fig. 2. Oscillograph record. Top trace = solenoid current; middle trace = heterodyne note; bottom trace = time scale.

shows a section of film. The topmost trace indicates changes of current in the solenoid, the middle trace is a record of the heterodyne beat note, the bottom trace is the time scale, each segment representing 1/60 sec. The figure shows how the film was marked and how the frequency was determined for a given value of the magnetizing current.

To convert frequency changes into length changes it was necessary to calibrate the device. The following method was used. A leveling screw at F was adjusted till the heterodyne beat note emitted by the telephone receiver was in accurate tune with a tuning fork of pitch 1024. A micrometer microscope was then focussed on a fine scratch on plate A. By means of the leveling screw the plate A was now moved either up or down, so as to lower the pitch of the heterodyne note down through zero frequency and up to the frequency 1024 again. A total frequency change of 2048 was thus secured and the motion of A was large enough to be measured with considerable accuracy. For very small displacements of A (or B) such as were used in the experiment, it may be shown that the frequency change of the heterodyne note is proportional to the displacement. Thus the length change of the wire per cycle of frequency change is easily calculated. Throughout the experiments the value of this quantity was kept at 2.10×10^{-6} cm per cycle.

Magnetic hysteresis loops were secured by using a sensitive astatic magnetometer of the type described by Bozorth.[6] The vertical component of the

[5] G. R. Town, Rev. Sci. Inst. **1**, 449 (1930).

[6] R. M. Bozorth, J.O.S.A. and R.S.I. **10**, 591 (1925).

earth's magnetic field was neutralized by means of Helmholtz coils, both in the magnetometer experiments and in the magnetostriction experiments. Demagnetization of the nickel could be effected by using liquid rheostats to decrease a 60-cycle alternating current through the magnetizing solenoid.

The nickel wire was cold drawn from Eimer and Amend's *pure sheet nickel.* After the drawing the wire was heated electrically to a bright red in an atmosphere of carbon dioxide, and cooled slowly by gradual decrease of the heating current. It was loaded and unloaded several times up to the limiting tension used in the experiment before any records were taken. The wire was very soft and experiments on a short sample indicated a definite yield at about 14 kg per mm². In order to keep well within the elastic limit stresses greater than 7 kg per mm² were not used during the experiment.

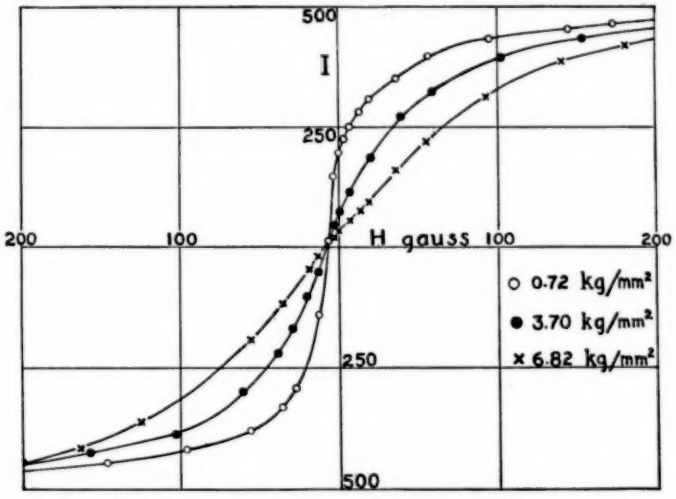

Fig. 3. The effect of tension on the descending branch of the hysteresis loop of nickel.

Discussion of Results

Fig. 3 shows how tension affects the magnetic hysteresis loop. These results agree, in general, with previous work.[7] Figs. 4 and 5 show the effect of tension on magnetostriction. A point of interest here is the fact that the curves for different tensions cross at large values of the magnetic field, H. In other words, it appears that tension applied to a nickel wire will decrease the magnetostriction in small fields and increase it in large fields. Bidwell[8] has observed a similar phenomenon. The explanation, as will appear later, lies in the way in which the intensity of magnetization varies with the field strength.

A second point of interest in connection with these curves is the effect of strain for very small fields. When the wire is loaded with 6.82 kg/mm² and saturated magnetically, the residual magnetostriction when the field is

[7] M. Kersten, Zeits. f. Physik **71,** 553 (1931).
[8] S. Bidwell, Proc. Roy. Soc. **47,** 469 (1890).

brought to zero is too small to be detected. Furthermore, a reverse field of at least 20 gauss must be applied before the magnetostriction becomes large enough to measure. The conditions are quite otherwise when the wire carries only 0.72 kg/mm². In this case the residual magnetostriction is quite large,

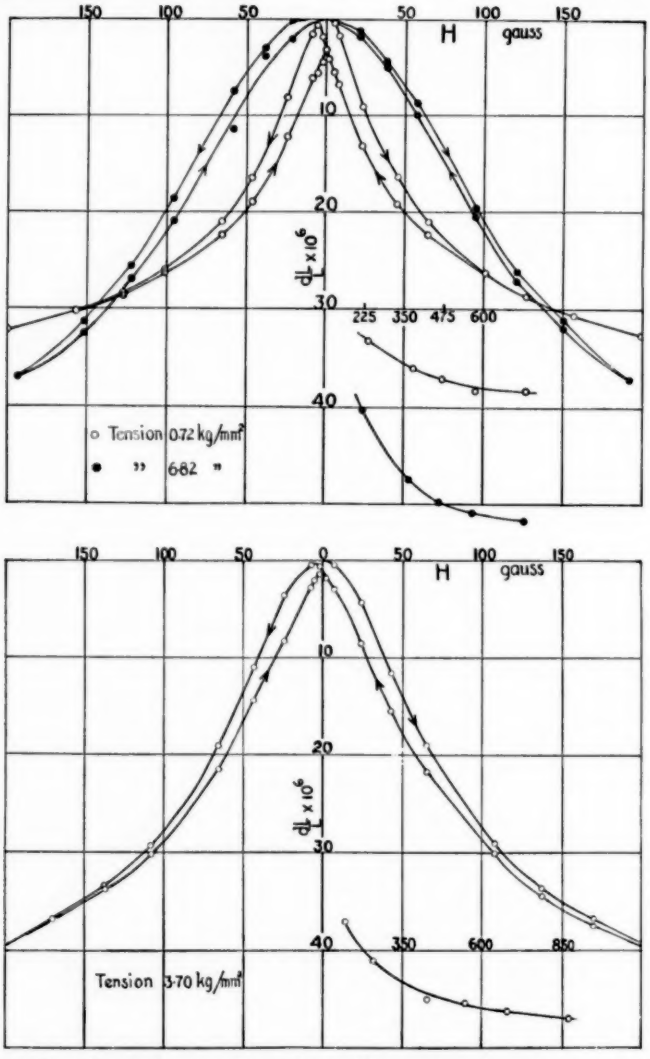

Figs. 4, 5. Fractional change of length, dL/L as a function of magnetic field, H. The short segments are extensions to large fields.

and the reverse field, as it increases, causes the wire to elongate[9] till a field of about 6 gauss is reached. At this point the residual magnetization is re-

[9] This elongation, of course, is really a diminution of contraction produced by a decrease of residual magnetization. Deitsch (reference 1) appears to consider it as actual positive magnetostriction of nickel. There seems to be little doubt, however, but that it may be accounted for in the work of Dietsch by incomplete demagnetization of his specimen. In such a case the origin of the magnetostriction curve is improperly located.

duced to zero and for further increase of field the wire contracts. As will be noted later, this difference of behavior of stretched and unstretched nickel is of special significance in relation to discontinuities of magnetization.

In Fig. 6 the magnetostriction is represented as a function of the intensity of magnetization. The plotted points are values taken from the curves of Figs. 3, 4, and 5. The line drawn through the points and designated by A is the graph of the equation $dL/L = -1.93 \times 10^{-10}\ I^2$. It appears that for the two tensions, 3.70 and 6.82 kg/mm², the one curve A represents the experimental results with considerable accuracy. It is somewhat surprising that an increase of tension from 3.70 to 6.82, which produces such marked changes in the magnetic hysteresis loop and in the magnetostriction loop as plotted against the magnetic field H, should really have no effect on magnetostriction considered as a function of I.

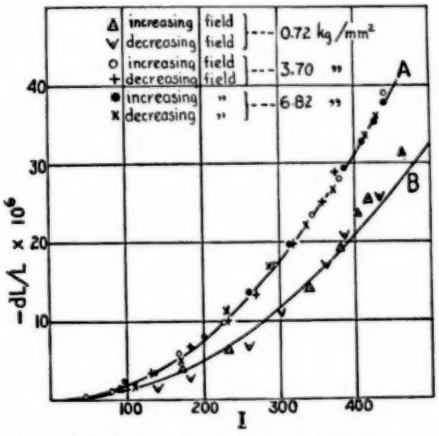

Fig. 6. Magnetostriction as a function of intensity of magnetization.

For the smallest tension the plotted points[10] are somewhat irregularly distributed. The curve drawn through these points and designated by B is the graph of the equation $dL/L = -1.30 \times 10^{-10}\ I^2$. It represents to a fair approximation the experimental results. However, for small values of I the plotted points indicate the existence of appreciable hysteresis. The work of McKeehan and Cioffi, and of A. Schulze, seems to show that hysteresis is present in the $dL/L - I$ curves for unstrained nickel, in agreement with the present work. From Fig. 6, curve A, the additional conclusion may be drawn that the application of sufficiently large strains makes this hysteresis effect negligibly small.

Recently some important theoretical work has been done on the subject of magnetostriction. The theories of Akulov[11] and of Becker,[12] in which the energy of a strained dipole lattice is taken as the starting point, have been shown by Powell[13] to be consistent with each other. Powell's equation for

[10] The points for this curve are obtained on the assumption that $dL/L = 0$ when $I = 0$.

[11] N. Akulov, Zeits. f. Physik **52,** 389 (1928); **59,** 254 (1930); **64,** 817 (1930); **69,** 78 (1931).

[12] R. Becker, Zeits. f. Physik **62,** 253 (1930); **64,** 660 (1930).

[13] F. C. Powell, Proc. Camb. Phil. Soc. **27,** 561 (1931).

dL/L makes the effect proportional to I^2. Powell states that his equation need not necessarily apply to values of dL/L determined experimentally because of the possibility of micromagnetization of crystals which as a whole are unmagnetized. In spite of this limitation it appears that where tension is applied to nickel the theoretical law of variation of dL/L is verified experimentally to a considerable degree of accuracy.

We may now consider why curve A of Fig. 6 represents equally well the data for the two large tensions. The obvious explanation is that either of the two large tensions is sufficient to produce a saturation effect. When tension is applied to nickel, current theories[14] agree in supposing that the atomic magnets are orientated across the axis of tension, or that the magnetization vectors, I, of small microscopic blocks into which the nickel is divided, are so orientated. For a sufficiently large tension there is complete transverse orientation. A longitudinal magnetic field, in order to magnetize the wire to saturation, must orientate all these atomic magnets along the axis of the wire, thus causing maximum magnetostriction. When no tension is applied the atomic magnets may be initially orientated at random and the magnetic field, in lining them up, cannot produce such a large net length change because of the less favorable initial distribution of axes.

It appears from the curves of Fig. 6 that tensions of 3.70 and 6.82 kg/mm^2 are equally effective in producing complete transverse orientation of atomic magnets in nickel. This conclusion may be drawn because for both of these tensions we get the same magnetostriction produced by a given intensity of magnetization. On the other hand, for the tension 0.72 a considerably smaller magnetostriction is produced by this same intensity of magnetization. It is probable that the atomic magnets of the nickel under the tension 0.72 are distributed more or less at random. There will not be completely random orientation, however, even with this small tension. The quantitative working out of the theory indicates that the maximum magnetostriction under large strain should be 1.5 times the maximum magnetostriction under no strain. This ratio for tensions 6.82 and 0.72 is only 51.8/38.3, or 1.35. Apparently, therefore, the small strain has produced an appreciable transverse orientating of atomic magnets.

The Effect of Strains on Residual Magnetism

The curves of Fig. 3 do not give a complete picture of the processes which may occur in the region of demagnetization. For example, from these curves, each obtained at constant tension, it might be concluded that compressing nickel in a demagnetizing field would increase the residual magnetism. However, since shock and vibration are known to facilitate demagnetization there might be some doubt about the correctness of this conclusion. In order to secure more detailed information regarding the region of demagnetization the following experiment was performed.

A wire of commercial nickel, 15 cm long and about 1 mm in diameter, was soldered to a strip of brass 15 cm long, 0.16 cm thick, and about 3 cm wide.

[14] L. W. McKeehan, reference 1; R. Becker and M. Kersten, Zeits. f. Physik **64**, 665 (1930).

The wire was soldered throughout its length to the brass and was parallel to the strip's long dimension. The brass strip was then suspended in a vertical solenoid beside the magnetometer, a second solenoid being arranged to balance the field of the first solenoid at the magnetometer. The effect of the magnetized nickel on the magnetometer could also be balanced by a third small solenoid. By bending the plate in one direction the nickel wire was stretched, by bending it in the opposite direction it was compressed. Furthermore, by clamping the strip with an initial bend, adjusting the demagnetizing field to the proper value, and then altering slightly the amount of bend, the effect of this small change of strain on the value of I could be determined by observing the direction of deflection of the magnetometer.

Fig. 7 gives qualitatively the results of the various experiments. Curve A is representative of compressed nickel, curve B of stretched nickel. The

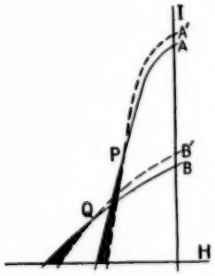

Fig. 7. The effect of strain on the intensity of magnetization of nickel in a demagnetizing field.

stretched wire has a smaller residual magnetism and a larger coercive force than the compressed nickel. The dotted curves associated with A and B indicate the effect of increasing the compression in each case.

The shaded areas represent regions where irreversible effects occur. In one case when the nickel was in a state of compression the point P was at about 8 gauss. For fields less than 8 gauss an increase of compression caused a reversible increase of residual magnetism. (However, as P was approached there was a decided tendency for irreversible decreases of magnetism to occur when the excess compression was removed.) For demagnetizing fields greater than that at P an increase of compression always caused an irreversible decrease of I. On the basis of these results the dotted curve A' was drawn as in Fig. 7.

It was found that in demagnetizing fields greater than that at P a decrease of compression produced an irreversible decrease of I. Hence the shaded area cannot be entered vertically starting from the dotted curve A'; any attempt to enter in this way results in a drop downwards.

Very similar results were obtained with nickel when initially in a stretched condition, the curves B and B' being obtained. In one case the point Q was at about 10 gauss.

Discontinuities of Magnetization

If a nickel wire is subjected to a bending torque its magnetization curve shows remarkably large discontinuities.[15] For the production of these discontinuities it appears necessary that part of the wire be in a state of compression and part in a state of tension. If a wire with no internal strains is bent into the arc of a circle and the elastic limit not exceeded, we probably have the simplest conditions for producing these large discontinuities. In this case we may make a rough approximation and consider the wire as behaving like two wires fastened together laterally, one wire being stretched, the other compressed. The magnetic and magnetostrictive behavior of these separate wires is known from experiment, hence the behavior of the composite wire should be predictable.

Assume the composite wire magnetized to saturation in one direction and then subjected to a gradually increasing field in the opposite direction. For small values of this field we may assume from Fig. 4 that there is negligible magnetostriction of the stretched component. The compressed component of the composite wire will increase its length as the field increases. This increase of length of the compressed section tends to increase the degree of compression, since the wire will be assumed not to bend. Also, the tension of the stretched section is increased. The situation is similar to that found where a straight, bimetallic strip is used on a thermostat. As the temperature rises and the strip is not allowed to curve, one metal is increasingly compressed, the other increasingly stretched.

It is easy to show that the magnetization of such a composite wire will be stable for demagnetizing fields less than those corresponding to points P or Q, Fig. 7. In demagnetizing fields greater than these, however, there is instability. For, consider a small increase, ΔH, occurring in a shaded region of Fig. 7, and assume outside forces applied so as to keep the tensions in the two parts of the composite wire constant during this change. We then get decreases, ΔI_A, and ΔI_B, respectively, in the magnetizations of the compressed and stretched segments. However, from Figs. 3 and 7 we conclude[16] that ΔI_B is much smaller than ΔI_A. Also from Fig. 4 we see that ΔH in this region produces negligible length change in the stretched segment B, as compared with that in the compressed segment A. Since the composite wire is not allowed to curve, the increase of length of A would produce a compressive stress in A and a tension in B, were it not for the external forces assumed to be applied. These forces are a pull on A and a compressive stress on B. Now remove these outside forces. From Fig. 7 it appears that decreases of magnetization, δI_A and δI_B, result, the value of δI_B being much less than δI_A. The effect of δI_A is to introduce magnetostrictive expansion of A, so that if the wire does not curve there results a compressive stress in A and a tensile stress in B. These new stresses now produce further increments of decrease of I.

[15] R. Forrer, reference 3; M. Kersten, reference 7.

[16] The curves for compressed nickel are not given in Figs. 3, 4, and 5. However, the differences between stretched and compressed nickel will be similar to the differences between stretched and unstretched nickel. The magnitude of the differences will, of course, be greater in the former case.

From the foregoing it is clear that conditions are such as to produce instability. The decrease of magnetization of the compressed segment, produced by a small increase of the demagnetizing, field, introduces strains which tend to increase the magnetization change which produced them. Discontinuities of magnetization of the composite wire will thus appear for demagnetizing fields beyond the point P.

The large changes of magnetization produced by the above means would end when the strains produced by magnetostriction tend to inhibit the magnetization changes which produce them. It appears that this condition is met with as soon as all the residual magnetism is removed and I begins increasing in the direction of the field.[17] In other words, a discontinuity of I, initiated above the H axis on the descending branch of the hysteresis loop, would not be expected to extend below the H axis.

It is a fact that the large Forrer discontinuities may be initiated in the demagnetization section of the hysteresis loop and that they frequently do not cross the H axis. On the other hand, there are instances where almost the entire left side of the hysteresis loop consists of a single discontinuity. It would appear, therefore, that conditions of instability must be present in many cases, even after all residual magnetization has disappeared and the I vector is increasing in the direction of the field.

Possibly it is not correct to assume, as we have done above, that nickel has its maximum length at the point where I passes through zero and begins increasing in the direction of the field. This assumption is not in agreement with the experimental work of Schulze, whose nickel begins to contract as soon as I is reduced below about 150. (It expands while I is being reduced from saturation to 150.) The curves of McKeehan and Cioffi, however, appear to indicate that $I=0$ when the slope of the dL/L curve is zero, in agreement with Fig. 6. Also from the standpoint of theories involving orientation of atomic magnets this assumption is the natural one to make. Schulze's curves, therefore, appear to require further experimental corroboration before they can be accepted.

The theory of the large discontinuities of magnetization given above may be applied to the much smaller Barkhausen discontinuities which usually require an amplifying device for their detection. Suppose that in a ferromagnetic substance there are small regions in a condition of strain similar to that assumed for the composite wire above. Then each of these small regions will contribute its own discontinuity to the magnetization curve. In this way the ordinary Barkhausen effect would be produced. The existence of these highly localized strains is not improbable. Recent experimental and theoretical work[18] has demonstrated that a ferromagnetic crystal is made up of small

[17] We assume that the contraction begins as soon as I begins increasing. In this case an increment, ΔH, causing an increment, ΔI_A, in the compressed segment, produces magnetostrictive strains which decrease the degree of compression of the compressed segment. A decrease of compression would produce a decrease of I. The strains produced by magnetostriction thus tend to inhibit the magnetization changes which produce the strains.

[18] F. Zwicky, Phys. Rev. [2] **38,** 1772 (1931); F. Bitter, Phys. Rev. [2] **37,** 91 (1931); **38,** 1903 (1931).

blocks which are more or less independent of each other in their magnetic behavior. These blocks will be the seat of local strains because of the differences in their magnetic condition. Webster's theory,[19] which accounts for magnetostriction in unsaturated states, assumes that small regions are magnetized to saturation in various directions, the crystal as a whole not necessarily showing any resultant magnetization. The small regions are supposed to possess natural directions of easy magnetization.

A system of this kind would inevitably lead to a complicated pattern of internal strains associated with the blocks. An increasing magnetic field merely rotates the magnetization vector of each element without changing its magnitude. However, since each block expands transversely to its magnetization vector and contracts parallel thereto, it is evident that rotation of the separate vectors, either into or out of the condition of random orientation would set up strains of an elastic character between separate blocks. Whenever these strains produce magnetic instability a Barkhausen jump of magnetization occurs.

Experimental evidence has been obtained by Preisach[20] that the Barkhausen effect is fundamentally of the same nature as the large Forrer discontinuity. Stretching a wire of Fe-Ni alloy caused the small discontinuities to merge into a single large one; we may therefore suppose them to arise from the same underlying cause. Although the large discontinuities sometimes obtained in alloys may not be as simply explained as in the case of pure nickel, it appears evident that no theory of the effect can be satisfactory unless it considers strains as of fundamental importance in the whole phenomenon.

[19] W. L. Webster, Proc. Phys. Soc. **42**, 431 (1930).
[20] F. Preisach, Ann. d. Physik [5] **3**, 737 (1929).

The Variation of Dielectric Constant with Temperature. II. Electric Moments of the Ethylene Halides

By Ernest W. Greene and John Warren Williams
Laboratory of Physical Chemistry, University of Wisconsin

(Received August 15, 1932)

Both the free and hindered rotation of atoms or groups of atoms about single chemical linkages may be studied with the Debye relation between the molar polarization, P, and the reciprocal of the absolute temperature, $1/T$. The quantitative treatment by one of us for the simplest case of a free rotation has been compared with the more recent and more general expressions of Eyring and of Zahn. For the case in which the relation between P and $1/T$ is nonlinear the use of Meyer's equation has been suggested for the calculation of the electric moment of the molecule. An apparatus has been described for measuring the dielectric constant of a vapor as a function of temperature. This apparatus includes a comparatively cheap vapor condenser of Monel metal, a means of obtaining vapor at any desired pressure up to that characteristic of 100°C, and a method of measuring vapor pressure in an all-glass apparatus. An experimental procedure has been designed to minimize as far as possible the systematic errors due to simplifying assumptions in the capacity equations of the measuring circuit. The results of dielectric constant and density measurements on ethylene chloride and ethylene bromide have been recorded. The experimental values for the total polarizations of these compounds have been plotted against the reciprocals of the absolute temperature. These results have been utilized for the calculation of the several electric moments by the usual methods based on the linear equation of Debye and by the application of Meyer's equation. All of the methods for the calculation of electric moments were found to give results approaching each other at higher temperatures but tending to deviate more and more at lower temperatures. It has also been possible to calculate the characteristic moments of the C−Cl bond and the C−Br bond from the experimental data. The characteristic moments of the bonds were found to bear the same ratio to each other as the moments of the methyl compounds. It has been further shown that Meyer's equation is applicable to the results for vapors and for solutions now existent in the literature. The indications are that the difference between the experimental results for vapors and for solutions may be due to changes in internal structure produced in the molecule by the solvent.

Introduction

DURING the last two decades dielectric theory has played an important role in the development of ideas concerning the electrical constitution of matter. Quantum theory has clarified the view of intra-atomic matter, while the older kinetic and thermodynamic theories have been concerned with intermolecular action of comparatively large aggregates. In the field between, where the interest lies in the relative positions and interactions of atoms and groups of atoms within the molecule, dielectric theory has found important and unique application.

The interpretation of the temperature effect on the mean electric moment $\bar{m}$ of a molecule in an external field F was presented by P. Debye in the year 1912 through the familiar equation:[1]

[1] Debye, Phys. Zeits. **13**, 97 (1912); See also *Polar Molecules*, Chemical Catalog Co., New York (1929).

$$\bar{m} = (\alpha_0 + \mu^2/3kT)F. \tag{1}$$

In this equation α_0 is the polarization due to deformation, μ is the permanent moment of the molecule, k is the Boltzmann constant (1.37×10^{-16}), and T is the absolute temperature.

The general formula for the polarizability is, therefore,

$$\alpha = \alpha_0 + \mu^2/3kT.$$

Experimental verification of this equation has followed its combination with the Clausius-Mosotti relation, written for the molar polarization P, as follows:

$$\frac{\epsilon - 1}{\epsilon + 2} \cdot \frac{M}{\rho} = P = \frac{4\pi N}{3}\alpha = \frac{4\pi N}{3}\left(\alpha_0 + \frac{\mu^2}{3kT}\right) \tag{2}$$

or

$$P = A + B/T. \tag{2'}$$

Here ϵ is the dielectric constant, M is the molecular weight, ρ is the density, N is the Avagadro constant (6.06×10^{23}), $A = 4\pi N\alpha_0/3$ (molar polarization due to deformation), and $B = 4\pi N\mu^2/9k$ (molar polarization due to the permanent moment of the molecule). The experimental determination of ϵ and ρ for a compound over a series of temperatures permits the calculation of the relation between the total polarization P and $1/T$. This affords a direct check on the linearity of the Debye relationship. It also distinguishes between nonpolar and polar molecules, and in the case of the latter, provides a means of calculating the permanent moment μ from the constant B. Such experimental studies have amply verified the fundamental correctness of the above equations.

From such results the electric moment μ has been obtained by one of the following methods:

(1) The constant B, and thus μ, can be obtained from the slope of the linear plot of P *vs.* $1/T$.

(2) Multiplying Eq. (2′) through by T gives:

$$PT = AT + B. \tag{2''}$$

The quantity B can now be obtained from the intercept, at $T=0$, of the plot of PT *vs.* T. This method does not differ essentially from the first.

(3) In Eq. (2′) the deformation polarization A can be approximated from refractivity data. Ten percent may be added to the molecular refractivity in order to allow for the contribution of the atoms. The ratio B/T is then obtained as the difference between P and A. This method must be used when data at only one temperature are available. Its use, in conjunction with the value of B given above, depends as much upon the linear form of the Eq. (2′) as does either of the other two methods.

Intra-Molecular Rotation

The possibility of rotation about some valence bonds has long been suspected. We will confine our attention in this article to what are probably the

simplest molecules in which this phenomenon is exemplified, namely, the ethylene halides. In these compounds rotation about the C–C bond would be expected from the purely chemical evidence that it has been impossible to separate cis and trans isomers. The fact that these molecules have finite dipole moments has been established by numerous investigators. The most important results for ethylene chloride and ethylene bromide have been brought together in Table I. If the trans form alone were present there would result a zero moment. The finite moment found experimentally may be due to one of three possibilities: (1) Molecules of only the cis form may be present. (2) There may be a mixture of molecules of the cis and trans form. (3) The moment may represent an average of the moments of a number of molecules

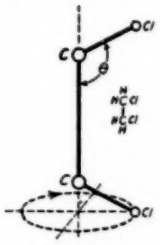

Fig. 1.

having effectively different dissymmetries due to the relative rotation of the two polar groups about the C–C linkage. The first of these is excluded because the cis form is the one having the higher potential energy (due to repulsion between like polar groups) and would thus hardly be formed in preference to the trans form. There is also evidence against this possibility in the fact that the moments in Table I are much lower than those of the corresponding cis forms of the acetylene dihalides. The second possibility, and indeed the first as well, would be at variance with all the evidence, both chemical and physical, for the rotation about such valence bonds. Evidence of a variation of moment with temperature further strengthens the supposition of such a rotation.

TABLE I. *Electric moments of ethylene chloride and ethylene bromide.*

Substance	In solution in: benzene $\mu\times10^{18}$	hexane $\mu\times10^{18}$	heptane $\mu\times10^{18}$	As vapor $\mu\times10^{18}$
Ethylene chloride	1.83[2] 1.86[3] 1.75[4]	1.26–1.42[2]	1.16–1.42[6]	1.56[7] 1.01[8] 1.12–1.54[9]
Ethylene bromide	1.46–1.55[5] 1.4[4]		0.79–1.05[5]	0.94–1.10[10]

[2] Meyer, Zeits. f. phys. Chem. **B8,** 27 (1930).
[3] Gross, Phys. Zeits. **30,** 504 (1929).
[4] Williams, Zeits. f. phys. Chem. **138,** 75 (1928).
[5] Smyth, J. Am. Chem. Soc. **53,** 2988 (1931).
[6] Smyth, J. Am. Chem. Soc. **53,** 4242 (1931).
[7] Ghosh, Mahanti and Sen Gupta, Zeits. f. Physik **54,** 711 (1929).
[8] Sänger, Phys. Zeits. **32,** 21 (1931).
[9] Zahn, Phys. Rev. **38,** 52 (1931).
[10] Zahn, Phys. Rev. **40,** 291 (1932).

In general there may be two types of rotation depending upon the energy state of the molecule. It will be recognized from the model in Fig. 1 that the cis configuration corresponds to a position of maximum potential energy of repulsion between the two moments, while the trans configuration corresponds to a position of minimum potential energy. In fact the resultant moment for the whole molecule would be largest for the cis form and zero for the trans form. This has been confirmed in the cis and trans forms of rigid double bond linkages. Calculations of Eucken and Meyer[11] have shown that free rotation occurs when the potential energy between the two halves of the molecule does not exceed $(1/10)kT$. However, if this potential energy exceeds $(1/10)kT$ there results a rotary oscillation about the position of minimum potential energy, which case we will call "hindered rotation" after the above authors. Obviously, in terms of the resultant moment of the molecule, there will be no sharp division between the two cases. When the rotation is hindered or oscillatory the amplitude of the oscillations will increase as the temperature is raised and the energy of the oscillations increases. The resultant moment of a molecule of this type will increase with the amplitude of the oscillations because the time average of the relative positions of the two polar groups will be further and further from the trans position. This is the theoretical basis for expecting the moment of the molecule to vary with temperature and thus produce a nonlinear relation between the total polarization and the reciprocal of temperature.

In the Debye theory the moment μ was assumed to be constant with respect to temperature. Consequently Eq. (2′) cannot be applied to the general case of intra-molecular rotation. However, in the limiting case of free rotation the moment will be constant as the temperature varies as long as the rotation remains free and unhindered. This case has been treated vectorially by Williams.[12] The resultant mean moment for the molecule, which is the one that would be obtained experimentally from Eq. (2′) if free rotation were actually the case, is given by:

$$\mu = 2^{1/2}\mu_1 \sin\theta \tag{3}$$

where μ_1 is the characteristic moment of the polar linkage and θ is the valence angle.

In applying Eq. (3) to the ethylene halides, using characteristic moments of 2.0 for C–Cl, 1.86 for C–Br, and 1.65 for C–I, Williams[12] found values of θ to be 38° for the chloride, 32° for the bromide, and 33° for the iodide. With tetrahedral carbon valences, the angle should be 180°–110° or 70°. We now know that the mutual repulsion of the two groups would not be likely to cause such a decrease in the angle, hence the natural conclusion is that the assumption of free rotation is not justified in these cases.

Eyring,[13] using the matrix algebra, has developed a general equation for the average resultant moment of a molecule having free rotation about certain bonds in terms of the individual permanent moments, the angles between

[11] Eucken and Meyer, Phys. Zeits. **30,** 397 (1929).
[12] Williams, Zeits. f. phys. Chem. [A] **138,** 75 (1928).
[13] Eyring, Phys. Rev. **39,** 746 (1932).

the valence bonds, the rotation angles, and the energy. From this equation he has obtained several equations for simpler cases. Smyth,[14] in conjunction with Eyring, has applied these equations to a number of organic compounds, comparing the calculated moments with the experimentally determined moments as a qualitative measure of the degree of freedom of the rotation. For the purpose of this discussion it will be sufficient to show that Eyring's equation reduces to the Williams equation above if applied to the simple case of free rotation about one single valence bond.

Eyring's equation for a paraffin chain of $n+1$ carbon atoms, with a free rotation about each C–C linkage, is:

$$\mu = \mu_1[2n + 2(n-1)\cos\theta + 2(n-2)\cos^2\theta + \cdots + 2\cos^{n-1}\theta]^{1/2} \quad (4)$$

where μ_1 is the characteristic moment of the C-X linkage and θ is the valence angle (110°). For the simplest molecules $n+1=2$, and the equation reduces to:

$$\mu = \mu_1[2 - 2\cos^2\theta]^{1/2}. \quad (5)$$

Eq. (5) is identical with that used by Smyth for ethylene bromide and is also identical with the Williams Eq. (3), thus:

$$\begin{aligned} \mu &= \mu_1 2^{1/2}(1 - \cos^2\theta)^{1/2} \\ &= \mu_1 2^{1/2}\sin\theta. \end{aligned} \quad (3)$$

Zahn[15] has used similar methods in discussing a number of special cases.

It has been pointed out above that the resultant moment μ would be expected to vary with temperature for the case of hindered rotation, and that consequently the polarization would no longer be a linear function of $1/T$. The theoretical treatment of this case thus requires a new derivation of the relation between P, μ, and T, which takes the hindered rotation into consideration. Meyer[2] was the first to do this quantitatively from the classical theoretical standpoint. Meyer's equation is

$$\left.\begin{aligned} P &= 4\pi N/3\{\alpha_0 + [2(\mu_1\sin\theta)^2/3kT](1-X)\} \\ X &= \frac{\alpha/kT + \beta/(kT)^2 + \gamma/(kT)^3 + \cdots}{m + n/kT + o/(kT)^2 + p/(kT)^3 + \cdots} \end{aligned}\right\} \quad (6)$$

where N is the Avagadro constant, k is the Boltzmann constant, α_0 is the molecular deformation polarization, μ_1 is the characteristic moment of the C-X linkage, θ is the valence angle, T is the absolute temperature, and $\alpha,\beta,\gamma,m,n,o,p$ are constants associated with the structure of the molecule.

Eq. (6) expresses the nonlinear relationship between P and $1/T$ for the simple case of hindered rotation in the ethylene halides. Meyer pointed out that at high temperatures the term X becomes negligible and Eq. (6) reduces to

$$P = 4\pi N/3\{\alpha_0 + [2(\mu_1\sin\theta)^2/3kT]\}. \quad (7)$$

[14] Smyth, J. Am. Chem. Soc. **54,** 2261 (1932).
[15] Zahn, Phys. Zeits. **33,** 400 (1932).

Comparing this with the Debye Eq. (2) it is seen that:

$$\mu = 2^{1/2}\mu_1 \sin\theta \tag{3}$$

which is the equation for free rotation previously developed.[12] Thus, at high temperatures Meyer's Eq. (6) is in accord with theory for the case of free rotation.

For the case of free rotation the resultant moment μ can be calculated from the experimental results by using the linear Debye equation in the three ways mentioned above. However, in order to calculate μ from experimental results when the rotation is hindered it is necessary to apply Eq. (6). This is a point which other experimenters either do not seem to have recognized or have thought unnecessary. At least we have been unable to find evidence of its use for the calculation in nonlinear cases.

On dividing the denominator of the function X of Eq. (6) into the numerator the function becomes:

$$\begin{aligned} X &= (\alpha/m)(kT)^{-1} + [(\beta m - \alpha n)/m^2](kT)^{-2} + \cdots \\ &= C(1/T) + D(1/T)^2 + \cdots \end{aligned} \tag{8}$$

where

$$C = \alpha/mk;\ D = (\beta m - \alpha n)/m^2k^2.$$

The expression for P in Eq. (6) then becomes:

$$\begin{aligned} P &= \frac{4\pi N}{3}\alpha_0 + \frac{4\pi N}{9k}2(\mu_1 \sin\theta)^2[(1/T) - C(1/T)^2 - D(1/T)^3 - \cdots] \\ &= A + B'[(1/T) - C(1/T)^2 - D(1/T)^3 - \cdots] \end{aligned} \tag{9}$$

where

$$A = (4\pi N/3)\alpha_0;\ B' = (4\pi N/9k)2(\mu_1 \sin\theta)^2.$$

In Eq. (9) the difference $P-A$ must be the polarization due to the resultant moment μ of the molecule at any temperature T. It is reasonable to suppose that the same relation holds between the resultant moment and the polarization caused by it as holds in the ordinary case where there is no intramolecular rotation. Then we can write from the ordinary Debye equation:

$$\begin{aligned} P &= A + (4\pi N/9kT)\mu^2 \\ \mu^2 &= (9kT/4\pi N)(P - A). \end{aligned} \tag{2}$$

Substituting for the value of $P-A$ in Eq. (9) we obtain the expression

$$\mu^2 = (9kT/4\pi N)B'[(1/T) - C(1/T)^2 - D(1/T)^3 - \cdots].$$

Putting in the value of B' and simplifying we find

$$\mu^2 = 2(\mu_1 \sin\theta)^2[1 - C(1/T) - D(1/T)^2 - \cdots]. \tag{10}$$

For the actual calculation of μ it is more convenient to retain the constant B', thus:

$$\mu^2 = (9k/4\pi N)B'[1 - C(1/T) - D(1/T)^2 - \cdots]. \tag{10'}$$

Now from the experimental plot of the total polarization P against $1/T$ the constants in Eq. (9) can be determined, and from these, substituted in Eq. (10′), the resultant moment μ can be calculated for any temperature.

Experimental

According to the results existent in the literature at the present time there is still some question as to whether or not ethylene chloride and ethylene bromide actually have nonlinear relationships between their total polarizations and the reciprocals of the temperature. Smyth,[5,6] studying solutions in heptane, and Meyer,[2] working with solutions in hexane, obtain a curvature in their plots of P against $1/T$. However, the results of these investigators for the corresponding solutions in benzene are inconclusive. It should be emphasized that experiments with solutions alone can hardly be sufficient to decide a question of this sort because of ignorance of the effect of the solvent. The experiments of Zahn[9] on the vapor of ethylene chloride show a nonlinear relationship while Ghosh and his associates[7] obtain a linear relation, and Sänger's results[8] are inconclusive.* Very recently Zahn[10] has reported data for ethylene bromide vapor. It is difficult to draw any conclusion from these data of Zahn when his total polarizations are plotted against the reciprocals of temperature. In view of this situation it was decided to complete the work, begun early in 1930, with the ethylene chloride and ethylene bromide vapors.

The object of the experimental part was, therefore, to obtain values of the total polarization P over as wide a temperature range as possible. The apparatus and method were designed for vapors having an appreciable vapor pressure in the neighborhood of 100°C. The determination of ϵ requires capacity measurements on a condenser in a vacuum and in an atmosphere of the vapor. The density term in the Clausius-Mosotti relation requires a knowledge of the pressure of the vapor and the temperature. To satisfy these requirements the apparatus must contain: (a) A condenser in a chamber holding the vapor; (b) apparatus for admitting and exhausting the vapor; (c) a means of determining the pressure of the vapor in the chamber; (d) a means of controlling and measuring the temperature of the condenser chamber; (e) apparatus for measuring the capacity of the condenser.

(a) The condenser was of the concentric cylinder type. Four cylinders of Monel metal (cold drawn, seamless, annealed tubing) were polished inside and outside and mounted concentrically as shown in Fig. 2. Four mica spacers were used in each end to keep the cylinders in position. The dimensions and spacings are listed below the figure. In cutting the outside cylinder to length three lugs were left on each end. These were shaped as indicated in the figure and used to support the condenser in a vertical position in a large Pyrex tube. Part of the Pyrex chamber is shown by dashed lines in the figure. Alternate cylinders were electrically connected through short lugs left projecting from their ends when they were cut to length. These lugs were simply spot-welded together. Leads to the outside were small tungsten wires, spot-welded

* In a recent communication to us Sänger has stated that a redetermination of several of his experimental points has brought his results to a practical agreement with those of Zahn.

to the Monel lugs, passing out through gas tight Pyrex-tungsten seals. The lead from the outside and second inner cylinders was taken off at the bottom and grounded as indicated, while the lead from the first and third inner cylinders was taken off at the top and served to connect the condenser to the capacity measuring apparatus.

(b) The condenser and chamber were mounted vertically as shown in Fig. 3. The entrance tube was at the top and led out through the three-way stopcock marked *A*. One of the tubes from this stopcock led directly to the tube *D* containing the liquid under investigation. The third outlet from stopcock *A* led to the evacuating system through stopcocks *B* and *C*. Stopcock *B* led to a "Hi-Vac" oil pump and stopcock *C* led through the trap shown, and a calcium chloride tube, to a water aspirator.

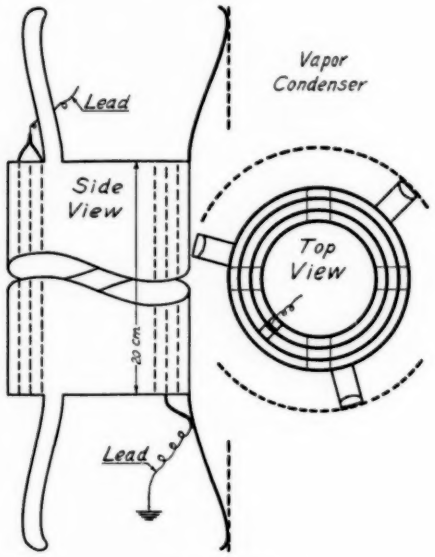

Fig. 2.

Cylinder	Outside Diam.	Spacing
Outside	4.76 cm	
1st inner	4.13	1.95 mm
2nd inner	3.65	1.50
3rd inner	3.18	1.50

Sufficient liquid for a whole series of determinations was placed in the tube *D* before it was sealed to the apparatus. The liquid was then cooled to a point where it solidified and the tube *D* was sealed to the apparatus through the small connecting tube. While the liquid was still frozen the stopcocks were turned so as to connect tube *D* through stopcock *B* to a source of carbon dioxide and the vacuum pump. In this way the space above the material was thoroughly flushed out several times with dry carbon dioxide, the carbon dioxide entering through stopcock *B* from auxiliary tubes not shown in the figure. Tube *D* was finally evacuated and then closed by means of stopcock *A*. By surrounding tube *D* with hot water contained in the vacuum flask the

liquid could be heated to give any desired vapor pressure up to that characteristic of 100°C.

In the meantime the rest of the apparatus was flushed out with dry carbon dioxide and evacuated. This was possible because the three-way stopcock *A* was mounted in such a way that the condenser chamber could be connected to the vacuum system while tube *D* was closed.

With the condenser chamber and connecting tubes evacuated stopcock *B* was closed and then stopcock *A* was turned to allow the vapor to flow from tube *D* into the condenser chamber until the desired pressure of vapor was obtained. Stopcock *A* was then set in an intermediate position so as to close both *D* and the condenser chamber. Condensation of vapor in the tube leading from stopcock *A* to the condenser chamber was prevented by means of the

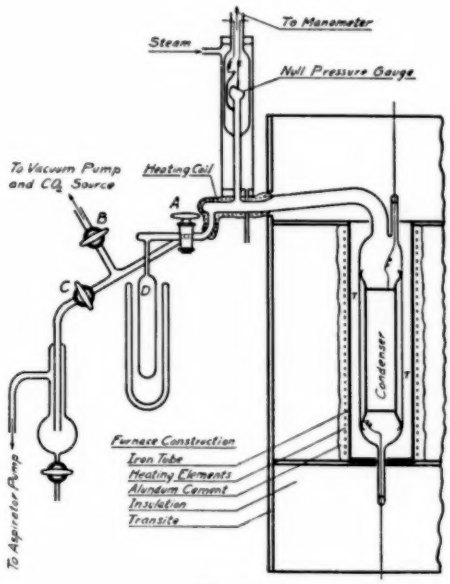

Fig. 3.

heating coil shown in the figure. Of course, the chamber itself was always kept at a temperature higher than that of the liquid in tube *D*.

After the measurements of temperature, pressure, and capacity (to be described later) the system was evacuated, keeping tube *D* closed as before. In evacuating the vapor, as much as possible was pulled out by the aspirator pump through stopcock *C*. Stopcock *C* was then closed and the system finally evacuated by the oil pump through stopcock *B*. In actual determinations the condenser chamber was flushed out several times with the vapor itself before it was finally admitted for the measurements. For the vapors of ethylene chloride and ethylene bromide stopcock *A* was lubricated with a paste made of P_2O_5, SiO_2, and phosphoric acid. Stopcocks *B* and *C* were lubricated with ordinary vacuum stopcock lubricant of the rubberized type.

(c) Pressure measurements were made by means of a null gauge of the

glass diaphragm type described by Daniels.[16] This gauge, with the glass diaphragm and the platinum wires leading from it, is shown in Fig. 3. The vapor side of the gauge was connected directly with the large tube leading to the condenser chamber. Steam was passed around the gauge to prevent condensation of vapor inside. The other side of the gauge was connected to a mercury manometer for reading the pressure. A system of stopcocks leading both to the atmosphere and to the vacuum system allowed adjustment of the pressure to the null point.

A gauge of this type always has an additive correction factor which must be determined in order to convert manometer readings at the null point into actual pressures. This correction factor was obtained when there was no vapor in the apparatus by connecting the gauge and manometer system to the inside system through stopcock *B*, allowing carbon dioxide to flow into both systems to any desired pressure, (measured now on the manometer)

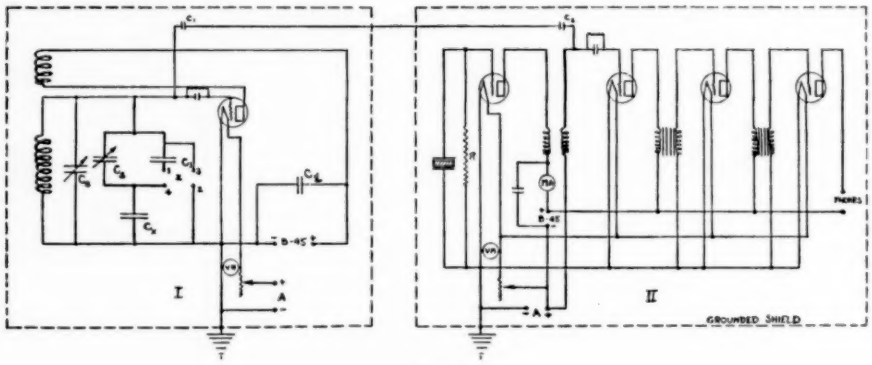

Fig. 4.

and then closing stopcock *B* and adjusting the pressure in the gauge and manometer system to the null point. The difference between the actual pressure and the pressure at the null point would then be the correction. The gauge was checked in this way after every two or three hours of operation. With a gauge of this type no vapors come into contact with the mercury manometer, the manometer can be operated at room temperature, and no mercury vapor enters the inside of the apparatus.

(d) The condenser chamber was mounted inside a verticle tube electric furnace. The furnace tube was of iron and was about four inches in diameter and sixteen inches long. It was closed at the top and bottom with metal ends and was grounded, thus serving as a shield for the condenser. The heating elements were nichrome wire wound non-inductively. There were about six or seven inches of insulation surrounding the tube. The heating current was drawn from a 220 volt a.c. circuit and was controlled by several *glow-coil* resistances and two slide wire rheostats. Temperature control was obtained by merely setting the resistance in the circuit and allowing the temperature to become constant.

[16] Daniels, J. Am. Chem. Soc. **50**, 1115 (1928).

Temperature measurements were made by means of two chromel-alumel thermocouples held against the outside of the condenser chamber at the points lettered T in Fig. 3. The cold junctions were kept in cracked ice and the voltage readings were made by means of a Leeds and Northrup Type-K potentiometer using a wall galvanometer.

(e) The dielectric constants were determined from capacity measurements made by the method of Pungs and Preuner.[17] The electrical apparatus was the same as that used and described by Schwingel and Williams,[18] and is shown in Fig. 4.

A rough control condenser C_8, a variable precision condenser C_s, a fixed mica condenser C_y of comparatively large capacity, and the vapor condenser C_x form the capacity of circuit I. The control condenser C_8 is used to adjust the capacity to any desired point on precision condenser scale, and is left fixed for any series of determinations. The total series capacity of the part of the circuit containing the vapor condenser C_x is given by:

$$1/\text{total capacity} = 1/C_x + 1/(C_y + C_s). \tag{11}$$

Let ΔC_x represent the change in the capacity of the vapor condenser C_x on the admission of a vapor and let ΔC_s represent the change in the reading on the precision condenser required to bring the circuit back to the original total capacity. Then,

$$1/\text{total capacity with vapor} = 1/\text{total capacity evacuated}.$$

From Eq. (11):

$$\frac{1}{C_x + \Delta C_x} + \frac{1}{C_y + C_s + \Delta C_s} = \frac{1}{C_x} + \frac{1}{C_y + C_s}. \tag{12}$$

Solving for ΔC_x:

$$\Delta C_x = \frac{C_x^2 \cdot \Delta C_s}{(C_y + C_s)^2 + (C_y + C_s + C_x)\Delta C_s}. \tag{13}$$

In Eq. (13) any capacity in the leads from the vapor condenser will be included in C_x. As we shall consider C_x as the true capacity between the plates of the vapor condenser it will be necessary to replace C_x in (13) by $C = C_x + X$, where X is the lead capacity. Eq. (13) then becomes:

$$\Delta C_x = \frac{C^2 \Delta C_s}{(C_y + C_s)^2 + (C_y + C_s + C)\Delta C_s}. \tag{13'}$$

Dielectric constant values can now be obtained from the equation

$$\epsilon - 1 = \Delta C_x / C_x. \tag{14}$$

Combining Eqs. (13′) and (14):

$$\epsilon - 1 = \frac{C^2}{(C_y + C_s)^2 + (C_y + C_s + C)\Delta C_s} \cdot \frac{\Delta C_s}{C_x}. \tag{15}$$

[17] Pungs and Preuner, Phys. Zeits. **20**, 543 (1919).

[18] Schwingel and Williams, Phys. Rev. **35**, 855 (1930).

Assuming that $(C^2/C_x) = C$, and taking the reciprocal of both sides of Eq. (15):

$$\frac{1}{\epsilon - 1} = \frac{(C_y + C_s)^2}{C} \cdot \frac{1}{\Delta C_s} + \frac{(C_y + C_s)}{C} + 1.$$

Let the constant coefficient, $(C_y + C_s)^2/C = a^2$;
then

$$(C_y + C_s)/C = a/C^{1/2}.$$

Therefore,

$$1/(\epsilon - 1) = a^2(1/\Delta C_s) + a/C^{1/2} + 1, \tag{16}$$

where ϵ is the dielectric constant, a is a constant of the circuit, C is the capacity of the vapor condenser and the leads, and ΔC_s is the *difference* reading on the precision condenser.

Absolute values of $\epsilon - 1$ can be determined from Eq. (15) if values of the capacities C_x, X, C_y and C_s are known. In this work it was thought preferable to determine the constant a from calibrations with carbon dioxide, using Stuart's[19] value of $\epsilon - 1$. Having determined a in this manner, $\epsilon - 1$ for a vapor is obtained directly from Eq. (16).

The vapor condenser has been described in part a of this section. Its capacity, including lead capacity, was found to be 530 mmf. The fixed condenser C_y was found to be 2834 mmf. In this work condenser C_y was mounted inside a vacuum flask in order to decrease fluctuations due to changes in room temperature and humidity.

The first step in the actual measurement of a dielectric constant is the determination of the constant a. As has already been mentioned, carbon dioxide is admirably suited for this purpose. Stuart's[19] value of $(\epsilon - 1)10^6$ for carbon dioxide is 987 at 273°K and one atmosphere. This value was converted to that corresponding to the pressure and temperature of the experiment by multiplying it by the density ratio. We then have, according to Eq. (16):

$$1/(\rho/\rho_0)(987)10^{-6} = a^2(1/\Delta C_s) + a/C^{1/2} + 1,$$

where ρ is the density under experimental conditions and ρ_0 is the density under standard conditions. The quotient ρ/ρ_0 was calculated from Berthelot's equation.

The procedure followed was to make two or more determinations of the constant a in this manner at each temperature at which vapor determinations were made. After the whole temperature range of the apparatus had been covered all of the a values were averaged and the average was used to calculate the dielectric constants of the vapor at the several temperatures by Eq. (16). The vapors of the ethylene halides were run in a manner similar to carbon dioxide, readings being taken first with the apparatus evacuated, then with the vapor in the apparatus at a desired pressure, and finally after re-evacuation. In this manner the quantity ΔC_s could be determined for the several capacity balances.

[19] Stuart, Phys. Zeits. **47**, 457 (1928).

The molar polarization P is calculated from the equation

$$P = [(\epsilon - 1)/3](M/\rho).$$

The quantity (M/ρ) is obtained from Berthelot's equation,

$$M/\rho = C_1(T/p) + C_2 - C_3(1/T^2).$$

The constants of this equation are given below:

$$C_1 = 760R \text{ (if } p \text{ is in mm)} = 62370$$

	Ethylene chloride	*Ethylene bromide*
$C_2 = 9RT_c/128p_c =$	61.2	48.8
$C_3 = 54RT_c^3/128p_c =$	11.60×10^7	9.8×10^7
$R = 82.07$ cc. atmos./deg.		
(Crit. temp.) $T_c^* =$	562.2°K	583.0°K
(Crit. press.) $p_c^* =$	53.06 atmos.	68.99 atmos.
*From	Nadejdine (1887)	Vespignani (1903)

Sources of Error

Pressure

For carbon dioxide the pressures were read directly on the mercury manometer because it was not necessary to use the null gauge with a noncondensing gas. Using a reading glass the manometer reading was accurate to ± 0.2 mm. For vapor pressure readings the null gauge was necessary. However, as this could be set as closely as the manometer could be read, the accuracy here was also ± 0.2 mm. There should be no systematic errors in pressure readings because the null gauge was frequently checked. Of course, at both high and low temperature extremes such an error would develop, due to chemical change in the vapor in one case, and adsorption on the condenser cylinders in the other. In these cases the pressure would no longer be an indication of the amount of material between the condenser cylinders.

Temperature

Thermocouple readings on the potentiometer could be checked without difficulty to ± 0.002 millivolts. This corresponds to ± 0.05°K. The two thermocouples used were calibrated against a third chromel-alumel thermocouple which had just been calibrated in steam, tin, cadmium, and zinc. The calibration points were sharp and probably as accurate as the temperature values given for them in the literature. Temperatures were reported to the nearest degree because this is within the limit of accuracy of the capacity readings.

Capacity

The pertinent reading was ΔC_s, the difference between the precision condenser readings when the apparatus was evacuated and when it was filled with gas or vapor. The precision condenser could be read to ± 0.1 of a scale

division. As ΔC_s was reported in tenths of a scale division the reading accuracy was ± 1. There are no systematic errors in $\epsilon - 1$ due to the method of calculation, because Eq. (16) does not involve any simplifying assumptions. Of course the practice of calibration with carbon dioxide depends upon the dielectric constant of this gas remaining constant over the temperature range used. This has been attested to by numerous investigators. It is further supported by the constancy of the a calculated from the determinations on carbon dioxide.

The accuracy of the total polarization P can be estimated by an analysis of the values of the constant a^2 obtained in a series of determinations on carbon dioxide. The least accurate of these series gave a mean absolute deviation of 2 percent.

Purification of Materials

Carbon dioxide was taken from a commercial cylinder and passed through concentrated sulphuric acid and a P_2O_5 tower.

Table II. *Data on ethylene chloride.* Run No. 1.

Temp. °K	$(1/T)\times 10^3$	Press. (mm)	ΔC_s	$(\epsilon-1)\times 10^6$	P (cc)
297.5		52.7	314	473	55.5
297.6		55.3	337	507	56.6
297.6		57.5	348	523	56.1
297.6		54.8	331	498	56.1
297.7		49.4	292	440	55.0
297.9		47.0	287	432	56.7
297.9		49.6	302	456	56.8
297.9		52.4	319	488	57.6
297.8		48.3	293	449	57.5
Av. 298	3.36				57.0
345.8		54.2	264	399	52.8
345.9		61.3	301	454	53.1
345.5		112.6	558	830	52.9
345.6		106.4	529	787	53.0
Av. 346	2.89				53.0
395.3		332.4	1458	2070	50.8
395.2		327.6	1450	2060	51.2
395.4		329.2	1471	2080	51.4
393.0		423.1	1909	2650	50.6
393.0		324.5	1468	2080	52.0
393.3		318.2	1431	2030	51.7
Av. 394	2.54				51.3
447.8		112.2	424	635	52.7
447.9		109.1	400	600	51.0
448.3		158.0	581	863	50.6
448.4		157.9	576	855	50.2
Av. 448	2.23				51.1
495.5		80.3	264	399	51.1
495.7		89.5	294	444	50.9
Av. 496	2.02				51.0

TABLE III. *Data on ethylene chloride.* Run No .2.

Temp. °K	$(1/T)\times10^3$	Press. (mm)	ΔC_s	$(\epsilon-1)\times10^6$	P (cc)
588.6		171.4	522	733	52.3
587.2		161.0	484	681	51.5
587.5		164.0	437	617	45.8
Av. 588	1.70				49.9
533.2		192.8	611	854	49.0
532.2		177.5	583	815	50.7
531.6		171.1	565	791	51.0
Av. 532	1.88				50.2
495.2		171.7	608	850	50.9
495.5		170.8	606	847	50.9
Av. 495	2.02				50.9
392.9		130.8	590	826	51.4
393.8		128.6	586	814	51.6
Av. 393	2.55				51.5

TABLE IV. *Data on ethylene bromide.* Run No. 1.

Temp. °K	$(1/T)\times10^3$	Press. (mm)	ΔC_s	$(\epsilon-1)\times10^6$	P (cc)
298.5		11.1	75	114	64
298.6		10.8	75	114	66
298.6		11.0	90	137	77
298.6		10.0	75	114	71
298.7		10.2	78	119	72
Av. 299	3.35				70
346.6		21.8	92	140	45.4
346.6		20.4	89	137	47.9
346.7		20.0	84	128	46.2
Av. 347	2.88				46.5
401.0		19.8	74	113	47.6
401.0		54.5	205	310	47.4
Av. 401	2.50				47.5
449.2		121.4	391	587	45.2
449.3		125.6	406	609	45.2
Av. 449	2.23				45.2
490.3		87.7	314	472	54.8
490.4		93.9	336	505	54.7
Av. 490	2.04				54.8

Ethylene chloride (from the Eastman Kodak Company) was washed twice with normal NaOH and three times with water. It was then dried over fused $CaCl_2$ for several days and fractionally distilled. The vapor of the distillate was kept in contact with P_2O_5 for several days. The liquid was then distilled directly into the apparatus as described above. B.P. 82.3–82.6°C.

Ethylene bromide (from the Eastman Kodak Company) was treated in the same way as the ethylene chloride except that the distillation was carried out under reduced pressure.

TABLE V. *Data on ethylene bromide.* Run No. 2.

Temp. °K	$(1/T)\times10^3$	Press. (mm)	ΔC_s	$(\epsilon-1)\times10^6$	P (cc)
611.9		130.1	324	510	49.8
613.2		103.6	254	400	49.2
Av. 612	1.64				49.5
562.2		89.4	410	642	84.0
562.2		61.7	283	447	84.6
Av. 562	1.78				84.3
494.5		109.3	481	750	70.5
494.9		89.8	391	613	70.2
Av. 495	2.02				70.4
454.0		87.0	285	449	47.3
454.2		80.1	268	422	49.8
Av. 454	2.21				48.6
425.5		80.5	265	419	45.9
425.2		71.8	238	376	46.3
425.2		65.2	224	354	47.9
Av. 425	2.36				46.7
392.3		67.1	249	392	47.6
392.0		67.4	248	391	47.3
Av. 392	2.55				47.5
363.5		45.4	196	311	51.7
363.4		46.5	202	320	51.9
Av. 363	2.76				51.8

CALCULATIONS WITH ETHYLENE CHLORIDE DATA

The Debye linear equation for the polarization as a function of the temperature is, $P=23.9+B/T$, where the value $A=23.9$ for the deformation polarization is that obtained by Hitchcock[20] for the solid substance and is,

TABLE VI.

Temp. °K	P (cc)	B	$\mu\times10^{18}$ e.s.u.
298	57.0	9,880	1.27
346	53.0	10,080	1.28
394	51.3	10,790	1.32
448	51.1	12,200	1.41
495	50.9	13,380	1.48
532	50.2	14,200	1.52
588	49.9	15,250	1.57

[20] Hitchcock, Quoted by Smyth, J. Am. Chem. Soc. **53,** 4242 (1931).

furthermore, in good agreement with estimates by the optical method. The constants B calculated from the experimental points, and the corresponding moments μ are given in Table VI.

The application of Meyer's equation will now be described, again taking the deformation polarization to be 23.9. Eq. (9) then becomes

$$P = 23.9 + B'(1/T) + B'C(1/T)^2.$$

The constants in this equation can be obtained from two experimental points. These points were selected so as to give the best approximation to all the experimental results.

Points selected.

$1/T$	$(1/T)^2$	P
2.02×10^{-3}	4.08×10^{-6}	51.0
2.55	6.50	51.5

The results of the calculation are $B'=23.3\times10^3$ and $B'C=4.89\times10^6$, so that the equation for the total polarization is

$$P = 23.9 + 23{,}300(1/T) - 4{,}890{,}000(1/T)^2.$$

The equation for the moment is,

$$\mu^2 = (9k/4\pi N)[23{,}300 - 4{,}890{,}000(1/T)].$$

From this equation the values of μ in Table VII are obtained. Assuming

TABLE VII.

T	$(1/T)10^3$	$\mu\times10^{18}$ e.s.u.
298	3.36	1.05
346	2.89	1.22
394	2.54	1.33
448	2.32	1.42
495	2.02	1.48
532	1.88	1.52
588	1.70	1.56
(∞)	(0.00)	(1.94)—for free rotation

the valence angle θ to be 70° the characteristic moment μ_1 for $C-Cl$ can be obtained from:

$$B' = (4\pi N/9k)2(\mu_1 \sin\theta)^2,$$

with the result that

$$\mu_{C-Cl} = 1.46 \times 10^{-18} \text{ e.s.u.}$$

CALCULATIONS WITH ETHYLENE BROMIDE DATA

The Debye linear equation in this case is, $P=29.7+B(1/T)$, where the deformation polarization is 29.7.[10] The individual experimental points, substituted in this equation give the results of Table VIII.

TABLE VIII.

Temp. °K	P (cc)	B	$\mu\times10^{18}$ e.s.u.
347	46.5	5830	0.97
392	47.5	6980	1.05
401	47.5	7130	1.07
425	46.7	7220	1.08
449	45.2	6960	1.04

In applying Meyer's equation to the ethylene bromide data it was found that the points for the higher temperatures cannot fall on a parabola whose constant A has the value 29.7 and which represents the more reliable data at the lower temperatures. For this reason, the Meyer equation was applied only to the points corresponding to the lower temperatures in the case of ethylene bromide.

Points selected.

$(1/T)$	$(1/T)^2$	P
2.5×10^{-3}	6.25×10^{-6}	47.5
2.88	8.29	46.5

The equation for the total polarization is,

$$P = 29.7 + 15600(1/T) - 3{,}390{,}000(1/T)^2,$$

and the equation for the moment becomes,

$$\mu^2 = (9k/4\pi N)\left[15600 - 3{,}390{,}000(1/T)\right].$$

From this equation the values of (μ) in Table IX are obtained:

TABLE IX.

T	$(1/T)10^3$	$\mu\times10^{18}$ e.s.u.
357	2.8	0.99
385	2.6	1.05
417	2.4	1.10
455	2.2	1.15
(∞)	(0.0)	(1.59)—for free rotation.

Since $B' = 15600$ and $\theta = 70°$,

$$\mu_{C-Br} = 1.20 \times 10^{-18} \text{ e.s.u.}$$

DISCUSSION OF RESULTS

The results of Zahn and Sänger for the vapors and the results of Smyth and Meyer for solutions are plotted, together with our results, in Fig. 5. The dashed curves represent the experimental curves of the various investigators while the full curves are the parabolas used in the calculation of our results. The circles represent results from vapor determinations and the

squares are results from solutions. The horizontal line separates the ethylene chloride points from those for ethylene bromide. Results for both compounds are plotted on the same axes and to the same scale. The low temperature values for the vapor and the high temperature values for the solutions are probably the least accurate.

For ethylene chloride our two points at the lowest temperatures undoubtedly are high due to adsorption of vapor on the condenser cylinders. This was confirmed by purposely coating the condenser cylinders with some thermal decomposition products of the vapors by admitting vapor to the condenser chamber at 400°C. With the adsorptive properties of the surface increased in this manner the P values obtained at the low temperatures were considerably higher than those shown on the graph. The range of temperature avail-

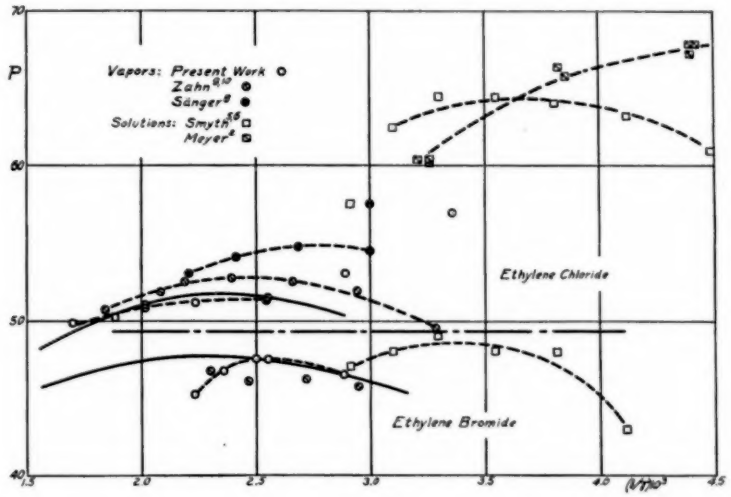

Fig. 5.

able for the investigation of ethylene bromide was much less than that for ethylene chloride. The erratic effects at high and low temperatures are indicated by the high values of the polarization P in Tables IV and V.

The dashed curves represent our interpretation of the experimental data reported by other investigators and by us. They support the theory that this type of compound should have a nonlinear relation between P and $1/T$.

For ethylene chloride the full curve on the graph, representing a parabolic relation between P and $1/T$ and calculated from our data, is a fair approximation to the experimental points. This theoretical curve has a greater curvature than the experimental curve and the maxima do not come at the same place. This is undoubtedly due to the particular selection of the deformation polarization in the calculation of the theoretical curve. A parabola could be drawn through three points on the experimental curve, and in this way the constant A in the equation could be evaluated directly from experiment. However, this procedure could hardly be expected to give an accurate measure of the deformation polarization.

The characteristic moment of (1.46×10^{-18}) for the $C-Cl$ bond, obtained from the constant B', compares well with the value of (1.5×10^{-18}), usually accepted. However, the figure (1.46×10^{-18}) is low compared to the experimental moment of methyl chloride, which is (1.86×10^{-18}) according to the tables of Smyth.[21]

Although our experimental points for ethylene bromide fall on a smooth curve it will be noticed that there is a rather sharp change in curvature at the peak. This, together with the large slope of the curve to the left of the peak, indicates that the two points for the higher temperatures may be too low. Even a straight line through these two points would give an intercept too small for the deformation polarization.

The constant B' for the parabola chosen as the representation of the data gives a characteristic moment for the C-Br bond of (1.20×10^{-18}). This seems low compared to the value of (1.5×10^{-18}) usually accepted. In this connection, however, the question arises as to why the bonds C-Cl and C-Br should both have characteristic moments of (1.5×10^{-18}) when the moments of the corresponding methyl compounds are (1.86×10^{-18}) and (1.45×10^{-18}), respectively.[21] It may be worth while to point out that the ratio of the characteristic moments obtained from ethylene chloride and ethylene bromide is very close to the ratio of the moments for the methyl compounds. Thus,

$$(\mu_1 \text{ for } C-Br)/(\mu_1 \text{ for } C-Cl) = 1.20/1.46 = 0.82$$

$$(\mu \text{ for } CH_3Br)/(\mu \text{ for } CH_3Cl) = 1.45/1.86 = 0.78.$$

The Table X contains a comparison of our moments for ethylene chloride calculated by the optical method and by the parabolic equation, with those reported by Zahn[9] for the vapor. The moments of Zahn were obtained by graphical interpolation for the temperatures listed in our table. Zahn calculated his moments by means of Eq. (2''). Since his experimental curve for the polarization P agrees very well with ours his values for the moment can be used as a comparison of the method of calculation. The results of all three columns approach each other at the higher temperatures, while at lower temperatures the first and third columns deviate from the second and from each other. The optical method is definitely the least reliable.

TABLE X. *Values of* $\mu\times10^{18}$. (*Ethylene chloride.*)

Temp. °K	Optical method	Parabolic equation	Zahn
298	1.27	1.05	1.10
346	1.28	1.22	1.25
394	1.32	1.33	1.36
448	1.41	1.42	1.44
495	1.48	1.48	1.49
532	1.52	1.52	1.53
588	1.57	1.56	
(∞)		(1.94)	

[21] Smyth, *Dielectric Constant and Molecular Structure*, Chemical Catalog Co. (1931).

The comparison of μ values calculated for ethylene bromide vapor by the optical method, by the method of the parabola, and as reported by Zahn[10] are given in Table XI. These results cannot be used for a study of the several methods of calculation because the different columns are not based upon the same experimental points. In view of this it is surprising how well they agree.

TABLE XI. *Values of* $\mu \times 10^{18}$. (*Ethylene bromide.*)

Temp. °K	Optical method	Parabolic equation	Zahn
357	0.99	0.99	0.98
385	1.04	1.05	1.01
417	1.08	1.10	1.05
455	1.02 ?	1.15	1.13 ?
(∞)		(1.59)	

The striking thing about the results for ethylene chloride, both in solution and as vapor, is that, with the exception of a few points in individual cases, they could all be represented as a family of parabolas having a common intercept. The parabola used by us would be a typical one for the family. The difference in the various parabolas is to be found in the heights and positions of the maxima. The same thing could probably be said for the data on ethylene bromide. The difference between the results for vapor and solution appears to be the same type of difference but of a larger order of magnitude. The horizontal position of the maximum is governed by the constant C in the equation. This can be seen at once by setting the derivative with respect to $1/T$ equal to zero. It has been pointed out that the constant C is a function of structural constants of the molecule. Consequently the difference between the curves for the vapor and for solutions may be due to some structural change within the molecule when it is dissolved. The difference between the results with the vapor and with solutions for ethylene bromide is much less than in the case of ethylene chloride. This might be expected on the above basis due to the heavier bromine atoms resisting structural changes more strongly than the chlorine atoms. It is not meant to suggest here that the discrepancies between different experiments with the vapor are due to structural changes since these differences are of the order of the absolute experimental error.

CONCLUSIONS

(1) The results of the present experimental work are in accord with previous work which shows both ethylene chloride and ethylene bromide to give a nonlinear relationship between the total polarization P and the reciprocal of the absolute temperature $(1/T)$.

(2) At the lowest temperatures adsorption on the condenser cylinders tends to give high values of the total polarization and thus tends to decrease or even reverse the curvature of the P *vs.* $1/T$ relation.

(3) At the highest temperatures ethylene bromide vapor gives abnormally high values for the total polarization, due, it is supposed, to the beginning of a thermal decomposition of the material.

(4) The relation between the total polarization P and the reciprocal of absolute temperature $1/T$ for the ethylene halides can be represented by an equation of the form

$$P = A + B'(1/T) - B'C(1/T)^2.$$

This equation should be applied to such systems in which the relationship between P and $1/T$ is nonlinear.

(5) The differences between the P *vs.* $1/T$ relationships for vapor and for solution can possibly be explained as due to changes in the internal structure of the molecule in question, due to the influence of the solvent.

(6) The theoretical ideas presented permit the calculation of the characteristic moments of the C-Cl and the C-Br bonds from the experimental data. In this computation it is assumed that the angle between the line joining the centers to the two carbon atoms and the direction of the carbon to halogen bond is that required by the normal undeformed tetrahedra used to represent the spatial configuration of the molecule.

LETTERS TO THE EDITOR

Prompt publication of brief reports of important discoveries in physics may be secured by addressing them to this department. Closing dates for this department are, for the first issue of the month, the twenty-eighth of the preceding month; for the second issue, the thirteenth of the month. The Board of Editors does not hold itself responsible for the opinions expressed by the correspondents.

Probabilities of *K*-Electron Ionization of Silver by Cathode Rays

The work reported here is an extension of a research described in previous papers[1] on the probabilities of K-electron ionization of silver by cathode rays, as measured by the intensities of the $K\alpha$ lines. To make it possible to have all collisions producing x-rays for any one measurement occur at the same cathode-ray speed, we are using constant potentials, of course, and also targets thin enough to avoid serious retardation of the cathode rays while they are in the silver.

The previous work extended only to 85 kv, or 3.3 V_K (where V_K is the K-series excitation voltage), but we are now working to $7V_K$. Because of the difficulty of exact absolute measurements of x-ray intensities, or even of the thicknesses of these very thin targets, we are reckoning all probabilities in terms of the most convenient arbitrary standard, the probability at $2V_K$. The ratio of the probability at any other voltage to this standard, we call $j(U)$, where $U=V/V_K$.

In these terms, $j(U)$ is of course zero up to $U=1$, and there it begins its rise abruptly, its graph starting upward from $U=1$ with a finite slope. The graph is concave downward, and reaches a very flat maximum, $j(U)$ remaining with 2 percent of 1.21 from $U=3.5$ to $U=7$. Aside from the standard, $j(2)=1.00$, some values at other points are as follows: $j(1.2)=0.39$, $j(1.5)=0.72$, $j(2.5)=1.11$, $j(3)=1.18$. All these values confirm the earlier work to within ± 0.01, except at $U=3$, where the earlier value was lower by 0.025, probably because of gas in the tube. The values of j given here are all corrected for cathode-ray diffusion effects, as explained in the Physical Review paper cited above; but for the rediffusion constant of beryllium, the material on which the silver was deposited, we are now using 0.025, a fair representative of the values found by Neher.[2] These new data are all based on one film, about 500A thick. We therefore plan to make further measurements, for greater accuracy and for certainty that there was nothing radically wrong with that film, before publishing the results in detail.

In the meantime, however, assuming for the present that they are at least a good first approximation, we can make some statements about their relation to various theories. The theories of Rosseland,[3] Thomas,[4] Ochiai,[5] and Bethe[6] are all based on the inverse-square law of repulsion between the cathode ray and the K electron, though with various differences in other assumptions. Rosseland and Thomas used classical quantum mechanics, and therefore were definite in their predictions. The theories of Ochiai and Bethe, on the other hand, are based on single-term approximations by Born's perturbation method, and are therefore restricted to values of $U \gg 1$. Whether this restriction keeps them from being applicable in the range $U \leqq 7$ or not, we cannot say; nor can we be quite sure of what can be assumed, under conditions straining the above restriction, as to possible variations in some quantities treated as constants. But if we interpret them correctly, all these inverse-square-law theories agree in predicting a notable decline in the ionization probability in the region where we find our flat maximum.

[1] Phys. Rev. **37**, 115 (Jan. 15, 1931) and Proc. Nat. Acad. Sci. **14**, 769 (1928).

[2] H. V. Neher, Phys. Rev. **37**, 655 (Mar.1, 1931). (Letter to the Editor.)

[3] S. Rosseland, Phil. Mag. **45**, 65 (1923).

[4] L. H. Thomas, Proc. Camb. Phil. Soc. **23**, 829 (1927).

[5] K. Ochiai, Proc. Phys.-Math. Soc. of Japan **11**, 43 (1929).

[6] H. Bethe, Ann. d. Physik **5**, 325 (1930).

The only other quantum theory of x-ray line intensities that we have seen is the oldest of them all, that of Davis,[7] who assumed the collisions to be equivalent to those of hard spheres. This theory predicted a deviation from our data in the direction opposite to that of the inverse-square theories.

To explain these deviations, several ideas present themselves. One is that the inverse-square law ought to be the best basic hypothesis, but that the deviations of these inverse-square theories from the data are caused by relativity effects, which might well be large at these voltages. Another idea is that the inverse-square law may fail between electrons at distances less than 10^{-11} cm, such as are demanded by these theories for the transfer of the large amounts of energy carried by our cathode rays. Still another idea is that the inverse-square law may fail for some other reason, connected with the dynamics of electrons within an atom, rather than with high energy. This last idea is the only one of these three, at least, that will explain observations on the inert gases by Hughes and Klein,[8] Compton and Van Voorhis,[9] and Smith.[10] Their data cover argon, neon and helium, and in all cases show the same sort of departure from the inverse-square theories that we find here. Helium may perhaps be the best for comparison with our data, since it contains only K electrons; and Smith's data show most clearly a very flat maximum around 4.5 V_K, remarkably like that given by our silver K electrons. Here at least, at 110 volts, there is no relativity or high energy problem.

To test the possibilities of laws other than the inverse-square, therefore, we have tried an interpolation between it and Davis's inverse-infinity power. For this purpose we made all other assumptions exactly like those of Rosseland's theory, the simplest of the inverse-square theories, but substituted an inverse-cube law for the inverse-square. The result is the equation

$$j(U)=\frac{6}{U\left\{\left(\frac{\pi}{2\cos^{-1}U^{-1/2}}\right)^2-1\right\}}$$

This equation fits our present experimental values of $j(U)$ to within ± 0.01 for all values of U up to 3, though it is low by 0.04 at $U=5$ and by 0.08 at $U=7$. Altogether, it fits far better than any of the other theories, unless possibly the changes with U in the parameters of Bethe's theory may make it fit better than it appears to.

We must recognize, of course, that any theory such as this, based on the classical concept of force, with the introduction of quanta as extraneously imposed prohibitions, is at least antiquated. We must also remember that there is no basis for an inverse-cube hypothesis other than *ad hoc*. We therefore offer this hypothesis, not as one to be taken literally, but as a suggestion on the direction in which it may prove worth while to change the potential energy functions used in better theories.

D. L. WEBSTER
W. W. HANSEN
F. B. DUVENECK

Stanford University,
California,
August 25, 1932.

[7] B. Davis, Phys. Rev. **11**, 433 (1918).

[8] A. L. Hughes and E. Klein, Phys. Rev. **23**, 450 (1924)

[9] K. T. Compton and C. C. Van Voorhis, *ibid.* **26**, 436 (1925) and **27**, 724 (1926).

[10] P. T. Smith, *ibid.* **36**, 1293 (1930).

Concerning the Production of Groups of Secondaries by the Cosmic Radiation

The experiments with counters and cloud chambers have shown that the ionization attributed to the cosmic radiation is produced by ionizing corpuscular rays (capable of discharging a counter or of producing a cloud track) of energies ranging from 10^6 to 10^{10} electron volts. At least some of these corpuscular rays are secondaries originating within the surrounding matter, but whether the primary radiation which ejects these secondaries itself consists of ionizing corpuscles or is of a non-ionizing gamma-ray or neutron character has been an unanswered question.

Experiments by Rossi[1] and by the writers[2] have shown that there are frequent groups consisting of two or more divergent ionizing rays which emerge simultaneously from a

[1] B. Rossi, Phys. Zeits. **33**, 304 (1932); Rend. Lincei XV, 734 (1932).

[2] Johnson and Street, Phys. Rev. **40**, 638 (1932).

block of lead, and a similar grouping phenomenon has been observed by those who have worked with cloud chambers. These observations could be explained by any one, or all of three postulates. I. The primary may be an ionizing ray which in passing through matter produces other ionizing rays by close collisions with electrons or nuclei. II. The primary may be a non-ionizing ray whose energy is at once transferred by a single nuclear collision to a group of secondary ionizing rays.

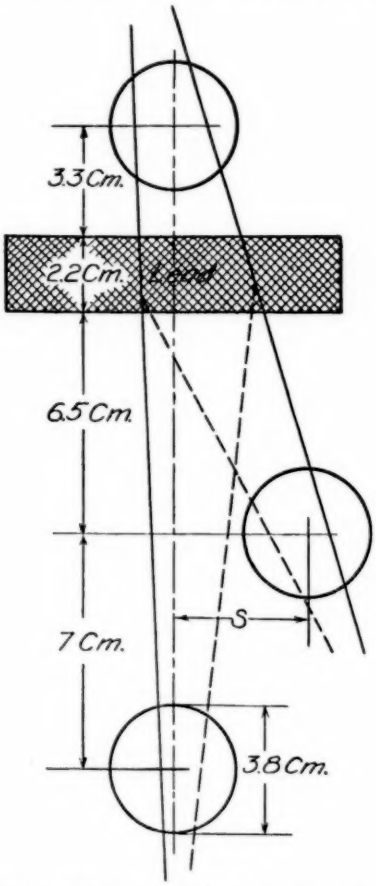

Fig. 1. Effective length of counter 9 cm.

III. The primary may be a non-ionizing ray whose energy is degraded by the formation of a succession of ionizing rays along an extended path.

To distinguish between these postulates we have made some experiments with the arrangement of three counters and the lead block shown in Fig. 1. If II is the correct hypothesis the presence of the lead block in the position indicated should have only an absorbing effect on the triple coincidence counting rate whereas an increase due to the lead should be noticed if I or III is right. The results in Table I show an increase due to the lead which is well above the statistical probable error, proving that at least a part of the grouping phenomenon must be accounted for either by postulate I or by III or perhaps by both.

To determine which of these two postulates applies, some experiments with the arrange-

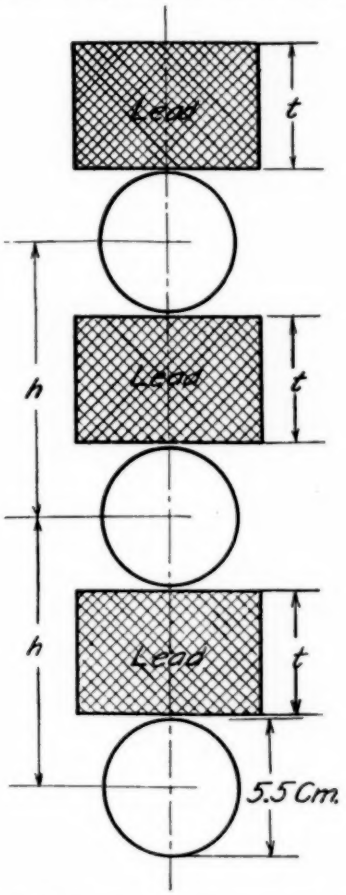

Fig. 2. Effective length of counter 12 cm.

ment of counters and lead blocks shown in Fig. 2 have been carried out. In this case the circuits were arranged for counting the double coincidences between counters 1 and 3 simultaneously with the triple coincidences. Counts were made both with the three lead blocks in position and with all of the lead removed. An explanation[3] of the transition effects dis-

[3] T. H. Johnson, Phys. Rev. **41**, 545 (1932).

covered by Schindler[4] and by Rossi[1] requires that, whether I or III is correct, the secondaries which enter any one of the lead blocks from above shall, for the most part, be absorbed in the thickness of lead used so that the probability that a primary be accompanied by a secondary below a lead block is independent of the condition above. However, most of the secondaries are sufficiently penetrating to pass through all three counters in the absence of the lead. If E is the efficiency of counter 2, the ratio T/D of triple to double counts without the lead is E whereas, with the lead in place, this ratio is EP, where P is the probability of any element of the path of the primary in lead being traversed by at least one ionizing ray (whether it be the primary itself or one of its secondaries). The results obtained are shown in Table II, from which it appears that there is no change in the ratio T/D due to the lead within the limits of error. Hence P is equal to unity. We must conclude, therefore, that the primary ray is either itself an ionizing ray or, if it is a non-ionizing ray, it is always accompanied by at least one of its secondary ionizing rays. This latter possibility must be excluded on other grounds. In the first place, the groups observed in the cloud chamber seldom contain more than two ionizing rays, and in the second place, a comparison of ionization measurements with counter data indicates an average of only two to three ionizing rays per group. These considerations necessitate the conclusion that if the primary is a non-ionizing ray it would be unaccompanied by ionizing secondaries over such a large fraction of its path that P would be less than unity by an easily detectable amount. (If three were the average density of independently formed secondaries 20 percent of the path of the primary should be non-ionizing.) We are, therefore, left with the conclusion that all of the groups observed in the first experiment arise from an ionizing primary. This ray, of course, may itself have been produced by a non-ionizing gamma-ray or neutron and, furthermore, it is still possible that a part of the groups observed by other arrangements of counters or in the cloud chamber may arise according to postulate II.

TABLE I.

Distance s		Total counting period	Total counts	Counts per minute	Difference due to lead
4 cm	with lead	2484 min.	136	0.055 ± 0.003	0.015 ± 0.004
	without lead	3971	159	0.040 ± 0.002	
5 cm	with lead	3069	132	0.043 ± 0.002	0.014 ± 0.003
	without lead	2512	73	0.029 ± 0.002	
7 cm	with lead	5795	194	0.034 ± 0.002	0.018 ± 0.002
	without lead	3886	63	0.016 ± 0.001	

TABLE II.

Spacing between counters (h)	Thickness of lead (t)	Total counting period	Total double counts (D)	Total triple counts (T)	T/D
13 cm	5 cm	1228 min.	2289	1913	0.84 ± 0.01 with lead
		1072	2389	1954	0.82 ± 0.01 without lead
18 cm	10 cm	1993	2074	1731	0.84 ± 0.01 with lead
		1497	2014	1615	0.81 ± 0.01 without lead

We are indebted to Dr. E. C. Stevenson for his help in arranging the circuits and in recording the data.

J. C. STREET
THOMAS H. JOHNSON

The Bartol Research Foundation of The Franklin Institute, Swarthmore, Pa., August 29, 1932.

[4] H. Schindler, Zeits. f. Physik **72**, 625 **(1931)**.

Structure of Atomic Nuclei. II

It seems to be possible to regard the lighter nuclei as if their only constituents were protrons and neutrons. The writer[1,2] has suggested that closed shells exist, and that this may explain the presence of the "clusters" of nuclei discovered by Barton.[3] The center of the cluster seems to lie about where the shells would be half-completed, provided that the closed shells correspond to the masses 36, 64, 100, 144, etc. On the simple model above, Zn 64 would have 30 protons and 34 neutrons, and it is hard to attach any particular significance to this arrangement. Also, one is rather at a loss to explain just what the constitution of Cl 37 is, unless it is admitted that after a closed shell has once become filled, stability conditions may favor the existence of holes in the closed shell for certain heavier isotopes.

To avoid these difficulties, one way is to adopt a tentative suggestion made to the writer by Prof. Dirac. This is that electrons may have a separate existence in certain nuclei, since β-type disintegrations exist. That is, that there are at least three types of primary particles, namely proton, neutron, and electron. The neutron is not to be thought of as a combination of proton and electron, but simply as a fundamental building-stone. Finally, the total angular momentum of the nucleus is integral or half-integral according as the total number of such independent particles is even or odd. This suggestion throws light on other phenomena and necessitates a revision of some earlier concepts.

In the central field of A 36, which has 18 protons and 18 neutrons, a neutron and an electron seem to be stabler than just a neutron. When they are added, Cl 37 is the result. One added proton gives A 38, and another proton K 39, where branching occurs. A neutron may be added, and an electron either added or taken away, resulting in the isobars A 40 and Ca 40, respectively. The existence of these isobars seems to support the hypothesis of nuclear electrons.

If to Ca 40 a neutron and electron be added, there is obtained the nucleus K 41, which emits β- and γ-rays. This nucleus contains 20 protons, 21 neutrons, and one electron. It may be that the presence of this electron is partly responsible for the radioactivity of K 41, and that Sc 45 (and possibly Cl 37) will also have similar properties. Nuclei up to A 36 cannot disintegrate with emission of primary β-rays, owing to the absence of free electrons.

The isotopes thus far reported for the mass range $36 < M \leqq 64$ are Cl 37, K 39, Ca 40, A 40, K 41, Ca 44, Sc 45, Ti 48, Cr 50, V 51, Cr 52, Cr 53, Cr 54, Fe 54, Mn 55, Fe 56, Ni 58, Co 59, Ni 60, Cu 63, and Zn 64. It has already been noted[4] that "isotopes only become numerous for atomic numbers >29." A glance at the distribution of isotopes seems to show one that a new regularity begins at $M=64$, and this we associate with the hypothesis that a closed shell has been formed. That is, Zn 64 is to consist of 32 protons, 32 neutrons, and two electrons. Though many points are missing in this mass range, still there are certain regularities apparent. For instance, the groupings Cr 50—V 51—Cr 52, Fe 54—Mn 55—Fe 56, and Ni 58—Co 59—Ni 60 are similar. It is probable that a fourth, Zn 62—Cu 63—Zn 64, exists. From Fe 54, Mn 55 may be formed by the addition of a neutron and an electron, and Fe 56 by the further addition of a proton. The total angular momentum of the Mn 55 nucleus is half-integral, so that it must contain an even number of electrons, namely two, as one would also expect for Fe 56. The nuclei Cr 50, Fe 54, Ni 58, and Zn 62 should, on the above basis, contain one electron and have half-integral spin values.

In addition to the isotopes A 38, Ca 42, Ti 46, K 43, and Sc 47 predicted by Beck,[5] we would suggest V 49 or Ti 49, Fe 57 and 58, Ni 61 and 62, and Zn 62 as rather probable.

The isotopes which have been found for the mass range $64 < M \leqq 100$ are Cu 65, Zn 66–68, and 70, Ga 69 and 71, Ge 70–77, As 75, Se 74, 76–78, 80, and 82, Br 79 and 81, Kr 78, 80, 82–84, and 86, Rb 85 and 87, Sr 86–88 Y 89, Zr 90, 92, and 94, Nb 93, Mo 92, 94–98, and 100, and Ru 96, 98–102, and 104. For most elements of even atomic number in this range, the isotopes have a mass range of about eight, as is exemplified by Zn 64–70, Ge 70–77, Se 74–82, Kr 78–86, Mo 92–100, and Ru 96–104. Accordingly, it might be expected

[1] J. H. Bartlett, Jr., Nature **130**, 165 (1932).

[2] J. H. Bartlett, Jr., Phys. Rev. **41**, 370 (1932).

[3] H. A. Barton, Phys. Rev. **35**, 408 (1930).

[4] Rutherford, Chadwick, and Ellis, "Radioactive Substances," p. 524.

[5] G. Beck, Zeits. f. Physik **47**, 407 (1928).

that strontium has isotopes between 84 and 92, and zirconium isotopes between 88 and 96. We note the groupings Zn 64—Cu 65—Zn 66, Ge 70—Ga 71—Ge 72, Se 74—As 75—Se 76, Kr 78—Br 79—Kr 80, Mo 92—Nb 93—Mo 94, and Ru 96—(Ma 97)—Ru 98.

In the mass range $100 < M \leqq 144$, the known isotopes are Ag 107 and 109, Cd 110–114, and 116, In 115, Sn 112, 114–122, and 124, Sb 121 and 123, Te 122–128 and 130, I 127, Xe 124, 126, 128–132, 134, and 136, Cs 133, and Ba 135–138. Since Sn and Xe have isotopes covering a mass range of twelve, this is probably true for other elements of even atomic number, and we should expect Te 118–130, Cd 106–118, Pd 100–112, and Ba 130–142.

Finally, a determination of the spin value for each isotope would be invaluable in deciding what the makeup of the nucleus is. For instance, Cl 35 has supposedly 17 protons and 18 neutrons, so that the closed shell lacks one *d*-proton. The ground state should therefore be an inverted *D*-doublet, the lower level of which would have a total angular momentum $I=5/2$, which is the value actually observed.[6] If Cl 37 does have an electron, then its spin should be either 2, 3, or 4. For this reason, it is not safe to assume, in unraveling a fine-structure pattern, that the nuclear spin for elements of odd atomic weight is capable of only half-integral values. At present, the information about nuclear spins is relatively meager, so that the rate of progress with nuclear stability questions is thereby limited.

JAMES H. BARTLETT, JR.

Quincy, Mass.,
August 30, 1932.

[6] A. Elliott, Proc. Roy. Soc. **127,** 638 (1930).

Luminosity of Sodium Flames

In a recent article by Bonner (Phys. Rev. **40,** 105, 1932) on the luminosity of sodium flames attention was called to the fact that the greater part of the absorption of the sodium light by such flames occurs at their surfaces. It follows from this that a sodium flame which does not have any cool surface, such as was used by Bonner, must show less absorption than those with which other experimenters have worked. It is, therefore, surprising to find the opposite of this indicated by Bonner's data for concentrated solutions of NaCl.

That this difference is due neither to a difference in the apparatus used for measuring the light nor to the system of units employed is shown by the fact that Bonner found with dilute solutions less absorption than did either Locher (Phys. Rev. **31,** 466, 1928) or myself (Phys. Rev. **38,** 699, 1931). Similarly this difference can not be explained by any uncertainty in my measurements regarding the effective center of the flames, as was suggested by Bonner, since an error due to such a cause would have made my results different from his in the same way and to the same extent with both dilute and concentrated solutions and such was not the case.

Because Bonner's data was so different from what one might expect, I repeated his experiments as nearly as I could with the apparatus which I had previously used. I found, however, that it was impossible to make accurate measurements of the length of the flame. Bonner had placed a non-luminous flame in front of the one into which salt was being sprayed, in order to keep the surface o the sodium flame hot. Due to diffusion of the sodium from one part into the other it was impossible to determine accurately the boundary between the two. If I measured the length of the sodium flame as if there were no diffusion from one part into the other, I obtained results which were much the same as those obtained by Bonner; but if I assumed that the sodium flame ended where it appeared to the eye to end, I obtained data similar to those which others have obtained. Bonner apparently assumed that it makes no difference how much diffusion there is from one part to the other. This would be entirely allowable, if it had been proven that a given amount of sodium gives the same amount of light irrespective of the number of flames into which it may be sprayed, but this is the assumption which Bonner is attempting to prove by his experiments and should not be assumed in the proof.

I believe, therefore, that one is justified in refusing to accept Bonner's experiments as definite proof of his conclusion.

C. D. CHILD

Colgate University,
Hamilton, New York,
September 8, 1932.

The Gyromagnetic Ratios for Nickel and Cobalt

In a paper recently published by the *American Academy of Arts and Sciences* (Proceedings, vol. 66, No. 8, pp. 273–348) I have given an account of an elaborate investigation of the *rotation* of permalloy and soft iron *by magnetization*. The gyromagnetic ratios for the two substances were found to be, respectively, $1.05\times m/e$ and $1.04\times m/e$, with errors probably less than $\frac{1}{2}$ percent.

Many successful observations have now been made on the less tractable substances nickel and cobalt. Preliminary values for the gyromagnetic ratios for these substances are, respectively, $1.06\times m/e$ and $1.07\times m/e$. The method, an alternating-current one, had to be modified to reduce the effects of certain sources of error, including magnetostriction, before any success was obtained with cobalt. Inasmuch as serious errors not suspected by other investigators have been eliminated in all of this work, the results obtained are far more reliable than those obtained by others, who have always obtained $1\times m/e$ within the limits of their supposed experimental errors (with the exception of Einstein and de Haas, who, in 1915, thought they had found $2\times m/e$).

The gyromagnetic ratios obtained in this investigation agree with those published by L. J. H. Barnett and myself in 1925 (*Proceedings American Academy of Arts and Sciences*, vol. 60, No. 2) as the result of an elaborate investigation of the *magnetization* of many ferromagnetic substances *by rotation*, the mean for all these being $1.06\times m/e$, with an error estimated as not greater than 2 percent. They also agree with the results obtained by me for iron when the effect was discovered in 1914, in view of the relatively large experimental error (some 10 or 15 percent) in these early observations. A complete account of this new work will be published later.

S. J. Barnett

The University of California at Los Angeles,
and
The California Institute of Technology
September 12, 1932.

Angular Distribution of Electrons Scattered in Mercury Vapor

In a recent paper (Phys. Rev. **40,** 731, 1932) describing an investigation on the scattering of electrons in mercury vapor, Tate and Palmer conclude that Mott's theory is quite inadequate to account for the angular distribution of the electrons which are scattered elastically. Mott's theory leads to a formula

$$I(\theta, v)=\left(\frac{e^2}{2mv^2}(Z-F)\operatorname{cosec}^2\frac{\theta}{2}\right)^2$$

where $I(\theta, v)$ is the number of electrons having a velocity v and scattered through an angle θ, Z the atomic number of the scattering atom, and F the atomic structure factor. Their conclusion is based on the fact that the experimental curve representing the number of electrons scattered as a function of the angle is far *less steep* than the curve representing $\operatorname{cosec}^4(\theta/2)$. This method of testing the formula implicitly assumes that F is independent of θ, an assumption which is not correct. F values are given by James and Brindley (Phil. Mag. **12,** 81, 1931) for caesium ($Z=55$), together with a formula which enables one to calculate the F values for any other heavy element from those listed for caesium. In this way a table of F values for mercury was constructed. On using these values in the formula given above, Mott's function $I(\theta, v)$ could be calculated. It was then found that there was a much better agreement between the theoretical curve and the experimental curve. The experimental curve is now somewhat *steeper* than the curve representing $(Z-F)^2\operatorname{cosec}^4(\theta/2)$, a result which is in accord with that obtained by Hughes, McMillen and Webb (Phys. Rev. **41,** 154, 1932) for the scattering of electrons by helium atoms over the same range (0° to about 60°). They found that, when the experimental curves began to deviate from the Mott curves which is the case when electron energies less than about 400 volts are involved, the experimental curves are *steeper* than the theoretical curves.

The F values used for mercury are probably to be regarded only as a fairly close approximation. When such values are used to calculate a *difference*, $(Z-F)$, it is evident that we cannot at present expect to construct

a highly accurate theoretical curve. However the deviation between the theoretical curve and the experimental curve given by Tate and Palmer for 700 volt-electrons is probably real and not to be accounted for by the uncertainty in the F values. It would be interesting to see whether or not the theoretical, and experimental curves would coincide for mercury when higher electrons speeds are used.

A. L. HUGHES

Washington University,
St. Louis, Missouri,
September 14, 1932.

On the Radiation Originating from a Beam of Electrons in Mercury Vapor and the Mean Life of the 2^3S_1 State

Previously the writer[1] has obtained photographs of the mercury spectrum produced by a beam of electrons in mercury vapor. The optical arrangement consisted of projecting the image of the electron beam on to the slit of the spectrograph perpendicular to the length of the slit. It was found that some of the lines extended beyond the image of the electron beam, this being particularly true for the resonance line 2537A. This result has recently been confirmed by Lees and Skinner.[2] The extension of the lines beyond the image of the electron beam is caused by the radiation of atoms lying outside of the boundaries of the beam. In Table I is included the most prominent lines obtained which are classified into two groups; extended lines and normal lines. Fig. 1 illustrates a typical spectrogram obtained. In this particular case the electrons

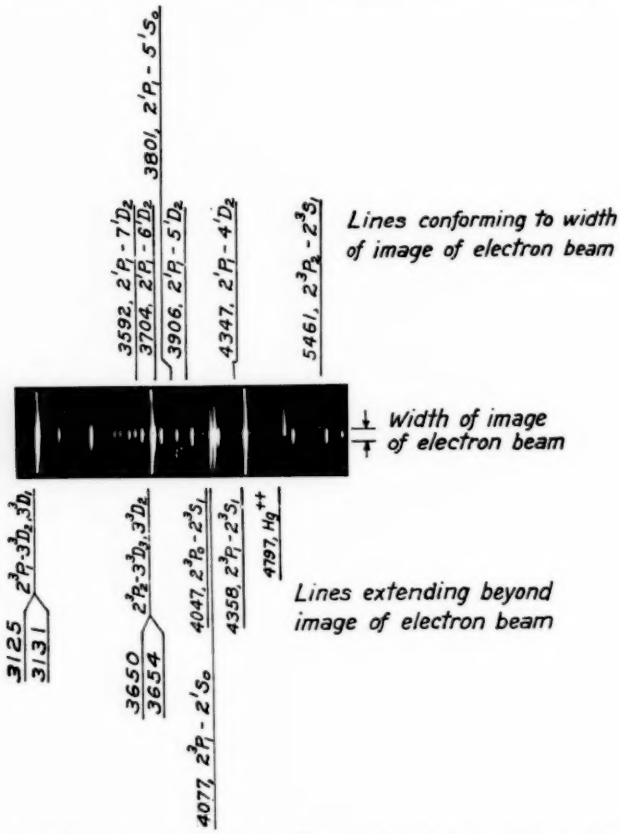

Fig. 1. A portion of the mercury spectrum illustrating the lengthening of lines beyond the image of electron beam.

[1] Maxwell, Phys. Rev. **32**, 715 (1928).

[2] Lees, and Skinner, Proc. Roy. Soc. **137A**, 186 (1932).

were accelerated to a velocity of 200 volts. A transverse electric field was applied for the purpose of drawing out the spark line 4797A as shown in Fig. 1. The shape of the lines was not particularly dependent upon the speed of the electrons. In general the lines having the levels 2^3P_0, 2^3P_1, 2^3P_2, as the final state are lengthened, whereas the lines terminating in the 2^1P_1 state do not show spreading beyond the image of the electron beam. An exception to this rule, however, occurs for the line $2^3P_2 - 2^3S_1$ (5461A) which does not show any appreciable elongation. The lines of the series $2^1P - n^1S_0$ (4916A, 4108A) showed slight extension beyond the image of the electron beam, but the line 3801A, $2^1P_1 - 5^1S_0$ showed practically no spreading.

The lengthening of the resonance line (2537A) is obviously caused by absorption since it is very easily absorbed at the pressures of about 0.001 mm of Hg used in this case.

TABLE I. *Lines of the mercury arc spectrum.*

Lines extending beyond image of the electron beam		Lines conforming to the width of image of electron beam	
$1^1S_0 - 2^3P_1$	2537	$2^1P_1 - 4^1D_2$	4347
$2^3P_0 - 2^3S_1$	4047	$2^1P_1 - 5^1D_2$	3906
$2^3P_0 - 3^3S_1$	2752	$2^1P_1 - 6^1D_2$	3704
$2^3P_0 - 3^3D_1$	2967	$2^1P_1 - 7^1D_2$	3592
		$2^1P_1 - 5^1S_0$	3801
$2^3P_1 - 2^3S_1$	4358	$2^3P_2 - 2^3S_1$	5461
$2^3P_1 - 3^3S_1$	2893		
$2^3P_1 - 4^3S_1$	2576		
$2^3P_1 - 2^1S_0$	4077		
$2^3P_1 - 3^3D_2$, 3^3D_1	3125, 3131		
$2^3P_1 - 4^3D_2$, 4^3D_1	2653		
$2^3P_1 - 5^3D_2$, 5^3D_1	2482		
$2^3P_2 - 3^3D_3$	3650		
$2^3P_2 - 3^3D_2$	3654		

It has been proposed[3] that the lengthening of the other lines was caused by absorption of atoms in the 2^3P_0, 2^3P_1 and 2^3P_2 state located in the vicinity of the electron beam.

Similar lengthening or spreading of spectrum lines has been found for helium[4] and for the case of the lines $2^3P - n^3D$. Lees and Skinner suggested that it was caused by collisions of the type

$$\mathrm{He}(n^1P) + \mathrm{He}(1^1S) = \mathrm{He}(1^1S) + \mathrm{He}(n^3D)$$

occurring outside the electron beam where the energy differences between the n^1P and n^3D states are of the order of the thermal energy. For mercury, similar atomic collisions resulting in a change from n^1P_1 to $n^3D_{1,2,3}$ states may be possible. Transitions of this kind to populate the 2^3S_1 state from any of the n^1P_1 levels will be very unlikely on account of the large energy differences involved.

Randall and Webb[5] have measured the mean life of the 2^3S_1 state of mercury by using the lines $2^3P_2 - 2^3S_1$ (5461A), $2^3P_1 - 2^3S_1$ (4358A) and $2^3P_0 - 2^3S_1$ (4047A) and found that the lines 4358A and 4047A gave the mean life of 5.75×10^{-8} sec. while the line 5461A gave an entirely different value of 2.37×10^{-7} sec. In this connection it is very interesting to notice from Table I that the line 5461A which gave the greater mean life shows no lengthening while on the other hand the other two lines 4358A and 4047A have prominent spreading. This shows that outside of the electron beam there are atoms in the 2^3S_1 state which will give rise to transitions to the 2^3P_0 and 2^3P_1 levels but with practically the exclusion of transitions to the 2^3P_2 state. This undoubtedly means that the fine structure of the 2^3S_1 level plays an important part in the radiation phenomena, in support of the conclusion arrived at by Randall and Webb to account for the dis-

[3] Maxwell, Phys. Rev. **31**, 711 (1928); see also for instance, for absorption of excited states: Turner, and Compton, Phys. Rev. **25**, 606 (1925); Wood, Phil. Mag. **50**, 774 (1925); *ibid.* **4**, 466 (1927).

[4] Lees, Proc. Roy. Soc. **137A**, 173 (1932); Lees and Skinner, reference 2; Maxwell, Early issue of Jour. Frank. Inst.

[5] Randalls and Webb, Phys. Rev. **35**, 665. 1161 (1930); see also Richter, Ann. d. Physik, **7**, 293 (1930).

crepancies found for the mean life of this state.[6]

There exists the possibility that the photograph plate characteristics may vary for the triplet lines in such a manner as to weaken the spread of the line 5461A in comparison with the lines 4047A and 4358A, since the green line is nearer to the less sensitive portion of the plate. Exact intensity measurements were not obtained, however the difference in shape of the line 5461A in comparison with the other lines of this triplet appears too great to be accounted for by errors of this kind.

This work was done in the laboratory of the Bartol Research Foundation.

LOUIS R. MAXWELL

5336–42nd St., N.W.,
Washington, D.C.,
September 15, 1932.

[6] For further discussions see; Morozoroski, Zeits. f. Physik **68,** 278 (1931); Frisch and Pringsheim, Zeits. f. Physik **67,** 169 (1931).

The Disintegration of Lithium by Swiftly-Moving Protons

We have recently carried through preliminary experiments on the disintegration of lithium by swiftly-moving protons and have obtained results in confirmation of those of Cockcroft and Walton (Proc. Roy. Soc. **A137,** 229–242, 1932).

Using the apparatus of Lawrence and Livingston (Phys. Rev. **40,** 19–35, 1932) as the source of high-speed protons, we have bombarded a crystal of lithium fluoride with protons having energies of 360,000, 510,000, and 710,000 volts. Radiations emanating from the crystal were detected by a Geiger point counter with a mica window (stopping power 2.2 cm of air) adjacent to the crystal, subtending a solid angle of $\pi/10$. Counts were ob-

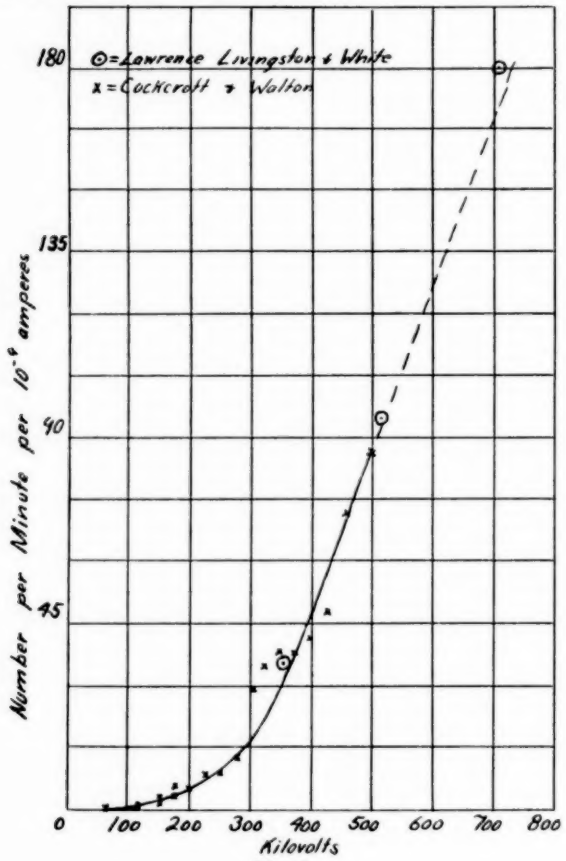

Fig. 1.

tained proportional to the bombarding proton current (about 10^{-9} amp.), there being for 500,000 volt-protons about 95 counts per minute per milli-microampere. Fig. 1 is a plot of our observed number of counts per minute per milli-microampere for the three voltages and also the corresponding observations of Cockcroft and Walton adjusted to our curve at 500,000 volts. It is seen that our observed variation is in excellent agreement with theirs over the overlapping region and that our observation at 710,000 volts agrees with a linear extrapolation (dotted line) above their range of observation. In the above figure the two sets of data have been adjusted to agree at 500,000 volts. Actually there is an apparent disagreement in that when account is taken of geometrical considerations, our observed number of counts per unit current per unit solid angle is about five times that of one set of observations of Cockcroft and Walton (Fig. 4 of their paper) and about equal to that derived from another set of their observations (their Fig. 2)—while on the other hand, one would expect the observed rate of disintegration of lithium in a lithium fluoride crystal to be about one-fourth the rate for the pure metal.

There are numerous possible sources of this slight difference in observations. There is the possibility that our counter was registering counts in excess of the number of alpha-particles entering the counting chamber. The counter was operated with voltages above its gamma-ray threshold and therefore was sensitive to such radiations. However, some counts were obtained below the gamma-ray threshold showing that some of the counts certainly were due to alpha-particles. On the other hand, Cockcroft and Walton's values may be too low because of an appreciable lack of homogeneity of velocities of their bombarding protons or because of an appreciably rough lithium target which would diminish the number of alpha-particles escaping to the counter, i.e., at right angles to the proton beam.

At this early stage of the work we of course would not urge our absolute values as more likely nearer the truth; but it is interesting to note that they are in excellent accord with the predictions of Gamow's theory. Professor J. R. Oppenheimer has kindly calculated for us, along the lines of Gamow's theory, the probability that an alpha-particle will be liberated by a proton striking a lithium fluoride crystal, taking account of the range and velocities of the proton within the crystal. His calculation for 500,000 volt-protons indicates that there should be from one to ten alpha-particles liberated for every 10^7 protons, while we observed six alpha-particles per 10^7 protons (assuming each count of the Geiger counter represents one disintegration alpha-particle). Dr. Oppenheimer also calculated the variation with energy of the proton of the probability of disintegration, obtaining the relative values of 1.0, 2.6 and 5.2 for the voltages 360,000, 510,000, and 710,000, respectively. These values, as may be seen from the above figure, are also in splendid agreement with our observations. Thus, these calculations, though still rough and schematic, show that the simple extension of Gamow's theory is fully able to account for the order of magnitude and voltage dependence given by observation.

These experiments were begun by Dr. James A. Brady who was joined later by Drs. Donald Cooksey and F. N. D. Kurie. They were successful in detecting radiations from the bombarded lithium fluoride but unfortunately because of insufficient available time had to abandon the experiments which we have carried on. We are much indebted to them for their participation in the earlier stage of the work as well as to Dr. Malcolm C. Henderson who has taken an active part in the work since their departure and is continuing with the experiments.

ERNEST O. LAWRENCE
M. STANLEY LIVINGSTON
MILTON G. WHITE

Radiation Laboratory,
Department of Physics,
University of California.
September 15, 1932.

BOOK REVIEWS

A History of Experimental Physics. C. T. CHASE. Pp. 195, Figs. 15. D. Van Nostrand Company, New York, 1932. Price $2.25.

This book deserves the attention of all teachers and serious students of physics. The perspective to be gained by a study of the historical development of physics is valuable and leads to a better understanding of the subject. That the treatment is non-mathematical will appeal to some readers, but it seems to the reviewer that an essential part of physics is thereby omitted. It is striking that nearly half of the book deals with developments since 1895, an era of very rapid growth and of many new ideas. Since much of this material has not yet won its way into the usual general course in physics, this text makes an excellent supplement to such a course. The subject matter is very well selected and the style is clear and interesting. The few slips are not serious.

JOSEPH VALASEK
University of Minnesota

Vision and Colour Vision. R. A. HOUSTOUN. Pp. 238, Figs. 102. Longmans, Green and Company, New York, 1932. Price $4.50.

When a physicist departs from a discussion of intensity and wave-length in connection with light, he is stepping over the boundary between physics and psychology. However, several of the great physicists have strayed in this way because of the many interesting phenomena involved in vision. The present volume will be an inducement to others to follow in their steps.

This volume gives, first of all, a resumé of existing knowledge on vision and color vision. It differs from the usual summary in that the author himself has performed many experiments in the field and has some pertinent criticisms and suggestions to offer. However, many readers will disagree with some of his conclusions. In particular, the association of the two reticular and nuclear layers of the retina with the red-green and yellow-blue processes of Hering will require further investigation. Can it be reconciled with the zonal color characteristics of the human eye? This particular phase of color vision is scarcely mentioned.

The author raises a mathematical objection to the Young-Helmholtz theory. It is not noticed that this will also apply to the author's theory for any stimulus which excites both processes. However it is not hard to make a plausible modifying assumption in either case.

It is to the credit of the author that he has devised experiments which make it possible to obtain a numerical measure of the normality or abnormality of color vision of an individual. As a result of such a measurement of color vision, it is found that there are no fixed types of color blindness, but that natural variation from the mean accounts for practically all of the abnormalities. The data in support of this are very impressive, but the reviewer thinks that at least the microscope experiment can be attacked on the ground that colors may be sensed by their darkness, i.e., that red may be detected as "the darker color" by the red blind. However, a wide circle of readers should find much food for thought and suggestions for further experiments in this interesting and stimulating book.

JOSEPH VALASEK
University of Minnesota

CURRENT LITERATURE OF PHYSICS

Extracts from the Tables of Contents of Some of our Contemporaries

NATURE

VOL. 130, NO. 3278 — AUGUST 27, 1932

Letters to the Editor:

X-Ray Interpretation of the Molecular Structure of Feather Keratin. By **W. T. Astbury and Thora C. Marwick** 309
Some Characteristics of Ultimate Lines. By **Adolfo T. Williams** 313
Magnetic Analysis of Molecular Orientations in Crystals. By **K. S. Krishnan** 313
Electric Dipole Moment of Nickel Carbonyl. By **L. E. Sutton and J. Breeze Bentley** 314
Hall Effect in Beryllium. By **A. Ciccone** 315
Absorption of Boron Neutrons by Lead. By **M. de Broglie and L. Leprince-Ringuet** 315

NATURE

VOL. 130, NO. 3279 — SEPTEMBER 3, 1932

Letters to the Editor:

Photography of Penetrating Corpuscular Radiation. By **P. M. S. Blackett and G. Occhialini** 363
Intensity of Cosmic Radiation in the High Atmosphere. By **E. Regener** 364
α-Rays of Ionium. By **Frederick Soddy** 364
Glow in Photoelectric Cells. By **Lord Rayleigh** 365
Possible Connection between the Troposphere and the Kennelly-Heaviside Layer. By **Ivo Ranzi** 368
Dimensions of Fundamental Units. By **William Cramp** 368

ZEITSCHRIFT FÜR PHYSIK

VOL. 77, NOS. 7 AND 8 — AUGUST 6, 1932

Comparison of the Elementary Photographic Processes in Alkali and Silver Salts. By **R. Hilsch and R. W. Pohl** 421
Electron Impact on Crystal Surfaces as a Proof of Optical Energy States. By **Rudolf Hilsch** 427
Magnetic Rotation among the Zeeman Components. By **Wilhalm Schütz** 437
Rotation-Vibration Spectrum of Acetylene. By **K. Hedfeld and P. Lueg** 446
Determination of the Transition Probability $2P-1S$ of Sodium by Absolute Intensity Measurements in Flames. By **E. F. M. van der Held and L. S. Ornstein** 459
Influence of Screening on the Intensities of X-Ray Diagram Lines. By **J. A. Prins** 478
Significance of the Line Emission and Absorption Spectra of the Chromium Phosphors. By **Otto Deutschbein** 489
Second Spark Spectrum of Neon, Ne III. By **T. L. de Bruin** 505
Stark Effect in the Argon Spectrum. By **Nils Ryde** 515
Variation with Electron Energy of the Fluorescence Brightness of Calcium Tungstate under Electron Impact. By **A. Güntherschulze and F. Keller** 528
Mass Defect and Binding Energy of the Neutron. By **Werner Braunbek** 534
Characteristic Temperature for Seignette Salt Crystals. By **R. D. Schulwas-Sorokin** 541
Uniform Distribution of Admixtures in Crystals when Tempered. By **B. Hochberg** 547
Investigations of Vibrating Fluids under the Influence of Alternating Electric Fields. By **B. Claus** 553

ZEITSCHRIFT FÜR PHYSIK

VOL. 77, NOS. 9 AND 10 — AUGUST 24, 1932

Measurement of the Lifetime of Excited NO_2. By **Oskar Heil** 563
Influence of Plastic Deformation on the Susceptibility of Dia- and Para-Magnetic Metals. By **A. Kaussmann and H. J. Seemann** 567
Ionizing Power of Artificial H-Rays. By **K. Diebner** 581
Range and Total Ionization of α-Rays in Gases. By **Martin Mäder** 601
Raman Effect of Aqueous Nitrate Solutions. By **Peter Grassmann** 616
Slow Rays of Mercury Ions. By **Fr. Beyerlein** 632
Elementary Wave Theory of Image Formation by Concave Mirrors and Lenses. By **Wilhelm Westphal** 644
Time of Establishment of Vibration Energy in CO_2 and N_2O. By **H. O. Kneser and J. Zühlke** 649
Quantum Physics of the Biological Action of X-Rays. By **R. Glocker** 653
Optical Investigation of Spark Formation in Air at Atmospheric Pressure. By **W. Holzer** 676
Anomalous Behavior of the Magnetic Permeability of Iron in High-Frequency Fields. By **G. R. Wait** 695
Remark on the Paper by H. Schüler and E. G. Jones: Hyperfine Structure and Nuclear Moments of Mercury. II. By **K. Murakawa** 699
Reply to the Preceding Remark. By **Schüler and E. G. Jones** 701

DIE NATURWISSENSCHAFTEN

VOL. 20, NO. 34 — AUGUST 19, 1932

Possibilities of the Formation of Complex Molecules. The Application to $(H_2O)_x$. By **Von Erich J. M. Honigmann** 635
Short Original Communications:
Occurrence of Highly Magnetic Intermediate Stages during the Thermal Disintegration of Nontronits. By **Von W. Geilmann, W. Klemm and K. Meisel** 639
Occurrence of Highly Magnetic and Catalytically Very Active Disintegration Stages during the Thermal Formation of Zinc-Chromium-Spinells. By **Von G. F. Huttig, H. Kittel and H. Radler** 640
Crystal Structure of Red Manganese Sulphide. By **Von Horst Schnaase** 640

DIE NATURWISSENSCHAFTEN

VOL. 20, NO. 35 — AUGUST 27, 1932

Method for Investigating Small Crystalline Powders by Electron Diffraction. By **F. Trendelenburg** 655
Short Original Communications:
Intensity Alternation in the Rotation-Vibration Spectrum of Water Vapor (Ortho- and Para-Water). By **R. Mecke** 657
Specific Coincidence Probability of Cosmic Rays at Sea Level after Passing 10 cm of Lead. By **W. Kolhörster and L. Tuwim** 657
Atomic Rays of Selenium and Tellurium. By **Otto Hönigschmid** 659

DIE NATURWISSENSCHAFTEN

VOL. 20, NO. 36 — SEPTEMBER 2, 1932

Short Original Communications:
27 Day Period of Air Disturbances of Wireless Telegraphy (Preliminary Communication). By **F. Schindelhauer** 672
New Class of Absorption Series as a Transition from the Optical to the X-Ray Spectra. By **H. Beutler** 673

PHYSIKALISCHE ZEITSCHRIFT

VOL. 33, NO. 15 — AUGUST 1, 1932

Conductivity of Dielectric Liquids. By **A. Nikuradse** 553
Addenda to the Report on Atomic Structure Factors. By **W. Ehrenberg and K. Schäfer** .. 575

Original Communications:

Remark on the Origin of the Field in the Positive Column. By **F. Ollendorff and R. Seeliger** 577
Determination of Planck's Constant as a Quantitative Demonstration Experiment. By **R. Suhrmann** 579
Optical Investigation of the Reflection of Hydrogen Canal Rays on Solid Bodies. By **E. Horovitz** 579
Production of Circularly Polarized Electric Waves by a Single Total Reflection. By **L. Bergmann** 582
Some New Facts Concerning the Contact Layer Photoelectric Effect. By **F. Waibel and W. Schottky** 583
Mechanical Vibrations of High-Frequency Conductors. By **J. Grunow** 585
Scattering of X-Ray from Chlorine. By **H. Richter** 587

PHYSIKALISCHE ZEITSCHRIFT

VOL. 33, NO. 16 — AUGUST 15, 1932

X-Ray Interference of Fluids in Liquids (Hg, Ga, CCl_4). By **H. Menke** 593
X-Ray Interference in Molecules with Two Carbon Atoms. By **F. Erhardt** 605
Crystal Oscillator and its Technical Form. By **E. Habann** 615
Theory of the Crystal Photoelectric Effect. By **H. Th. Wolff** 621
Investigation of the Emission of Glasses of the Composition $B_2O_3+Na_2O$. By **H. Bölling** 625

ANNALEN DER PHYSIK

VOL. 14, SERIES 5, NO. 4

Electrical Properties of Mixed Crystal Alloys. II. Resistance of Silver Alloys. By **J. O. Linde** 353
Application of Conformal Representation in Electrostatics. By **E. Kehren** 367
Electrical Properties of Dust and Mist. By **H. Sachsse** 396
Remark of the Paper of L. Wesch: "On the Proof of the *K*-Absorption Edges for Phosphors and a New Sensitive Method for Spectral Analysis of High-Frequency Rays." By **E. Rupp** 413
Breakdown Investigations in Compressed Gases and in Liquid Carbon Dioxide. By **O. Zeier** 415
Intensity Relations in the Helium Spectrum in the Case of Superposition of Canal Ray Motion and Electric Field. By **H. Kirschbaum** 448
Variation with Surface Orientation of the Maximum Velocity and of Work Function of Photoelectric Electrons on Zinc Single-Crystal Cleavage Surfaces. By **Albert Nitzsche** 463

COMPTES RENDUS

VOL. 195, NO. 6 — AUGUST 8, 1932

Raman Effect in Salt Solutions. By **A. Silveira and E. Bauer** 416
Sensitometry with a Cylindrical Lens and Profile Diaphragm. By **Duffieux and Leon Grillet** 419
Photochemical Oxidation of Aqueous Solutions of Ammonia. By **Leon Gion** 421
Double Sulphate of Aluminum and Sodium. By **Astruc and Mousseron** 423

COMPTES RENDUS

VOL. 195, NO. 7 — AUGUST 17, 1932

Constitution of Atomic Nuclei. By **D. Iwanenko** 439
Contribution to the Study of Ternary Systems Magnesium-Aluminum-Copper. By **A. Portevin and P. Bastien** 441

REVUE D'OPTIQUE

VOL. 11, NOS. 7–8 — JUNE–JULY, 1932

Corrections due to Size of Slit in Photometric and Pyrometric Measurements Applied to Spectrophotometry. By **G. Ribaud and J. Peychès** 241

that the scattering by the atom would then be Z^2 times the intensity due to a single free electron. If, on the other hand, the electrons in the atom are separated by distances large compared with the wave-length of the x-rays, we may suppose them to scatter independently, in which case the intensity should be only Z times that due to a single free electron. Depending, then, upon the concentration of the electrons in the atom, the intensity of the x-rays scattered from it will vary by a factor of Z. If the electrons are at distances comparable with the wave-length of the x-rays, interference, constructive as well as destructive, will take place between the x-rays scattered by the different electrons of the atom, and as a result the intensity scattered by the atom as a whole will then be between Z^2 and Z times that due to a single free electron. Compton,[2] Debye,[3] Schott[4] and others have calculated the intensity scattering function for various atomic models.

The intensity of x-rays scattered by a number of atoms depends not only upon the configuration of the electrons within each atom but also upon the configuration of the atoms in the molecules, as well as upon any special orientation of the molecules themselves. In the particular case, where the atoms are grouped in a crystal lattice, we have the so-called *Laue or Bragg Reflection* which, therefore, is only a special case of scattering. In the case of liquids or amorphous solids, the phenomenon known as "excess scattering" is probably the result of the cooperation of the three factors just mentioned. Debye[5] has shown that the last two of these factors play no roll when perfect gases are used for scattering and hence excess scattering must in that case be ascribed solely to the configuration of the electrons within the atoms. On account of this simplification of the problem great progress has been made in the theories of scattering for monatomic gases. So far as the writer is aware, only Jauncey[6] has made an attempt to solve the problem for amorphous solids.

The quantum theories predict a scattering function different from Thomson's formula. They are, however, based upon the assumption that for the limiting case of long wave-lengths, where the motion imparted to the scattering electron is negligible, the intensity of the scattered rays should approach that assigned to it by Thomson's classical formula. The older forms of the quantum theory were not successful in giving a unique solution for the scattering function. The newer forms do give such a solution and it is,

$$I_\phi = I_0 \frac{e^4}{2m^2r^2c^4} \frac{(1 + \cos^2 \phi)}{(1 + \alpha \operatorname{vers} \phi)^3}$$

where $\alpha \equiv h\nu/mc^2$, h being Planck's constant, ν the frequency of the x-rays, and the other symbols have the same significance as before.

[2] A. H. Compton, Washington University Studies **8,** 99 (1921).
[3] P. Debye, Ann. d. Physik **46,** 809 (1915).
[4] G. A. Schott, Proc. Roy. Soc. Lon. **A96,** 395 (1920).
[5] P. Debye, Phys. Zeits. **28,** 135 (1920).
[6] G. E. M. Jauncey, Phys. Rev. **37,** 1193 (1931).

Breit[7] was the first to suggest this formula on empirical grounds and reasoning from the correspondence principle. Dirac[8] derived it theoretically with the help of the quantum dynamics of Heisenberg and Born, and Waller[9] as well as Gordon[10] did the same on the principles of the de Broglie-Schroedinger wave theory. It is true, that more recently, Klein and Nishina,[11] on the hypothesis of the spinning electron using Dirac's relativistic quantum dynamics, have derived a scattering function which differs somewhat from the above. However, deviations of the two formulae are of the order of $(h\nu/mc^2)^2$, while the Breit-Dirac expression differs from the classical Thomson formula by quantities of the order of $h\nu/mc^2$. In the x-ray region, where $h\nu/mc^2$ is small the deviations between the two quantum expressions are virtually negligible. Even for an $\alpha=0.5$, which corresponds to a wave-length of 0.05A the deviation amounts to only about 10 percent.

The only experimental tests of the quantum formula for sufficiently hard rays, that have so far been published, are the indirect ones of Fricke and Glasser,[12] for effective wave-lengths of 0.18 and 0.115A, and those of Ishino,[13] and Owen, Fleming and Fage,[14] for the γ-rays from RaC. The first consisted in determining the ratios of the coefficients of photoelectric absorption to those of true absorption due to scattering in carbon, and in the latter two cases, in measuring the ratios for aluminum of the coefficients of true absorption due to scattering to the total scattering coefficients. A direct test, by comparing I_ϕ with the experimental values of scattered intensities, is attended by considerable difficulties. In the earlier technique of various authors,[15] the wave-lengths used were too long to show appreciable deviations from the predictions of the classical theory. Where short wave-lengths were used the results are difficult to interpret on account of the comparatively large corrections that would have to be made in the ionization effects at different angles. This is due to the small absorption in the ionization chamber.

The work described in this paper was undertaken with a view of testing the scattering function given by the quantum theory. For hard x-rays and scattering materials of low atomic number, we may suppose, in view of the Compton effect, that the scattered rays are more or less completely modified. In that case the intensity of scattering should most nearly approximate that predicted by the quantum theory. Paraffin was selected as the light scatterer and in addition the scattering distribution curves were determined for aluminum, copper and lead.

[7] G. Breit, Phys. Rev. **27,** 362 (1926).
[8] P. A. M. Dirac, Proc. Roy. Soc. Lond. **A111,** 422 (1926).
[9] Ivar Waller, Phil. Mag. **4,** 1228 (1927).
[10] W. Gordon, Zeits. f. Physik **39,** 117 (1926).
[11] Klein and Nishina, Zeits. f. Physik **52,** 852 (1928).
[12] H. Fricke and O. Glasser, Zeits. f. Physik **29,** 374 (1924).
[13] M. Ishino, Phil. Mag. **33,** 140 (1917).
[14] E. A. Owen, N. Fleming, and W. E. Fage, Proc. Phys. Soc. **36,** 355 (1924).
[15] For a summary see Compton's *X-rays and Electrons* p. 306, D. Van Nostrand Co. N.Y.C. (1926).

II. Apparatus and Experimental Procedure

A diagram of the apparatus is given in Fig. 1. A tungsten target x-ray tube was operated at 120 peak k.v. and 5 m.a. with half-wave rectification. The

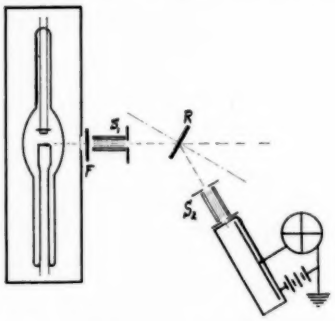

Fig. 1. Arrangement of apparatus.

tube was water cooled and immersed in oil in a heavy lead box. In the front of the box was fitted a heavy lead glass plate having a thin celluloid window. This arrangement permitted the tube to be brought very near to the spectrom-

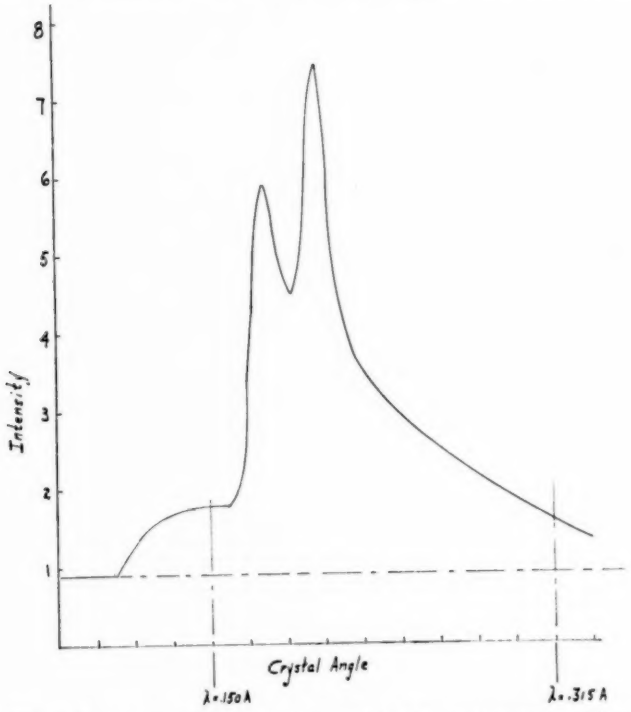

Fig. 2. Spectrum of radiation transmitted through tungsten filter.

eter with a consequent increase of intensity in spite of the absorption in the oil.

An effort was made to work with homogeneous radiation. It was hoped, that by designing all component parts of the apparatus for maximum effi-

ciency, it would be possible to use crystal-reflected rays. Unfortunately, however, the intensities obtained were too low for accurate measurements and the attempt had to be abandoned. Also, the balanced filter method could not be used as the two necessary elements for such filter, when using tungsten radiation, erbium and ytterbium, were not procurable anywhere in the United States. Finally, it was decided to use a tungsten filter, as shown at F in Fig. 1. The spectrum of the radiation transmitted through this filter, which consisted of two metallic tungsten foils each 0.065 mm thick, is given in Fig. 2. It is seen that the filtered band extends practically from about 0.15 to 0.315A.

Soller collimators were used for both the primary and scattered beams. They are shown as S_1 and S_2 in Fig. 1. They were 10 cm long and the distance between adjacent lead spacers was 0.1 cm, so that a maximum angular divergence of a little over one degree was obtained in the horizontal plane. The width of the collimators could be varied by proper slits, the height of which was 1 cm. This made the scattering angle slightly larger than recorded on the spectrometer circle, but the corrections were too small to be taken account of.

R in Fig. 1. represents the scattering substance mounted in the center of the spectrometer. In the case of paraffin and aluminum thin plates of these materials were placed so that the normal to the plate always made an angle of $\phi/2$, where ϕ is the scattering angle. This so-called "Crowther position" has certain obvious advantages over other ways of mounting the scatterer. The copper and lead plates, for reasons of greater intensities, were mounted so that the angle between the face of the plate and the primary beam was always one half the scattering angle. These plates were thick enough to absorb all of the primary radiation.

The intensities were measured with a Compton electrometer, mounted over the axis of the spectrometer, having a sensitivity of 8900 divisions per volt on a scale 150 cm away. The ionization currents could be measured with a reproducibility of about 3 percent.

At first an ionization chamber 7 cm long filled with xenon at two atmospheres pressure was used. Due to the insufficient absorption in this chamber and the large fluorescent yield of xenon certain corrections had to be made which, considering the nature of the experiment, were felt to be too large. Accordingly, another high pressure ionization chamber was constructed and filled with argon at a pressure of 1000 lbs. per sq. in. It was made of cylindrical, seamless steel tubing, 40 cm long and 4.45 cm inside diameter. The window was of 0.7 mm celluloid. The absorption in the window for the wave-lengths used was negligible and hence no corrections were made for it. The absorption in the chamber of a wave-length of 0.21A is 90 percent and the fluorescent yield for argon is, according to Auger,[16] only 0.07. The corrections are discussed in more detail below. The potential across the electrodes of the ionization chamber was 135 volts, which was about twice the value needed for saturation.

All parts of the apparatus were carefully shielded. The electrometer system, including the connections to the ionization chamber, was protected by

[16] Auger, Ann. de Physique **6**, 183 (1926).

large lead baffles. Other lead baffles, suitably disposed, prevented all stray radiation from reaching the ionization chamber.

The procedure consisted in a determination of the angular distribution of the intensities scattered from paraffin, aluminum, copper and lead. In the case of the last two, care was taken to exclude the characteristic radiations from entering the ionization chamber. This was accomplished by using an aluminum filter 0.65 mm thick for copper and one 1.3 mm thick for lead. Wave-lengths of the scattered rays at the different angles were determined by measuring the absorption in several sheets of aluminum. The final step was to make an accurate measurement of the scattered intensities at 90° from the different materials under experimental conditions as nearly alike as can be realized in actual practice.

The constants of the scattering materials are as follows: paraffin, 0.276 g per sq. cm; aluminum, 0.103 g per sq. cm; copper, 5.09 g per sq. cm; lead, 3.80 g per sq. cm.

The paraffin was from a block of commercial "Parowax." The aluminum and lead were from the usual rolled sheets of these materials. The copper was of electrolytic origin. An attempt to work with finely powdered aluminum failed because no good binding material was available.

III. Experimental Results and Calculations

The ratios of the ionization currents at any angle ϕ to those at 90° are given in the second column of Tables I to IV for each of the four materials.

Table I. *Paraffin at λ0.23A.*

Angle ϕ	Exp. ratio of ionization $i\phi/i_{90}$	Ratio from Crowther's formula	Corrected ratio $P\phi/P_{90}$	Scattering per gram s/ρ	S
10	3.23	4.46	4.9	0.0432	1.84
20	2.50	3.42	3.72	0.0328	1.46
30	2.10	2.80	3.04	0.0268	1.28
40	1.75	2.28	2.46	0.0216	1.14
50	1.53	1.92	2.01	0.0177	1.03
60	1.33	1.59	1.67	0.0147	0.99
70	1.18	1.35	1.39	0.0122	0.92
80	1.06	1.15	1.16	0.0102	0.83
90	1.0	1.0	1.0	0.0088	0.74
105	1.15	1.26	1.24	0.0109	0.85

Table II. *Aluminum at λ0.23A.*

Angle ϕ	Exp. ratio of ionization $i\phi/i_{90}$	Ratio from Crowther's formula	Corrected ratio $P\phi/P_{90}$	Scattering per gram s/ρ	S
10	9.50	12.60	13.80	0.1290	5.70
20	4.50	6.20	6.80	0.0636	2.95
30	3.00	4.05	4.40	0.0410	2.04
40	2.20	2.90	3.13	0.0293	1.61
50	1.60	2.03	2.15	0.0201	1.22
60	1.30	1.58	1.65	0.0154	1 08
70	1.20	1.39	1.43	0.0134	1.05
80	1.05	1.13	1.14	0.0106	0.905
90	1.0	1.0	1.0	0.0093	0.81
105	1.20	1.33	1.31	0.0122	1.0

TABLE III. *Copper at λ0.19A.*

Angle ϕ	Exp. ratio of ionization	Scattering per gram	S
10	22	0.2340	11.0
20	7.95	0.0855	4.20
30	4.75	0.0510	2.69
40	3.25	0.0350	2.04
50	2.30	0.0247	1.59
60	1.70	0.0182	1.35
70	1.40	0.0150	1.19
80	1.15	0.0123	1.10
90	1.0	0.0107	0.99
105	1.07	0.0115	1.0

TABLE IV. *Lead at λ 0.19A.*

Angle ϕ	Exp. ratio of ionization	Scattering per gram	S
10	22.0	0.557	30.0
20	11.20	0.284	16.05
30	5.00	0.127	7.73
40	3.13	0.0792	5.30
50	2.15	0.0545	4.02
60	1.65	0.0418	3.56
70	1.35	0.0342	3.26
80	1.12	0.0284	2.94
90	1.0	0.0253	2.70
105	1.0	0.0253	2.53

These ratios were, of course, corrected for the leak in the electrometer system. The third column of Table I and II is derived from the second by evaluation from Crowther's formula.[17] This formula for the intensity of x-rays scattered in a direction ϕ from a thin plate of material of thickness t is,

$$I_\phi = AIts/R^2 \cos(\phi/2) \tag{1}$$

where I_ϕ is the intensity scattered in a direction ϕ, I is the intensity of the primary rays *after* penetrating the plate in the Crowther position, s is linear scattering coefficient per unit solid angle in a direction ϕ, A is the area of the ionization chamber window, and R is the distance between the window and the plate. Also, I is given by

$$I \equiv I_0 e^{-\mu t/\cos(\phi/2)}$$

where I_0 is the intensity of the primary rays at the incident face of the scattering plate, and μ is the linear absorption coefficient of the primary rays in the plate.

From Eq. (1) an expression may be set up giving the ratio of the scattering per gram per unit solid angle in any direction ϕ relative to that at 90° with the primary beam, thus cancelling out I_0.

Measurements of absorption in aluminum of the rays scattered from paraffin at 90° gave an absorption coefficient which by interpolation from the values given in Compton's table[18] corresponded to a wave-length of 0.25A. At

[17] J. A. Crowther, Proc. Roy. Soc. **A86,** 478 (1912).

[18] Compton's *X-rays and Electrons,* p. 184.

30° the result was 0.23A. The values for aluminum were the same within the uncertainty of the measurement. Considering the hardness of these rays, the scattered radiation from paraffin may be assumed to be completely modified at 90° and that from aluminum is virtually so. Accordingly, for these two materials, the change in wave-length at the different scattering angles was computed from the formula for the Compton effect,

$$\Delta\lambda = (h/mc)(1 - \cos\phi)$$

where $\lambda = 0.25$ at 90°. The wave-lengths so obtained were used in the correction computations given below.

When x-rays of different wave-lengths enter an ionization chamber, the ionic saturation currents which one measures, are not in general proportional to the intensities in the beams. Allison and Andrew[19] give an expression which enables one to calculate the true intensities. This expression is

$$I = cPFR \tag{2}$$

where I is the measured ionic saturation current, P is the power of the beam of x-rays entering the chamber, F is the fraction of the primary energy absorbed in the chamber, c is a constant for a given gas, which is inversely proportional to ϵ, where ϵ is the energy spent in producing a pair of ions, and R is given by

$$R = 1 - \frac{\tau_k}{\mu}\omega_k\lambda_i \sum_i \frac{f_i}{\lambda_i} e^{-\tau_i r} - \frac{\sigma_s}{\mu} e^{-\tau r} + \frac{\sigma_r}{\mu} \tag{3}$$

where τ_k is the absorption coefficient of the gas corresponding to frequency ν for the ejection of photoelectrons from the K-level, μ is the absorption coefficient of the gas for the wave-length of the primary beam, ω_k is the fluorescent yield for K-series as defined by Auger, f_i is the fractional part of the total number of quanta emitted, having the frequency ν_i of the i^{th} line of the K-series, τ_i is the fluorescent absorption coefficient of the gas for the i^{th} line of its own K-series, r is the effective path length of the radiation to the walls, σ_s is the true scattering coefficient, σ_r is the coefficient of absorption due to scattering or simply the recoil electron coefficient, and τ is the absorption coefficient for the scattered rays.

The last term of Eq. (3) has been added to Allison's original expression to take care of the Compton scattering. The σ_s is merely σ in Allison's expression, the usual scattering coefficient.

σ_s and σ_r were calculated from Compton's expressions,[20]

$$\sigma_s = \sigma_0(1 + \alpha)/(1 + 2\alpha)^2$$
$$\sigma_r = \sigma_0\,\alpha/(1 + 2\alpha)^2$$

where σ_0 is the classical linear scattering coefficient, and α has the same significance as before.

[19] S. K. Allison and V. J. Andrew, Phys. Rev. **38**, 1424 (1931).
[20] Compton's *X-rays and Electrons*, p. 312.

The second term of Eq. (3) is negligibly small, if we consider that the K-series of argon is around 4A and hence strongly absorbed on its way to the walls; and also, that the fluorescent yield, as stated above, is only 0.07. It may be emphasized that the last term of Eq. (3) is based on the assumption that the recoil electrons are completely absorbed in their journey to the walls. This assumption is permissible as a short calculation from Whiddington's formula for the "reach" of a photoelectron will show.

The constant c in Eq. 2 may be eliminated by taking the ratio between the ionization due to a given wave-length as compared with that due to any other. In this manner the corrected ratios given in column 4 of Tables I and II were arrived at, using the wave-lengths at the different angles as determined from the formula for the Compton effect, with the experimental determination of wave-length at 90° serving as the basis.

With a thick scattering plate, in which there is complete absorption of the primary rays, which are incident on it at a glancing angle of $\phi/2$, it can easily be shown that the ratio of the scattering per gram per unit solid angle in any direction ϕ to that at 90° with the primary beam, is given by

$$(s/\rho)_\phi/(s/\rho)_{90} = I_\phi/I_{90} \tag{4}$$

where the symbols have the same significance as above. Hence in the case of copper and lead in Tables III and IV the experimental ratios are the true ratios, if, for the moment, we leave aside possible corrections for the wave-lengths at different angles.

The absorption measurements in aluminum of the scattered rays from copper and lead gave almost identical wave-lengths. There was no difference, within experimental error, between the wave-lengths at different scattering angles. The effective wave-length, determined as above from Compton's table, was 0.19A.

It was thought desirable to place the ratios of the intensities of scattering upon an absolute basis by a comparison with paraffin, as Coven[21] had done.

For unpolarized x-rays, the Breit-Dirac formula for the scattering per gram per unit solid angle in a direction ϕ, may be written,

$$\left(\frac{s}{\rho}\right)_\phi = N\frac{Z}{W}\frac{e^4}{2m^2c^4}\frac{(1+\cos^2\phi)}{(1+\alpha\ \text{vers}\ \phi)^3} \tag{5}$$

where N is Avogadro's constant, Z is the atomic number of the scatterer and W its atomic weight, and where the other symbols have the same significance as above.

This formula is, of course, strictly valid for free electrons only. But, considering the low effective atomic number of paraffin and the hardness of the primary rays in this experiment, we may assume as a first approximation that the value it gives for paraffin at 90° is the true value for paraffin. In that way we obtain a unit of measure. The average formula for paraffin is $C_{24}H_{50}$ which makes Z/W approximately equal to 0.5. Substituting this in Eq. (5),

[21] A. W. Coven, Phys. Rev. **38**, 1424 (1931).

we get for σ/ρ at 90° the value of 0.0088, for a wave-length of 0.23A. With this basic value for paraffin at 90° and the corrected ratios for the other angles, the column in Table I giving the scattering per gram has been calculated.

Similar calculations for the other material were made by using the separately determined ratios at 90°. These were:

paraffin/aluminum	2.43	by transmission
copper/lead	1.12	by reflection.

Also, the scattering from a 2 mm plate of aluminum, arranged for reflection, was compared with that from copper and lead. The ratios were:

aluminum/copper	2.02	by reflection
aluminum/lead	2.26	by reflection.

Since the 2 mm aluminum plate did not absorb all of the primary radiation, the latter ratios had to be divided by $(1-e^{-\mu l})=0.37$, where l is the maximum path of the x-rays in the aluminum plate.

Correcting all ratios for the different effects in the ionization chamber due to the different wave-lengths, we finally get the following relations:

$$(s/\rho)\text{Al } 0.23\text{A} = 1.06(s/\rho)\text{Par. } 0.23\text{A}$$

$$(s/\rho)\text{Cu } 0.19\text{A} = 1.22(s/\rho)\text{Par. } 0.23\text{A}$$

$$(s/\rho)\text{Pb } 0.19\text{A} = 2.88(s/\rho)\text{Par. } 0.23\text{A}.$$

The effective wave-length of the x-rays in the 2 mm aluminum plate was found to be 0.22A and in the above relations there is a small correction for the difference in the scattering power of aluminum at 0.23A and at 0.22A.

Using these relations at 90° and the corrected experimental ratios at the other scattering angles, the columns for the scattering per gram in Tables II, III and IV for aluminum, copper and lead, respectively, were calculated.

The S-columns in the tables give the scattering per electron relative to the classical scattering from a free electron. They were calculated on the assumption that the rays scattered from paraffin are completely modified, in which case we have from Eq. (5) that,

$$S = (1 + \alpha \operatorname{vers} \phi)^{-3}$$

which is then the actual value for paraffin. This value at 90° is 0.74. With the help of Eq. (5) and the experimentally determined values of (s/ρ), the S-values at other angles and for the other materials were computed.

IV. Discussion of Results

In Fig. 3 the dots represent the experimental values of the ratios of scattering from paraffin at a given angle compared with that at 90°. For convenience of comparison with Dirac's theory of scattering by free electrons, three curves have been drawn, evaluated from Eq. (5) for different values of α. Curve 1 corresponds to an α of 0.05A, curve 2 to an α of 0.1 and curve 3 to an α of 0.23A. The broken curve is plotted from Thomsons classical formula for the scattering from a free electron. It is interesting to note, although

the fact is probably entirely without significance, that the experimental values for angles between 30° and 90° lie almost exactly along curve 2, whereas, if the scattering from paraffin were equal to that from free electrons, we should expect these values to lie more nearly along curve 3, assuming Dirac's theory to hold for paraffin also. For angles below 30° there is a radical departure of the experimental values even from curve 2, but this circumstance can most probably be ascribed to line interferences, as, strictly speaking, none of the substances investigated can be entirely amorphous. In the backward direction also, there is excess scattering over what one would expect from the theory. Unfortunately, one could not go beyond 105°, as the lead box, containing the x-ray tube, was so close to the spectrometer, as to prevent its arm from swinging beyond that point.

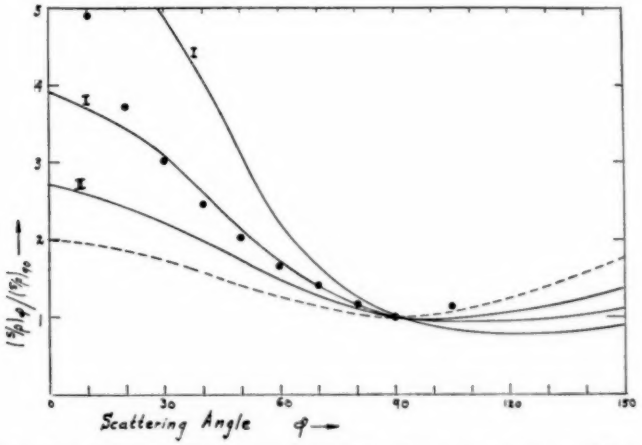

Fig. 3. Scattering from paraffin. Experimental values are represented by dots. Curves 1 2 and 3 are drawn from Dirac's formula for values of λ equal to 0.05, 0.1 and 0.23A respectively, The broken curve is from Thomson's classical formula.

But this value at 105° must be given some weight, for it, like all the other experimental values, represents the mean of the values obtained from three distribution curves for paraffin, each point on the latter being in turn the mean of four ionization measurements. It is estimated that the probable error of the dots in Fig. 3 is less than 1 percent.

There is some error introduced due to the use of Crowther's formula for the hard x-rays of this experiment. As Jauncey and Williams[22] point out, Eq. (1) was derived by Crowther when the Compton effect was still unknown. The scattered rays should be divided into coherent and incoherent rays and the simple Crowther formula should be replaced by

$$I_\phi = [AIt/R^2 \cos(\phi/2)](s_1 + s_2 T) \tag{6}$$

where s_1 and s_2 are respectively the coherent and incoherent linear spatial scattering coefficients per unit solid angle in a direction ϕ, and where T is a complicated expression involving the absorption coefficients of the coherent

[22] G. E. M. Jauncey and P. S. Williams, Phys. Rev. **41**, 127 (1932).

and incoherent scattered rays in the plate, in the air between the plate and the window of the ionization chamber.

Since we may consider the x-rays of wave-length 0.23A, scattered from paraffin at 90°, to be almost entirely modified and hence incoherent (unless, indeed, the modified ray is not entirely incoherent), s_1 in Eq. (6) becomes zero. A calculation for this particular case shows that the value of s_2 would be less than 1 percent larger than the value of s calculated from Eq. (1). This, therefore, places an upper limit upon the error from this source, as for the smaller angles the discrepancy would be smaller. The difference between the errors for 90° and 105° is trifling.

These results for paraffin are somewhat discordant with those obtained by Coven[21] at an effective wave-length of 0.32A. He finds closer agreement with the Dirac theory for free electrons. There is, however, in his case a question as to the magnitude of the error in determining the effective wave-lengths. Also, no corrections were made for the different ionization effects at different angles. Jauncey and Harvey[23] report good agreement between the scattering from paraffin and the Dirac theory at an effective experimental wave-length of about 0.30A. They measured the ratios of the scattering at 97.5° and 120° as compared with that at 75°. Their corrections for the different ionization effects are more difficult than in this experiment. They used methyl iodide and ethyl bromide in their ionization chamber which require comparatively large corrections for the fluorescent yield.

It is difficult to see how the agreement with the theory from free electrons can be perfect, if we recall what has been said about interferences, unless, indeed, our conception of the mechanism of scattering should be modified.

In Fig. 4 are plotted the S-values against $[\sin(\phi/2)]/\lambda$ for the different scattering materials. These curves show very clearly how the scattering per electron increases with the atomic number of the scatterer. For paraffin at the larger angles, the scattering is practically that from free electrons, which condition seems to be approached also for the other materials as $[\sin(\phi/2)]/\lambda$ is increased.

The largest errors involved in measuring the scattering per electron are probably those of comparing the scattering from one material with that of another. The smallest of these is in the case of the comparison of the intensity of scattering from paraffin with that from aluminum. This is estimated to be of the order of 1 percent. Also, in the comparison of the intensity of scattering of lead to copper the error is of about the same magnitude. This is because in one case the transmission and in the other case the reflection method was used for the two materials in question. But when we come to compare the scattering from paraffin with that from copper or lead we have to use the scattering from aluminum by the reflection method as a sort of connecting link. A little thought on the calculation involved will show that it is not entirely satisfactory. This doubt is strengthened by the fact that an attempt to get the ratio of paraffin to copper, by scattering from a copper foil by the transmission method, gave a result which did not agree with the other within

[23] G. E. M. Jauncey and G. G. Harvey, Phys. Rev. **37**, 1203 (1931).

experimental uncertainty. There is a possibility that multiple scattering[24] may have some bearing on this, and this point will be investigated in the near future.

The possible error of method involved in determining the S-values for copper and lead is estimated, in view of the above, to be of the order of 5 percent. On account of this large error it was thought inadvisable to attempt a

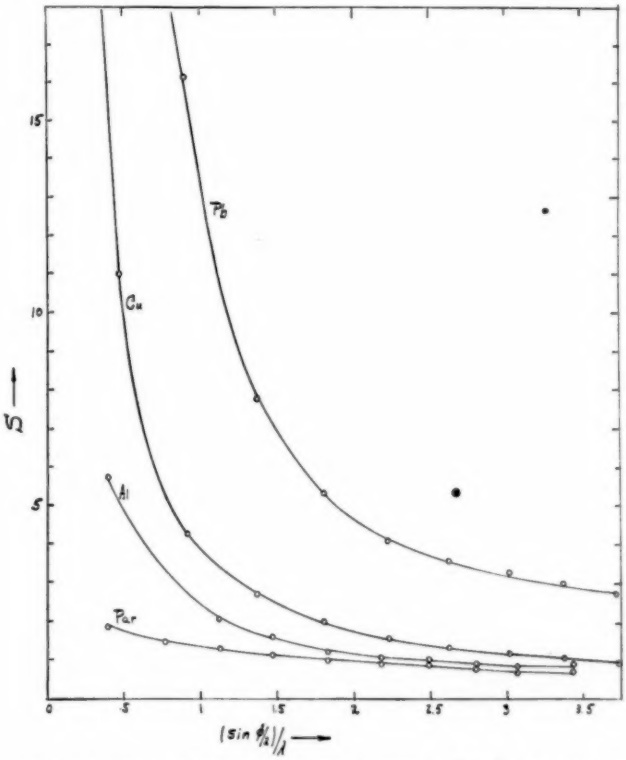

Fig. 4. Experimental values for the scattering per electron with the classical scattering from a free electron taken as a unit.

correction for the coherent and incoherent scattered radiations from copper and lead. Besides, this error is probably slight, as the radiation scattered from lead is almost entirely coherent and that from copper is mostly so.

Considering all sources of error, the most probable error for the S-values is estimated to be less than 2 percent for paraffin and aluminum, and less than 6 percent for copper and lead. Included in these calculations is the error involved in the determination of the effective wave-length. It must be emphasized that in experiments of this kind where one works with more or less heterogeneous radiation, the concept of "effective" wave-length is not a closely defined one, as one learns by reading the divergent opinions expressed by different authors.[25]

[24] J. W. M. Dumond, Phys. Rev. **36**, 1685 (1930).

[25] See discussions under *X-Rays*, International Critical Tables, Vol. VI, 1928 Ed.

Jauncey,[6] in his theory of diffuse scattering of x-rays by solids, arrives at an expression given by

$$S = 1 - (Z - 1)(f'^2/Z^2) + (F^2/ZN)X$$

where S is the scattered intensity per electron, relative to the scattered intensity from a single electron, Z is the atomic number, F is the atomic structure factor which includes the effect of thermal agitation, f' is related to f, the true atomic structure factor, N is the total number of atoms, and X is a complicated double summation.

So far, the double summation X has been evaluated only for a simple cubic crystal consisting of atoms of one kind.[26] It has not been determined for an amorphous solid and hence no comparison can as yet be made between Jauncey's theory and the present experimental results.

It is interesting, in connection with what has been said above about the excess scattering by paraffin at 105°, to note Chao's experimental result.[27] Working with γ-rays from ThC he finds at 135° an intensity of scattering by lead approximately three times that which one would expect from the formula of Klein-Nishina. This *anomalous* scattering he attributes to a cooperation of the nuclear electrons in the process of scattering.

In concluding, I wish to express my gratitude to Professor A. H. Compton for help in the course of this work.

[26] G. E. M. Jauncey and G. G. Harvey, Phys. Rev. **37**, 1203 (1931).
[27] C. Y. Chao, Phys. Rev. **36**, 1519 (1930).